# THE HYDRAULIC BEHAVIOUR OF SAND AND SILT SOILS AROUND THE RESIDUAL-STATE CONDITION

A Thesis Submitted to the College of

Graduate Studies and Research

in Partial Fulfillment of the Requirements

for the Degree of

Doctor of Philosophy

in the

Department of Civil and Geological Engineering

University of Saskatchewan

Saskatoon

Canada

By

Nader Ebrahimi-Birang

## ABSTRACT

Geotechnical and geo-environmental engineering problems may require the computation of near-ground-surface water balances. Evaluation of the unsaturated coefficient of permeability function is often necessary in order to undertake numerical simulations associated with the water balance evaluations. Evaporation at ground surface has the potential to reduce the water content of the soil to values less than the residual water content. However, it appears that the accuracy of commonly used methods for the determination of the permeability function around residual-state conditions is unknown. There may be lack of accuracy due to an oversimplification of the physics of water movement around the residual-state condition. Evaluation of the coefficient of permeability function around the residual-state condition requires reliable experimental data in the low water-content range.

In this study, the concept of residual-state condition is reviewed, and a definition of the conditions suitable for geotechnical engineering practice is suggested. A transition zone for the soil-water content/soil-suction profile is defined for steady-state flow systems. A possible link between the limits of the transition zone and the residual-state condition is proposed. A method is developed for predicting the unsaturated coefficient of permeability, based on a new definition of the residual-state condition. The method is based on the theory of vapour-phase flow and on the soil-water characteristic curve.

A series of evaporation tests were conducted in an environmentally controlled room on two different types of soil samples: sand and clayey silt. The unsaturated coefficient of permeability functions for the selected soils were established. The steady-state evaporation method used in this study proved to measure the unsaturated coefficient of permeability function in the low-water content range.

The results obtained from the predictive method proposed in this thesis are compared to the experimental data and to the data predicted by the previously proposed methods. Predictions computed when using the new method appear to be more accurate than those from previously proposed methods.

It was not possible to draw firm conclusions from the tests performed regarding the relationship between the residual-state condition and the upper and lower limits of the transition zone of the water-content/soil-suction profile.

## ACKNOWLEDGMENTS

To *Nooshin* and *Karina*

and

To the memory of *Naser Ebrahimi-Birang*

**CONTENTS** .......................................................................................................... PAGE

## LIST OF FIGURES

xiii

xv

xvi

xvii

# LIST OF TABLES

CHAPTER 1

**INTRODUCTION**


**1.1   BACKGROUND**

With an increasing world population and the extension of the geotechnical and geo-environmental problems associated with human activities, geotechnical engineers have become more involved in solving unsaturated soil problems in the low water content range. One such problem is related to the unsaturated coefficient of permeability function. Engineering problems may require the computation of near-ground-surface water balances, the prediction of potential volume changes, or the prediction of the unsaturated shear strength of the soil. Evaporation at ground surface has the potential to reduce the water content of the soil to values less than the residual water content. The design of engineered cover systems and water balance evaluations in the top part of earthen embankments or natural slopes often requires an evaluation of the unsaturated coefficient of permeability function in order to undertake numerical simulations.

Acid drainage has been found to be a serious environmental issue that the mining industry has had to address. More than 15,000 hectares of land have been covered with potentially acid-generating tailings in Canada (Wheeland and Feasby, 1991). Feasby et al. (1991) estimated $2 billion in liability costs for reclamation of acid-generating mines in Canada. The MEND (Mine Environment Neutral Drainage) program was initiated by the Government of Canada in 1988 to confront the issue of acid-generating mine tailings (Yanful et al. 1999). Many acid-generating mine tailings have been controlled using engineered soil covers since the initiation of the MEND program.

Engineered soil covers have continued to be of interest in controlling acid-generating mine tailings in Canada and worldwide (Yanful et al. 1999; Barbour et al. 1993). Water balance calculations form the basis for the design of moisture-retaining cover systems. In arid and semi-arid regions, the evaporation component of the water

balance controls the degree of saturation and the unsaturated coefficient of permeability within the soil cover. Quantifying the evaporation component is fundamental to soil cover design (Carey et al. 2005). The unsaturated coefficient of permeability must be accurately defined in order to estimate the evaporation component of the water balance equation for the design of moisture-retaining covers.

Commonly used methods for determining the unsaturated coefficient of permeability have been developed by Mualem (1976c), van Genuchten (1980) and Fredlund et al. (1994). The methods rely on the SWCC and the saturated coefficient of permeability for predicting the unsaturated coefficient of permeability.

Two key features of the soil-water characteristic curve that have often been used to identify the form of the unsaturated coefficient of permeability function are the air-entry value and the residual water content. There is a general consensus on the definition, physical description, and determination of the air-entry value among researchers; however, differences have been observed on the definition, physical description, and determination of the residual water content (Luckner et al. 1989; Nimmo, 1991; Luckner et al. 1991).

The concept of residual water content has been previously introduced in various disciplines, such as petroleum engineering, agriculture, and soil science. The residual water content has been estimated as a point on the SWCC. Methods for estimating the residual water content have been proposed in different disciplines (Brooks and Corey, 1964; Mualem, 1976c; van Genuchten, 1980; Vanappali, 1990).

Considering the residual water content as a point on the soil-water characteristic curve may lead to an inaccurate prediction of the liquid-phase coefficient of permeability around the residual state condition. The lack of an accurate prediction of the unsaturated coefficient of permeability around the residual water content can in turn lead to an inaccurate simulation of the soil-suction profile. Discrepancies have been observed between experimental and simulated soil-suction profiles within the transition zone obtained from the laboratory tests and flow models (Wilson, 1990; Gitirana, 2005; Choo and Yanful, 2000).

Wilson (1990) developed a theoretical-based approach to evaluate the evaporative rate from a soil surface. A drying test using a fine, uniform column of sand was

conducted in an environmentally controlled room for 42 days. The developed theory was evaluated using experimental data obtained from the drying test. Figure 1.1 shows the measured and computed suction profiles for day 29 of the column-drying test. The water content profile was divided into three distinct zones: i) a predominant liquid-water flow zone, ii) a transition zone, and iii) a predominant water-vapour flow zone. A sharp change in suction values was observed between the predominant water-vapour flow region at the bottom of the column and the predominantly liquid-water flow at the top (i.e., within the transition zone of the profile). There are discrepancies between the experimental and computed data within the transition zone. The thickness of the transition zone of the suction profile is about 60 mm. It was suggested that discrepancies observed between the data might be attributed to the difficulty in defining the unsaturated coefficient of permeability around the residual-state condition.

Although some literature is available on the definition and description of the transition zone of the water-content profile, little research is available on the definition of the residual-state condition for engineering practices. As previously explained, most of the previous research has considered the residual-water content as a well-defined or definite point on the SWCC. It is hypothesized in this thesis that there may be a one-to-one relationship between the residual-state condition and the transition zone of water-content profile. That is, the residual-state condition is hypothesized to be a zone on the SWCC; the water contents at the lower and upper limits of the transition zone are assumed to mark the initial and final residual-state condition, respectively. The hypothesis will be evaluated through an experimental program in this research.

From the examples described in the previous paragraphs, it appears that an inaccurate prediction of the unsaturated coefficient of permeability within the residual-state condition may result in inaccurate simulations for the soil-suction profile within the transition zone. An inaccurate prediction of the unsaturated coefficient of permeability may be due to a simplification of the residual-state condition as a point on the SWCC along with the use of the point as a lower limit for the liquid-phase coefficient of permeability in most prediction methods.
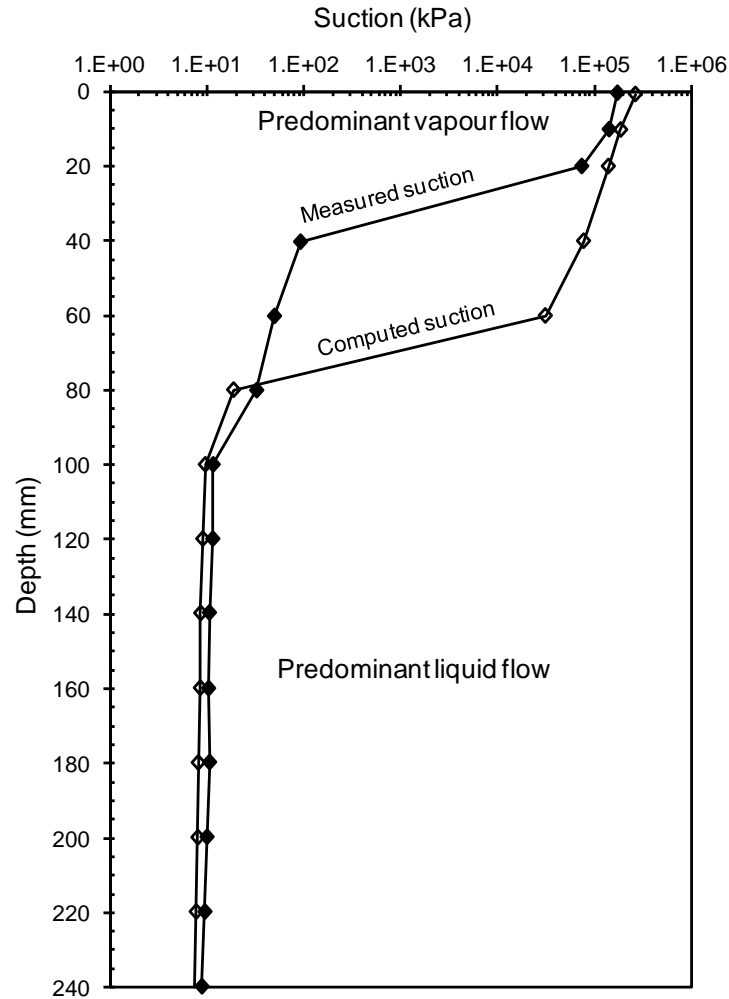
Figure 1.1 Measured and computed suction profiles for day 29 of the column-drying test
for Beaver Creek Sand (Modified from Wilson, 1990)

The author considers that the definition of the liquid-phase coefficient of
permeability within the transition zone of soil-suction profile or around the residual-state
condition needs to be modified to improve the accuracy of the simulation of the soil-
suction profile within the transition zone. The prediction methods for the liquid
coefficient of permeability have been mostly based on limited experimental data in the
high range of water contents. The first step in the modification requires a set of reliable
experimental data to observe the true form of the liquid-phase coefficient of
permeability function within the transition zone or within the residual-state condition.

Numerous methods have been used to measure the unsaturated coefficient of
permeability in the laboratory. The methods have been classified into two categories:

steady-state and transient-flow methods. Most of the methods have been limited to high water-content ranges. Two of these methods, however, may be suitable for measuring the unsaturated coefficient of permeability for low water-content ranges. A modified form of the evaporation method for the measurement of the liquid coefficient of permeability has been shown to result in a reasonable liquid-phase coefficient of permeability for low water content ranges (Mehta et al., 1994; Fujimaki and Inoue, 2003). A modified form of the evaporation method is given consideration in this thesis for the measurement of the coefficient of permeability in the residual zone.

## 1.2 RESEARCH OBJECTIVES AND SCOPE OF THE THESIS

The general objective of this research program is to study the hydraulic flow properties of sand and clayey silt soils around residual-state conditions.

The specific objectives of the research are as follows:

1) to review research in associated disciplines and determine an appropriate definition and description of the residual-state condition (RSC) for geotechnical engineering practice,

2) to measure the unsaturated coefficient of permeability in the moderate to low water content ranges,

3) to evaluate relationship between the residual-state condition and the transition zone of water-content profile, and

4) to propose a methodology, or modify an existing methodology, in order to predict the unsaturated coefficient of permeability around the residual-state condition.

Throughout this thesis, the porous media are assumed to be rigid in the sense that volume changes are assumed to be insignificant. Evaporation is considered as the main process involved in the desaturation of the soil. The evaporation method is considered to measure the coefficient of permeability around the residual-state condition. Soil columns at the start of the evaporation tests are considered to be saturated. The evaporation system needs to reach steady-state flow conditions at the end of the tests. Therefore, only steady-state flow condition will be considered in development of the flow equations as well as in the analysis. The transient flow at the beginning of the evaporation tests is

discarded from the analysis. The shear strength and volume change in the low water content range is considered to be beyond the scope of this thesis.

## 1.3 OUTLINE OF THE THESIS

Chapter 2 presents a review of literature on the SWCC, on the residual-water content concept and its various definitions, physical descriptions, and determinations, and on the drying soil system subjected to evaporation. It will also include a discussion on the development of evaporation methods to measure the unsaturated coefficient of permeability function and a review of literature on methods for predicting the unsaturated coefficient of permeability function.

Chapter 3 proposes a physical description for the residual-state condition. The residual-state condition is theoretically defined through the development of a conceptual model of desaturation. Mathematical equations are developed to describe the flow and heat fluxes for the steady-state evaporation process. A combination of the liquid-phase and vapour-phase flows is considered for the flow mechanism within the transition zone of water-content profile. Challenges regarding the definition of the liquid-phase unsaturated coefficient of permeability within the transition zone of the water-contents profile are described. A modified procedure is proposed for the prediction of the liquid-phase unsaturated coefficient of permeability within the transition zone. The modified procedure is based on Buckingham's (1907) hypothetical definition for liquid-phase coefficient of permeability function, the definition of the residual-state condition, and the theory of vapour flow.

Chapter 4 outlines the laboratory program for the entire thesis. As part of the experimental program, a series of steady-state evaporation processes on two different types of soil, namely, a sandy soil and a clayey silt soil, was conducted within an environmentally-controlled room.

Chapter 5 presents the experimental test results and discussion.

Chapter 6 presents the analyses and interpretations of the experimental data, including determination of the residual-state condition using the proposed theoretical method; validation of the existence of a relation between the residual-state condition and the transition zone of soil-suction profile; calculation of the unsaturated coefficient of permeability function using laboratory testing data; prediction of the coefficient of

6

permeability function using the proposed method in chapter 3; and evaluation of the proposed method using the experimental data.

Chapter 7 presents the summary, conclusions, and recommendations for future research.

CHAPTER 2

**LITERATURE REVIEW**

**2.1 INTRODUCTION**

This chapter provides a review of the research literature related to: i) various aspects of the soil-water characteristic curve (section 2.2); namely, the concept of the residual-state condition (section 2.3); ii) drying-soil systems, including flow equations and key soil parameters (section 2.4); iii) methods for measuring the coefficient of permeability function (section 2.5); and iv) methods for predicting the coefficient of permeability function (section 2.6).

The soil-water characteristic curve (SWCC), discussed in section 2.2, plays a significant role throughout this research program. The residual-state condition is considered to be a key feature on the SWCC. In the analysis of the experimental data from an evaporation test, an independent measurement of the SWCC is often required and is used along with the water content profile to determine the coefficient of permeability. A water content profile can be converted to a soil suction profile using the independently measured SWCC. Additionally, the SWCC plays an important role in some commonly used methods for the prediction of the coefficient of permeability function. The SWCC has other applications which are outside the scope of this thesis and are not considered in this review.

Thorough review on the concept of the residual-state condition is presented in section 2.3. The objectives of the review are: i) to highlight previous research related to the definition, physical description and determination of the residual-state condition described in different disciplines, ii) to understand how the concept has been interpreted in the literature when dealing with flow problems through unsaturated soils, iii) to establish a foundation to develop an appropriate definition and determination procedure

8

for the residual-state condition for geotechnical engineering practice. A new procedure to determine the residual-state condition will be proposed in Chapter 3.

Section 2.4 presents a review on drying soil systems. Water content profiles have been widely used in the analysis of water flow through unsaturated soils. The water content profile has been used to determine the location of the drying surface and dominant flow mechanisms along a soil column during evaporation processes. Water content profiles can also be used to determine when steady-state flow conditions have been reached. A steady-state flow condition is assumed to have been reached when the water content profile remains constant with respect to time. In addition to water content profiles, temperature profiles may also be required to determine steady-state flow conditions. Examples are presented from the literature to provide information on the application of the water content and temperature profiles in a drying soil system. Separation of the liquid water and water vapour flow mechanisms using the water content and salt profiles is also considered.

Section 2.4 also provides a review of literature on the flow equations and key soil parameters (i.e. coefficient of permeability and vapour diffusion) associated with water transport through unsaturated soils. Determination of the coefficient of permeability function using the evaporation method requires thorough understanding of flow equations. Darcy's equation has been used to represent the liquid water movement within a soil profile. Fick's law has been used to represent the water vapour flow within the soil. The combination of the two equations (i.e. Darcy's equation and Fick's law) has been used to represent a combined liquid water and water vapour flow within the soil profile. A concise review on the experimental data from the laboratory and field tests is also presented.

Section 2.5 presents a concise review on the methods used for measurement of the coefficient of permeability function, with an emphasis on the evolution of the evaporation method. To assess the effect of defining the residual-state condition as a zone, on the prediction of the coefficient of permeability function, it is necessary to have a set of reliable experimental data for the coefficient of permeability function. A modified form of the evaporation method is considered for measuring the coefficient of permeability function around the residual-state condition in this thesis.

Section 2.6 presents a review of the prediction methods for the coefficient of permeability function. A method will be outlined in Chapter 3 to predict the coefficient of permeability function by considering the residual-state condition as a zone. Laboratory data from the evaporation method will be used in order to assess the newly proposed predictive method. The results from the new predictive method will also be compared with the results from some commonly used predictive methods.

## 2.2   SOIL-WATER CHARACTERISTIC CURVE (SWCC)

Many studies have been done on different aspects of the SWCC, including its measurement, representing equations, hysteresis, estimation, and application (Barbour, 1998; Fredlund, 2006). The SWCC has been used in determining the unsaturated coefficient of permeability through measurement and prediction methods. Many research papers have related the definition and determination of the residual-water content to the SWCC (e.g., Barbour 1998, Fredlund 2006). Although there are several references on the SWCC, there is not a particular reference to cover all of the aspects of the SWCC that are needed for the current research. The following sections presents a concise review on the aspects of the SWCC associated with the current research. The review is written with the intention to help the reader comprehend the concepts associated with the SWCC throughout the thesis.

### 2.2.1   Definition of the Soil-Water Characteristic Curve (SWCC)

The soil-water characteristic curve indicates the relationship between water content and soil suction (Fredlund and Xing, 1994; Williams, 1982). Water content is a quantitative parameter used to define the amount of water within the pores of a soil specimen. The soil water content is generally presented as gravimetric water content, w, or volumetric water content, $\theta_w$. The degree of saturation, $S$, is another commonly used measure to indicate the percentage of the voids that are filled with water. In geotechnical engineering, gravimetric water content, $w$, is commonly used, while in soil science and agricultural disciplines, the volumetric water content, $\theta_w$, is more common.

Soil suction is an indicator of the energy level of water in the soil. Soil suction may be either matric suction or total suction (i.e., matric suction plus osmotic suction). Matric suction is defined as the difference between pore-air pressure and pore-water pressure

within the soil pores. In their development of the theory for unsaturated soil mechanics, Fredlund and Morgenstern (1977) introduced matric suction as a stress-state variable for unsaturated soils. In developing theories for unsaturated soil mechanics, Fredlund and Rahardjo (1993) chose matric suction as one of two required stress-state variables. Net normal stress was chosen as the second stress-state variable. Typical drying SWCCs, from saturation to oven dry conditions (i.e., 0–1,000,000 kPa), are shown for four soils from Saskatchewan, Canada in Figure 2.1 (Fredlund, 2000).

The key features of the SWCC are the air-entry value and the residual-state condition. The air-entry value has been seen to represent the suction at which drainage of the largest soil pores begins (Fredlund, 2006). Researchers seem to have reached a general consensus on the definition for air entry value. On the other hand, the literature shows that there have been considerable differences in the definition of the residual water content. A comprehensive review on the concept of the residual water content is presented in section 2.3.

### 2.2.2 Hysteresis of the Soil-Water Characteristic Curve

Desorption and adsorption branches of the soil-water characteristic curve exhibit hysteresis (Fredlund and Rahardjo, 1993). Figure 2.2 shows a schematic of the initial drying, main drying and main wetting soil-water characteristic curves from saturation to a completely dry condition (Ebrahimi-Birang et al. 2007).

For many applications, it becomes necessary for a geotechnical engineer to decide which branch of the SWCC to use (Tami et al. 2004). For some cases, it might be suitable to use an average curve between the wetting and drying SWCCs (Fredlund, 2006). The main drying curve has been most commonly measured in the laboratory since it is easier than the wetting curve to measure. Experimental data for the wetting branch of the SWCC is limited. Therefore, some procedures have been proposed to predict or estimate the wetting branch from the drying branch of the SWCC (e.g., Feng and Fredlund, 1999). Some complex models that represent the hysteretic SWCC have also been proposed (Mualem 1974, 1976 a,b; Pham et al. 2003).
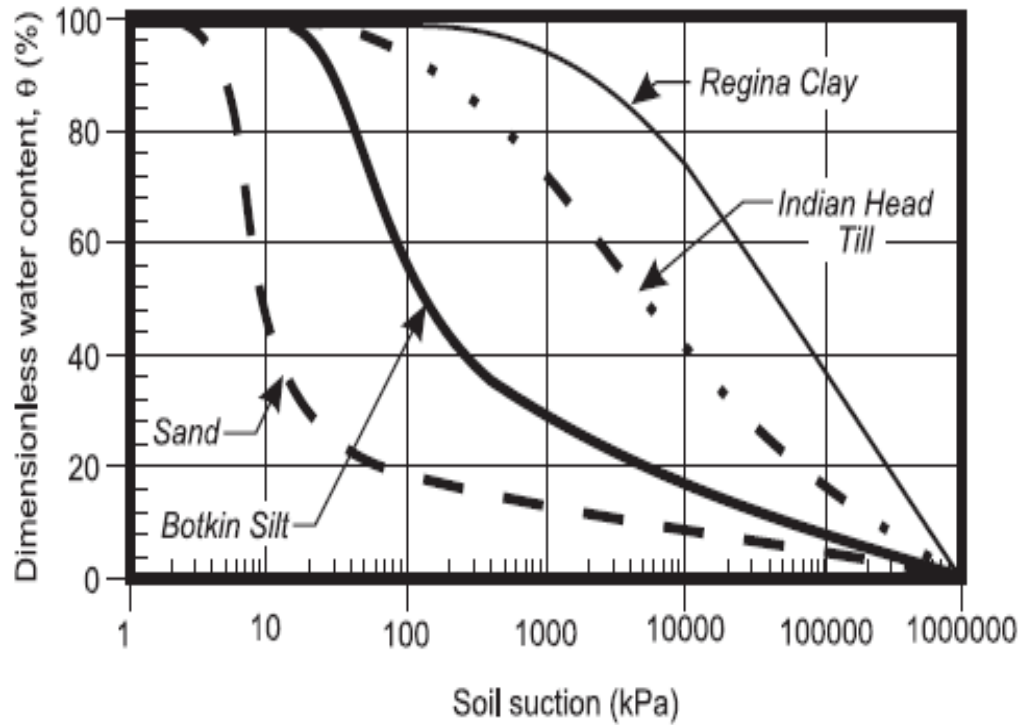
Figure 2.1 Typical drying SWCCs for four soils from Saskatchewan, Canada (Fredlund, 2000)
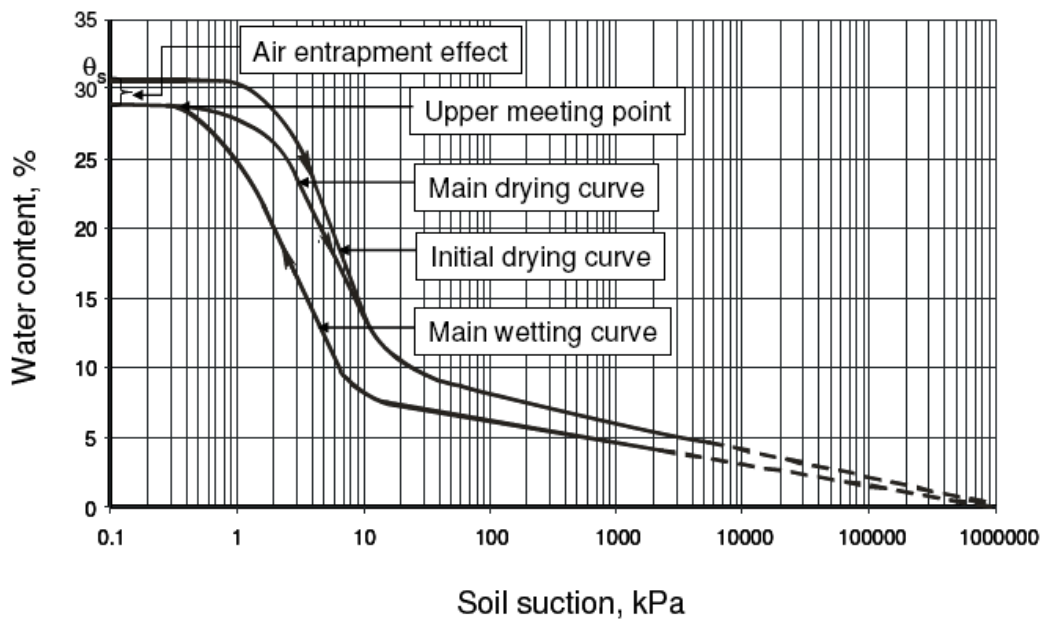


Figure 2.2 A schematic diagram of initial and main drying and main wetting SWCCs (Ebrahimi-Birang et al. 2007)

Most studies on the hysteresis phenomena have focused on the low suction range of the SWCC. There is limited information on the SWCC hysteresis in the high suction range of the SWCC. It is hypothesized in this research program that there may be a suction value beyond which the main drying and wetting SWCCs essentially become the same. It is also assumed that this meeting point of the SWCCs may be located at the residual-state condition. The existence of the aforementioned suction value has not yet been verified with experimental data. Some measurements on the SWCC hysteresis in the high suction range will be a part of the proposed research program.

### 2.2.3   Measurement of the Soil-Water Characteristic Curve

An accurate SWCC is required for a precise estimation of the evaporation component of the water balance in engineering cover design (Yanful and Choo 1997). The SWCC is also an essential part for estimating the unsaturated coefficient of permeability a soil. A variety of methods have been used to measure the soil-water characteristic curve. Information on laboratory methods of measuring the SWCC in agriculture and soil science may be found in the reference by Dane and Topp (2002). Reference for geotechnical engineering discipline can be made to ASTM D 6836- 02 (2003). Similar methods have been used in geotechnical engineering practices and agronomy-related disciplines to determine the entire soil-water characteristic curve.

Different apparatuses should be used for different ranges of suctions in order to obtain an accurate SWCC in the laboratory. Laboratory devices are usually limited to a specific range of suctions. All laboratory methods used for the measurement of the SWCC have a common theoretical base. Moisture within the soil pores is thermodynamically equilibrated to a known energy level through a water reservoir (Barbour, 1998).  Mechanical energy-based methods are used for the wetter portion of the SWCC curve (i.e., the soil suction range of 0 to 1500 kPa) and physico-chemical energy-based methods are used for the drier portion of the SWCC (i.e., beyond 1500 kPa).

To establish the SWCC, often a pressure plate apparatus is used in the low- to moderate-suction ranges (i.e., 0–500 kPa), and a desiccator is used in the high-suction range, (i.e., 1500–1,000,000 kPa). The pressure plate apparatus designed and manufactured at the University of Saskatchewan, Saskatoon will be referred to as "U of

S Pressure Cell" hereafter. The cell has been used for much of the research carried out in the University of Saskatchewan. The suction range of the U of S Pressure Cell has been limited to a maximum applied suction of 500 kPa. Recently, a device called "GCTS SWC 100" was designed by Fredlund and commercialized by GCTS Testing Systems. Through the GCTS SWC 100 device, the measurement range for the SWCC can be extended to 1500 kPa. As the GCTS SWC 100 device is relatively new, not many experimental data are available from it. Both the U of S Pressure Cell and the GCTS SWC 100 will be used for the measurement of the SWCC for the suction range from 10 to 1500 kPa in this thesis. Details of the features of U of S Pressure Cells and GCTS SWC 100 devices will be described in Chapter 4.

Different methods have been used to measure soil suction in the high suction range. The primary method has involved using equilibration of small soil samples over salt solutions of known osmotic suction (Fredlund, 1964; and Campbell and Gee 1986), or by using thermocouple psychrometry (Fredlund and Rahardjo, 1993; and Rawlins and Campbell, 1986). The former method is time consuming, while the latter method is limited to a maximum suction of 8000 kPa (Fredlund and Rahardjo, 1993).

Another method of measuring high soil suction involves the measurement of water activity. The principle involved in this method is similar to those of the hygrometric technique associated with thermocouple psychrometry (Gee et al. 1992). The method is rapid and involves the measurement of soil suction from 0 to 316,000 kPa. The device was first introduced as a water-activity meter (Gee et al. 1992), and it was later commercialized by Decagon Company.

The dew-point Water PotentiaMeter (WP4) has been used by several geotechnical researchers (Leong et al. 2003; Thakur et al. 2006; Agus and Schanz, 2005; Campbell et al. 2007) and is a modified form of the water-activity meter. The dew-point Water PotentiaMeter (WP4) has also been called the chilled-mirror dew-point psychrometer (Cardoso et al. 2007), or chilled-mirror hygrometer (ASTM D 6836-02, 2005).

Figure 2.3 shows a schematic diagram of a Dew-Point Water PotentiaMeter (WP4) (Leong et al. 2003). The device consists of a sealed chamber with a fan, a mirror and a photodetector cell, and an infrared thermometer.  The soil sample is placed in a stainless steel or plastic container of approximately 40 mm diameter and is slid into the chamber

using a tray. The sample thickness may vary between 1 to 5 mm. The chamber is closed and the sample becomes thermodynamically equilibrated with the environment inside the chamber before measurements can be made. The fan helps to accelerate the equilibration process. A Peltier cooling system is used to reduce the temperature on the surface of the mirror to dew-point temperature. The photodetector cell detects the condensation on the mirror which first appears at dew point. The dew-point temperature is then measured by a thermocouple. The infrared thermometer is used to measure the temperature of the chamber which is assumed to be the same as the temperature of the soil specimen at equilibrium.

Vapour pressure above the soil sample in the chamber and the saturated vapour pressure at the same temperature are computed using the dew-point and specimen temperatures. The calculations are done using software within the device and the value of the soil-water potential in MPa units, along with the specimen temperature, is displayed on an LCD panel. The soil suction is numerically equal to the negative soil-water potential.
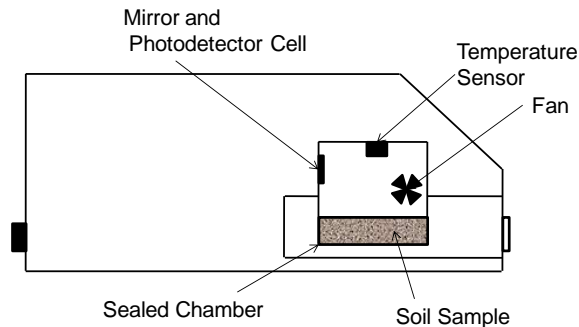
Figure 2.3 A schematic diagram of a dew-point Water PotentiaMeter (WP4) (after
         Leong et al. 2003)

Leong et al. (2003) evaluated the performance of a WP4 device for total suction measurements. It was reported that the quantities of total suctions determined from the individual measurements of osmotic and matric suctions were less than total suctions measured with the WP4 device. The difference increased with total suction. It was

suggested that the WP4 device could be used for rapid measurement of the total suction of unsaturated soils.

Agus and Schanz (2005) quantified inaccuracy involved in the measurements of the total suction using WP4 and three other commonly used sensors, including filter paper, the psychrometer, and the capacitance sensor. They found that the WP4 resulted data with the greatest accuracy. Agus and Schanz (2005) suggested that WP4 could be used for evaluating performance of the other sensors. They also suggested that for adequate accuracy, the total suction measurements should not be considered for suctions less than 1000 kPa.

Thakur et al. (2006) used the WP4 device to determine the soil water characteristic curve for a locally available silty soil and commercial white clay. Thakur et al. (2006) reported that the study revealed the practicality of the WP4 for the measurement of the total suction for fine grained soils to maximum total suction of 80,000 kPa.

Campbell et al. (2007) verified the performance of a WP4 device using five saturated salts and an unsaturated salt of known suctions. They found that the accuracy of the total suction measurements using the WP4 device was within 1% or better. Campbell et al. (2007) also determined the soil-water characteristic curve for four soil samples with different textures from sand to bentonite using a WP4 device for suction ranges from 1,000 to 400,000 kPa. They found that the relationship between the gravimetric water content and the logarithm of total suction was linear.

As described on the performance of the WP4 in the previous paragraphs, some research has been shown to have high accuracy for the measurement of the total suction using the WP4 device (e.g., Agus and Schanz, 2005; Campbell et al. 2007). On the other hand, there has been research where the accuracy of the WP4 appeared not to be adequate (Leong et al. 2003).

The manufacturer's instructions request that the WP4 be calibrated prior to operation with a standard solution of 0.5 M KCl, which should yield a suction of 2.19 ± 0.1 MPa, at 25 $^{o}$C. Cardoso et al. (2007) found that the calibration procedure suggested by the manufacturer for the WP4 device was not satisfactory.

Decagon Company recently added a new feature to the WP4 in order to minimize the influence of the ambient temperature fluctuation on the suction measurements. The

new device with internal temperature control is called WP4-T. The most important advantages of the WP4-T over the conventionally used desiccator method is its much shorter equilibrium time (e.g., 5–10 minutes).

Further experimental investigation will be conducted as part of this research program in order to evaluate the performance of the WP4-T.

### 2.2.4 Equations to Represent the Soil-Water Characteristic Curve

A variety of equations have been proposed to represent the SWCC. Some of these equations are tabulated in Table 2.1 (Fredlund, 2006). Most of the proposed empirical equations in Table 2.1 result in a SWCC description in which the suction goes towards infinity at some water content value. To more accurately represent the true form of the SWCC in high suction ranges, some researchers have proposed modifications to the SWCC equations. Some of the modified equations are summarized in Table 2.2.

Ross et al. (1991) suggested a method to extend any SWCC equation into high suction ranges provided the equation could be solved for the corresponding water content.

Ross et al. (1991) suggested that a modified form of the van Genuchten (1980) empirical equation with a residual water content taken as zero could be written as follows (see Tables 2.1 and 2.2):

$$\theta = \theta_s[1 + (\alpha\psi)^n]^{-m} - \theta_s[1 + (\alpha\psi_o)^n]^{-m} \qquad [2.1]$$

Rossi and Nimmo (1994) proposed two equations to represent the SWCC for the entire range of suction. Both equations were developed based on a modified form of the Brooks and Corey (1964) equation with a residual saturation taken as zero.

Fredlund and Xing (1994) developed an equation to represent the SWCC over the entire suction range from 0 to 1,000,000 kPa. A correction factor, $C(\psi)$, was used to extend the SWCC curve beyond the residual-state condition to a totally dry condition. The correction factor, $C(\psi)$, was defined as follows:

$$C(\psi) = 1 - \frac{Ln\left(1 + \frac{\psi}{\psi_r}\right)}{Ln\left[1 + \left(\frac{1,000,000}{\psi_r}\right)\right]} \qquad [2.2]$$

where $\psi_r$ is the residual suction. Other variables in the equation were defined in Table 2.1. Fredlund and Xing (1994) suggested selecting 3000 kPa as the residual suction for situations where the residual suction was not known. Sillers and Fredlund (2001) showed that shape of the correction factor was insensitive to $\psi_r$.

Table 2.1 Representing equations for the soil-water characteristic curve (after Fredlund, 2006)

| References | Equations | Description |
|---|---|---|
| Gardner (1958) | $$\Theta_d = \frac{1}{1 + \alpha_g \psi^{n_g}}$$ | $\alpha_g$ = soil parameter which is primarily a function of the air entry value of the soil and $n_g$ = soil parameter which is primarily a function of the rate of water extraction from the soil, once the entry value of the soil has been exceeded |
| Brooks and Corey (1964) | $$\Theta_n = 1, \quad \psi \leq \psi_{aev}$$ $$\Theta_n = \left(\frac{\psi}{\psi_{aev}}\right)^{-\lambda_{bc}}$$ | $\psi_{aev}$ = air entry value of the soil and $\lambda_{bc}$ = pore size distribution index |
| Brutsaert (1967) | $$\Theta_n = \frac{1}{1 + \left(\frac{\psi}{a_b}\right)^{n_b}}$$ | $a_b$ = soil parameter which is primarily a function of the air entry value of the soil and $n_b$ = soil parameter which is primarily a function of the rate of water extraction from the soil, once the entry value of the soil has been exceeded |
| Laliberte et al. (1968) | $$\Theta_n = \frac{1}{2} erfc\left[a_l - \frac{b_l}{c_l + \frac{\psi}{\psi_{aev}}}\right]$$ | $a_l$, $b_l$, and $c_l$ = unique functions of the pore size distribution index, $\lambda$ |
| Farrel and Larson (1972) | $$w = w_s - \frac{1}{\alpha_f} Ln \frac{\psi}{\psi_{aev}}$$ | $\alpha_f$ = medium parameter |
| Campbell (1974) | $$\theta = \theta_s \left(\frac{\psi}{\psi_{aev}}\right)^{\frac{-1}{b_c}}, \quad \psi \leq \psi_{aev}$$ | $\psi_{aev}$ = air entry value of the soil; $b_c$ = a constant; and $\theta_s$ = saturated water content |

Table 2.1 Continued from previous page

| van Genuchten (1980) | $$\Theta_n = \dfrac{1}{\left[1 + \left(\dfrac{\psi}{a_v}\right)^{n_v}\right]^{m_v}}$$ | $a_v$ = soil parameter which is primarily a function of air entry value of the soil; $n_v$ = soil parameter which is primarily a function of the rate of water extraction from the soil, once the air entry value has been exceeded; and $m_v$ = soil parameter which is primarily a function of the residual water content |
|---|---|---|
| van Genuchten (1980) | $$\Theta_n = \dfrac{1}{\left[1 + \left(\dfrac{\psi}{a_v}\right)^{n_v}\right]^{m_v}}, \quad m_v = 1 - \dfrac{1}{n_v}$$ | |
| van Genuchten (1980) | $$\Theta_n = \dfrac{1}{\left[1 + \left(\dfrac{\psi}{a_v}\right)^{n_v}\right]^{m_v}}, \quad m_v = 1 - \dfrac{2}{n_v}$$ | |
| McKee and Bumb (1987) | $$\Theta_n = \dfrac{1}{1 + exp\left(\dfrac{\psi - a_m}{n_m}\right)}$$ | $a_m$ and $n_m$ = curve fitting parameters |
| Fredlund and Xing (1994) | $$w(\psi) = C(\psi)\dfrac{w_s}{\left\{Ln\left[e + \left(\dfrac{\psi}{a_f}\right)^{n_f}\right]\right\}^{m_f}}$$ $$C(\psi) = 1 - \dfrac{Ln\left(1 + \dfrac{\psi}{\psi_r}\right)}{Ln\left[1 + \left(\dfrac{1{,}000{,}000}{\psi_r}\right)\right]}$$ | $a_f$ = soil parameter which is primarily a function of air entry value of the soil; $n_f$ = soil parameter which is primarily a function of the rate of water extraction from the soil, once the air entry value has been exceeded; $m_f$ = soil parameter which is primarily a function of the residual water content; and $C(\psi)$ = correction which is primarily a function of the suction at which the residual water content occurs |

Note: $\Theta_n = \dfrac{(\theta - \theta_r)}{(\theta_s - \theta_r)}$ = normalized water content; $\theta$ = volumetric water content; $\theta_r$ = residual water content; $\theta_s$ = volumetric water content at saturation; $\Theta_d = \dfrac{\Theta}{\Theta_s}$ = dimensionless water content; and $\psi$ = soil suction

Fayer and Simmons (1995) modified the SWCC equations proposed by Brooks and Corey (1964) and van Genuchten (1980) in order to represent the SWCC for entire range of soil suctions from 0 to 1,000,000 kPa. The adsorption function proposed by Campbell and Shiozawa (1992) (i.e., Eq. 2.3) was substituted into the Brooks and Corey (1964) and van Genuchten (1980) equations for $\theta_r$.

$$\theta_r = \left(1 - \dfrac{Ln(\psi)}{Ln(\psi_0)}\right)\theta_a \qquad\qquad [2.3]$$

19

where $\theta_a$ is a curve fitting parameter representing the volumetric water content at 1 kPa suction and $\psi_o$ represents the matric suction at oven-dry water content (i.e., $\psi = 1{,}000{,}000$ kPa).

Table 2.2 Modifications proposed to represent the SWCC for entire suction ranges from 0 to 1,000,000 kPa

| References | Equations | Description |
|---|---|---|
| Ross et al. (1991) | $\theta = f(\psi) - f(\psi_o)$ | $\theta = f(\psi) = $ a general equation for the SWCC; $\psi_o = $ total suction at zero water content |
| Rossi and Nimmo (1994) | $\Theta_r = 0$ | modified form of the Brooks and Corey (1964) equation with a residual saturation taken as zero |
| Fredlund and Xing (1994) | $C(\psi) = 1 - \dfrac{Ln\left(1 + \dfrac{\psi}{\psi_r}\right)}{Ln\left[1 + \left(\dfrac{1{,}000{,}000}{\psi_r}\right)\right]}$ | $C(\psi) = $ correction factor was used to extend the curve below residual water content to totally dry conditions |
| Fayer and Simmons (1995) | $\theta_r = \left(1 - \dfrac{Ln(\psi)}{Ln(\psi_0)}\right)\theta_a$ | The adsorption function proposed by Campbell and Shiozawa (1992), was substituted into the Brooks and Corey (1964) and van Genuchten (1980) equations for $\theta_r$ |

## 2.2.5  Prediction Methods of the SWCC

Measurement of the SWCC is relatively expensive and time consuming. The required accuracy of the SWCC may vary depending on the sensitivity of the solutions for the unsaturated soil problem. Some solutions may be quite sensitive to the accuracy of the soil-water characteristic curve; others may not. Some methods have been proposed for prediction of the SWCC. The proposed methods may be useful for some applications. Most of the prediction methods use some easily obtained soil characteristics to describe the SWCC. Prediction methods that describe the SWCC through other easily obtainable soil characteristics are termed Pedo-Transfer Functions, PTFs (Bouma and van Lanen, 1987). Estimation methods for the SWCC can be classified into three categories: i) point prediction of the SWCC, ii) functional parameter prediction methods, and iii) physico-empirical methods (Tietje and Tapkenhinrichs, 1993; Wosten et al. 2001).

Point prediction of the SWCC or point regression methods constitute the earliest form of PTFs in which the water content corresponding to specified soil suctions is related to easily obtainable soil parameters such as dry density and the percentage of soil particles sand, silt, and clay (Gupta and Larson, 1979; Rawls et al., 1982; Ahuja et al., 1985). In functional parameter prediction method, the parameters of a SWCC representing equation (see Table 2.1) are usually related to easily obtainable soil parameters (Cosby et al., 1984; Rawls and Brakensiek, 1985; Vereecken et al. 1989; and Aubertin et al., 2003). Physico-empirical models for the prediction of the SWCC often use information such as grain-size distribution and dry density. These types of models first translate the grain size distribution curve into an equivalent pore size distribution curve, which is then related to a distribution of water contents and associated suctions (Bloemen, 1980; Arya and Paris, 1981; Arya and Dierolf ,1992; Fredlund et al., 2002).

In addition to the three types of prediction methods presented in this section, a series of research papers has been published where the SWCC was determined from measured pore-size distributions (Simms and Yanful, 2002; Simms and Yanful, 2004). Pham et al., (2005) studied models for predicting the hysteresis soil-water characteristic curves.

## 2.2.6 Relevance of the SWCC in Geotechnical Engineering

Prediction methods have become quite routine for unsaturated soil property functions such as unsaturated coefficient of permeability function (Childs and Collis George, 1950; Brooks and Corey, 1964; Campbell, 1974; Mualem, 1976c) and shear strength (Vanapalli et al., 1996; Fredlund et al., 1996; Oberg and Sallfors, 1997; Khalili and Khabbaz, 1998). Proposed prediction methods have been generally based on the SWCC (Barbour 1998; Fredlund, 2006).

There are two essential bases for the prediction of the unsaturated soil properties: i) understanding of the geometry and distribution of the water within the pores, and ii) the effect of the geometry and water distribution within the pores on the special predictive soil property. Figure 2.4 reveals that the form of the relationship between the degree of saturation and various unsaturated properties might be different due to the fact that soil properties are controlled by different interphase relations (Barbour, 1998).

In addition to its role in the predictive methods for unsaturated soil properties, the SWCC may also play a significant role in experimental determination of the unsaturated coefficient of permeability. The SWCC may be used for conversion of the water content profile into the soil suction profile for calculation of the unsaturated coefficient of permeability function. The SWCC often provides an indication of soil suction from the measured water content. However, the prediction of the soil suction from the measured water content is often approximate due to the hysteresis associated with the SWCC.
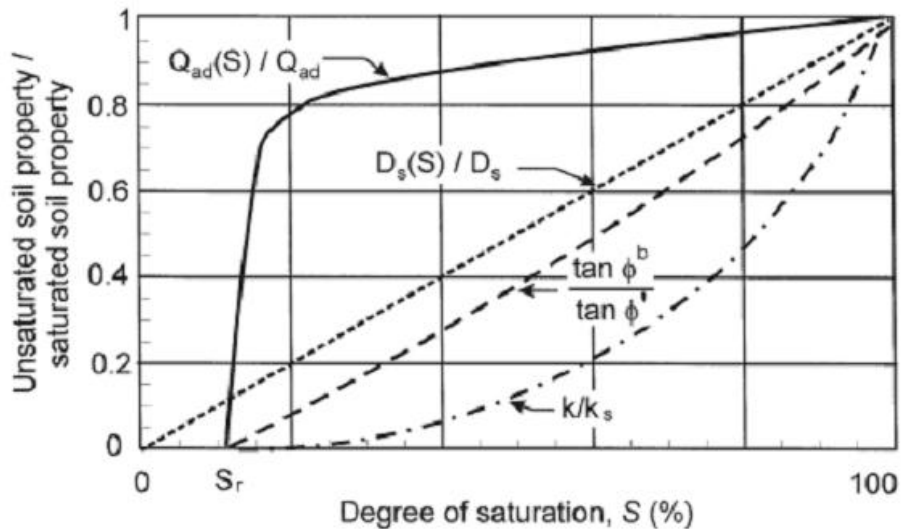


Figure 2.4 A typical functional relationship for unsaturated soil property normalized to saturated soil property versus degree of saturation (Barbour, 1998)

## 2.3 RESIDUAL-STATE CONDITION

Different terms in the literature have been used for describing the concept of residual state. Terms related to the concept of the residual-water content in the literature have been *irreducible saturation*, *residual saturation*, and *residual water content*. The terms irreducible saturation and residual saturation have often been used in the field of petroleum technology, while in agriculture and geotechnical disciplines, the terms residual-water content, residual degree of saturation, or residual saturation are more often used. Vanapalli et al. (1998) and Rassam and Cook (2002) introduced the residual suction, the residual state, and the residual conditions to the geotechnical engineering field.

A review on the residual-state concepts associated with unsaturated porous media in various disciplines is described in this section. Definitions and determination methods for residual-water content or residual suction are classified into three approaches: empirical and semi-empirical, conceptual, and experimental. These three categories, along with the references, are summarized in Table 2.3. A concise review on these three approaches will be described in this section.

Table 2.3 Definitions and determination methods of the residual-state concept for unsaturated soils

| Approach | References |
|---|---|
| Empirical and semi-empirical approach | Brooks and Corey (1964), Mualem (1976c), van Genuchten (1980), Haverkamp et al. (2005) |
| Conceptual approach | White (1968), White et al. (1970), Gvirtzman et al. (1987), Luckner et al. (1989), Couture et al. (1996) |
| Experimental approach | Haines (1923), Morrow (1970), Knight et al. (1996), Huang et al. (1998), Aoda (2000), Reinson et al. (2005) |

### 2.3.1   Empirical and Semi-Empirical Approach

The residual concept (usually the residual water content) have been assumed either as a fitting parameter for an equation representing the SWCC (van Genuchten, 1980; Haverkamp et al., 2005) or as a lower water-content limit for the unsaturated water flow models (Brooks and Corey, 1964; Mualem, 1976c) in empirical and semi-empirical approaches. In both cases the residual-state concept has been assumed as a definite.

The residual water content has often been determined by the means of the least square methods when taken as a fitting parameter in the SWCC representing equations. In the case of the lower limit for the unsaturated water flow models, the residual water content has been estimated using the graphical method proposed by Brooks and Corey (1964), or the mathematical approach proposed by Mualem (1976c).

In petroleum engineering, the concept of the residual saturation has been defined as the lowest saturation below which flow of the wetting phase cannot occur. The concept has been brought to the field of irrigation and drainage by Brooks and Corey (1964) in order to develop a theory for modeling liquid flow in an unsaturated porous medium.

The theory was developed based on the principles used in the field of petroleum science. The slow flow of liquid water at low degrees of saturation was not included in the Brooks and Corey (1964) model.

The unsaturated coefficient of permeability function is a key function for the models involving the liquid flow in porous media. Brooks and Corey (1964) developed a procedure to predict the unsaturated coefficient of permeability function using an empirical relationship between the effective saturation, $S_e$, and capillary pressure. In the equation proposed by Brooks and Corey (1964), the relative permeability of soil was also related to the effective saturation.

Brooks and Corey (1964) defined the effective saturation as:

$$S_e = \frac{S - S_r}{1 - S_r}$$  [2.4]

where $S$ is degree of saturation, and $S_r$ is "residual saturation."

Brooks and Corey (1964) defined the "residual saturation" as the

> "saturation at which theory assumes that effective permeability of the wetting phase, $k_{ew}$, is zero and effective permeability of the non-wetting phase, $k_{enw}$, is a maximum".

In unsaturated soils, the terms "wetting phase" and "non-wetting phase" refer to water and air phases, respectively. Brooks and Corey (1964) proposed a graphical method for determining the residual saturation from a relationship between effective saturation and capillary pressure.

Considering the relevance of the unsaturated coefficient of permeability function in flow modelling through porous media, Mualem (1976c) proposed a method to predict the relative permeability of a soil using the SWCC. The equation derived by Mualem (1976c) included a parameter called the effective volumetric water content, defined as:

$$\Theta = \frac{\theta - \theta_r}{\theta_s - \theta_r}$$  [2.5]

where $\theta$ is the volumetric water content, $\theta_s$ is the volumetric water content at saturation, and $\theta_r$ is the residual water content.

Mualem (1976c) defined the residual water content as follows:

"$\theta_r$ is defined as the residual water content for $\frac{d\theta}{d\psi} \to 0$ for $\theta \to \theta_r$ because it fulfills the other basic requirements that $k(\theta_r) = 0$".

Mualem (1976c) observed that for most of the available measurements, SWCCs were limited to water contents above the residual water saturation. To make the prediction methods for the unsaturated coefficient of permeability function more practical, Mualem (1976c) suggested that the SWCC must be extended to the residual water content. Therefore, he developed a method termed "an analytical standard method" to determine the residual water content by extrapolating the available data for the SWCC.

Van Genuchten (1980) proposed a closed-form equation to predict the relative permeability function from the SWCC. To represent the SWCC data, an empirical equation with four independent parameters was proposed. The parameters were saturation-water content, $\theta_s$, residual-water content, $\theta_r$, a parameter related to the air entry suction, *a*, and a parameter related to the slope of the SWCC, *n*. Van Genuchten (1980) presumed that two of the parameters—saturation-water content and the residual-water content—could be measured experimentally. The residual-water content was assumed to be the water content corresponding to the permanent wilting point (i.e., water content at 1500 kPa suction). The saturated-water content was measured as one of the routine parameters; however, the residual-water content might not routinely be available for all soils. Therefore, similar to Mualem's procedure, the value of the residual-water content was assumed to be extrapolated from the available SWCC data.

Van Genuchten (1980) defined the residual-water content as

"the water content for which the gradient, $\frac{d\theta}{d\psi}$ [slope of the SWCC], becomes zero excluding the region near saturation".

It was suggested that significant increases in suction may further decrease the amount of water below the residual-water content; however, from a practical point of view, such further decreases in water content were assumed not to be important.

Definitions given by Brooks and Corey (1964), Mualem (1976c), and van Genuchten (1980) are similar in that there is a consensus that the unsaturated coefficient of permeability function becomes zero at the residual-water content.

25

The equation proposed by van Genutchen (1980) to represent the SWCC has been used in research in agriculture disciplines to simulate unsaturated flow problems. In most of the research, the residual water content has been taken as one of the fitting parameters in the SWCC equation (Haverkamp et al. 2005). In such cases, the residual-water content does not have any physical description or definition. It is not uncommon to see negative values for residual-water content during the analysis.

Several researchers have used the Brooks and Corey (1964) method in order to determine the residual saturation (e.g., Wilson, 1990; Bruch, 1993). Table 2.4 shows values of the residual saturation, $S_r$, determined by the Brooks and Corey (1964) method for different soils. Values of the residual saturation, $S_r$, vary from 8.5% to 57.7% for the soils presented in Table 2.4.

Generally, clean sands have small residual saturations and sands containing some clay contents have larger residual saturations; however, Brooks and Corey (1966) indicated that the residual saturation was not solely a function of the clay content. Amarillo Silty Clay Loam (Table 2.4) and Pullman Clay Loam (see Figure 2.5) are two soils with high clay contents. While the residual-saturation value for Amarillo Silty Clay Loam is relatively high ($S_r = 25\%$,), it is almost zero for Pulman Clay Loam. In Figure 2.5, $\lambda$ and $\eta$ were defined as the slope of the capillary pressure head versus the effective saturation ($S_e$) line, and the slope of the capillary pressure head versus the relative coefficient of permeability ($k_{rw}$) line, respectively.

Table 2.4 Some residual saturation values obtained using the method proposed by Brooks and Corey (1966)

| References | Soil | Residual Saturation, $S_r$ (%) |
|---|---|---|
| Brooks and Corey (1966) | Volcanic Sand | 15.7 |
| Brooks and Corey (1966) | Glass Beads | 8.5 |
| Brooks and Corey (1966) | Fine Sand | 16.7 |
| Brooks and Corey (1966) | Touchet Silt Loam | 27 |
| Brooks and Corey (1966) | Berea Sandstone | 29.9 |
| Brooks and Corey (1966) | Hygiene Sandstone | 57.7 |
| Brooks and Corey (1966) | Poudre River Sand | 12.5 |
| Brooks and Corey (1966) | Amarillo Silty Clay Loam | 25 |
| Wilson (1990) | Beaver Creek Sand | 24 |
| Bruch (1993) | Beaver Creek Sand | 26 |
| Bruch (1993) | Processed Silt | 11 |
| Bruch (1993) | Natural Silt | 10 |

In functional parameter prediction methods for prediction of the SWCC using Pedo-Transfer Functions (see section 2.2.5), the residual-water content has been usually taken as a dependent variable of easily obtainable physical properties of the soil, such as dry density and porosity.
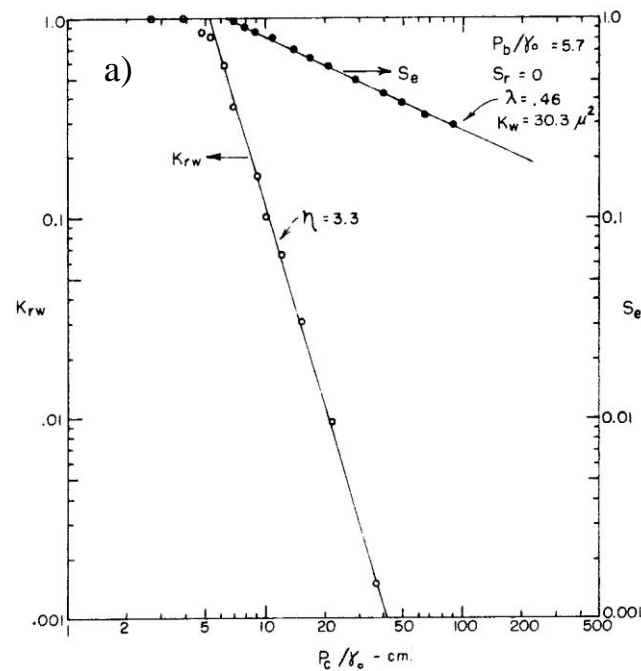


Figure 2.5 Relative permeability and effective saturation as a function of capillary pressure head for Pullman Clay Loam (Brooks and Corey, 1964)

### 2.3.2 Conceptual Approach

Conceptual approaches for the definition of the residual-state concept associated with unsaturated soils have been developed based on the water distribution within soil pores during desaturation of an initially saturated soil. While most of the conceptual models have assumed the residual state concept as a point (e.g., Gvirtzman et al. 1987), White (1968) has proposed the residual-state concept as a zone on the capillary pressure versus water-content plot.

Ever since the residual-water-content concept has been introduced, some authors have attempted to propose a physical description of the concept. There has been a consensus among the authors that when degree of saturation reaches the residual state, liquid water in the soil does not exist as a linked phase. In other words, the liquid-water

27

phase becomes discontinuous below the residual degree of saturation. This stage of the water distribution is known as the pendular rings stage. In the pendular rings stage, water is isolated as separated rings between joining points within grains.

In the case of the residual state condition as a point, the water distribution within the pores is assumed to take the form of pendular rings. The capillary model has generally been used to estimate the capillary pressure at the pendular rings stage. Geometry of the pores and distribution of water within the pores in the pendular ring stage have been used to estimate the water content corresponding to the pendular ring stage (Gvirtzman et al. 1987).

Gvirtzman et al. (1987) investigated the stage of pendular rings for an unsaturated clay loam using cold stage Scanning Electron Microscopy (SEM). Figure 2.6 shows an isolated pendular ring. Pendular rings of water were observed in the form of concave and convex curvatures (see "W" and "L" arrows in Figure 2.6). Bear (1979) and Barbour and Yanful (1994) suggested that although there might still be a hydraulic connection between isolated water rings through thin layer of water films, these water films do not appear to be able to effectively transmit the pressure between pendular rings.
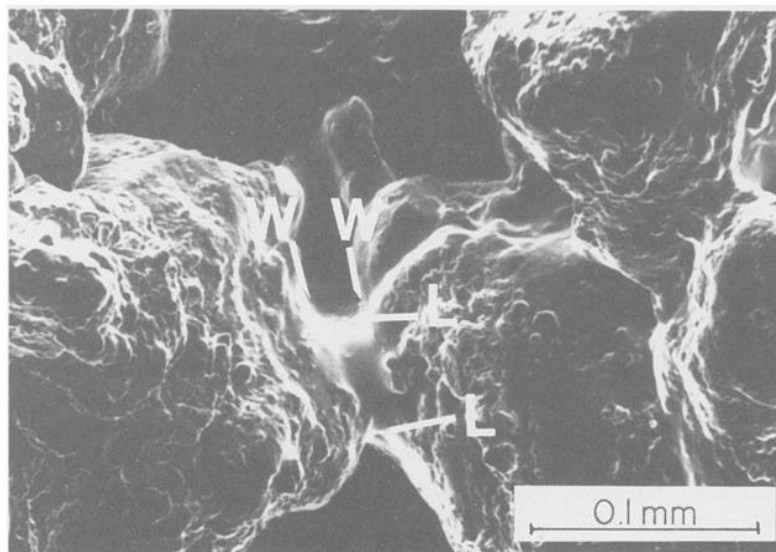


Figure 2.6 SEM micrograph of pendular rings with the convex and concave curvatures marked by "L" and "W" arrows, respectively (Gvirtzman et al., 1987)

Gvirtzman and Roberts (1991) proposed a conceptual model based on geometry to quantitatively analyze the interfacial area between the wetting and non-wetting phases

28

within a porous medium as a function of degree of saturation. Reinson et al. (2005) used the conceptual theory proposed by Gvirtzman and Roberts (1991) to predict the residual water content. Reinson et al. (2005) compared the predicted and measured data for the residual saturation. It was suggested that capillary theories and pendular rings could be used for the prediction of the residual saturation point on the soil-water characteristic curve for uniform coarse soils.

Luckner et al. (1989) presented a physical description of the residual fluid (e.g., water and air) content based on continuum mechanics. Continuum mechanics assumes that in a three phase system such as an unsaturated soil system, all phases (i.e., air, water, and solids) are distributed continuously. Figure 2.7 shows possible mobility domains in a soil system that includes two immiscible fluids, a wetting and a non-wetting fluid. Luckner et al. (1989) described the residual fluid (e.g., water and air) contents as follows: "the residual fluid contents $\theta_{w,r}$ and $\theta_{nw,r}$ characterize the transitions from coherent to incoherent fluid phase distributions. These two residual parameters are important geo-hydraulic variables affecting fluid flow in the subsurface"

Luckner et al. (1989) went on to say:

> we emphasize that incoherency of a fluid phase does not necessarily mean that the material making up the fluid phase is fixed in space or time. Incoherency only means that the fluid is immobile as a linked phase. Because of trans-phase exchange and transport as a dissolved phase in the other fluid phase, the incoherently distributed phase can still undergo significant changes. Evaporation and condensation, and de-gassing and dissolution between the liquid and gasses phase are examples of such trans-phase exchange processes.

The values of $\theta_{w,r}$ and $\theta_{nw,r}$ are wetting and non-wetting phase residual contents. For an unsaturated soil system, $\theta_{w,r}$ is water residual content and $\theta_{nw,r}$ is air residual content.

In Figure 2.7, $k_w$ and $k_{nw}$ are the coefficient of permeability for wetting and non-wetting phases, respectively; $\overline{S}$ and $\overline{S^*}$ are degree of saturations for wetting and non-wetting phases, respectively; and $\phi$ is total porosity of the soil.

In addition to defining the residual saturation as a point, it has been also defined as a designated zone on the SWCC. Conceptual modeling of desaturation for an initially

saturated porous medium has often been considered to define the residual saturation as a zone (White, 1968; White et al., 1970; Sjoblom, 2000).

White (1968) and White et al. (1970) developed a conceptual model to describe the residual-state condition as a zone on the capillary pressure versus saturation plot. White (1968) proposed a hypothetical model to describe desaturation of a porous medium. The model assumed that two types of desaturation mechanisms occur in a porous medium: i) *discrete mechanism* in which the capillary pressure needs to exceed the air-entry value of the medium in order to create changes in saturation and ii) *continuous mechanism* in which finite change in capillary pressure causes finite change in saturation. The concepts of discrete and continuous mechanisms have been also used by Bethel and Calhoun (1953) and Miller and Miller (1958) to describe the change in saturation of a porous medium.
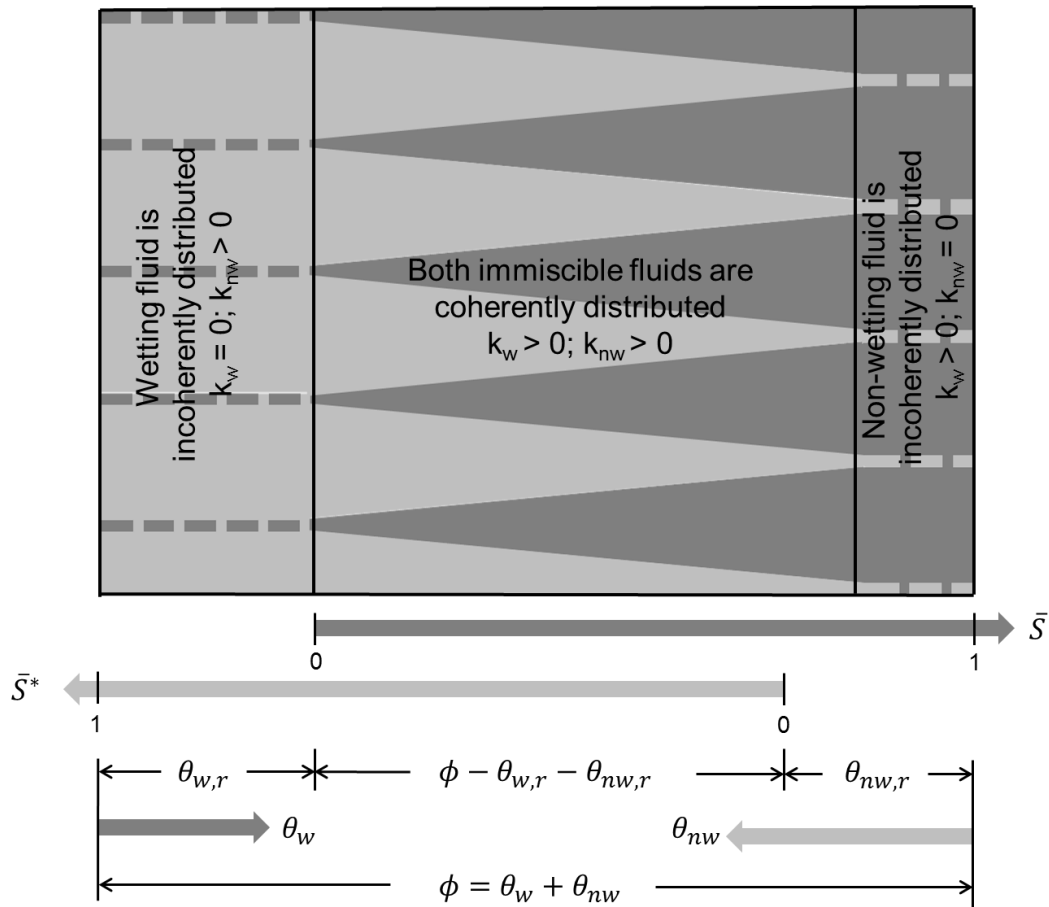


Figure 2.7 Possible mobility domains for two immiscible (wetting and non-wetting) fluids in a porous medium (Luckner et al., 1989)

30

Using the concept of discrete and continuous mechanisms of flow, White (1968) divided a saturation-capillary-pressure curve into four desaturation zones: i) boundary-effect zone, ii) primary-transition zone, iii) secondary-transition zone, and iv) residual-desaturation zone (Figure 2.8).

Boundary-Effect Zone

During initial times of desaturation of a porous medium, the capillary pressure is not great enough to drain any pores; however, desaturation begins at the exterior boundary of the medium. The range of capillary pressure over which this type of desaturation is dominant is termed the "boundary-effect zone." All equations and models developed for saturated soil mechanics are valid and applicable in this zone.

Transition Zone

Discrete desaturation begins when the capillary pressure is great enough to force the water through the largest throat in the exterior boundary toward a pore. The range of capillary pressure from this stage to the stage where discrete mechanism becomes insignificant is termed the "transition zone" of desaturation.
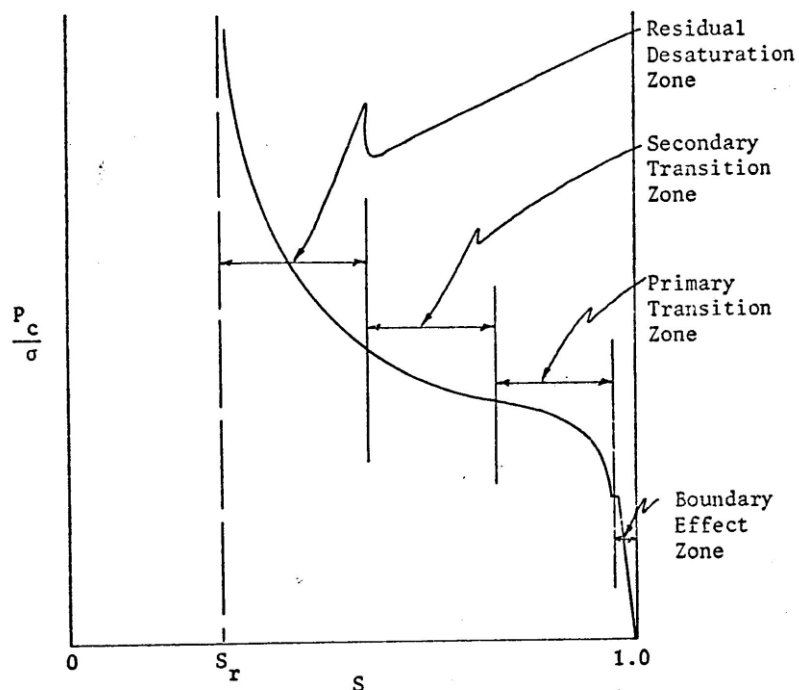


Figure 2.8 Saturation-capillary pressure curve for a hypothetical porous medium (White, 1968)

31

<u>Residual Zone</u>

The residual zone of desaturation is defined as the range of capillary pressure which begins when the continuous mechanism of desaturation becomes dominant over the discrete mechanism and extends to the residual saturation, $S_r$, at which point the liquid phase practically becomes immobile. White (1968) proposed graphical methods to determine the saturation at the beginning and termination of the residual-desaturation zone.

Vanapalli et al. (1996) proposed a probable distribution of water at different stages of desaturation by considering the description of the hypothetical desaturation model given by White (1968). The SWCC was divided into four independent zones, as shown in Figure 2.9. The residual condition was introduced as a point on the soil-water characteristic curve and a method of determination was proposed (Vanapalli et al., 1998).
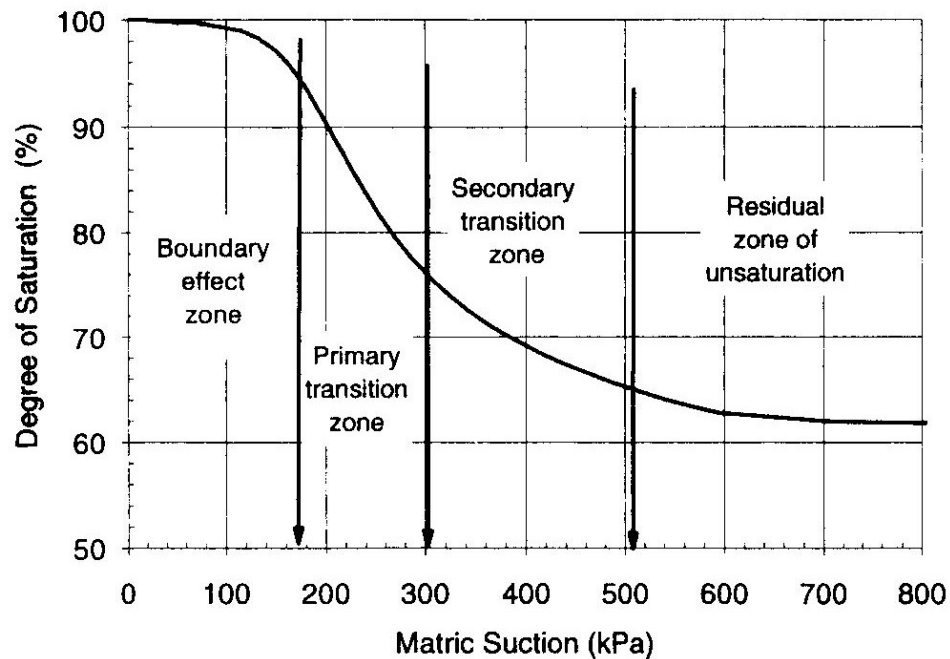
Figure 2.9 Soil-water characteristic curve indicating different stages of desaturation (Vanapalli et al., 1996)

The method of construction proposed by Vanapalli et al. (1998) has simplified definition of the residual-state condition from a zone on the saturation-capillary-pressure plot (i.e., a definition proposed by White, 1968) to a definite point on the SWCC. This

interpretation of the residual-state condition may retain the debate on the accuracy of the numerical simulations of suction profiles around the residual-state condition in unsaturated flow problems (see Chapter 1).

In chapter 3 of this thesis, interpretation of the residual-state condition as a designated zone on the saturation-capillary-pressure plot, proposed by White (1968) (Figure 2.8), is used to establish a definition for the initial residual-state condition on the SWCC.

### 2.3.3 Experimental Approach

Experimental approaches for the description and determination of the residual-state condition have been based on conceptual models where the residual condition was assumed to be a point. As explained in the previous paragraphs, it was assumed that at the stage of pendular rings, the water phase became discontinuous and the capillary pressure could not be transferred between the water rings.

Some laboratory methods have been used to estimate the residual saturation. Knight et al. (1996) used drying rate information from thin soils to estimate the residual saturation. From a series of evaporation tests they concluded that the hydraulic connectivity within the soil specimen breaks at a transition point from a constant rate to a falling rate of evaporation. Knight et al. (1996) suggested that the transition point from a constant rate to a falling rate of evaporation may provide an estimate for the residual water content.

Wilson (1990) conducted similar evaporation tests to those of Knight et al. (1996) using thin soil layers. Wilson (1990) and Wilson et al. (1997) concluded that although the transition from constant rate to falling rate of evaporation occurs at different water contents for different type of soils, the corresponding suction values are independent of soil type. It was suggested that at an approximate soil suction value of 3000 kPa, there was a transition point regardless of the type of soils. The 3000 kPa value has been used in other research studies since it was initially suggested by Wilson (1990). Bruch (1993) used the 3000 kPa suction value as a separation point between liquid and vapour mechanisms of flow within the soil. Fredlund and Xing (1994) used the value as residual soil suction in development of their SWCC equation to represent the soil-water characteristic curve for entire suction range from 0 to 1,000,000 kPa. Vanapalli (1996)

used the 3000 kPa value for predicting the shear strength from the soil-water characteristic curve and indicated that the estimated value and experimental data showed closer agreement with a value of 3000 kPa. Rassam and Williams (1999) conducted laboratory evaporation column tests and numerical studies on tailings materials. It was concluded from the evaporation studies that a soil suction value of around 3000 kPa corresponded to an increase in the gradient in the soil relative humidity. It is not clearly explained in the literature why an application of 3000 kPa resulted in closer agreement between simulated and experimental data.

Haines (1923) has defined the "residual shrinkage" as a zone on the shrinkage curve of a soil. It appears that Haines's definition is the first instance of the residual concept in the literature associated with unsaturated soil studies. However, most of the definitions associated with the residual water content in the literature have been based on the relationship between the capillary pressure and water content or between the water content and the soil suction (i.e., SWCC).

Barbour and Yanful (1994) investigated the pore-water pressure response within sand columns during prolonged drainage using two different tensiometers (i.e., "NTC" and "U of S"). After the applied pressure head was dropped below -0.35 m for coarse sand, the measured values commenced to depart from the applied hydrostatic pressure head (Figure 2.10). As the water distribution approached the condition where the liquid phase became discontinuous, it appeared that the applied pressure could not be transmitted between the soil and tensiometers.

Aoda (2000) conducted a column drainage test using glass beads with a diameter of 24 mm in a constant-temperature environment. The pore-water pressure was measured in three different points using a pressure transducer through an injection needle with an inside diameter of 0.2 mm (Figure 2.11). Starting from saturated conditions, different pressure heads were applied by changing the water level. The radius of meniscus curvatures of pendular rings was also photographed.

The relationship between pressure heads and the height from the water table were plotted for measurement point No. 1 (Figure 2.12). The results of the test showed that the pressure head was constant and independent from change in water level, beyond a pressure head of -2.84 cm. Analyses of photographs also showed that the radius of the

meniscus curvatures of the pendular rings were independent of changes in water level (Aoda, 2000).
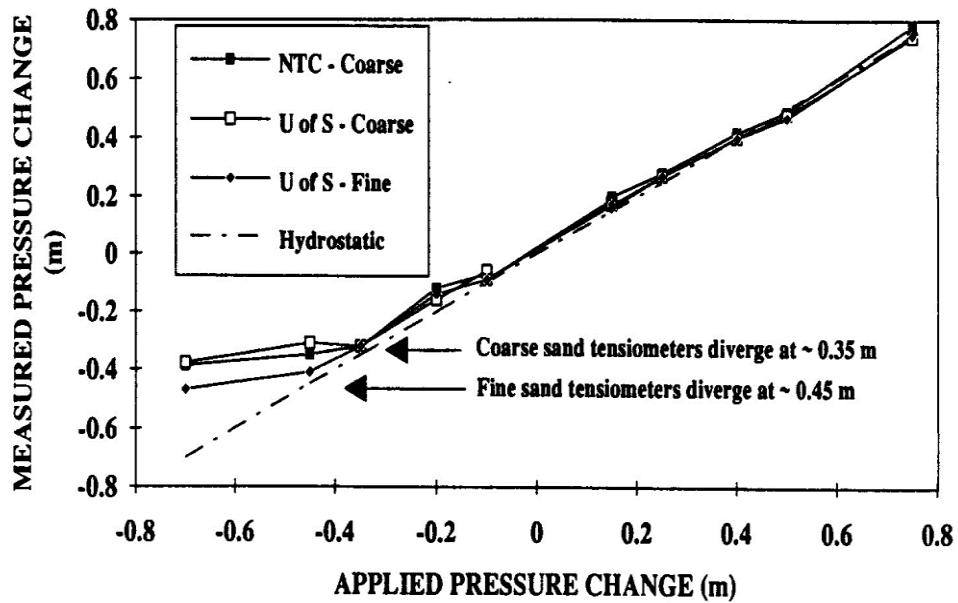


Figure 2.10 Relationship between applied and measured pressure changes (Barbour and Yanful, 1994)
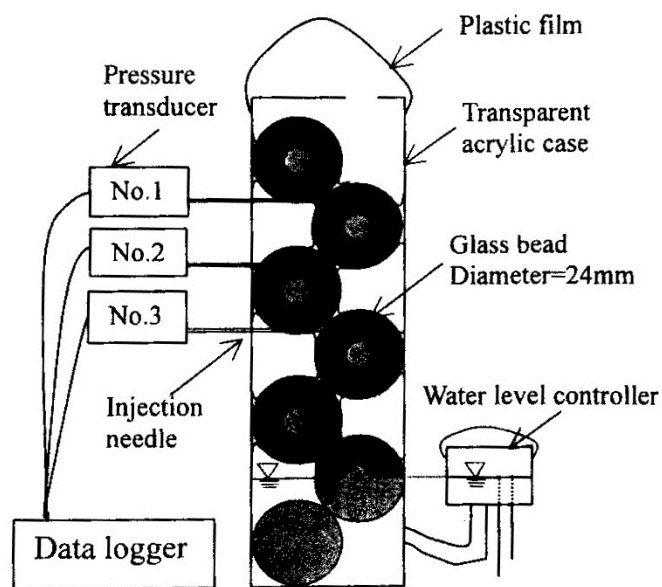


Figure 2.11 Schematic diagram of experimental apparatus (Aoda, 2000)
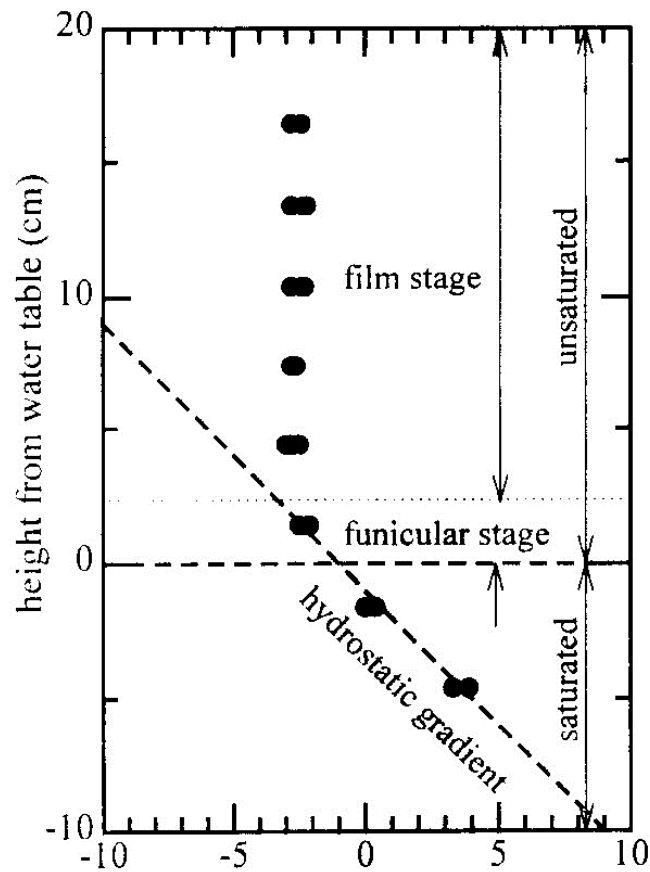
Figure 2.12 Relationship between pressure heads and water level at measurement point
No.1 (Aoda, 2000)

The aforementioned review on the residual-state condition revealed that most researchers have considered the residual-state condition as a definite point. On the other hand, considering the residual-state condition as a point may lead to an inaccurate prediction of the liquid-phase coefficient of permeability around the residual-state condition. Inaccurate simulation of the water contents or soil suctions profile have been observed between the experimental suction profile and simulated data obtained from flow models within transition zone of a suction profile (Gitirana, 2005; Choo and Yanful, 2000). This discrepancy between the experimental and simulated suction profiles has been suggested to be due to the lack of accurate prediction of the

unsaturated coefficient of permeability around the residual water content (Wilson, 1990; Choo and Yanful, 2000).

Wilson (1990) developed a theoretical based approach to simulate the unsaturated flow condition during evaporation. In order to evaluate the performance of the theoretical model, Wilson (1990) conducted a drying test using a fine uniform column of sand in an environmentally controlled room for 42 days. The moisture profile in terms of the mechanism of flow was divided into three distinct zones: i) the predominant water-vapour flow zone, ii) predominant liquid-water flow zone, and iii) the transition zone. Gitirana (2005) simulated Wilson's column test results using a heat and moisture flow model solved through FlexPDE, a Partial Differential Equation solver (PDE Solutions Inc., 2003). Results of the simulations by Wilson (1990) and Gitirana (2005) along with the measured results for suction profile for day 29 are shown in Figure 2.13. There was a clear discrepancy between the simulated and measured results in the transition zone. Wilson (1990) suggested that the difference between the simulated and measured profiles within the transition zone might be attributed to the difficulty in defining the unsaturated coefficient of permeability within the zone (Wilson 1990).
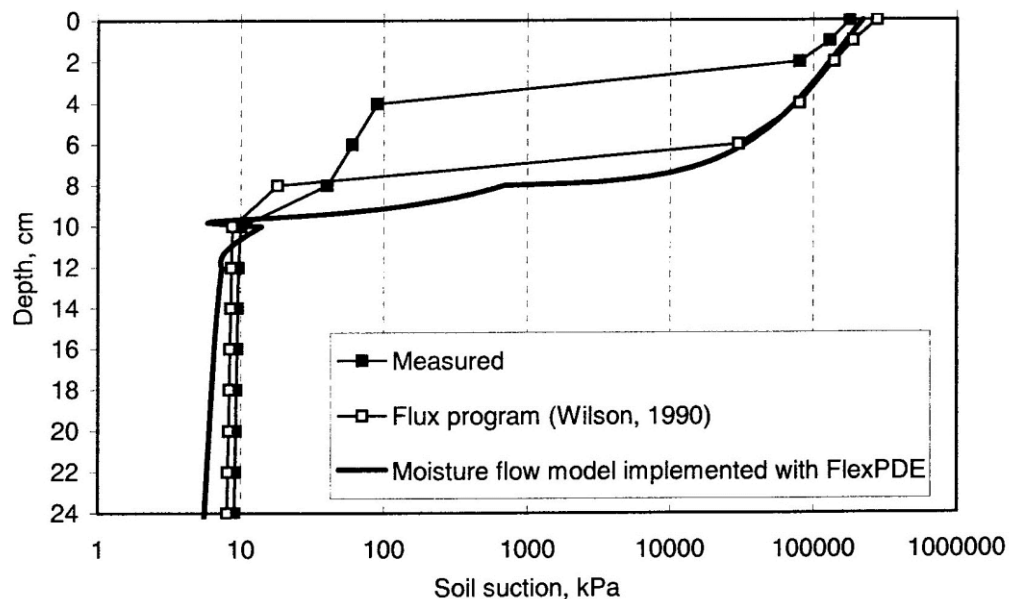


Figure 2.13 Measured and computed suction profiles for day 29 of the column-drying test for Beaver Creek Sand (Gitirana, 2005)

37

Choo and Yanful (2000) observed a discrepancy between measured and simulated water-content and pressure-head profiles for a three-layer soil column. A finite element and analytical methods were used for simulations. For times equal to and greater than 3 days, reasonable simulations were obtained by modifying the estimated coefficient of permeability function, $k(\psi)$. Choo and Yanful (2000) suggested that the method used for predicting the coefficient of permeability function, $k(\psi)$, could not capture the behaviour of soil around the residual-state condition.

It appears that the lack of accurate simulation of the suction profile within the transition zone may be caused by inaccurate prediction of the unsaturated coefficient of permeability around the residual-state condition. Inaccurate prediction of the unsaturated coefficient of permeability might be attributed to the simplification of the residual-state condition as a point.

## 2.4 DRYING SOIL SYSTEM

Three stages of drying are often recognized during evaporation from a saturated soil (Campbell, 1985; Wilson, 1990). The actual evaporation rate is almost constant and equal to the potential evaporation rate during the first stage. The second stage begins where the evaporation rate starts to decline. The third stage of drying commences when the rate of decrease in evaporation becomes small. These three stages are shown in Figure 2.14 along a typical evaporation curve for sand.

Evaporation may be analyzed in terms of the liquid-water flow rate throughout the first stage. Following the first stage to some degree of saturation, evaporation might still be analyzed as liquid-water flow. Campbell (1985) and Wilson (1990) proposed that there may be an unknown point within the third stage beyond which vapour flow is the only important mechanism of flow that must be considered.

### 2.4.1 Water Content Profile in a Drying Soil System

The water-content profile is commonly measured in the study of water movement in unsaturated soils. Based on the drying process stage, the type of soil and evaporation rate, water-content profiles can exhibit different shapes. If the evaporation process continues for a sufficiently long time, the evaporation front and hence the vapour-flow zone may develop. The primary mode of water movement near the surface within the

vapour-flow zone is due to vapour diffusion. The depth of drying front depends on different factors. The main factors are the depth of water table and potential rate of evaporation (Rose et al. 2005). The drying front can be characterized by an inflection in the soil water content profile, as illustrated in Figure 2.15 (after Hillel, 1998).
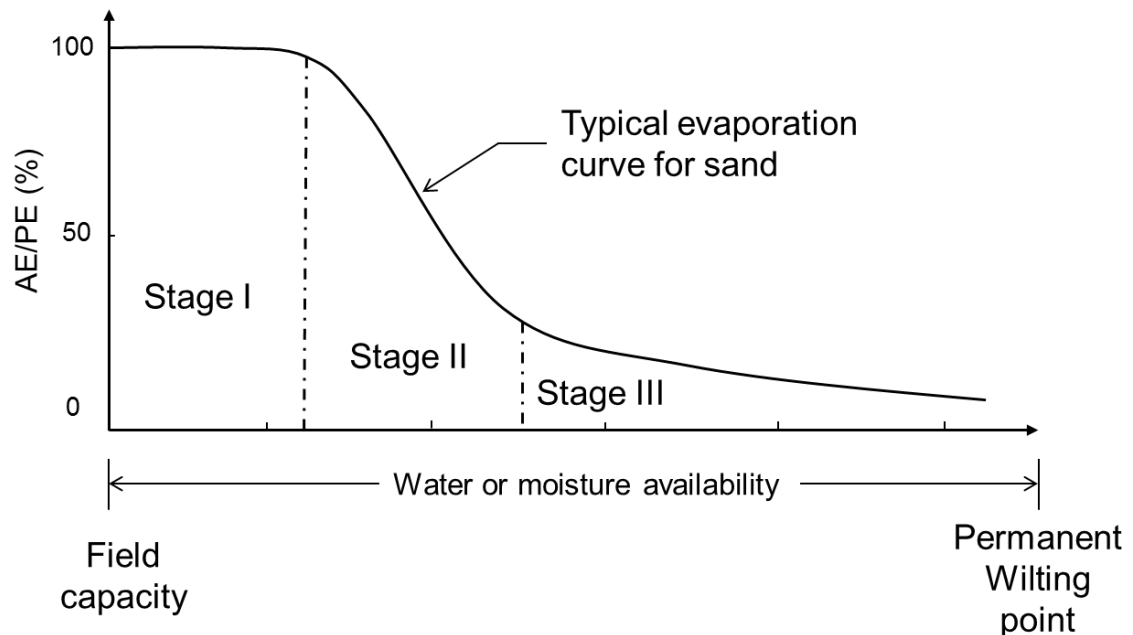


Figure 2.14 Three stages of drying process (after Wilson et al., 1994)

Bruch (1993) conducted a series of evaporation tests on soil columns in an environmentally controlled room with "constant water head" and "zero water head" boundary conditions at the bottom of the soil columns. Figure 2.16 shows the gravimetric water-content profiles for the processed silt soil column at some selected times for the zero flux condition (i.e., no water table). A drying front is developed for this case, but a drying front was not developed for the constant head boundary condition. The results for the constant head boundary condition are not shown here.

Development of a drying front has been observed for some evaporation tests with the existence of a water table. Rose et al. (2005) conducted a series of column evaporation tests with different water table depths. The development of the drying front was observed for all three cases on the water content profiles (Figure 2.17).

39
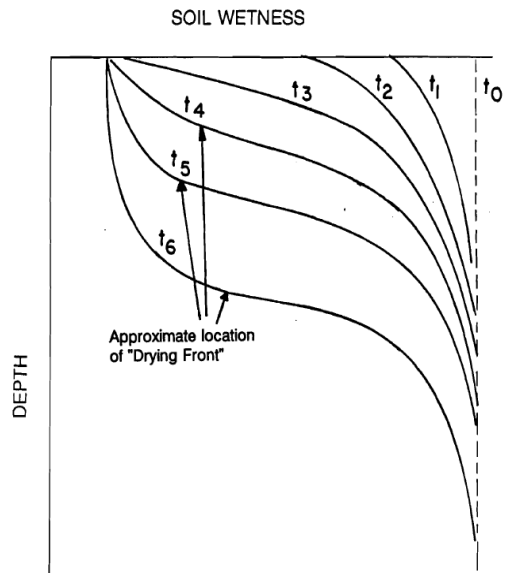
Figure 2.15 Hypothetical development of drying front and its movement into the soil during the course of soil moisture evaporation (after Hillel, 1998)
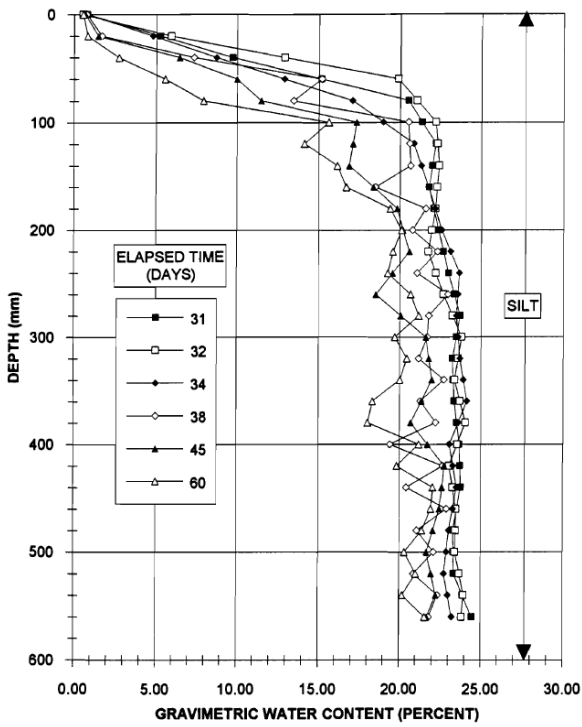


Figure 2.16 Gravimetric water-content profiles for the homogeneous processed silt column at selected times during the zero-flux phase in the column evaporation tests (Bruch, 1993)
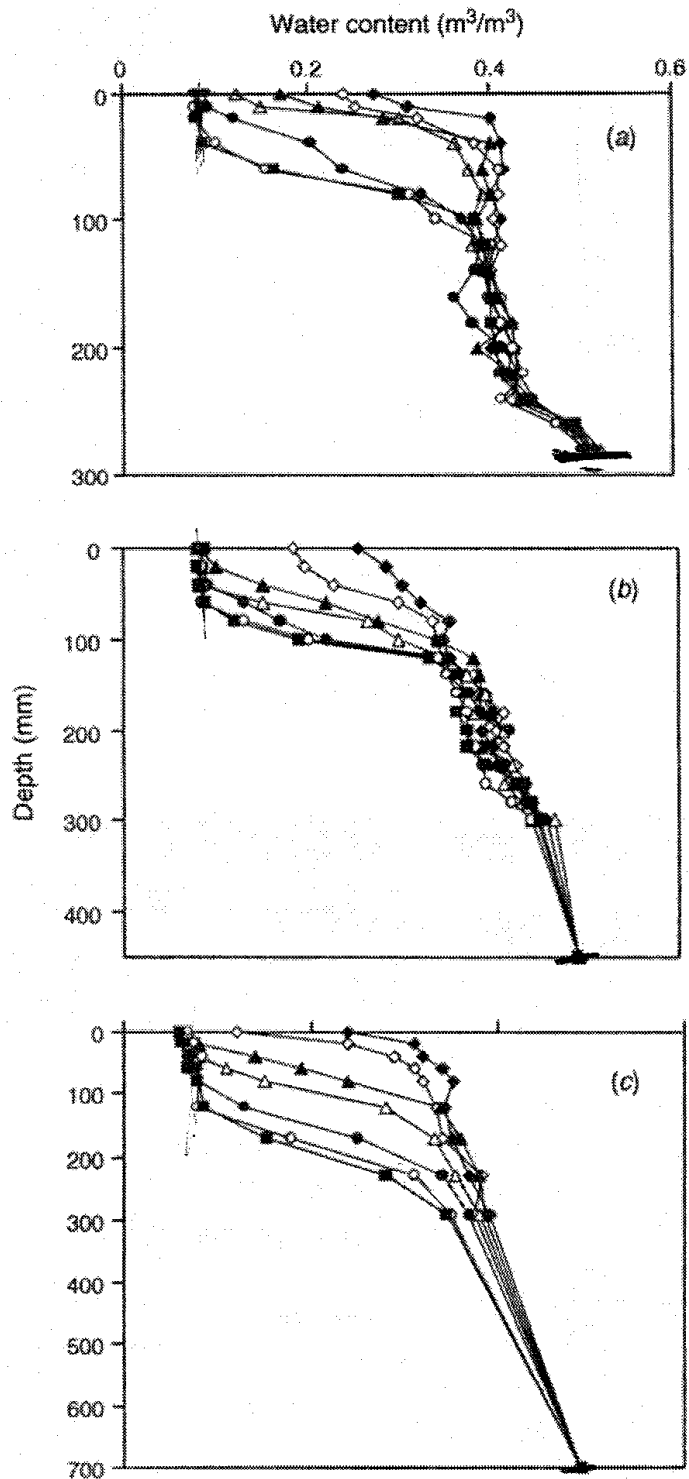
Figure 2.17 Soil-water profiles at different times above saline water tables a) 300, b)
450, and (c) 700 mm deep. Times: ◆, 1 day; ◇, 3 days; ▲, 7 days; △, 16 days;
●, 36 days; ○, 50 days; ■, 70 days  (after Rose et al., 2005)

## 2.4.2 Temperature Profile in a Drying Soil System

Two different source of energy are used to promote evaporation during evaporation processes in the experimental part of this thesis. This section presents a review of some of the temperature profiles resulted from different source of energy in experimental conditions similar to the conditions used in this thesis.

Hanks et al. (1967) studied the effect of different sources of energy on the temperature profiles along a drying soil system. Two different sources of energy used in the test were radiation and wind. The results from his research are shown in Figure 2.18. With radiation as a source of energy for evaporation, soil temperatures near the surface of the soil were greater than the ambient temperature. The soil temperatures increased at the surface as the soil became drier. Except for the first day, the temperature was generally higher near the surface and it decreased with depth. With wind as a source of driving evaporation, the temperature near the surface of the soil was lower than the air temperature. The temperature increased with time as the surface of the soil became drier. The temperature was generally lower near the soil surface and increased with depth into the soil.
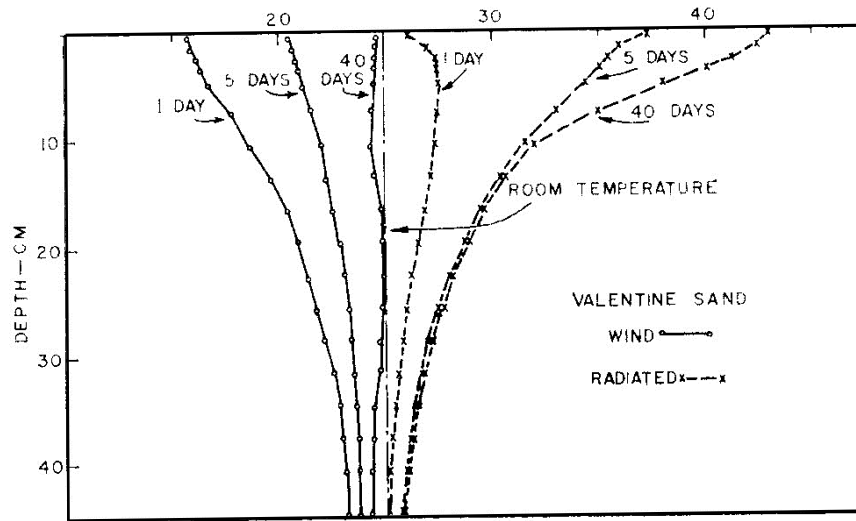


Figure 2.18 Temperature profiles as a function of time and type of drying for Valentine sand (Hanks et al., 1967)

Temperature profiles for the Beaver Creek sand column tests conducted by Bruch (1993) for "zero flux" and "constant head" boundary conditions are shown in Figures

2.19 and 2.20, respectively. With radiation as a source of energy for evaporation, soil temperatures near the surface of the soil were lower than the ambient temperature due to the latent heat of evaporation. As the soil surface became drier, the temperature at the surface of the soil column increased and reached around the ambient temperature.

Further evaporation column tests will be conducted on Beaver Creek sand as part of this research program and the data will be analyzed in further detail.
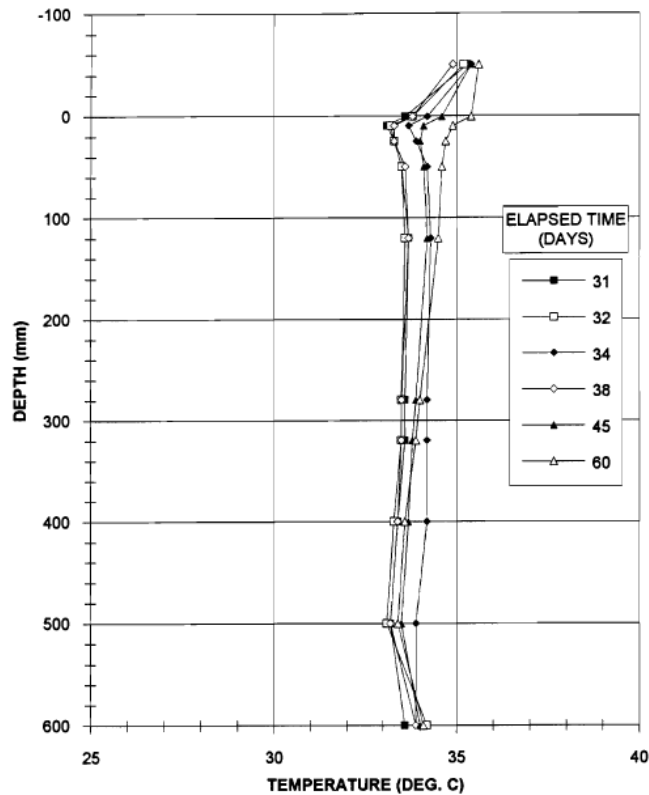


Figure 2.19 Temperature profiles for the homogeneous sand column during the zero flux boundary condition phase of the column evaporation test (Bruch, 1993)

### 2.4.3   Separation of the Liquid Water and Water Vapour Flow

During the drying process, there is a mixed form of vapour and liquid flow that occurs within the transition zone. Therefore, both liquid-water flow and water-vapour flow must be taken into consideration when performing numerical simulations. Separating the liquid-water flow and water-vapour flow within the transition zone is important in water transport analyses. To simplify the flow analysis, researchers have often selected a surface within the water-content profile above and below which vapour flow and liquid

flow are essentially independent processes. In other words, it is assumed that there is a definite water-content or soil-suction value where the vapour and liquid flow can be separated. This assumption essentially neglects the transition zone or simultaneous occurrence of the liquid water and water vapour flow.
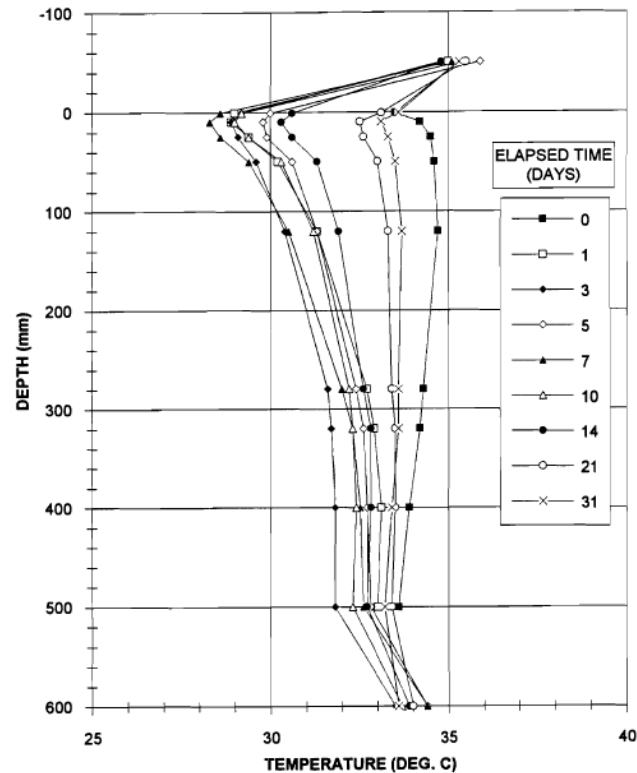


Figure 2.20 Temperature profiles for the Homogeneous Sand column during the constant head boundary condition phase of the column evaporation test (Bruch, 1993)

The experimental research on the separation of the vapour and liquid phase flow does not support a sharp separation between the vapour and liquid phase flow. This section presents a concise review on experimental study of the liquid and vapour phase flow during evaporation.

Marshal and Gurr (1954) used the redistribution of chloride and water in soil to separate liquid-water and water-vapour flow. Soil specimens with uniform chloride and water distribution were prepared. The transport of chloride from the lower half of the specimen to upper half of the specimen was observed after 24 hours of evaporation. Identical soil specimens with different initial water contents were tested. Figure 2.21 shows the results of the tests for different types of soils. Marshal and Gurr (1954)

44

suggested that the lower limit of liquid water flow was at or below the plant wilting point. The plant wilting point values for different type of soils are shown in Figure 2.21 with vertical dashed lines.
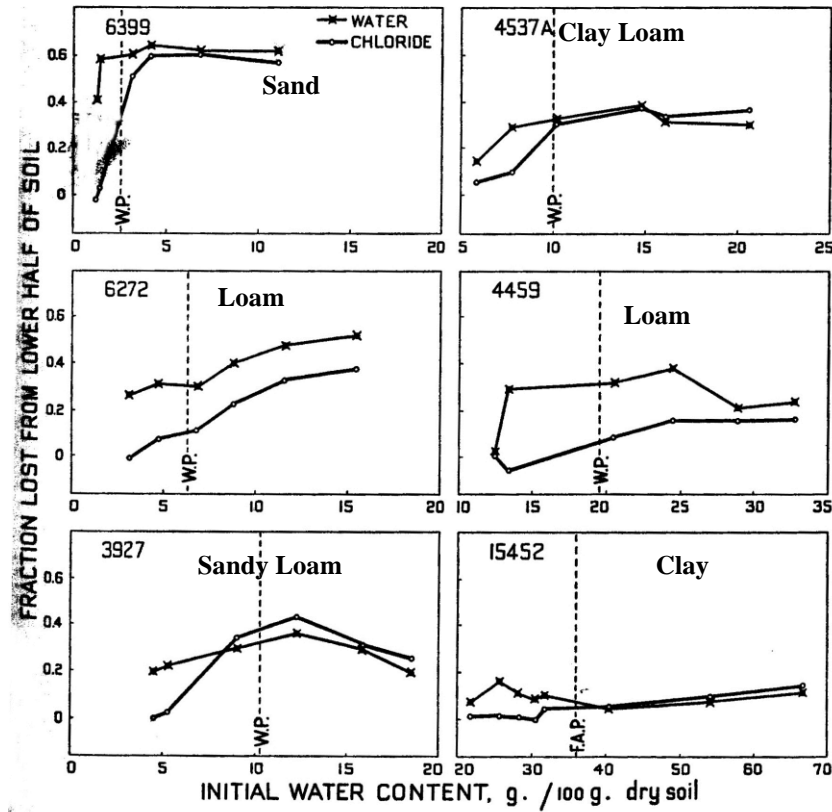


Figure 2.21 Distribution of water and chloride after 24 hours of evaporation in different types of soil (Marshal and Gurr, 1954)

Fritton et al. (1967) used chloride transport to distinguish the liquid water from water vapour movement in soil columns. Thirty columns containing silt loam soil were subjected to various evaporation potentials. The soils were initially wetted with 0.02 N $CaCl_2$. Various parameters were recorded during the evaporation tests including cumulative evaporation, water distribution, chloride distribution, and thickness of the dry surface (i.e., depth of the vapour-phase dominant flow zone). Evaporation flux potentials ranging from 5 to 20 mm/d were used in the tests. Figure 2.22 shows the initial water content and chloride profiles before the start of evaporation. Figures 2.23

45

and 2.24 show the distribution of water and chloride contents for various elapsed time periods under different potential evaporative rates.
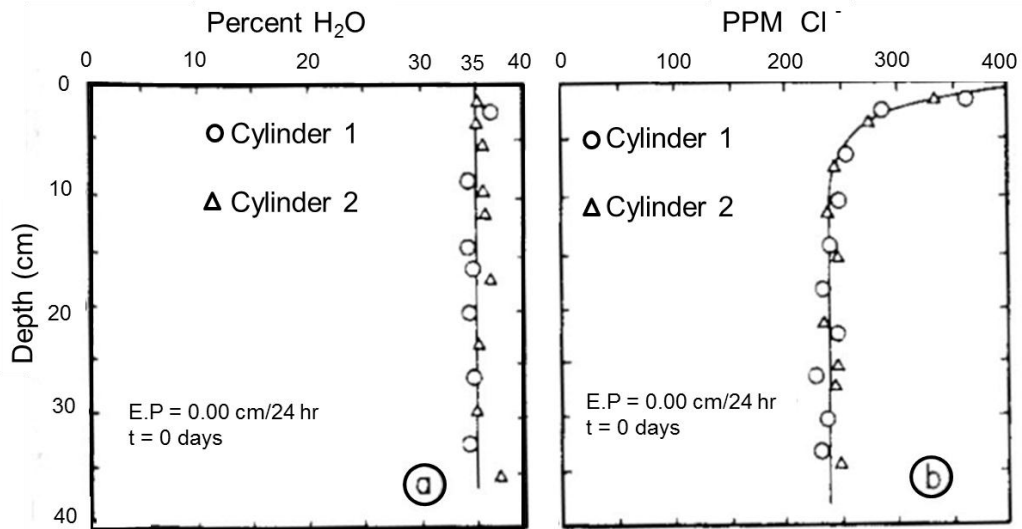


Figure 2.22 Initial water and chloride distribution in the soil columns (after Fritton et al. 1967)

Fritton et al. (1967) assumed that depth of the visible dry layer was near the upper limit of the transition zone and the depth of chloride deposition was near the lower limit of the transition zone. Table 2.5 shows the depth of the transition zone inspected from the water-content and chloride-content profiles for different evaporation rates. Gardner and Hanks (1966) pointed out that the transition zone was almost 10 mm thick. In Table 2.5 the thickness of the transition zone exceeded 10 mm in only two cases; both cases were in the high evaporation rates and long evaporation durations.

Nakayama et al. (1973) studied the chloride transport to the soil surface by allowing evaporation from a bare soil (clay loam) under field conditions. A bare plot (72 x 90 m) was irrigated with about 100 mm of well water containing 12 meq/lit cl-. Starting 3 days after irrigation, soil samples were obtained from different depths every 0.5 hours for 2 weeks. The maximum depth of soil sampling was 90 mm. Water content and chloride concentrations were measured on the soil samples. Observed chloride contents for different periods of time in the top layers of the soil (i.e., 0–5 mm, 5–10 mm, and 10– 20 mm are shown in Figure 2.25. Below 20 mm depth, the concentrations of chloride were

almost constant, indicating that liquid water movement was the predominant form of flow.
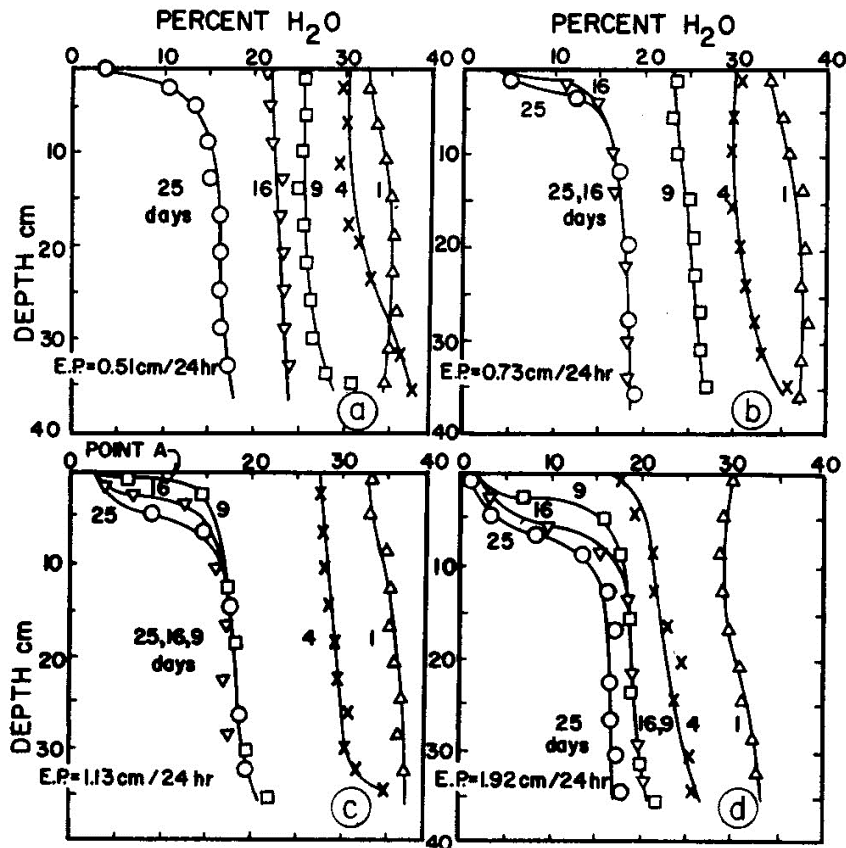


Figure 2.23 Water profiles at different elapsed times (Fritton et al., 1967)

Movement of chloride was noticed to stop at about 4% water content (i.e., a suction value of about 100,000 kPa), leading to the conclusion that water could move as liquid water at very high suctions. The same results were obtained for different depths, (i.e., 0–5 mm, 0–10 mm, and 10–20 mm) (Nakayama et al., 1973).

Wilson (1990) showed that regardless to the type of soil, the actual evaporation rate started to decrease below the potential evaporation rate at a suction value of approximately 3000 kPa. Taking this suction value as a suction beyond which vapour flow becomes dominant over liquid flow, Bruch (1993) analyzed the dominant flow mechanism for three types of soils. The results for Beaver Creek sand are shown in Figure 2.26.

47
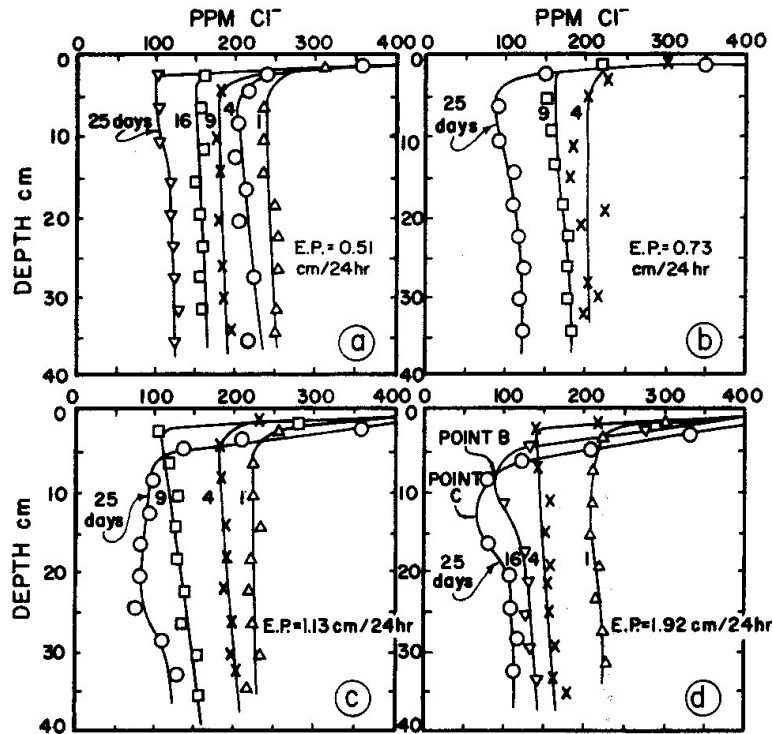
Figure 2.24 Distribution of chloride for different time periods (Fritton et al., 1967)

Based on experimental observations given in this section, during the evaporation process it can be inferred that there is a transition zone within which the flow mechanism is the combination of liquid-phase and vapour-phase mechanisms. The existence and thickness of the transition zone is a function of the potential evaporation rate, duration of evaporation, type of soil, and depth of water table. The form of water content and chloride distribution profile during the evaporation process may be used as an indication of the lower and upper limit of the transition zone.

### 2.4.4 Key Soil Parameters Associated with Water Transport through Unsaturated Soils

There are two primary mechanisms for water transport in a drying soil system: conduction in the liquid-water phase and diffusion in the vapour phase. Liquid-water flux results from total pressure gradient along a soil specimen. Diffusion primarily results from a gradient in the water-vapour concentration. Darcy's law is used to describe the flow of water in a saturated soil (Darcy, 1856). Darcy's law is also used to describe the flow of liquid water through an unsaturated soil (Buckingham, 1907; Richards, 1931; Childs and Collis-George, 1950; Fredlund and Rahardjo, 1993). Fick's

law (1855) was derived to describe the diffusion of gas through liquids. Modified forms of Fick's law have been developed to describe the diffusion of water vapour through the soil (Dobchuk et al., 2004). Equations governing these two mechanisms used in this thesis will be proposed in the theory chapter (i.e., Chapter 3).

Table 2.5 Estimates of the vapour flow zone depth (mm) using different methods, observation, water profile, and chloride profile (after Fritton et al., 1967)

| Duration of Evaporation (day) | Method of Estimation | Potential Evaporation (mm/d) | | | |
|---|---|---|---|---|---|
| | | 5.1 | 7.3 | 1.13 | 1.92 |
| 9 | visually observed | 0 | 0 | 6 | 25 |
| 9 | inspection of water profile | 0 | 0 | 10 | 25 |
| 9 | inspection of chloride profile | ---- | ---- | 18 | 29 |
| 16 | visually observed | 0 | 8 | 25 | 45 |
| 16 | inspection of water profile | 0 | 15 | 30 | 55 |
| 16 | inspection of chloride profile | ---- | ---- | 33 | 55 |
| 25 | visually observed | 15 | 25 | 37 | 60 |
| 25 | inspection of water profile | 15 | 25 | 45 | 65 |
| 25 | inspection of chloride profile | ---- | 35 | 75 | 80 |

The liquid-phase coefficient of permeability is the primary soil parameter used in describing liquid-water flow through an unsaturated soil. For vapour-flow analysis, the primary soil property is the coefficient of vapour diffusion. When liquid-phase and vapour-phase flow simultaneously occur in the soil, the coefficients of liquid-phase permeability and vapour diffusion are not readily comparable in their original forms because of their different units of measurement.

49
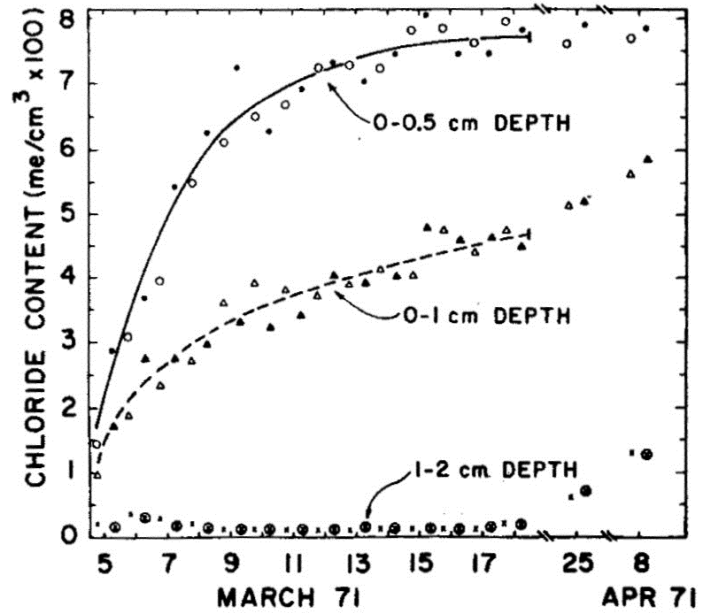
Figure 2.25 Chloride content versus time at top layers of the plot (Nakayama et al. 1973)
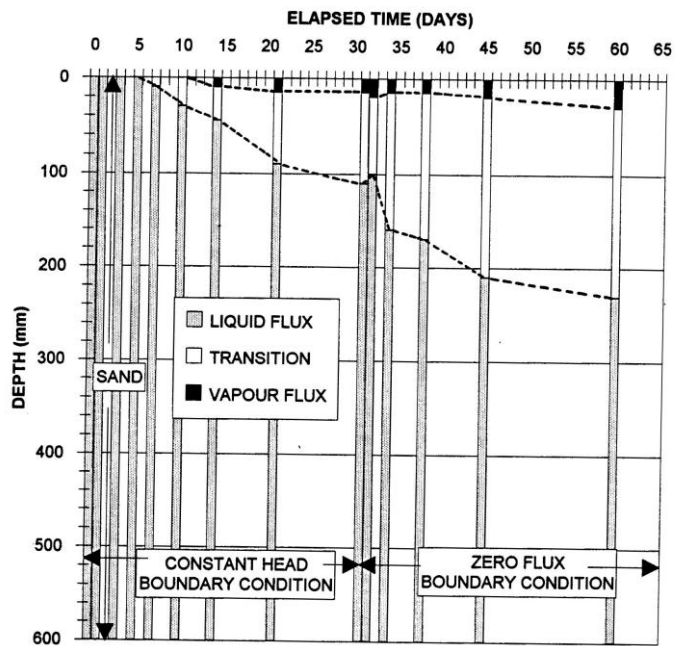


Figure 2.26 Dominant flux mechanisms for the homogeneous Beaver Creek Sand during evaporation test (Bruch, 1993)

The literature shows that there are two options for comparing these two soil properties: i) the coefficient of permeability has been converted into hydraulic diffusivity, or ii) vapour diffusivity has been converted into vapour conductivity. Both conversions may be performed through application of the SWCC.

Rose (1963a) used the following equation as the general equation for isothermal vapour flow:

$$\frac{q_v}{\rho_l} = -k_v \nabla \psi = -D_v \nabla \theta \qquad [2.6]$$

where $q_v$ is water vapour flux, g cm$^{-2}$s$^{-1}$; $\rho_l$ is density of liquid water, 0.997 gcm$^{-3}$; $k_v$ and $D_v$ were defined as isothermal vapour conductivity, cm s$^{-1}$, and isothermal vapour diffusivity, cm$^2$s$^{-1}$, respectively. $\nabla \psi$ and $\nabla \theta$ are soil suction and water content gradients, respectively.

$k_v$ and $D_v$ were defined as follows:

$$k_v = D_a f(\varepsilon) \frac{v h \rho_v g}{\rho_l R T} \qquad [2.7]$$

$$D_v = k_v \frac{\partial \psi}{\partial \theta} \qquad [2.8]$$

where $D_a$ is molecular diffusion coefficient of water vapour in free air, 0.262 cm$^2$s$^{-1}$; $\varepsilon$ is volumetric air content, cm$^3$ air cm$^{-3}$; $v$ is mass flow factor = *P/(P-e); P* is total gas pressure, mm Hg; e is partial pressure of water vapour at *T*, mm Hg; *T* is temperature, K; *h* is relative humidity; $\rho_v$ issaturation density of water vapour, 2.3 x 10$^{-5}$ g cm$^{-3}$; *g* is acceleration due to gravity, 981.2 cm s$^{-2}$; R is gas constant of water vapour, 4.615 x 10$^6$ erg g$^{-1}$ deg c $^{-1}$.

Rose (1963a) conducted laboratory experiments to determine the SWCC and the liquid-phase coefficient of permeability function for different type of soils. The results of the laboratory experiments are shown in Figures 2.27 and 2.28. In most cases, three zones can be recognized from either SWCC or coefficient of liquid-phase permeability function.

Mehta et al. (1994) calculated the vapour coefficient permeability, $k_v$, using Eq. 2.9, derived by Campbell (1985), and compared the calculated values with the liquid-phase coefficient of permeability, $k_l$ (Figure 2.29). The effect of temperature gradient on water flow was assumed to be negligible.

$$k_v = \frac{D_v \rho_s Mg}{\rho_w RT} exp\left(\frac{\psi_w Mg}{RT}\right)$$

[2.9]

where $M$ is molecular weight of water; $R$ is universal gas constant, $T$ is absolute temperature, $\rho_s$ is density of solids.
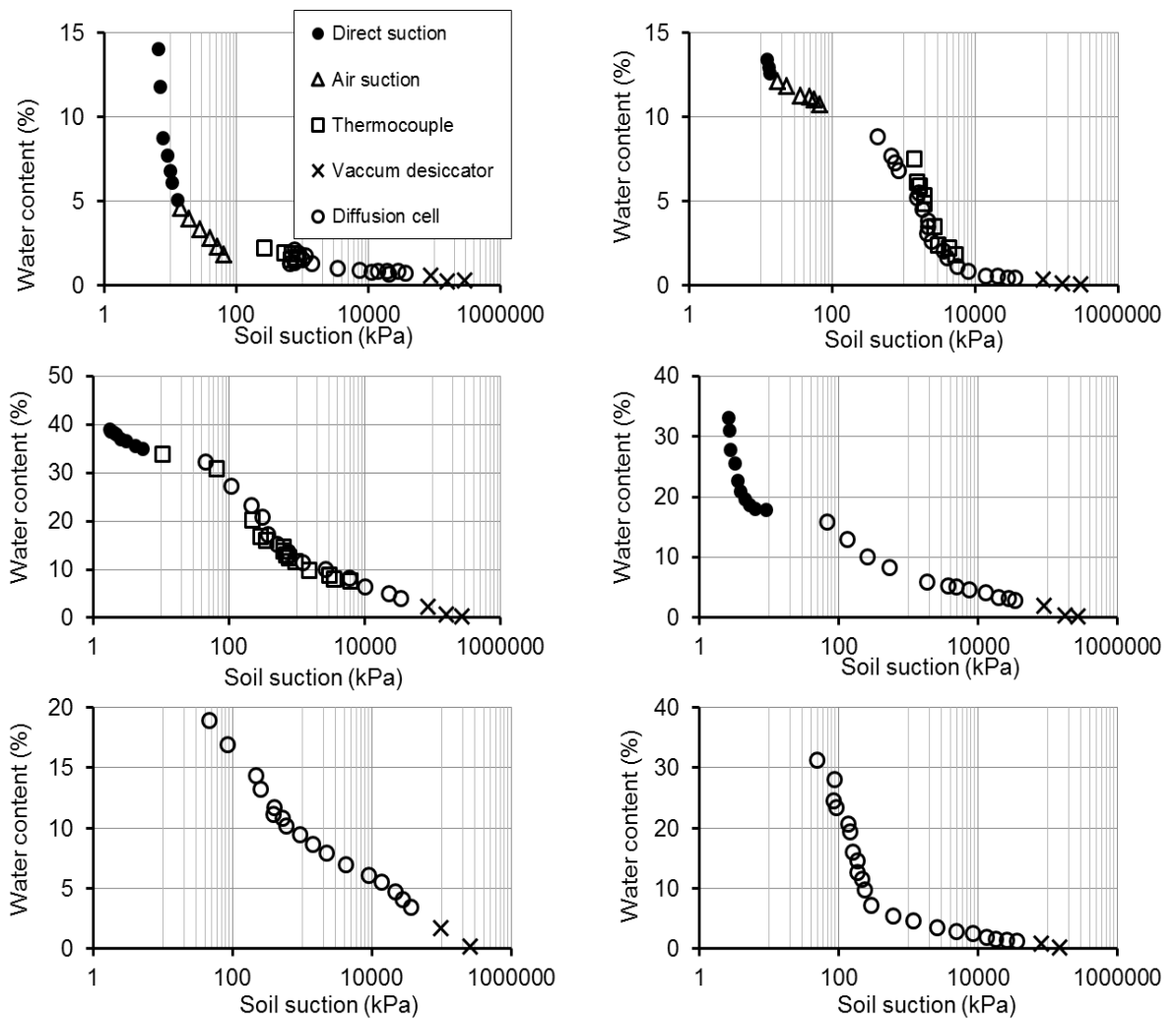


Figure 2.27 Relationship between volumetric water content and soil suction (modified from Rose, 1963a)

Mehta et al. (1994) also calculated and compared vapour and water coefficient of diffusivities (Figure 2.30).

Bachmann et al. (2001) conducted a series of evaporation experiments from sandy soils of different water repellency. The calculated water vapour flux based on Fick's law was 2 to 2.5 orders of magnitude smaller than the evaporation flux observed at the surface (Table 2.6). Comparing the isothermal vapour transport with the observed average moisture flux at the surface, Bachmann et al. (2001) suggested that the water transport in the upper part of the column (0 to 20 mm) occurred mainly in the liquid phase.
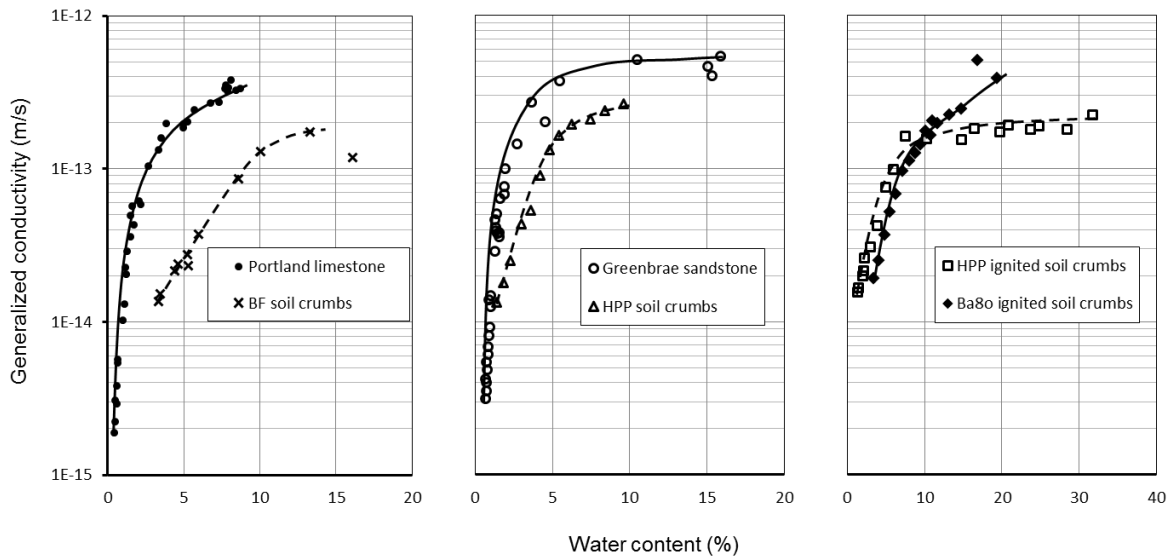


Figure 2.28 Relationship between volumetric water content θ and the liquid-water coefficient of permeability, $k_l$ (ψ) (modified from Rose, 1963a)

Konukco et al. (2004) compared liquid-water, water-vapour, and total (liquid and vapour) diffusivities using evaporation tests on different type of soils. Figure 2.31 shows determined values of liquid-water diffusivity, $D_l$, water-vapour diffusivity, $D_v$, total diffusivities $D = D_l + D_v$, and the ratio of $D_v/D$ for a sandy loam soil. Using the variation in the ratio of $D_v/D$, water-content values were determined for the upper and lower limits of the transition zone. Above the upper limit of the transition zone, the dominant mechanism of flow was assumed to be water vapour and below the lower limit

53

of the transition zone the dominant mechanism of water flow was assumed to be liquid water.
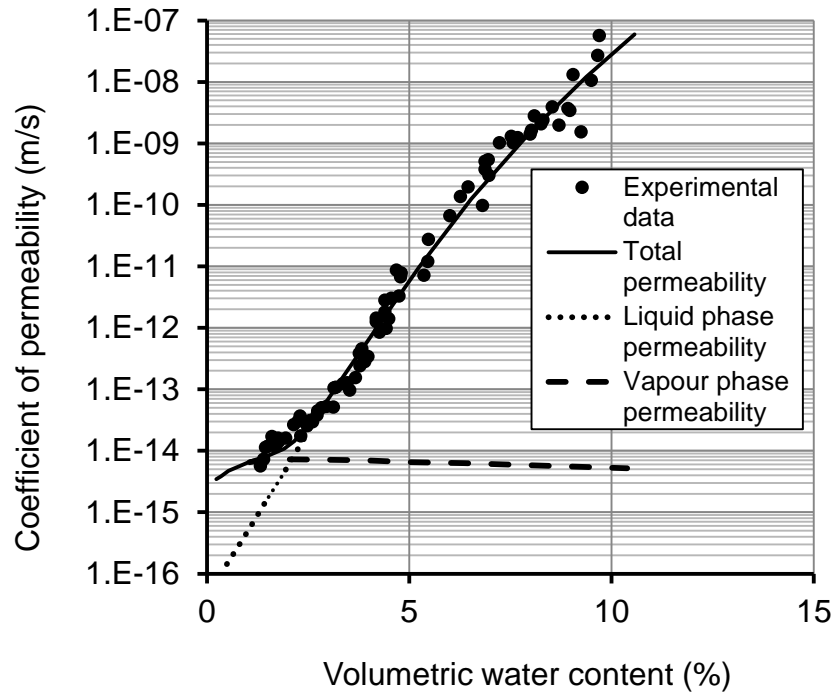


Figure 2.29 Comparison of the liquid-water and water-vapour components of permeability (modified from Mehta et al., 1994)
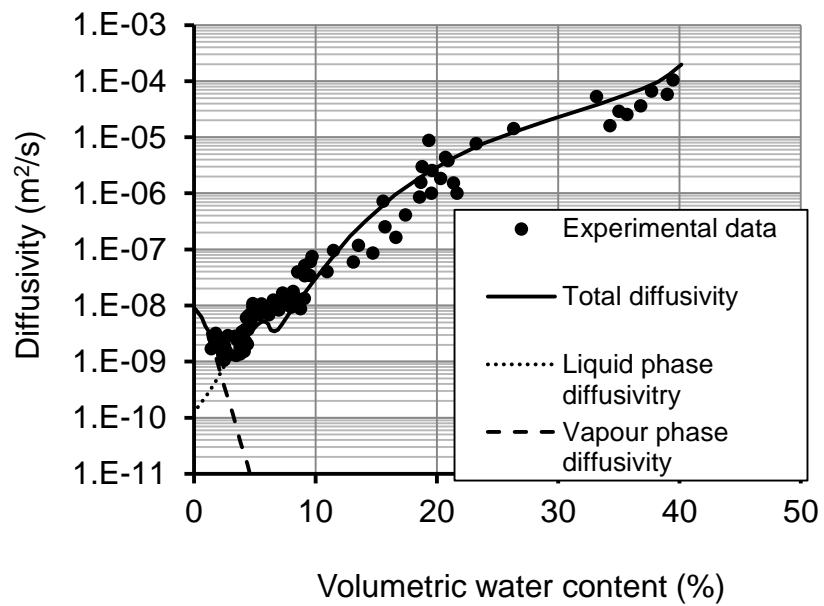


Figure 2.30 Comparison of the liquid-water and water-vapour components of diffusivity (modified from Mehta et al., 1994)

Table 2.6 Observed and calculated water-vapour flux in the surface layer (0–20 mm)
based on water content data of day 195 (after Bachmann et al., 2001)

| Soil Type | Observed Evaporation Flux (m/s) | Calculated Vapour Flux (Depth = 5-15mm), m/s |
|---|---|---|
| $A_w$ | $6.5 \times 10^{-10}$ | $6.1 \times 10^{-12}$ |
| $A_H$ | $5.4 \times 10^{-10}$ | $2.7 \times 10^{-12}$ |
| $B_w$ | $8.0 \times 10^{-10}$ | $6.3 \times 10^{-11}$ |
| $B_H$ | $5.9 \times 10^{-10}$ | $1.1 \times 10^{-13}$ |

Konukco et al. (2004) termed the water content at the upper limit of the transition zone as threshold or critical water content. The corresponding suction value was also called the critical or threshold suction value. These values were determined for different soils through analyzing salt and water content profiles during evaporation tests. The results are shown in Table 2.7.
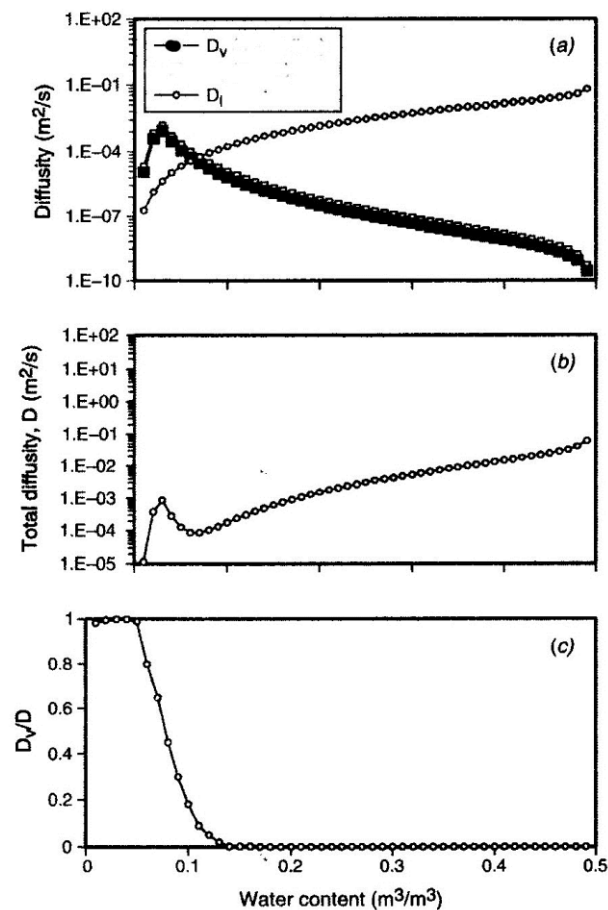


Figure 2.31 Liquid-water diffusivity, ($D_l$), water-vapour diffusivity ($D_v$), total diffusivity ($D = D_l + D_v$), and the ratio of $D_v/D$ versus water content for a sandy loam soil (after Konukco et al., 2004)

Table 2.7 Threshold water content for different soils (Konukco et al., 2004)

| Soil Texture | $\theta_e$(Konukco et al., 2004) | Rose (1963a) | Calculated range of $\theta$ in transition zone | $\Theta$ when $D_l = D_v$ |
|---|---|---|---|---|
| Clay Loam | 0.10 | 0.24 | 0.1-0.28 | 0.17 |
| Silty Loam | 0.06 | 0.09 | 0.06-0.17 | 0.1 |
| Sandy Loam | 0.05 | 0.06 | 0.05-0.14 | 0.07 |
| Coarse Sand | 0.02 | 0.01 | 0.02-0.09 | 0.05 |

The laboratory experimental test results presented in this section suggest that it might be possible to use the liquid-phase and vapour-phase coefficient of diffusions to locate the upper and lower limits of the transition zone.

## 2.5 EXPERIMENTAL DETERMINATION OF THE LIQUID-PHASE COEFFICIENT OF PERMEABILITY FUNCTION

A variety of methods for measuring the unsaturated coefficient of permeability have been proposed in the literature. Benson and Gribb (1997) and Dane and Topp (2002) summarized some of the laboratory methods. The methods for the measurement of the liquid-phase coefficient of permeability function have been classified into two categories: steady state methods and transient methods. Most of the methods are limited to measuring the coefficient of permeability at relatively high water contents. Two of the methods proposed in the literature have been shown to have potential for measuring the coefficient of permeability under low water-content conditions. These two methods are the centrifuge method (Nimmo et al., 1987, 1990) and the evaporation method (Wind, 1968; Arya et al, 1975). The evaporation method will be further pursued as part of the research program in this thesis. The evolution of the evaporation method is briefly discussed in this section.

Wind (1968) introduced the evaporation method (or the wind method) to measure the liquid-phase coefficient of permeability function in an unsaturated soil. In the wind method, a saturated soil column is placed in constant environmental conditions and water evaporates from top of the soil column. The amount of evaporated water is monitored by weighing the column with time.

The main disadvantage of the wind method is that its data are limited to suctions in the range where tensiometers can be used to measure suction. Barbour and Yanful (1994) showed that for a sandy soil, tensiometer suction measurements were limited to

the residual suction condition, which could be as low as 3 to 5 kPa for sandy soils. Therefore, the method cannot be used for the measurement of the liquid-phase coefficient of permeability beyond the residual suction condition.

Arya et al. (1975) developed what is called the hot-air method. Water diffusivity could be determined for a wide range of soil water contents using the hot-air method. The water diffusivity function was then converted to the unsaturated coefficient of permeability provided the soil-water characteristic curve was available.

In the hot-air method, an initially saturated soil column is forced to dry using hot air flow above the soil sample. Mass of the column is monitored during drying. Drying of the soil must happen under the following initial and boundary conditions:

$$\theta = \theta_i \qquad \text{for} \qquad x > 0 \qquad t = 0 \qquad [2.10]$$
$$\theta = \theta_0 \qquad \text{for} \qquad x = 0 \qquad t > 0$$

where $\theta_i$ is initial water content, $\theta_0$ is the air-dry water content, $x$ is distance, and $t$ is the elapsed time.

The water content distribution data are measured at the end of the test. The data are analyzed in order to calculate the water diffusivity function using the following equation:

$$D(\theta) = 0.5t(\frac{dx}{d\theta})_x \int_{\theta_x}^{\theta_i} x d\theta \qquad [2.11]$$

where $D(\theta)$ is the water diffusivity, $t$ is elapsed time, $x$ is distance, and $\theta$ is water content.

If the SWCC is known, then the water diffusivity can be converted to the unsaturated coefficient of permeability using the following equation:

$$k(\theta) = D(\theta)\frac{d\theta}{d\psi} \qquad [2.12]$$

The hot-air method is based on two conditions: i) the existence of a linear relationship between the cumulative evaporation and $t^{0.5}$ and ii) the availability of the water-content profile at the end of the test. The water content at the bottom of the column (i.e., lower boundary condition) must remain unchanged.

Although the hot-air method can be used to measure the water diffusivity function for a wide range of water contents, there are some concerns related to this method. The method is not considered accurate since the theoretical assumptions are not fully satisfied in the experimental procedure. Some redistribution of water may also occur during sampling for gravimetric water content determinations. Pushing the sample from the wet end of the core (i.e., the portion used for sampling at the end of the test) may cause some compression and possibly squeezing out some water. The most serious concern appears to be related to the temperature effects on water flow. Because the samples are dried using hot air, a rise in soil temperature is expected. The increase in air temperature violates the assumption of isothermal conditions.

A non-steady state evaporation method was used by Mehta et al. (1994) to determine the liquid-phase coefficient of permeability function for a sandy soil at low water contents. Six identical soil columns with saturated initial condition were used in the experimental program. Each soil column had a height of 120 mm and was composed of 12 acrylic rings with a thickness of 10 mm and an inner diameter of 49 mm. The soil columns were placed on a turntable (1 rpm) and evaporation was allowed to take place at a constant wind speed of 0.1 m/s in a room with a constant temperature of 20 $^\circ$C and relative humidity of 70%. Soil columns were sectioned at different elapsed times and the volumetric water-content profiles were determined. The following equation was used to calculate the average water flux at any measured depth over specified time intervals:

$$q(x) = \frac{1}{\Delta t}\left[\int_x^L \theta(x)_{t+\Delta t}dx - \int_x^L \theta(x)_t dx\right] \qquad [2.13]$$

where $q(x)$ is the average liquid-phase flux at any measured distance, $\Delta t$ is time difference, $\theta(x)$ is the volumetric water content of the soil at $x$, $x$ is distance, and $L$ is the total length of the soil column.

Darcy's law was used to calculate the average coefficient of permeability over a time increment, $\Delta t$, as follows:

$$k(x) = \frac{q(x)}{0.5[I(x)_t + I(x)_{t+\Delta t}] + 1} \qquad [2.14]$$

where $I(x)_t$ and $I(x)_{t+\Delta t}$ are suction gradients corresponding to the times $t$ and $t + \Delta t$, respectively.

Figure 2.32 shows the SWCC of Shonai sand dune soil that was tested by Mehta et al. (1994). A wide range of suctions were applied in the measurements of the SWCC (i.e., 1–100,000kPa).

Figure 2.33 shows the measured liquid-phase coefficients of permeability function for the sandy soil from saturation to a volumetric water content of 1%. The coefficient of permeability varies from $10^{-4}$ to about $10^{-15}$ m/s.
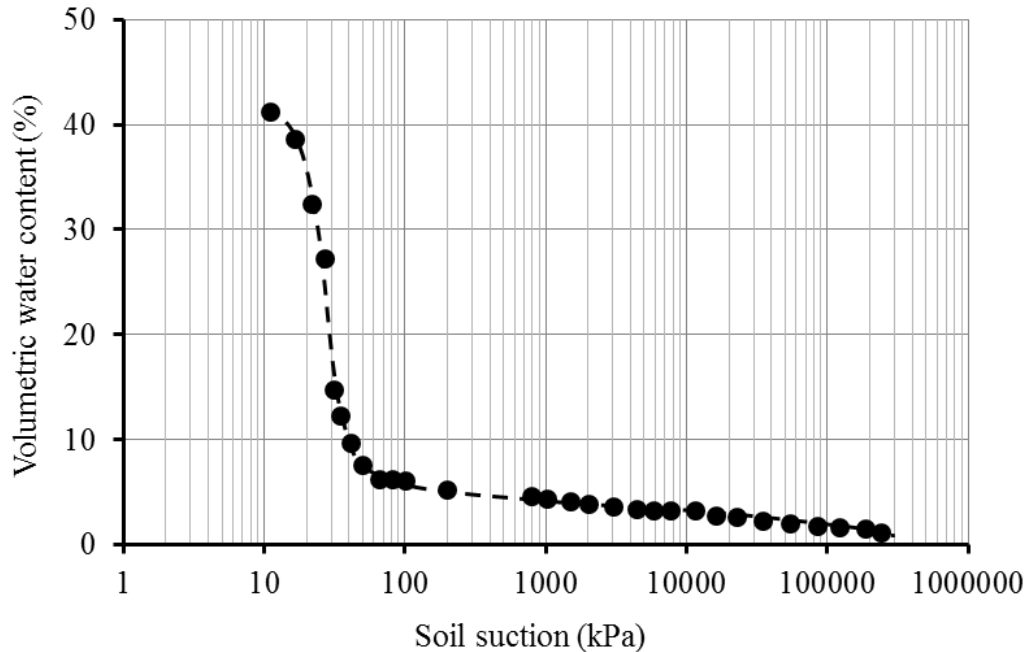


Figure 2.32 SWCC of Shonai sand dune soil (modified from Mehta et al., 1994)
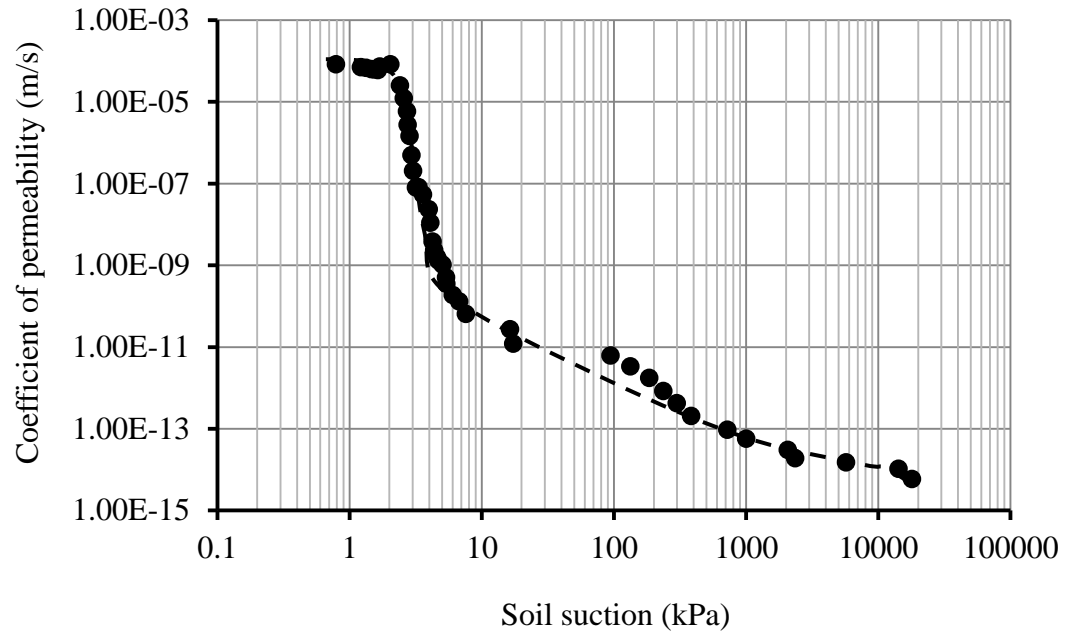
Figure 2.33 Relationship between the liquid-water coefficient of permeability and volumetric water content for a Shonai sand dune soil (modified from Mehta et al., 1994)

Fujimaki and Inoue (2003) developed a flux-controlled steady-state evaporation method for determining the liquid-phase coefficient of permeability function at high suction values. Figure 2.34 shows a schematic of the experimental set-up used to measure the coefficient of permeability under environmentally-controlled conditions. The soil column was comprised of acrylic rings that were 5 to 10 mm thick. The soil was washed with distilled water applied from the top of the column in order to produce a salt free soil sample. An electric fan was used above the soil column to accelerate the rate of evaporation and a lamp was placed above the column. The lamp was automatically controlled to keep the soil column surface temperature at a constant value of 25 $^o$C. At the same time, a peristaltic pump was attached to the middle of the bottom ring through a hypodermic needle. The pump was used to apply a small amount of water flow at a constant rate of 10.2 mm/d. Relative humidity of the room during the test was maintained at 37 $\pm$ 3%. The column was placed on a balance to monitor its mass. Polystyrene foam was used for thermal insulation. A thermocouple was inserted horizontally to a depth of 2 mm in the column to monitor the temperature. The evaporation rates were measured using an electronic balance.

60
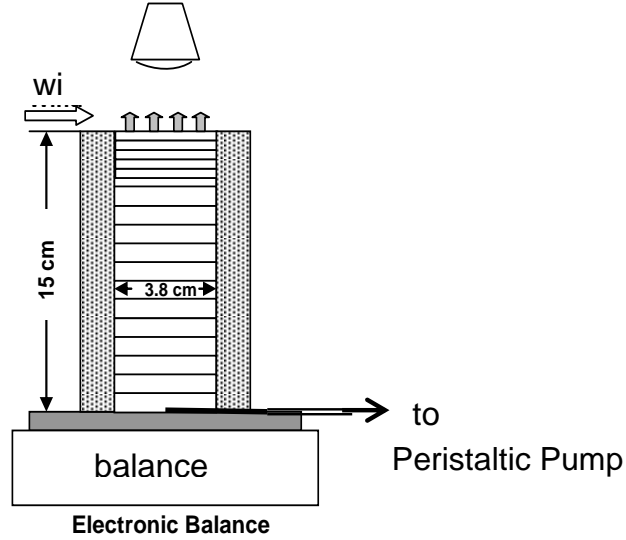
Figure 2.34 A schematic of the evaporation experiment set-up (modified from Fujimaki and Inoue, 2003)

The mass of the soil column was monitored over time. The evaporation test was started at an initially saturated condition. The rate of evaporation was greater than the applied inflow rate and therefore the mass of the column decreased with time. Since the suction in the top layer of the soil was increasing with time, the rate of evaporation and the mass of the column decreased with time until the rate of evaporation became equal to the water inflow rate, indicating that steady-state flow conditions had been reached (Figure 2.35). After achieving steady-state flow conditions, the column was sectioned to measure the water content and suction profiles. Water contents corresponding to each section were determined by an oven drying the soil samples at 105 $^{o}$C.

The following equation was used to calculate the unsaturated coefficient of permeability:

$$k(\psi) = \frac{q - \frac{a\tau D_{va}\rho_v^*}{\rho_w R_v T}\exp(\frac{\psi}{R_v T})\frac{\partial \psi}{\partial z}}{\frac{\partial \psi}{\partial z} - 1} \qquad [2.15]$$

where, $q = q_l + q_v$, $q_l$ and $q_v$ are the liquid water and water vapour fluxes respectively, cm/s; z is the depth, cm; a is the air-filled porosity, mm$^3$/mm$^3$; $\tau$ is the

tortuosity factor; $D_{va}$ is the diffusion coefficient of water vapour in free air, g/(cm$^2$.s); $\rho_v^*$ is saturated water-vapour density; $\rho_w$ is the density of water, 0.997 g/cm$^3$; $R_v$ is gas constant for water vapour, 4697 cm/K; T is temperature, K; and $\psi$ is soil suction,
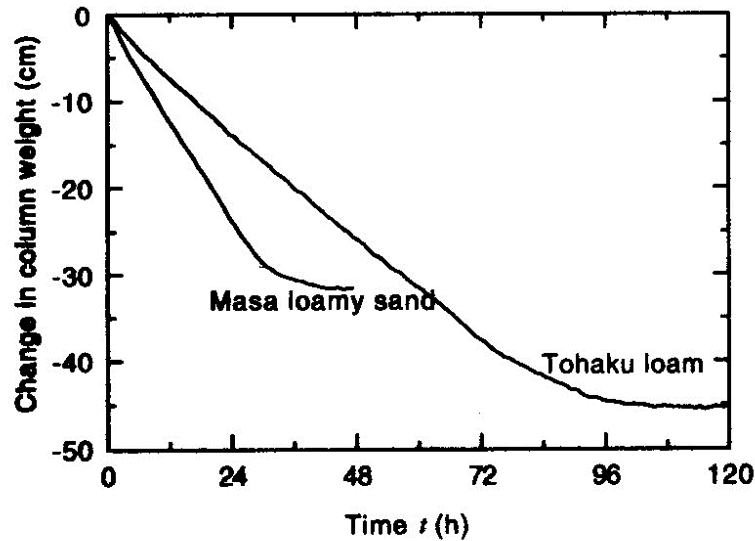


Figure 2.35 Change in column weight from the beginning of evaporation (Fujimaki and Inoue, 2003)

Figure 2.36 shows the measured values of the unsaturated coefficient of permeability for Masa Loamy Sand using three different methods: i) the steady-state downward flow method (SDFM), ii) the steady-state evaporation method (SEM), and iii) the instantaneous profile method (IPM) (Fujimaki and Inoue, 2003).

Fujimaki and Inoue (2003) used numerical analysis to find the time required to reach steady state conditions under different inflow rates and aerodynamic resistance. Figure 2.37 shows the final water contents near the surface of the soil column (i.e., at 10 mm depth). The results show that the lower the inflow rate, the lower the water content at 10 mm depth and the more the time required reaching steady-state conditions. Therefore, with the controlled flux steady-state method, lower inflow rates are required to calculate lower values for the coefficient of permeability. Under the experimental conditions imposed by Fujimaki and Inoue (2003), steady state conditions were established within two weeks.
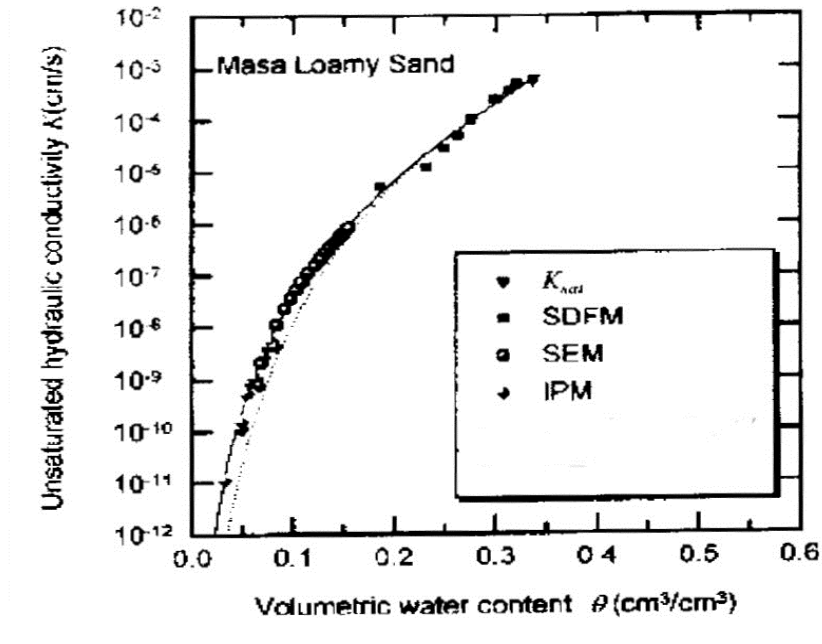
Figure 2.36 Experimental values of the unsaturated coefficient of permeability versus volumetric water content (Fujimaki and Inoue, 2003)
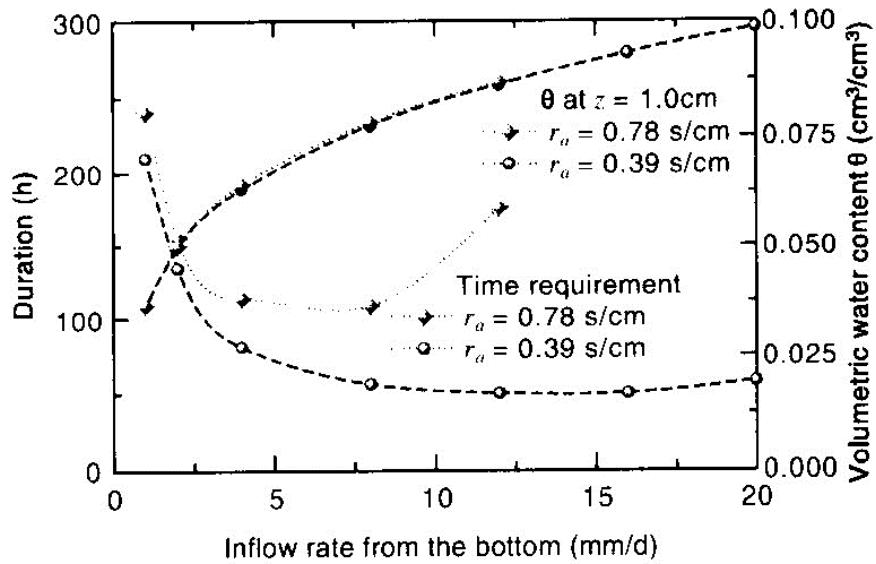


Figure 2.37 Dependence of duration required to attain steady-state and water content at $z$ = 1 cm on inflow rate (Fujimaki and Inoue, 2003)

The method proposed by Fujimaki and Inoue (2003) will be modified and used for the measurement of the liquid-phase coefficient of permeability function in the

laboratory experimental program as part of this thesis. Details pertaining to the modified method will be presented in Chapter 4.

## 2.6   PREDICTIVE METHODS FOR THE UNSATURATED COEFFICIENT OF PERMEABILITY FUNCTION

Numerous models have been proposed for the representation or estimation of the liquid-phase coefficient of permeability function, $k_l$ $(\theta)$ or $k_l$ $(\psi)$. These models have been classified by Mualem (1986, 1992). Figure 2.38 shows various categories of the unsaturated coefficient of permeability models according to the Mualem classification. The models were classified into two categories: theoretical and empirical models. The theoretical models were classified into two groups: macroscopic and microscopic models. This section presents a concise review of each group of the unsaturated coefficient of permeability predictive models. A review of the relationship between the unsaturated coefficient of permeability and water content, presented by Buckingham (1907), is also presented.
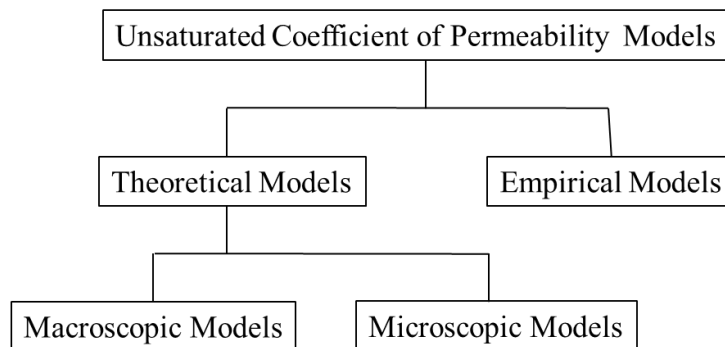


Figure 2.38 Classification of the unsaturated permeability models

### 2.6.1   Empirical Models

Empirical models are equations describing the variation of the unsaturated coefficient of permeability with soil suction, $k_l$ $(\psi)$, or with volumetric water content, $k_l$ $(\theta)$. Parameters required for the empirical equations are generally determined using a curve-fitting procedure. Some of empirical equations along with appropriate references are given in Table 2.8.

### 2.6.2 Theoretical Models

Theoretical models are based on the relationship between water flux and the hydraulic head gradient. There are two different groups of theoretical models: i) macroscopic models, and ii) microscopic models. These models are based on the statistical interpretation of the soil-water characteristic curve.

Table 2.8 Some of the empirical equations representing the unsaturated coefficient of permeability

| References | Equations | Description |
|---|---|---|
| Averjanov (1950) | $k_r = S_e^n$ | $S_e$ is "effective degree of saturation" , n = 3.5 |
| Wind (1955) | $k = \alpha|\psi|^{-n}$ | |
| Gardner (1958) | $k_r = exp(\alpha\psi)$ | |
| | $k = \dfrac{a}{(|\psi|^n + b)}$ | |
| | $k = \left(\dfrac{\theta}{\theta_s}\right)^b$ | |
| Brooks and Corey (1964) | $k = k_s$ for $\psi \geq \psi_{cr}$ | |
| | $k_r = \left(\dfrac{\psi}{\psi_{cr}}\right)^{-n}$ for $\psi < \psi_{cr}$ | |
| Rijtema (1965) | $k = k_s$ for $\psi \geq \psi_{cr}$ | |
| | $k_r = exp[\alpha(\psi - \psi_{cr})]$ for $\psi_1 < \psi < \psi_{cr}$ | |
| | $k = k_1\left(\dfrac{\psi}{\psi_1}\right)^{-n}$ for $\psi < \psi_1$ | |
| Campbell (1974) | $k = k_s\left(\dfrac{\theta}{\theta_s}\right)^{2b+3}$ | $b = \dfrac{\Delta\log(\psi)}{\Delta\log(\theta)}$ |

Note: $k_r$ is the relative permeability, $S_e$ is effective degree of saturation, $\theta_s$ and $\theta_r$ are the saturated water content and residual water content; respectively.

### 2.6.2.1 Macroscopic Models

The objective of the macroscopic models is to derive an analytical equation for the unsaturated coefficient of permeability function. All macroscopic models have the following general form:

$$k_r = S_e^{\eta} \qquad\qquad\qquad [2.16]$$

where $k_r$ is the relative permeability, $S_e$ is effective degree of saturation (see Eq. 2.4), and $\eta$ is a constant value.

The value of $\eta$ depends on the assumptions made in deriving the permeability equation. Numerous researchers have suggested values for $\eta$ (e.g., Averjanov, 1950, $\eta = 4$; Yuster, 1951, $\eta = 2$; Irmay, 1954, $\eta = 3$).

The effect of pore-size distribution is neglected in macroscopic models and this is the main criticism of this group of models (Childs and Collis George, 1950; Brooks Corey, 1964). Brooks and Corey (1964) showed that for a soil with uniform pore-size distribution index the exponent $\eta$ is 3, and in general $\eta = \frac{2+3\lambda}{\lambda}$, where $\lambda$ is a positive pore-size distribution index. Mualem (1976c) suggested that $\eta = 3 - 2m$, where m is a soil water parameter that is positive for granular soils and negative for fine-grained soils.

### 2.6.2.2 Microscopic Models

In microscopic models, the porous media is assumed to consist of a set of interconnected, randomly distributed pores. This group of models assumes the validity of the Hagen-Poiseuille equation at the level of a single pore, and hence uses this equation to estimate the permeability of an elementary pore unit. In this sense, statistical models may be considered to be a microscopic approach. The coefficient of permeability of an unsaturated soil is then determined by integration over the contribution of the liquid-filled pores. Numerous statistical models have been proposed by authors (e.g., Purcell, 1949; Gates and Lietz, 1950; Childs and Collis-George, 1950; Fatt and Dykstra, 1951; Burdine, 1953; Wyllie and Gardner, 1958; Farrel and Larson, 1972; Mualem, 1976c; Mualem and Dagan, 1978).

All of different statistical models can be represented by three general mathematical equations as follows:

$$k_r(\theta) = \Theta_n^q \frac{\int_0^{\theta} \frac{(\theta - \vartheta)}{\psi^2 + b_{(\vartheta)}} d\vartheta}{\int_0^{\theta_s} \frac{(\theta_s - \vartheta)}{\psi^2 + b_{(\vartheta)}} d\vartheta} \qquad\qquad [2.17]$$

66

$$k_r(\theta) = \Theta_n^q \frac{\int_0^\theta \frac{d\theta}{\psi^{2+b}}}{\int_0^{\theta_s} \frac{d\theta}{\psi^{2+b}}} \qquad\qquad [2.18]$$

$$k_r(\theta) = \Theta_n^q \left[\frac{\int_0^\theta \frac{d\theta}{\psi^{1+b}}}{\int_0^{\theta_s} \frac{d\theta}{\psi^{1+b}}}\right]^2 \qquad\qquad [2.19]$$

The statistical models proposed by Childs and Collis-George (1950), Burdine (1953), and Mualem (1976c) appear to be more commonly referenced in the literature. Eq. 2.17 results in the Childs and Collis–George model if n =1 and b = 0. Eq. 2.18 is the form of the Burdine model if n = 2 and b = 0, and the Mualem model is a form of Eq. 2.19 with n = 0.5 and b = 0. To solve the integral form of the statistical models and obtain the coefficient of permeability functions, the saturated coefficient of permeability and the soil-water characteristic curves are required. Numerous equations have been proposed to represent the soil-water characteristic curves (see Table 2.1). Van Genuchten (1980) suggested Eq. 2.20:

$$\Theta_n = \frac{1}{\left[1+\left(\frac{\psi}{a_v}\right)^{n_v}\right]^{m_v}} \qquad\qquad [2.20]$$

Where $a_v$ = soil parameter, which is primarily a function of air entry value of the soil; $n_v$ = soil parameter, which is primarily a function of the rate of water extraction from the soil once the air entry value has been exceeded; and $m_v$ = soil parameter, which is primarily a function of the residual water content.

A closed-form equation for the permeability function cannot be obtained when the parameters m and n are independent. However, the permeability models of Mualem (1976c) and Burdine (1953) can be solved when the restrictions $m_v = 1 - \frac{1}{n_v}$ and $m_v = 1 - \frac{2}{n_v}$ are applied, respectively. The closed-forms of the permeability function, $k_r(\psi)$, derived under these restrictions, are given in Table 2.8.

67

Fredlund and Xing (1994) proposed the following equations to represent the soil-water characteristic curve:

$$w(\psi) = C(\psi) \frac{w_s}{\left\{Ln\left[e+\left(\frac{\psi}{a_f}\right)^{n_f}\right]\right\}^{m_f}}$$ [2.21]

$$C(\psi) = 1 - \frac{Ln\left(1+\frac{\psi}{\psi_r}\right)}{Ln\left[1+\left(\frac{1,000,000}{\psi_r}\right)\right]}$$

Where $a_f$ = soil parameter, which is primarily a function of air entry value of the soil; $n_f$ = soil parameter, which is primarily a function of the rate of water extraction from the soil once the air entry value has been exceeded; $m_f$ = soil parameter, which is primarily a function of the residual water content; and $C(\psi)$ = correction, which is primarily a function of the suction at which the residual water content occurs.

Fredlund et al. (1994) used Eq. 2.21, and solved the Childs' and Collis–George's integral equation to find the coefficient of permeability at various suction values (Table 2.9).

Numerous investigators have contributed to the verification and improvement of the statistical models, including Nielson et al. (1960), Brooks and Corey (1964), Mualem (1976c, 1986), amongst others.

By analyzing experimental data for 30 soil samples, Ebrahimi-Birang et al. (2004) showed that while most of the predictive models were effective in predicting the liquid-phase coefficient of permeability function in the high water-content range, they appeared not to be able to successfully predict the complete form of the liquid-phase coefficient of permeability for the low water-content range. The firm conclusion was not made due to lack of the trustful experimental data for the liquid-phase coefficient of permeability in the low water-content range.

Over a century ago, Buckingham (1907) proposed a general qualitative relation between capillary conductivity (i.e., the liquid-phase coefficient of permeability) and the water content based on some theoretical reasoning. The relationship between the liquid-

phase coefficient of permeability and water content was extended from saturation to an oven-dry condition.

Table 2.9 Statistical unsaturated permeability models (Ebrahimi-Birang et al., 2004)

| Permeability Models | van Genuchten (1980) | Fredlund and Xing (1994) and Fredlund et al. (1994) |
|---|---|---|
| Childs and Collis George (1950) | --------------------- | $k_r = \dfrac{\int_{Ln(\psi)}^{b} \dfrac{\theta(e^y) - \theta(\psi)}{e^y} \theta'(e^y)dy}{\int_{Ln(\psi_{aev})}^{b} \dfrac{\theta(e^y) - \theta_s}{e^y} \theta'(e^y)dy}$ $\theta(\psi) = C(\psi) \dfrac{\theta_s}{\left\{ Ln\left[ e + \left( \dfrac{\psi}{a_f} \right)^{n_f} \right] \right\}^{m_f}}$ |
| Burdine (1953) | $k_r(\psi) = \dfrac{1 - (\alpha\psi)^{n-2}[1 + (\alpha\psi)^n]^{-m}}{[1 + (\alpha\psi)^n]^{2n}}$ $m = 1 - \dfrac{2}{n}$ | ---------------------- |
| Mualem (1976c) | $k_r(\psi) = \dfrac{\{1 - (\alpha\psi)^{n-1}[1 + (\alpha\psi)^n]^{-m}\}^2}{[1 + (\alpha\psi)^n]^{0.5}}$ $m = 1 - \dfrac{1}{n}$ | ---------------------- |

Figure 2.39 shows the relationship between the liquid-phase coefficient of permeability and water content proposed by Buckingham (1907). Point *A* of the curve shows the value of the saturated coefficient of permeability. At point *B*, due to initiating the formation of film paths, the permeability starts to decrease (air-entry value). As the film paths become longer, capillary conductivity decreases rapidly towards point *C*. From *C* to *D*, the flow is taking place almost exclusively through film paths, but the length of these is not increasing proportionately as rapidly as before, so the curve does not fall as rapidly from *C* to *D* as it does from *B* to *C* and is concave upward. At *D*, the soil has reached such a state of dryness that the films begin to break and the conductivity falls toward zero, possibly reaching this value before the water content become zero. In other words, the curve may not go from *D* to point *O* but to some point, *F*, to the right of *O*.

The general form of the experimental data for the liquid-phase coefficient of permeability function obtained by Rose (1963a), Mehta et al (1994), and Fujimaki and Inuo (2003) (see section 2.4) seem to reasonably agree with the theoretical form of the function proposed by Buckingham (1907). On the other hand, commonly used predictive methods have often resulted in inaccurate prediction of the entire function. For instance, Wilson (1990) used the method proposed by Brooks and Corey (1964) for predicting the unsaturated coefficient of permeability in order to determine the coefficient of permeability function for the simulations of evaporation column test results (see Table 2.10). The coefficient of permeability began to decrease as soil suction exceeded the air entry value of 3.8 kPa. The coefficient of permeability sharply decreased to an extremely small value once the water content reached the residual saturation. This sharp change resulted in a distinct transition from a liquid-flow dominant mechanism to a vapour-flow dominant mechanism on the water content/suction profile once matric suction exceeded 15 kPa or the water content fell below approximately 6%.
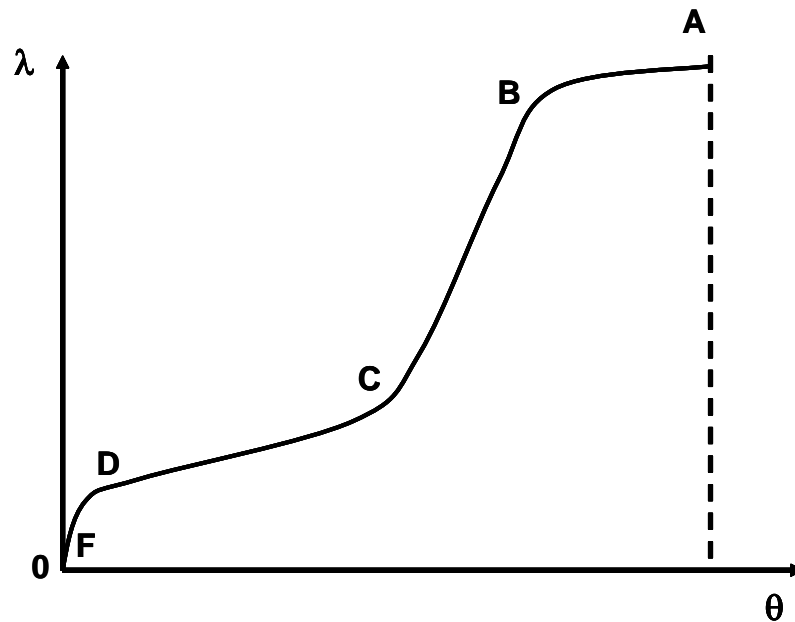


Figure 2.39 Variation of conductivity with water content (after Buckingham, 1907)

Failure of the commonly used prediction methods for the unsaturated coefficient of permeability function rationalizes to propose a proper method in order to improve the predicted results. A modified prediction method for the coefficient of permeability

function that considers modification on the definition of the residual-state condition will be outlined in chapter 3. The proposed predictive method will be then assessed using a series of reliable experimental data. The experimental data will be obtained using modified form of the steady-state evaporation method. A testing program in order to obtain the experimental data will be outlined in chapter 4.

Table 2.10 Predicted value of the coefficient of permeability in different suction- and water-content conditions using the Brooks and Corey (1964) method (after Wilson, 1990)

| Water Content (%) | Matric Suction (kPa) | $k$ (m/s) |
|---|---|---|
| 24.4 | 0.0 | $3.0 \times 10^{-5}$ |
| 23.5 | 2.0 | $3.0 \times 10^{-5}$ |
| 22.3 | 4.0 | $1.7 \times 10^{-5}$ |
| 9.8 | 6.0 | $2.0 \times 10^{-7}$ |
| 8.5 | 8.0 | $8.3 \times 10^{-9}$ |
| 7.3 | 10.0 | $7.2 \times 10^{-10}$ |
| 6.0 | 12 | $9.6 \times 10^{-11}$ |
| 5.9 | 15 | $8.3 \times 10^{-12}$ |
| 5.5 | 20 | $3.5 \times 10^{-13}$ |
| 5.6 | 25 | $3.0 \times 10^{-14}$ |
| 4.9 | 50 | $1.5 \times 10^{-17}$ |
| 3.4 | 100 | $7.2 \times 10^{-21}$ |

Note: $k_{sat} = 3.0 \times 10^{-5}$ m/s
$L = 3.0$

CHAPTER 3

**THEORY**


**3.1    INTRODUCTION**

This chapter describes a method of determining the residual-state condition that is suitable for geotechnical engineering practice. For this thesis, the residual-state condition (RSC) has been defined as a designated zone on the SWCC. The chapter also describes the theoretical framework and development of equations which are necessary to understand the experimental testing program outlined in Chapter 4, to analyze the data, and to interpret the test results. Flow equations are developed for isothermal steady-state conditions. The transient flow that occurs in the early stages of the evaporation tests has not been considered in the development of the flow equations. A procedure to predict the coefficient of permeability around the residual-state condition is also developed in this chapter.

A thorough understanding of the hydraulic behaviour of a soil around the residual-state condition requires a comprehensive description of this condition. The generally accepted methods for description and determination of the residual-state condition, reviewed in section 2.3, do not appear to satisfy the numerical simulations in the geotechnical literature (Wilson, 1990; Choo and Yanful, 2000; Gitirana, 2005).

In the literature on drying soil systems reviewed in section 2.4, discrepancies between numerical simulations and experimental data have been observed within the transition zone (Wilson, 1990) (section 2.3). It has been suggested that the discrepancies between simulated and observed data may be due to inaccurate determination of the unsaturated coefficient of permeability around the residual-state condition, which in turn is due to the inaccurate definition of the residual-state condition. It appears that there may be a link between the zone of the residual-sate condition and the transition zone.

The possible relationship between the residual-state condition and the transition zone has not been examined in the literature.

The residual-state condition has been considered in the geotechnical literature as a definite point in dealing with prediction of the coefficient of permeability (Wilson, 1990; Bruch, 1993; Gitirana, 2005). The effect of defining this condition as a zone does not appear to have been investigated.

Section 3.2 presents a conceptual description of the evaporation process from a bare soil column. The section provides information to help with understanding the procedure associated with the steady-state evaporation tests used in this thesis.

Section 3.3 describes three possible descriptions of the transition zone of the soil-water profile in a steady-state evaporation system. The information provided in this section will help with analysis and interpretation of data from steady-state evaporation tests in order to determine the transition zone of the water content profile.

Section 3.4 provides a physical description of the residual-state condition. Flow mechanisms of desaturation for a single pore as well as for a network of pores within a soil specimen are described in order to help with understanding the concept of the residual-state condition. A procedure is then developed to estimate the initial and final residual-state condition on the SWCC.

Section 3.5 describes the region of the residual-state condition on the SWCC and develops methods for determining the initial and final limits of the condition.

Section 3.6 describes development of the equations required for analysis of data from steady-state evaporation tests and for calculation of the coefficient of permeability.

Section 3.7 proposes a procedure to predict the coefficient of permeability around the residual-state condition by considering the condition as a zone. The accuracy of the procedure will be assessed later in this thesis using experimental data. The results of the proposed method will also be compared with results from some of the commonly used methods for predicting the coefficient of permeability.

## 3.2    EVAPORATION FROM A BARE SOIL COLUMN

Evaporation column tests in an environmentally controlled room are a main part of the laboratory testing program for this thesis. Details of the laboratory procedure on

evaporation column tests will be described in Chapter 4. This section provides a theoretical concept used to achieve steady-state flow conditions in the tests.

Figure 3.1 shows a schematic diagram of an ideal plot of the evaporation rate versus elapsed time for a column test with no flow from the bottom. Evaporation is assumed to start from a bared surface of a saturated soil column. The soil surface is exposed to a constant environmental condition during evaporation. The evaporation plot usually consists of three sections. In the first section, the rate of actual evaporation remains constant and equal to the potential evaporation rate. In the second section, called the falling-rate section, the rate of actual evaporation falls below the potential evaporation. The intersection of the constant-rate and falling-rate sections is the critical point of drying. In the third section, the rate of actual evaporation decreases gradually towards zero.
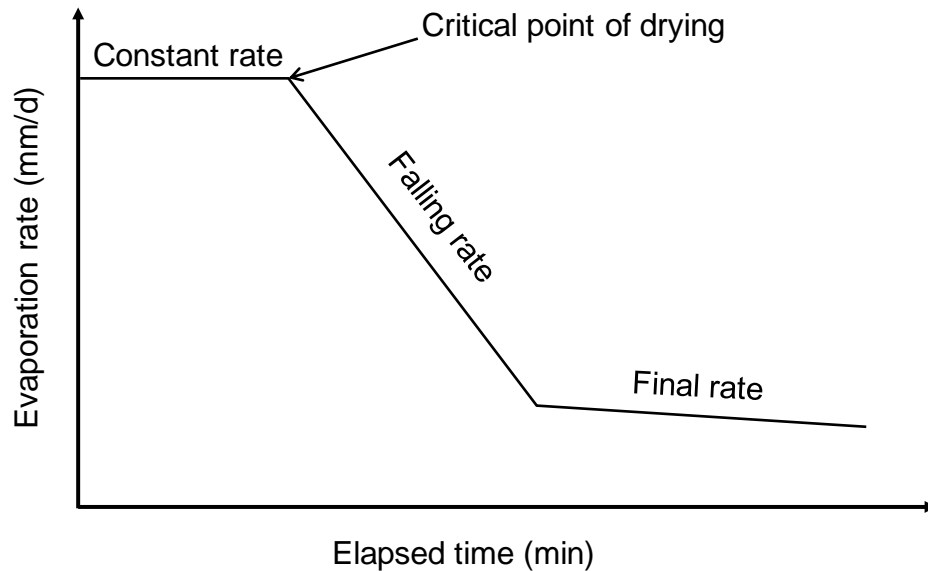


Figure 3.1 Schematic diagram of an ideal plot of evaporation rate versus elapsed time for a soil column

Theoretically, the steady-state condition may be reached at any evaporation rate on the evaporation plot, provided there is a continuous and constant inflow rate from the bottom boundary of the soil column. Figure 3.2 shows an example of an ideal plot of the evaporation rate versus elapsed time for a constant flow boundary condition at the bottom of the soil profile (ABCE'). The location of the horizontal line (CE') is a

function of the inflow rate at the bottom of the column and the evaporation rate from the top.
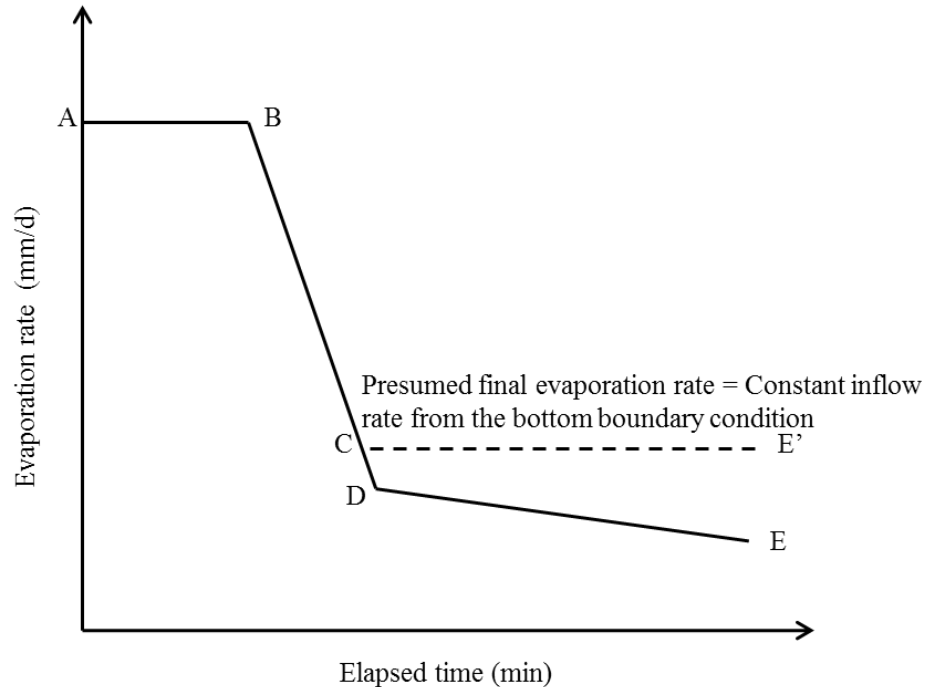


Figure 3.2 Schematic diagram of a drying test for a constant flow boundary condition at the bottom of the soil profile during steady-state evaporation process

The steady-state flow condition described in this section will be simulated in the laboratory. The ambient relative humidity and temperature at the top and the inflow rate from the bottom of the soil evaporation columns will be controlled. The inflow rate from the bottom of the column must be less than the potential evaporation rate.

## 3.3    TRANSITION ZONE OF THE SOIL-WATER PROFILE

This section presents three possible descriptions for development of the soil-water content profile after an evaporation test reaches steady-state flow conditions. The transition zone of the soil-water content profile is also discussed.

Figure 3.3 shows a schematic diagram of water content profile for a drying soil system after reaching the steady-state flow condition. The rate of evaporation from the top boundary and flow rate from the lower boundary are equal.
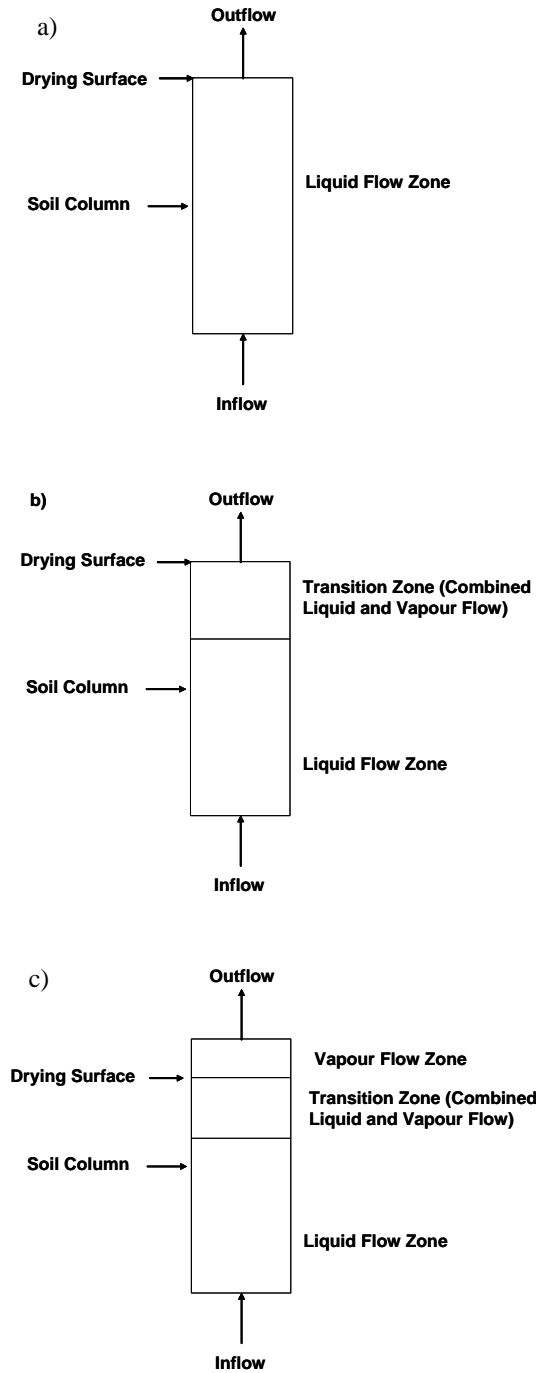
Figure 3.3 Schematic diagram of example cases of soil drying systems after reaching steady-state condition: a) drying surface remains at the surface of the soil column and only liquid flow zone develops, b) drying surface remains at the surface of the soil column and transition zone develops, and c) drying surface develops and receeds into the soil column, so that three zones are formed.

Figure 3.3a shows a case in which the drying surface remains at the surface of the soil column and only a liquid flow zone develops. Figure 3.3b shows a case in which the drying surface remains at the surface of the soil column. Transition and liquid-flow zones are developed. Figure 3.3c shows a case in which the drying surface develops and recedes into the soil column. Three zones may be developed:

1- a liquid-flow dominant zone, which starts from the bottom boundary of the soil column to the lower limit of the transition zone. The dominant flow mechanism is liquid-water flow within the liquid-flow zone.

2- a transition zone, which extends from the upper surface of the liquid-dominant flow zone to the drying surface. The flow mechanism in the transition zone consists of a combined liquid and vapour flow.

3- a vapour-flow dominant zone, which extends from the drying surface to the soil surface. The water-vapour flow mechanism dominates over the liquid water flow mechanism in this zone.

## 3.4    PHYSICAL DESCRIPTION OF THE RESIDUAL-STATE CONDITION

This section describes development of a physical description for the residual-state condition. The development procedure considers mechanism of the desaturation from a single pore and extends to a series of pores in a soil specimen. Physical evidence from the literature has been collected to describe distribution of the pore water during the desaturation of an initially saturated soil and to define the residual-state condition.

Rose (1963b) hypothesized water movement at the various stages in the wetting process of a porous material. Figure 3.4, a modified form of Rose's hypothetical model, describes water movement at the various stages in the drying process of a porous material. In stage 1, soil is saturated. As the soil dries, the pore empties and the soil becomes unsaturated (stage 2, Figure 3.4). In both stages (i.e., stages 1 and 2), the flow is in the liquid form. The mechanism of water flow in stage 3 is considered to be in both liquid and vapour phases. The liquid-water phase flows between water bridges (i.e., pendular rings) through film water. The water flow in stage 3 was termed as "surface creep."

77

Stage 4 shows the mechanism of "distillation" for vapour flow in soil (Philip and deVries, 1957). During the distillation process, water evaporates from one neck and condensates on the next neck. Vapour movement occurs between the two necks, and the necks work as short-circuits. Stage 5 is a condition in which the water bridges are diminished. The water flow occurs totally in the form of vapour flow. Stage 6 shows the condition in which there is only adsorbed water remaining in the soil and conductivity does not have actual meaning. Figure 3.4, as a whole, suggests that depending on the stage of drying, the water flow occurs in liquid form, in vapour form, or in the two forms combined.
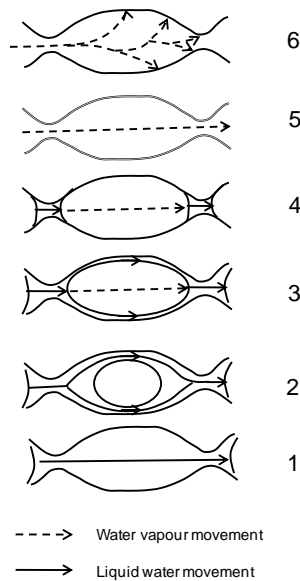
Figure 3.4 Mechanisms of moisture movement at various stages of drying (after Rose 1963b)

In this section, the residual-state condition is conceptually described for a single pore and for a series of pores within a soil specimen, based on the conceptual model proposed by Rose (1963b). Figure 3.5 shows the schematic diagram of a single soil pore during dewatering. Three stages of dewatering are considered. Let us apply a small suction and gradually increase the suction value on an initially saturated soil pore. Figure 3.5.a shows water distribution within the pore where the suction reaches its critical value (i.e., air entry value) and drains out a portion of water from the soil pore. The critical-suction value depends on the diameter of the pore; the smaller the diameter of the pore, the

greater the critical suction value. From zero to near the critical-suction value, the pore remains saturated; it releases its water at air-entry value. This step in the process of desaturation is called a *discrete mechanism* (White 1968).
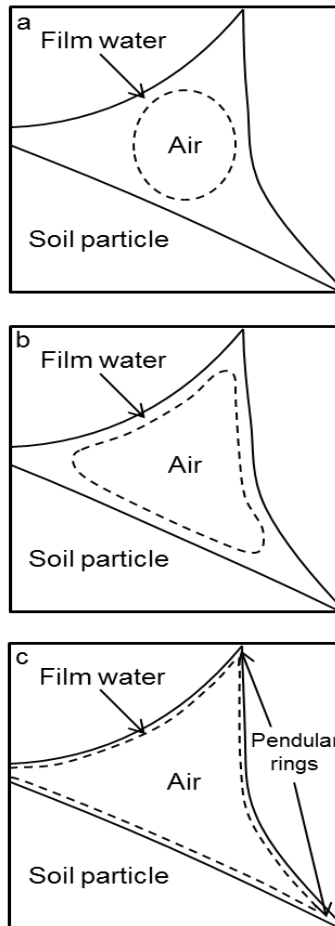


Figure 3.5 Schematic diagram of a single soil pore during dewatering

After the central part of the pore has been emptied, both air and water exist within it (Figure 3.5.b). The water inside the pore is assumed to be hydraulically connected through film water. The liquid-water flow can be transferred between water pockets through film water. The mechanism of desaturation at this stage is called a *continuous mechanism*. In other words, a finite change in suction value results in a finite change in water content (White 1968).

As the suction further increases, soil-water recedes toward the edges of the pore and pendular rings are formed. The film water becomes thinner with a further increase in the suction. At some suction value, the hydraulic connection between the water in the edge film water becomes weaker.

The structure of a soil specimen consists of a series of interconnected pores of various sizes. The desaturation mechanism of the soil specimen, as a whole, could result from a combination of the desaturation mechanisms within interconnected pores. Since pores of a soil specimen are of a variety of sizes, the different stages described for a single pore may happen simultaneously in the specimen. For instance, at a given suction value, large pores may be empty while the small pores may be fully saturated (Figure 3.6).
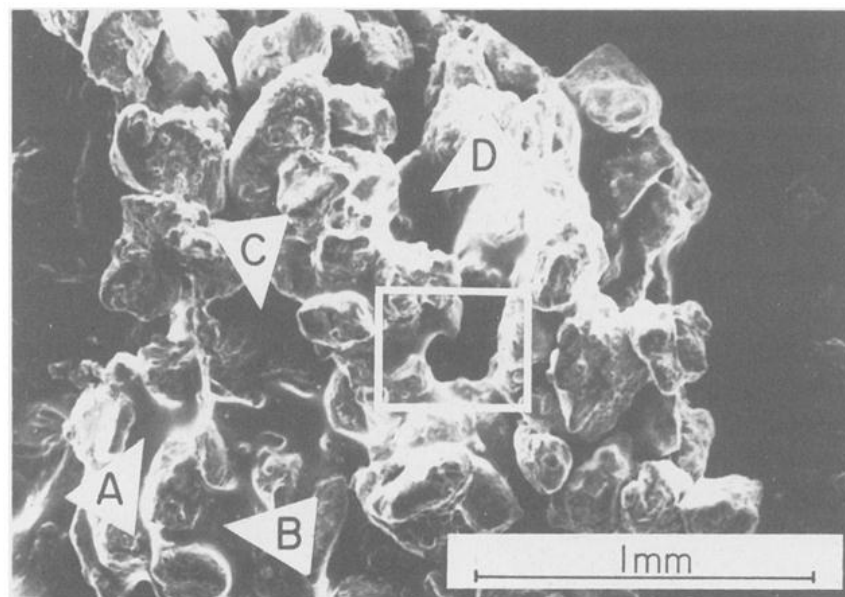


Figure 3.6 Low-magnification SEM micrograph of the unsaturated soil sample with some of the pores filled with water (A and B) and some empty (C and D) (Gvirtzman et al. 1987)

A conceptual model describing the desaturation mechanism of an initially saturated soil specimen has been proposed by various researchers (e.g., Childs, 1969; White, 1968; Nitao and Bear, 1996). Figure 3.7 shows a schematic diagram for a series of interconnected pores of different sizes within a soil specimen, assumed to be initially saturated. A small value of suction is applied from the bottom of the specimen. As the

suction increases, the water-air interface slightly recedes into the soil pores (Figure 3.7, interface 1). When the suction exceeds the air-entry value of the largest pore in the surface, $D_1$, the water-air interface recedes into the pore and empties the pore directly beneath $D_1$ (Figure 3.7, interface 2). A further increase in the amount of suction causes the interfaces to further recede into the soil through $D_2$ in two places. The discrete mechanism of desaturation is dominant at this stage. A further increase in the suction causes the interface to retreat deeper into the soil; and eventually all pores are emptied, and the discrete mechanism of desaturation is complete.
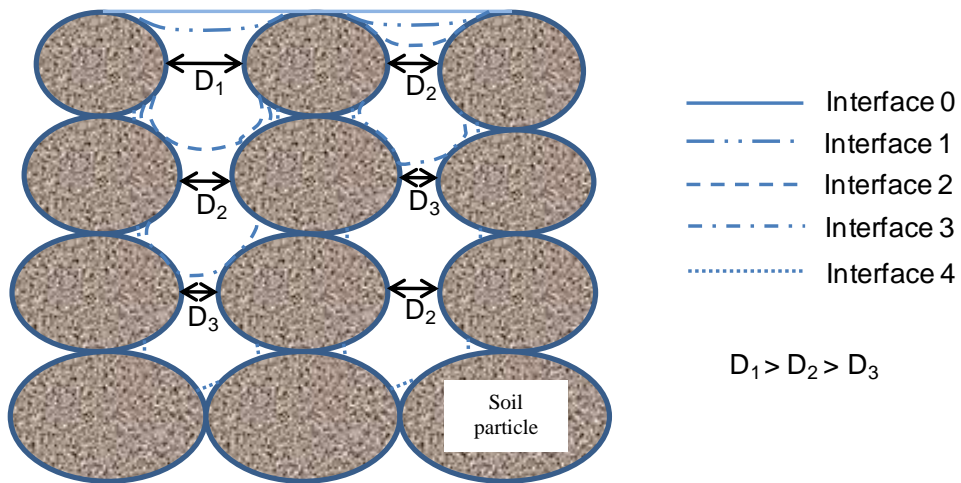


Figure 3.7 Cross-sectional view of a hypothetical set of pores indicating water-air interface at different stages during desaturation (after White, 1968)

As explained earlier, the continuous mechanism of desaturation within the soil specimen occurs when the applied suction value exceeds the air-entry value of a pore or series of pores. Upon drainage of the first pore within a soil specimen, the continuous mechanism of desaturation begins within the drained pore. At some state before completion of the discrete mechanism, the continuous mechanism becomes the dominant and primary means of desaturation.

The residual-state condition is hypothesized to begin when the continuous mechanism becomes the dominant mechanism of desaturation, and the effect of the discrete mechanism of desaturation becomes insignificant. The residual-state condition continues until the continuous mechanism once again becomes insignificant. The initial

and final state of the discrete and continuous mechanisms may not be definite points on the SWCC.

## 3.5 DETERMINATION OF THE RESIDUAL-STATE CONDITION

In dealing with unsaturated flow models, two key concepts on the SWCC must be defined: the air-entry value and the residual-state condition. While researchers agree on the definition of the air-entry value, there is no consensus about defining the residual-state condition.

Typical forms of the degree of saturation versus soil suction (SWCC) for different soils on the semi-log scale are shown in Figure 3.8 (modified from Zapata et al., 2000). In general, from sandy soils toward clayey soils, both the air-entry value and the residual saturation increase.

Most of the researchers mentioned in the previous chapter have defined the residual-state condition as a definite point on the SWCC (Brooks and Corey, 1964; Mualem. 1976; van Genuchten, 1980). The method for determining the condition introduced by White et al. (1970) considered it as a zone rather than a point. The White et al. (1970) method offers a procedure to determine the initial limit for the residual-state zone, but does not consider a final limit for it.

An empirical method developed by the author for this thesis considers initial and final limits for the residual-state condition. The SWCC of a soil from saturation to dryness is considered for the proposed method, with soil suction value at dry condition assumed to be 1,000,000 kPa. Methods for determining these limits are given below. The initial and final residual-sate conditions are assumed as definite points for simplifying the problem.

### 3.5.1 Determination of the Initial Residual-State Condition

The author proposes an empirical method for determining the initial residual-state condition, which is a function of soil type. The method is suggested based on thorough evaluation of the limited data available for both soil-water characteristic curve and coefficient of permeability function in the literature. The method may be modified in the future if more experimental data becomes available. Figure 3.8 shows the relationship between the soil suction and degree of saturation on the semi-log scale. Past air-entry

value, there are generally two distinguishable points on the curve where the rate of change of water content with suction decreases. Line tangent to the first point is drawn. Approximately 0.6 orders of magnitude from the point is defined as the start of the Residual-State Condition (iRSC).
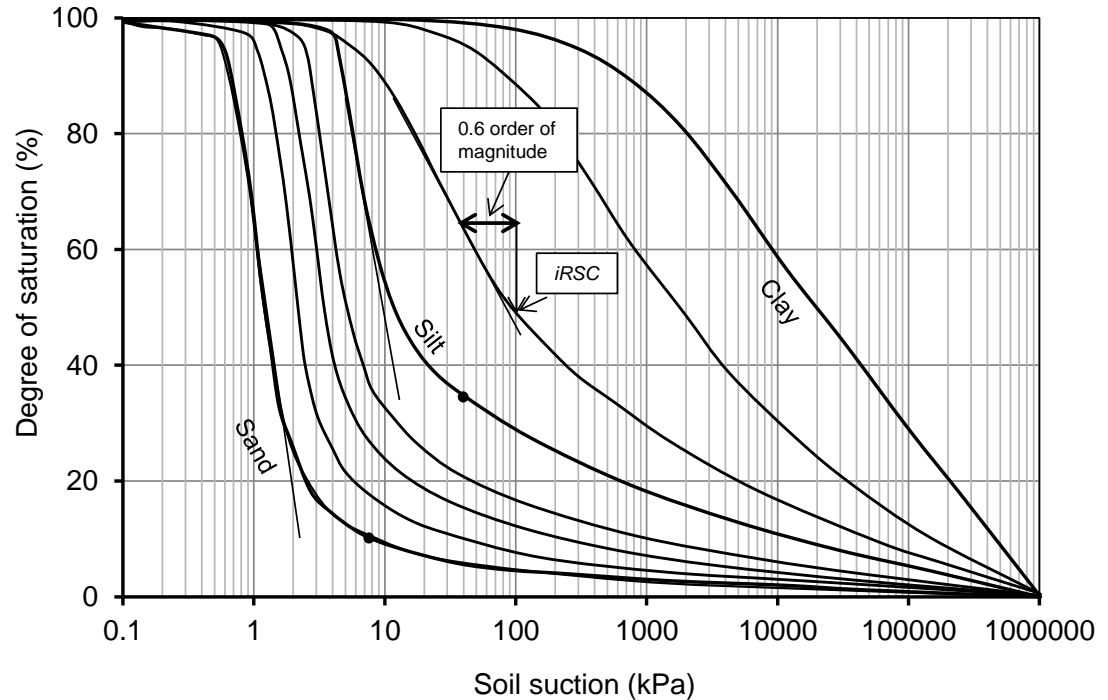


Figure 3.8 Determination of the initial residual-state condition (iRSC) (modified from Zapata et al., 2000)

### 3.5.2 Determination of the Final Residual-State Condition

The author proposes an empirical method for determining the final residual-state condition, which is a function of soil type. Figure 3.9 shows the relationship between the soil suction and degree of saturation on the semi-log scale. A line drawn from 1,000,000 suction value along the SWCC departs from the curve at a point, which is defined as the final Residual State Condition (fRSC).

Using the proposed method, suction values of about 10,000 kPa, 70,000 kPa and 200,000 kPa are determined for the final residual-state conditions of sand, silt and clay soils (Figure 3.9).
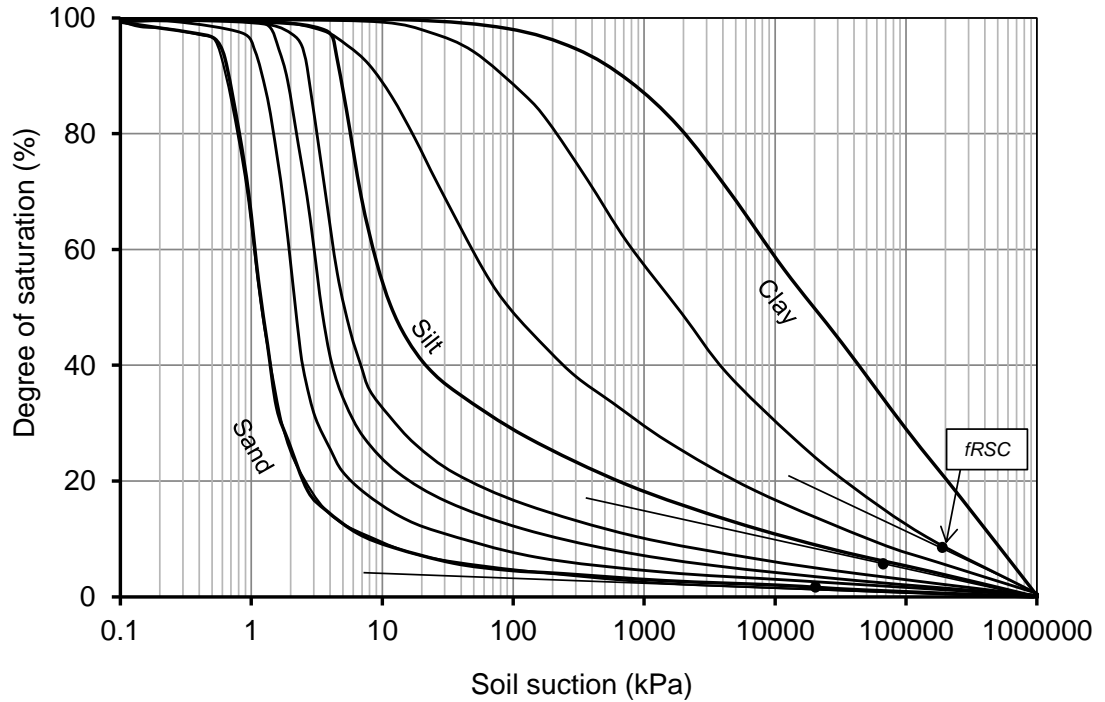
Figure 3.9 Determination of the final residual-state condition (fRSC)

## 3.6   UNSATURATED COEFFICIENT OF PERMEABILITY AROUND THE RESIDUAL STATE ZONE

The steady-state evaporation test is considered for the measurement of the unsaturated coefficient of permeability function around the residual-state condition for this thesis. In this section, the required flow equations for data analysis are developed for isothermal steady-state conditions. Transient flow conditions at the initial stages of the evaporation tests are not considered. Publications by Dakshanamurthy and Fredlund (1981), Wilson (1990), Dobchuk et al. (2004), and Gitirana (2005) are used for development of the equations.

The driving forces for the liquid-phase flow could be total hydraulic head gradient, concentration gradient (i.e., osmotic pressure gradient), and temperature gradient. The driving forces for water-vapour flow are the partial-vapour pressure gradient and the temperature gradient. The water-vapour flow associated with bulk-air flow usually occurs in the presence of the continuous-air phase within the pores. A phase change also occurs between liquid water and water vapour, due to temperature change and/or the evaporation-condensation phenomenon.

84

The one-dimensional flow equation for porous media given below is derived based on liquid-phase conductivity and vapour-phase conductivity. Equations are also derived in terms of liquid-water diffusivity and water-vapour diffusivity. The conductivity and diffusivity terms for the liquid and vapour phases are defined as follows:

Water conductivity or liquid-phase coefficient of permeability in soil ($k_l$) is defined as the rate of liquid-water transport in soil per unit area under unit total hydraulic gradient. The hydraulic gradient is the difference in total head over difference in distance.

Water diffusivity ($D_l$) is defined as follows:

$$D_l(\psi) = k_l\,(\psi)\frac{d\psi}{d\theta} \qquad\qquad [3.1]$$

where $k_l$ is the coefficient of permeability and $\frac{d\theta}{d\psi}$ is slope of the soil-water characteristic curve.

Vapour diffusivity or coefficient of vapour diffusion in soil ($D_v$) is defined as the rate of vapour transport per unit area under unit vapour concentration gradient.

Vapour conductivity ($k_v$) is defined as follows:

$$k_v(\psi) = \frac{D_v\,(\psi)}{\frac{d\psi}{d\theta}} \qquad\qquad [3.2]$$

### 3.6.1   Liquid Flow

Darcy's law is used to describe the flow of liquid water in a saturated soil (Darcy, 1856). Darcy's law is also used to describe the flow of liquid water through an unsaturated soil (Buckingham, 1907; Richards, 1931; Childs and Collis-George, 1950; Fredlund and Rahardjo, 1993). Darcy's law describes the liquid water flow through an unsaturated soil due to total head gradient (Fredlund and Rahardjo, 1993).

$$q_l = -k_l \frac{dh}{dy} \qquad [3.3]$$

where,

$q_l$  = liquid water flux, $m^3/(m^2.s)$,

$k_l$  = unsaturated coefficient of permeability with respect to liquid water phase, m/s, and

$\dfrac{dh}{dy}$ = total head gradient in the y-direction

$h$  $= y + \frac{u_w}{\gamma_w}$, m; $\gamma_w$ is unit weight of water, 9.81 $kN/m^3$; $u_w$ is pore water pressure, kPa.

Eq. 3.3 can be written as follows:

$$q_l = -(k_l + \frac{k_l}{\gamma_w} \frac{du_w}{dy}) \qquad [3.4]$$

The liquid flow equation can be written in terms of water diffusivity ($D_l$):

$$q_l = -(k_l + D_l \frac{d\theta}{dy}) \qquad [3.5]$$

where $D_l$ is water diffusivity, $m^2/s$, and is defined as:

$$D_l = \frac{k_l}{\gamma_w} \frac{du_w}{d\theta} \qquad [3.6]$$

Eq. 3.6 describes a relationship between the unsaturated coefficient of permeability and water diffusivity through use of the soil-water characteristic curve.

### 3.6.2   Vapour Flow

Fick's law (1855) was derived to describe diffusion of gasses through liquids. Through experimental observations, Buckingham (1907) showed that water-vapour diffusion through a soil obeyed the same laws as the diffusion of a gas (e.g., carbon dioxide) through the soil. Eq. 3.7 describes the water vapour flux through unsaturated soils.

$$q_v = -D_v \frac{dC_v}{dy} \qquad [3.7]$$

where

$q_v$ = water vapour flux, kg/(m$^2$.s),

$D_v$ = coefficient of vapour diffusion in soil, m$^2$/s,

$C_v$ = water vapour concentration, kg/m$^3$, and

$\frac{dC_v}{dy}$ = vapour concentration gradient.

Partial water-vapour pressure, $P_v$, and water-vapour concentration, $C_v$, are related through the ideal gas law (Eq. 3.8):

$$P_v = \frac{C_v}{\mu_v} RT \qquad [3.8]$$

$$\frac{dC_v}{dy} = \frac{\mu_v}{RT} \frac{dP_v}{dy} \qquad [3.9]$$

where,

$P_v$ = partial water vapour pressure, Pa;

$R$ = the universal gas constant, $R$ = 8.314 J /(mol °K);

$T$ = absolute temperature (°K); and

$\mu_v$ = molecular mass of water vapour, $\mu_v = 0.01802 \, kg/mol$.

By substituting Eq. 3.9 into Eq. 3.7, water vapour flux can be written in terms of gradient of the partial pressure of water vapour (Eq. 3.10) (Wilson, 1990).

$$q_v = -D_v \frac{\mu_v}{RT} \frac{dP_v}{dy} \qquad [3.10]$$

$D_v$ is the coefficient of vapour diffusion in the soil defined as:

$$D_v = n_a D^*$$ [3.11]

where $n_a$ is the air-filled porosity.

Lai et al. (1976) proposed the following equation for determining $D^*$,

$$D^* = n^{5/3} D_0$$ [3.12]

where $n$ is the total porosity and $D_0$ is the coefficient of water-vapour diffusion in the air, m$^2$/s.

Kimball et al. (1976) defined $D_0$ as:

$$D_0 = 0.229 \times 10^{-4} [\frac{T}{273}]^{1.75}$$ [3.13]

### 3.6.3 Combined Liquid and Vapour Flow Equations

Flow equations describing the combined liquid-water and water-vapour flow through an unsaturated soil can be written based on vapour and liquid diffusivities, and also based on vapour and liquid conductivities.

By combining equations 3.4 and 3.10, the moisture-flow equation can be written as follows (Eq. 3.14):

$$q = q_l + q_v = -(k_l + \frac{k_l}{\gamma_w} \frac{\partial u_w}{\partial y}) - D_v \frac{\mu_v}{\rho_w RT} \frac{\partial P_v}{\partial y}$$ [3.14]

During evaporation, phase change may be followed by a release of energy (condensation) and increase in temperature, or it may be followed by a consumption of energy (evaporation) and decrease in temperature. The evaporation-condensation mechanism often occurs in the second period of drying.

The following equation shows Equation 3.15 is a widely accepted equation by Edlefsen and Anderson, 1943) which represents the relationship between partial-vapour pressure ($P_v$) and total suction ($\psi$) in the soil.

$$\frac{P_v}{P_{vs}} = \exp\left(\frac{-\psi g \mu_v}{\gamma_w RT}\right) \qquad [3.15]$$

where

$P_{vs}$ = the saturated vapor pressure, kPa;

$\psi$ = total suction, kPa; $\psi = (u_a - u_w) + \pi$; $u_a - u_w$ is matric suction, kPa ; $u_a$ and $u_w$ are air and pore water pressures, kPa; and $\pi$ is osmotic suction, kPa;

g = acceleration of gravity, 9.81 m/s$^2$;

$R$ = universal gas constant, 8.314 J/(mole K);

$T$ = absolute temperature, K; and

$\gamma_w$ = unit weight of water, 9.81 kN/m$^3$

Differentiation of the water-vapour pressure with respect to total suction and temperature in Eq. 3.15 will result in the following equation:

$$dP_v = \frac{g\mu_v P_v}{\gamma_w RT}\left(\frac{\psi}{T}dT - d\psi\right) \qquad [3.16]$$

Substituting Eq. 3.16 into Eq. 3.14 gives:

$$q = -\left(k_l + \frac{k_l}{\gamma_w}\frac{\partial u_w}{\partial y}\right) - \frac{1}{dy}D_v\frac{\mu_v}{\rho_w RT}\frac{g\mu_v P_v}{\gamma_w RT}\left(\frac{\psi}{T}dT - d\psi\right) \qquad [3.17]$$

Eq. 3.17 can be written in short forms as Eqs. 3.18 and 3.19.

$$q = -k_l - \left(\frac{k_l + k_v}{\gamma_w}\right)\frac{\partial u_w}{\partial y} + \frac{k_v u_w}{\gamma_w T}\frac{dT}{dy} \qquad [3.18]$$

$$k_v = D_v\frac{\mu_v}{\rho_w RT}\frac{g\mu_v P_v}{RT} \qquad [3.19]$$

Vapour flow equation can be withdrawn from Eqs. 3.18 and 3.19:

$$q_v = \frac{-k_v}{\gamma_w}\frac{\partial u_w}{\partial y} + \frac{k_v u_w}{\gamma_w T}\frac{dT}{dy} \qquad [3.20]$$

89

### 3.6.4   Equations for Describing Heat Flow

Heat can be transferred within a soil by two main mechanisms: conduction and convection. Heat transfer by convection within soil is small compared to the other mechanism, and can often be neglected. Therefore, considering the conduction mechanism and latent heat due to phase change and conservation of energy, the equation for heat transfer is derived.

The conductive heat flow can be written as a function of thermal conductivity of the soil and temperature gradient:

$$h_c = -\lambda \frac{\partial T}{\partial y} \qquad\qquad [3.21]$$

where $\lambda$ is thermal conductivity of a soil, which is a function of moisture content and soil minerals J/(m.s.$^o$C).

The latent heat due to phase change ($h_l$) is equal to the amount of latent heat of evaporation multiplied by the evaporative flux. It should be noted that the evaporative and vapour fluxes for the steady-state flow condition are assumed to be the same (Eq. 3.22).

$$h_l = L_v\, q_v \qquad\qquad [3.22]$$

Substituting Eq. 3.10 into Eq. 3.22 will result in Eq. 3.23.

$$h_l = -L_v D_v \frac{\mu_v}{RT} \frac{dP}{dy} \qquad\qquad [3.23]$$

Total heat flux can be written by combining Eqs. 3.21 and 3.23:

$$h = -\lambda \frac{\partial T}{\partial y} - L_v D_v \frac{\mu_v}{RT} \frac{dP}{dy} \qquad\qquad [3.24]$$

90

## 3.7 PREDICTION OF THE UNSATURATED COEFFICIENT OF PERMEABILITY FUNCTION

In this section, a method for predicting the coefficient of permeability function is proposed by considering the residual-state condition as a zone. The proposed method is developed based on Buckingham's hypothetical definition for the liquid coefficient of permeability function (section 3.7.1), the definition of the residual-state condition described in section 3.4, and the theory of vapour flow (section 3.6).

### 3.7.1 Form of the Unsaturated Coefficient of Permeability Function for the Entire Range of Suction (Based on Buckingham's Conceptual Model)

Over a century ago, Buckingham (1907) described change in the coefficient of permeability versus water content for the entire range of water content from saturation to a totally dry soil condition. The conceptual plot proposed by Buckingham (1907), along with the theoretical explanation for each section of the plot, was given in the previous chapter (see section 2.6).

The unsaturated coefficient of permeability has often been plotted versus soil suction on a log-log scale for the analyses associated with the geotechnical engineering practice. Figure 3.10 shows the hypothetical change in the unsaturated coefficient of permeability versus soil suction on a log-log scale based on Buckingham's theory. The permeability function remains constant and equal to the saturated coefficient of permeability from point *A* to point *B* (i.e. from near-zero suction to the air-entry value). It should be noted that zero suction value cannot be shown at point *A* on a log scale plot because the logarithm of zero is not defined. Therefore, the start point of the abscissa on Figure 3.10 will be taken as a suction value close to zero, such as 0.1, 0.01 kPa, and so on. Past the air-entry value (i.e. point *B*), the coefficient of permeability decreases with soil suction with relatively constant rate to point *C*. Past point *C*, the rate of change of the unsaturated coefficient of permeability with soil suction decreases until the soil suction reaches point *E*. From *E* to *F*, the rate of change dramatically increases and the unsaturated permeability becomes zero at dry condition.

Geotechnical engineers often use a two-region curve to represent the permeability function. The accuracy of a two-region predictive method may be sufficient where the minimum unsaturated coefficient of permeability for the problem in hand remains

greater than the corresponding unsaturated coefficient of permeability at point $C$ (see Figure 3.10). There are engineering problems where the range of suction is greater than the corresponding suction at point $C$. Prediction of the permeability function beyond point $C$ may be required in the latter case.

As Buckingham stated from the theoretical standpoint, there are cases where section DE becomes a horizontal line. In some cases, the line DE may be so short that the line BC merges directly into DF and the permeability function may be shortened into two sections (i.e., AB and BF). The relative length of each line may differ from soil to soil.

### 3.7.2   Analysis of Vapour Coefficient of Permeability Using Eq. 3.19

Ebrahimi-Birang et al. (2004) determined the vapour coefficient of permeability, $k_v$, based on the vapour-flow theory for three different types of soil. They showed that the maximum vapour coefficient of permeability ($k_{vmax}$) was independent of the type of soil.
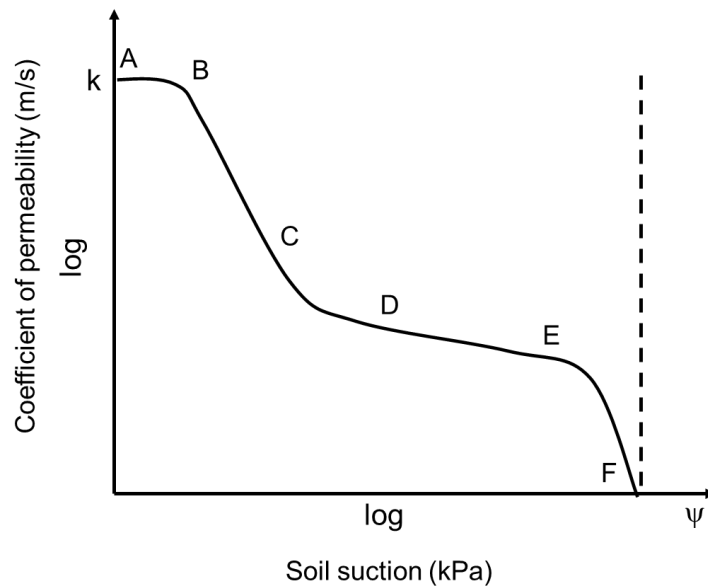


Figure 3.10 Variation of the liquid-water coefficient of permeability with soil suction, based on Buckingham's theory

To investigate the independence of the maximum vapour coefficient of permeability ($k_{vmax}$) to various soil specimens, the vapour-phase coefficient of permeability function was determined for three soils with different textures using Eq. 3.19. The soils were withdrawn from the SoilVision data base (2003).

Properties of the soils used in the analysis are given in Table 3.1. In addition to the soil properties given in Table 3.1, experimental SWCC data were available for all three soils.

The equation proposed by Lai et al. (1976) (i.e., Eq. 3.12) was used to determine the value of the coefficient of vapour diffusion in a dry soil. Several other empirical equations have been proposed for determining the coefficient of vapour diffusion in a dry soil (i.e., $D^*$ in Eq. 3.12) (Millington and Quirk, 1961; Millington, 1959; Marshall, 1959; Penman, 1940). The effect of using various equations for determining $D_v$ was found to be insignificant on $k_{vmax}$ values for the three selected soils (Ebrahimi-Birang et al. 2004).

Table 3.1 Properties of soils chosen for analysis of the vapour-phase coefficient of permeability function

| Soil ID | Reference and Specimen Counter | Saturated Coefficient of Permeability, m/s | Saturated Gravimetric Water Content, g/g |
|---|---|---|---|
| Sand | SoilVision Data Base, 11456 | 2.07E-06 | 0.2607 |
| Loamy Sand | SoilVision Data Base, 11178 | 2.92E-08 | 0.2644 |
| Silty Loam | SoilVision Data Base, 11408 | 2.55E-07 | 0.2662 |

Figure 3.11 shows the vapour-phase coefficient of permeability function for the three selected soils. The symbols on the graph indicate the points at which the SWCC was measured for each of the selected soil specimens. The results show that the maximum value of the vapour-phase coefficient of permeability is about $3 \times 10^{-15}$ m/s for all three soils.
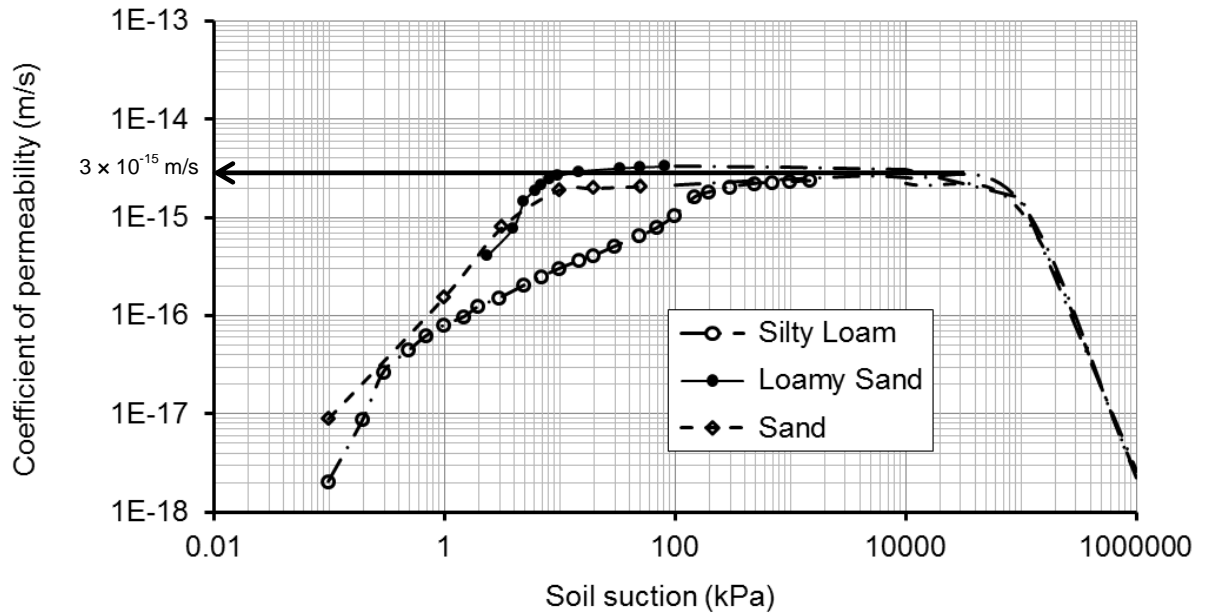
Figure 3.11 Vapour-phase coefficient of permeability for three selected soils

### 3.7.3 A Method to Predict the Liquid-Phase Unsaturated Coefficient of Permeability Function within the Residual-State Condition

Figure 3.12 shows a schematic diagram of the liquid-phase coefficient of permeability function. The function consists of five sections specified as AB, BC, CD, DE, and EF.

As previously described in section 3.4, when liquid becomes discontinuous at the end of the residual-state condition (point *D*), the film water still exists and water between the bridges is connected (see Figure 3.5.b).

A complete monolayer has been shown to be adsorbed onto the soil at a relative humidity of 20% ($\psi$ = 220,000 kPa) at 20 $^{\circ}$C (Quirk, 1955) (see Figure 3.5.c). At this suction value ($\psi$ = 220,000 kPa), the soil still contains liquid water. However, the liquid water occurs in isolated pockets, filling small pores, or forming wedges about the points of contacts between the grains of medium. The suction value of 220,000 kPa has been suggested based on observations on clayey soils and could probably be in the range of smaller suction for soils with lower clay contents.

Capillary contributions to the SWCC are due to liquid held in pore corners behind curved interfaces. Adsorptive contributions to the SWCC are attributed to van der Waals surface forces forming liquid films. Generally, capillary forces dominate at the wetter range of the curve, whereas adsorptive forces dominate at the dry end (Barbour, 1998;

Tuller and Or, 2005). Or and Tuller (1999) suggested that the capillary contributions become negligible for matric suction values larger than about 10,000 kPa.
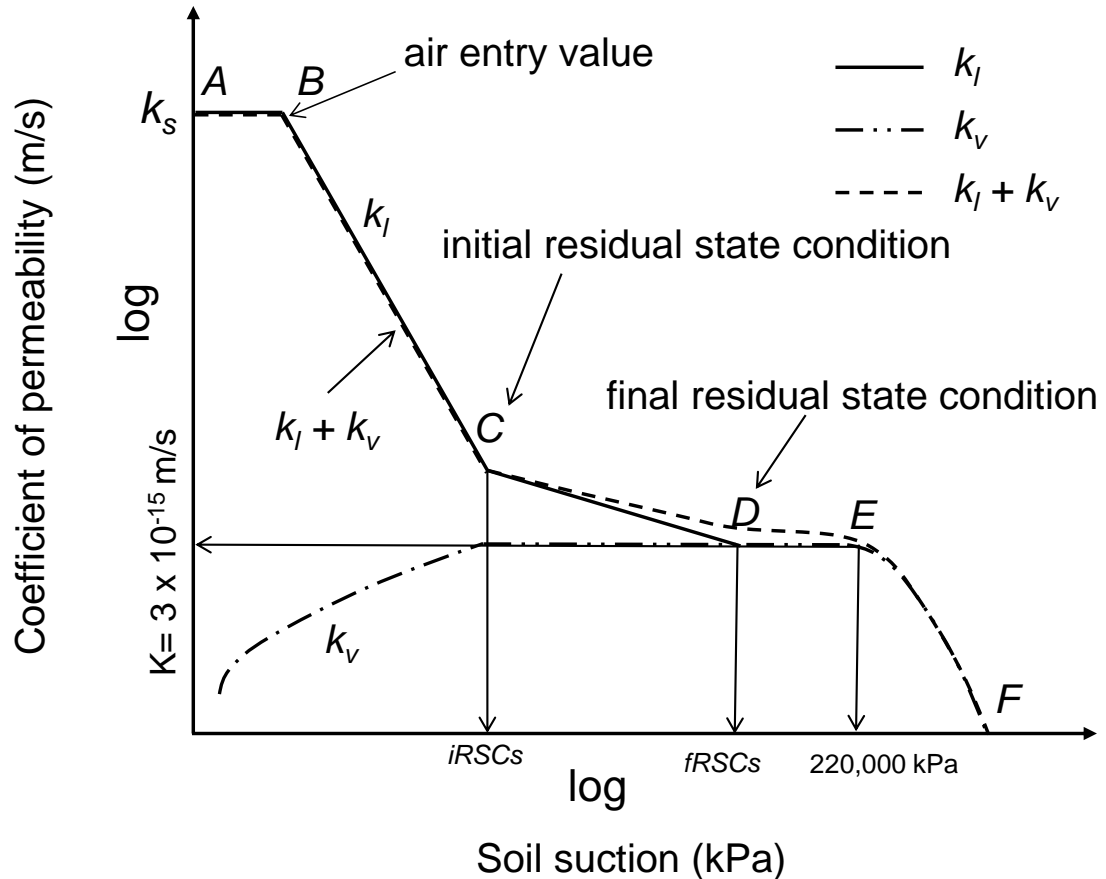


Figure 3.12 Schematic of the simplified proposed method for prediction of the unsaturated coefficient of permeability function

For the method proposed in this thesis, the liquid-phase coefficient of permeability is assumed to reach its minimum at the end of the residual-state condition (i.e., point *D*) and to remain constant from point *D* to point *E,* beyond which vapour flow is assumed to be a dominant flow mechanism. The suction value suggested by Quirk (1955) (($\psi$ = 220,000 kPa) is assumed to be reached at point *E*.

The dashed section (DE) on Figure 3.12 shows the maximum vapour-phase coefficient of permeability function, which is almost independent of the soil type (see section 3.7.2), and may be estimated using Eq. 3.19.

The methods proposed to predict the coefficient of permeability for each section on Figure 3.12 are described below.

Approaches for predicting the coefficient of permeability of sections AB and BC are available in the literature (see section 2.6, Chapter 2). The coefficient of permeability in section AB (i.e. from saturation to air-entry value) is considered as the saturated coefficient of permeability ($k = k_s$).

The Campbell (1974) method is used to determine the coefficient of permeability function in section BC (Eq. 3.25). Point $C$ is assumed as the initial residual state condition. The suction value at point $C$ can be estimated using the method described in section 3.5.1. The corresponding coefficient of permeability at point $C$ can then be determined using Eq. 3.25.

$$k = k_s(\frac{\psi_e}{\psi})^{n_1} \quad \text{for } \psi > \psi_e \quad \text{(see Chapter 2, table 2.8)} \qquad [3.25]$$

Where, $n_1 = 2 + 2/b$, $b = 1/\lambda$ and $\lambda$ is defined as the pore-size distribution index of the medium, and where $\psi_e$ is the air-entry value.

An alternative predictive method such as Brooks and Corey (1974) or Fredlund et al. (1994) may be used to determine the coefficient of permeability function in section BC.

Suction at point $D$ can be determined using the method described in section 3.5.2. The coefficient of permeability at point $D$ is assumed to be equal to the lower limit of the liquid coefficient of permeability function, which in turn is equal to the maximum value of the vapour coefficient of permeability. The maximum value of the vapour coefficient of permeability was shown to be equal to approximately $10^{-15}$ m/s, regardless of the type of soil (see section 3.7.2).

The coefficient of permeability function in section CD can be drawn using Eq. 3.26.

$$n_2 = \frac{\log(\frac{k_{fRSC}}{k_{iRSC}})}{\log(\frac{\psi_{iRSC}}{\psi_{fRSC}})} \qquad [3.26]$$

where $k_{fRSC}$ is equal to $3 \times 10^{-15}$ m/s.

The coefficient of permeability in section DE is assumed to remain equal to the minimum value of $3 \times 10^{-15}$ m/s.

The procedure given in this section will be later used in Chapter 6 to predict the liquid coefficient of permeability function for the soil samples under study, and the predictions will be evaluated using the measured values obtained from experimental tests. The procedure for the experimental tests will be described in the next chapter.

# CHAPTER 4

# LABORATORY TESTING PROGRAM

## 4.1   INTRODUCTION

In the experimental laboratory testing program for this thesis, three types of soils were used: sandy, silty, and clayey. Section 4.2 describes the soils and their preparation for the entire testing program.

Section 4.3 presents the primary geotechnical characteristic of the selected soils including grain-size analysis, specific gravity, and Atterberg limits.

Section 4.4 describes the procedure used for one-dimensional consolidation and saturated coefficient of permeability tests. The main objectives of conducting the one-dimensional consolidation tests were to measure the saturated coefficient of permeability and to prepare specimens with specified initial conditions for soil-water characteristic curve (SWCC) and steady-state evaporation tests.

Section 4.5 describes the testing program for establishing the soil-water characteristic curve, which plays a major role in achieving the objectives of this thesis. The performance of a relatively new device (i.e., WP4-T) for measuring the SWCC in the high suction range was assessed; study of the SWCC hysteresis in the high suction range was also considered.

Section 4.6 describes the steady-state evaporation tests. All of the evaporation tests were conducted on samples with saturated initial conditions in an environmentally controlled room. The design of evaporation columns, equipment, instrumentation, and testing procedure are described. Two evaporation columns were constructed: a primary and a modified column. A primary evaporation column was initially designed and constructed for the entire testing program. However, due to some technical difficulties on performing the evaporation tests on the clayey silt samples, a modified evaporation column with a shorter height was also constructed. The design of both columns is

described in this section. The main objective of the evaporation tests was to measure the coefficient of permeability function around the residual-state condition. The secondary objective was to obtain experimental data for the water-content and temperature profiles of the specimens at steady-state flow condition.

## 4.2    SELECTION OF THE SOILS FOR LABORATORY TESTING PROGRAM

The three soils selected to be used in this study were: i) a sandy soil, hereafter referred to as Beaver Creek sand, ii) a clayey silt soil, hereafter referred to as Botkin silt and iii) a clay soil, hereafter referred to as Regina clay. The Beaver Creek sand was available in the Department of Agriculture and Bio-resources, University of Saskatchewan, Canada. The sand soil was collected from sand deposits just South of Saskatoon, Canada. The Botkin silt and Regina clay soils were available in the Geotechnical Laboratory of the Department of Civil and Geological Engineering, University of Saskatchewan. All three soil samples were crushed, air-dried, and passed through a No. 10 sieve. The total soil samples of Beaver Creek and Botkin silt each weighed about 20 kg. The total sample of Regina clay was about 5 kg.

The Regina clay was used only for part of the laboratory testing program involving measurement of the drying and wetting soil-water characteristic curves (SWCCs) in high suction ranges.

The Beaver Creek sand and Botkin silt soil samples were washed to reduce the electrical conductivity of the saturated extracts in order to reduce the osmotic suction effect. The procedure for reducing electrical conductivity of the soils is discussed in this section. This section also presents the primary geotechnical characteristics of the soil samples before and after reduction of their electrical conductivity.

The washing procedure for the sand was easy, since over 99% of the soil consisted of sand-sized particles. The soil was placed in a 20-litre bucket, and distilled water was added. Each time distilled water was added to the bucket, the soil suspension was stirred and the sample was left overnight to allow the soil particles settle to the bottom of the bucket. Electrical conductivity of the water above the settled soil was measured and then the water was removed from the bucket. The remaining slurry at the bottom of the bucket was air-dried in the laboratory environment, crushed, and sieved through a No. 10 sieve (i.e., < 2 mm).

The washing procedure for the Botkin silt sample was the same as that used for the Beaver Creek sand; however, due to its consisting of 20% clay particles and 45% silt particles, the procedure was more challenging. The time required for settling the particles after stirring the soil with distilled water was longer. The number of times needed to wash the soil in order to reduce the electrical conductivity of the soil was larger.

Table 4.1 shows the gravimetric water content, electrical conductivity, and pH of the saturated paste of the Beaver Creek sand and Botkin silt soils before and after washing.

## 4.3    PRIMARY GEOTECHNICAL CHARACHTERESTICS OF THE SOILS

Grain-size analysis (GSA), specific gravity ($G_s$), and Atterberg limits of the soils were measured based on the ASTM standard designations (ASTM D 422, 1994; D 4318, 1994; D 854, 1994). The grain-size distribution curves for Beaver Creek sand, Regina clay, and Botkin silt soil samples are shown in Figures 4.1 to 4.3. Figure 4.3 shows the grain-size distribution curves for the Botkin silt sample before and after washing.

Table 4.2 presents the percentage of sand, silt, and clay size particles, specific gravity and Atterberg Limits of the Beaver Creek sand, Botkin silt and Regina clay soil samples, measured based on the ASTM designation before and after washing. A summary of the results of the grain-size analyses are given in Appendix A.

Table 4.1 Electrical conductivity, pH, and saturated paste water content of Botkin silt and Beaver Creek sand before and after washing

| Soil     Property | Botkin Silt before Washing | Botkin Silt after Washing | Beaver Creek Sand before Washing | Beaver Creek Sand after Washing |
|---|---|---|---|---|
| Electrical Conductivity, EC, dS/m | 4.2 | 0.86 | 0.8 | 0.4 |
| pH | 7.6 | 7.7 | 8.1 | 8.1 |
| Gravimetric Water Content of the Saturated Paste (%) | 36 | 36 | 27 | 27 |
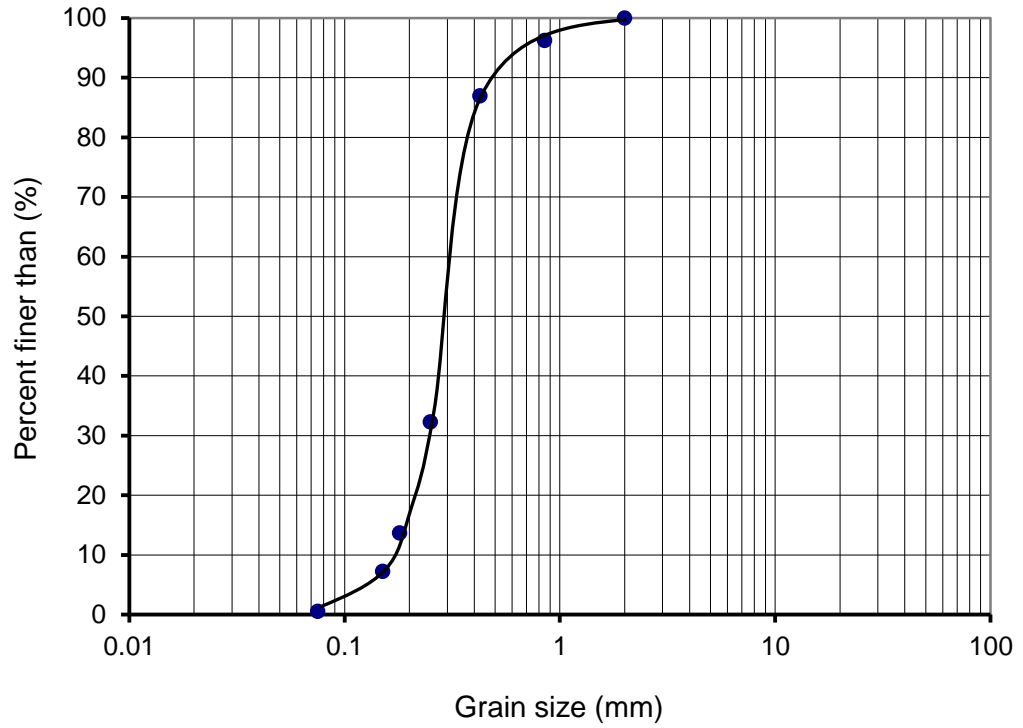
Figure 4.1 Grain-size distribution curve for Beaver Creek sand
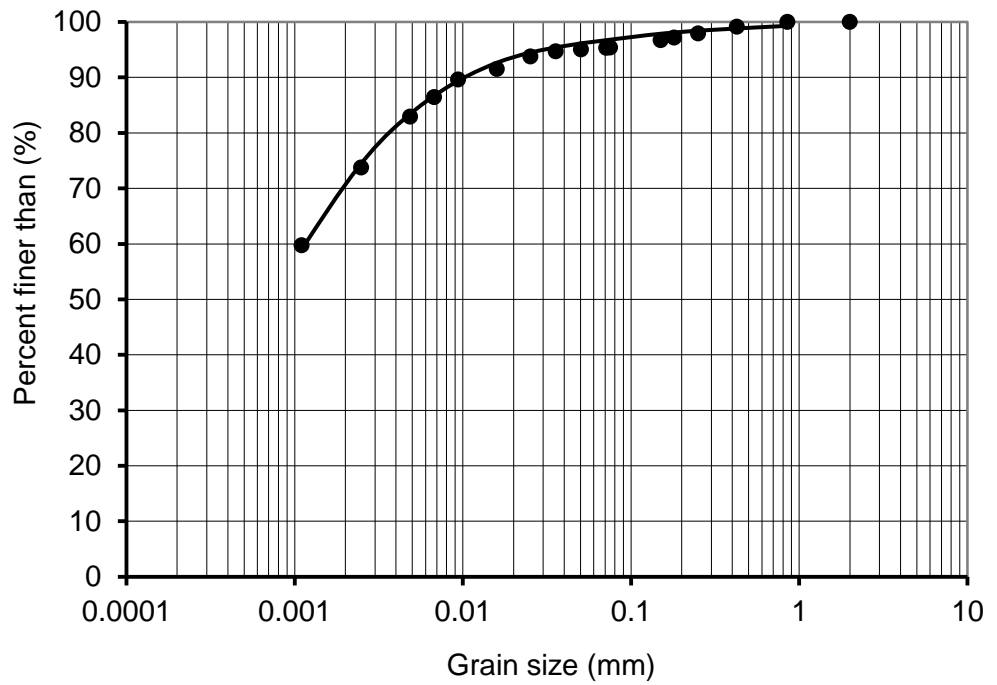


Figure 4.2 Grain-size distribution curve for Regina clay

101
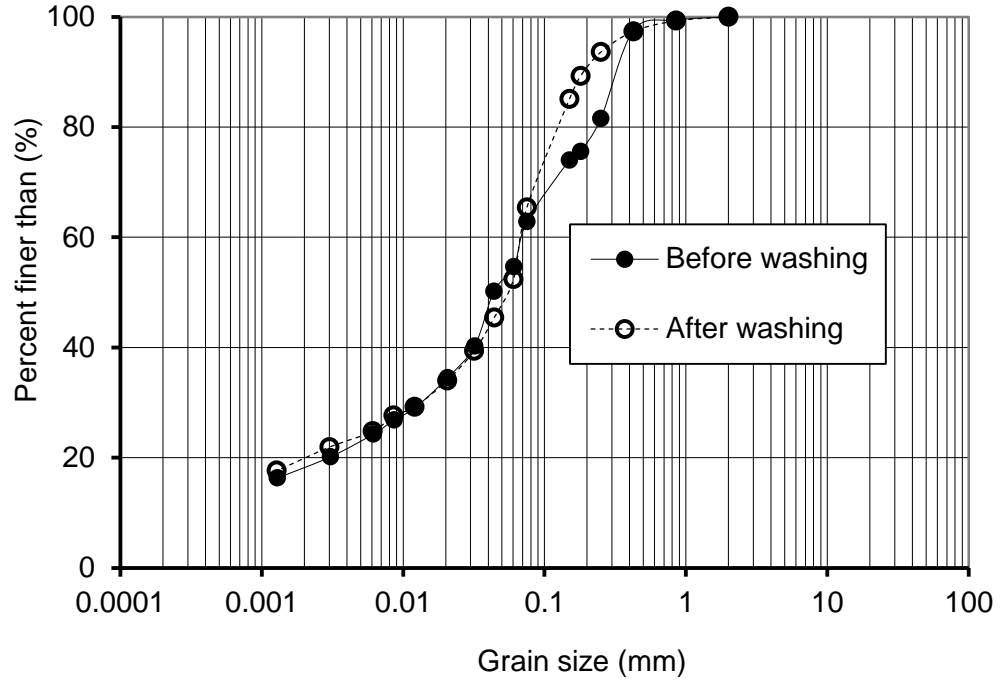
Figure 4.3 Grain-size distribution curve for Botkin silt before and after washing

Table 4.2 Primary geotechnical properties of the selected soil samples before and/or
after washing

| Soil<br><br>Property | Botkin Silt before Washing | Botkin Silt after Washing | Beaver Creek Sand after Washing | *Regina Clay |
|---|---|---|---|---|
| Sand Sizes, % | 37 | 35 | 99.5 | 5 |
| Silt Sizes, % | 45 | 45 | **0.5 | 21 |
| Clay Sizes, % | 18 | 20 | | 74 |
| Specific Gravity, $G_s$ | ----- | 2.71 | 2.65 | 2.7 |
| Liquid Limit, % | ----- | 20.3 | ----- | 81 |
| Plastic Limit, % | ----- | 15.1 | ----- | 23.1 |
| Plasticity Index, PI | ----- | 5.2 | ----- | 57.9 |

*Regina clay sample was not washed since it was not used for evaporation processes
**Total percentage of silt and clay sizes for Beaver Creek sand was 0.5

## 4.4 LABORATORY TESTING PROGRAM FOR ONE DIMENSIONAL CONSOLIDATION AND SATURATED COEFFICIENT OF PERMEABILITY

The objectives of this section are: i) to establish the saturated coefficient of permeability versus vertical stress relations through the consolidation process and ii) to prepare some of the specimens to be used for the measurement of the soil-water characteristic curve (section 4.5). This section describes the testing program for conducting the consolidation process and measurement of the saturated coefficient of permeability using the falling-head test at the end of the each loading increment during the consolidation process. A description of the laboratory equipment, as well as the sample preparation and the laboratory testing procedures, are presented.

### 4.4.1 Laboratory Testing Equipment

One-dimensional consolidation laboratory tests were conducted on the selected soils. The falling-head saturated coefficient of permeability tests were conducted after completion of the primary consolidation test associated with each of the applied vertical pressures. A consolidometer (i.e., consolidation cell) made of stainless steel, with a diameter of 101.5 mm and a total height of 62.6 mm, was used for conducting the consolidation test and for measuring the saturated coefficient of permeability at the end of each loading increment. Figure 4.4 shows a schematic diagram of the consolidation and saturated coefficient of permeability cell. The mass of the loading cap was 1093.5g. Details of the consolidation and saturated coefficient of permeability test used in this section can be found in Huang (1994).

### 4.4.2 Preparation of the Specimens

A saturated slurry of the Botkin silt and the Beaver Creek sand soil was prepared. The slurry was then poured into a consolidometer with dimensions shown in Figure 4.4. A total of three specimens were prepared, two for Botkin silt and one for Beaver Creek sand. Hereafter, the prepared specimens will be referred to as Specimens CS1-2 and CS2-2 for Botkin silt and Specimen S1-2 for Beaver Creek sand.
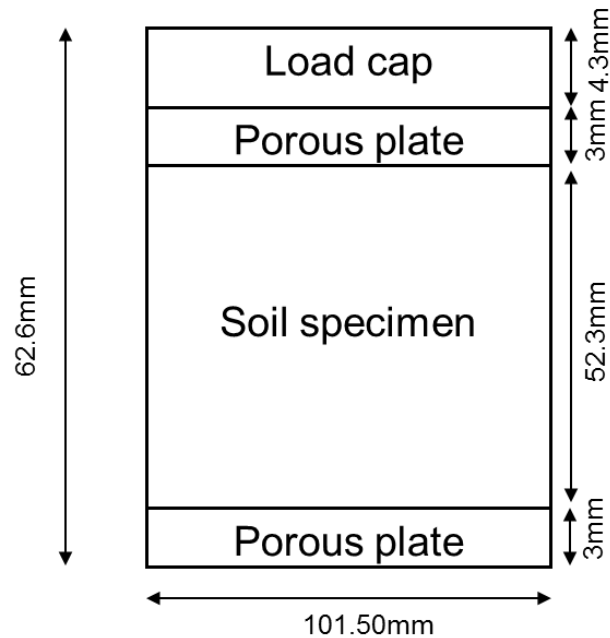
Figure 4.4 A schematic diagram of the consolidation and the saturated coefficient of permeability cell

### 4.4.3 Test Procedure of the Slurry Consolidation and Saturated Coefficient of Permeability

A small vertical pressure of 0.3 kPa was applied to the soil specimen using a consolidation loading frame. The deflection of the soil specimen with time during the consolidation test for each of the applied pressures was measured using a dial gauge. At the end of the each consolidation increment, the falling-head method was used to measure the saturated coefficient of permeability. The vertical pressures applied on Specimen CS1-2 were 12.5, 25, 50, 100 kPa. The vertical pressures applied on Specimens CS2-2 and S1-2 were 12.5, 25, 50, 100, 200 kPa. At the end of the consolidation tests, some of the consolidated specimens were used for measuring the soil-water characteristic curve (section 4.5).

### 4.5 LABORATORY TESTING PROGRAM FOR THE MEASUREMENT OF THE SOIL-WATER CHARACTERISTIC CURVE (SWCC)

This section is divided into three parts. Section 4.5.1 describes the equipment used for measuring the SWCC. The equipment used in this program was U of S Pressure Plate Cell, the GCTS SWC 100, the ATC, and the WP4-T. Section 4.5.2 describes the

procedure for preparing the soil specimens, and section 4.5.3 presents a description of the laboratory testing procedure used to measure the SWCC in soil suction ranges from 0 to 1500 kPa.

### 4.5.1 SWCC Testing Equipment

Different testing apparatuses were used to establish the SWCC of the selected soil for entire ranges of soil suction from 0 to 1,000,000 kPa. The apparatuses were divided into two main groups. The first group of the apparatuses (i.e., U of S Pressure plate Cell and GCTS SWC 100) was used to measure the SWCC in the suction ranges from 0 to 1500 kPa, and the second group of the apparatuses (i.e., ATC and WP4-T) was used to extend the SWCC beyond soil suction values of 1500 kPa.

### 4.5.1.1 University of Saskatchewan Pressure Plate Cell (U of S Pressure Plate Cell)

Figure 4.5 shows a schematic diagram of the U of S Pressure Plate Cell used in this study.
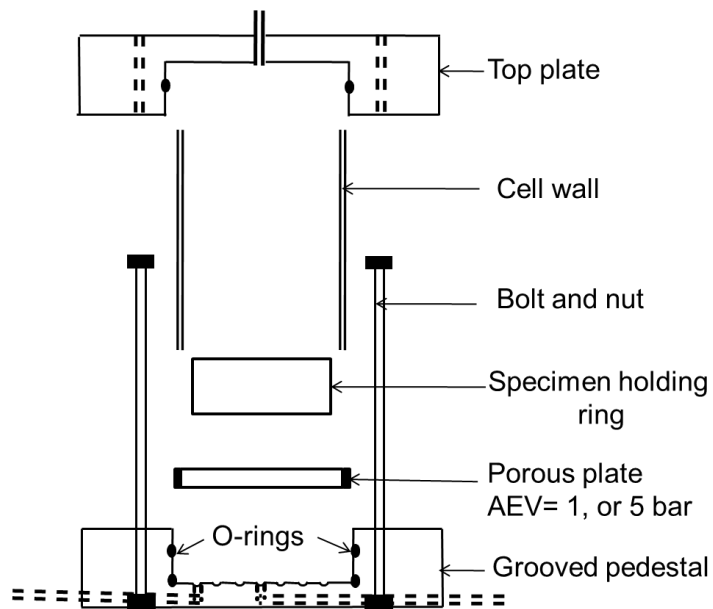


Figure 4.5 A schematic of the U of S Pressure Plate Cell

The ceramic porous plate placed at the bottom of the specimen was saturated prior to the test and assumed to remain saturated until the end of the test. The saturated porous plate was placed onto the grooved pedestal. Two O-rings were used on top and bottom of the ceramic plate in order to seal the space between the pedestal and the cell for air diffusion. There were two clear flexible tubes attached to the pedestal in order to drain the water out of the specimen and to flush diffused air accumulated under the porous plate.

### 4.5.1.2 Geotechnical Consultants and Testing System SWC-100 (GCTS SWC-100)

The GCTS SWC 100 device is a fairly new unsaturated soil testing apparatus, with the capability of controlling matric suctions from near zero to about 1500 kPa and applying one-dimensional loading to the specimen. The air pressure above the specimen is controlled using dual pressure regulators. In this research, the apparatus was only used for controlling matric suctions. The device also includes a plumbing system that allows for flushing water below the high air entry disk and measuring the diffused air. Water drained from the soil specimen can be measured using the volume tube readings.

The maximum supply pressure in the pipe network in the geotechnical laboratory was about 800 kPa. A pressure booster was used to increase the input air pressure from 800 kPa up to 2000 kPa. The maximum desired air pressure to complete SWCC tests using GCTS SWC 100 device was 1500 kPa. Figure 4.6 shows the pressure booster connected to GCTS SWC 100 device and pressure pipe network of the laboratory applied through high-pressure plastic tubes. There were two outlets on the pressure booster and this allowed the use of two GCTS SWC 100 SWCC devices.

### 4.5.1.3 Air-Tight Chamber (ATC) Equipment

One of the methods that has been used to measure the SWCC in the high suction range is the equilibration of the soil samples over salt solutions of known osmotic suction. Various types of salts can be used; however, in some cases the accuracy may decline with time due to chemical instability. A plastic container can be used as an air-tight chamber provided the salt solution is placed in a dish made of a suitable material such as glass (ASTM E 104-02, 2003).

Figure 4.6 GCTS SWC 100 apparatus and pressure booster

The air-tight chambers used in this research were built from PVC tubes at the University of Saskatchewan (Dadgar, 2005). Figure 4.7 shows an example of the air-tight chamber equipment used in this study. The chambers were composed of a PVC tube with a diameter of 190 mm and a height of 200 mm, with a plate at the top and one at the bottom. To prevent vapour diffusion, O-rings were used between the plates and the tubes.
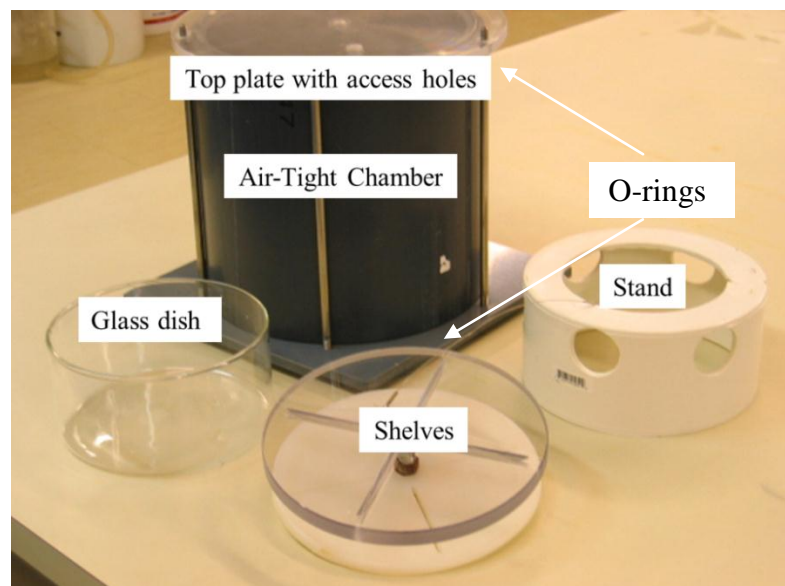


Figure 4.7 Air-Tight Chamber (ATC) Equipment

#### 4.5.1.4  Dew Point Water PotentiaMeter (WP4-T)

Dew-Point Water PotentiaMeter (WP4-T), a relatively new device, has been used in order to establish the SWCC beyond soil suction value of 1,500 kPa. A concise review on the development of the device was given in the literature review chapter (Chapter 2, section 2.2.3)

The manufacturer's instructions recommend that the WP4 be calibrated prior to usage with a standard solution of 0.5 M KCl, which should yield a suction of $2.19 \pm 0.1$ MPa, at 25 $^{\circ}$C. Cardoso et al. (2007) suggested that the calibration procedure provided by the manufacturer for the WP4 device was not satisfactory. A WP4-T device used for the measurement of the soil suction throughout this thesis was calibrated using the following procedure.

Different saturated salt solutions with known osmotic suction were prepared in the Environmental Engineering Laboratory in the Department of Civil and Geological Engineering at the University of Saskatchewan. The suction value of each of the prepared saturated salt solutions was measured using the WP4-T. Figure 4.8 shows the theoretical suction values versus the measured suction values using the WP4-T device for the selected saturated salt solutions. Good agreement was obtained between the theoretical and measured values.

#### 4.5.2  Preparation of the Soil Specimens for SWCC Measurement between Suction Ranges from 0 to 1500 kPa

Different procedures were used for the preparation of the soil specimens for Beaver Creek sand and Botkin silt. The procedures for preparation of the Beaver Creek sand and Botkin silt specimens are described in this section.

#### 4.5.2.1  Preparation Procedures of the Beaver Creek Sand Specimens for the SWCC Measurement

A total of 6 Beaver Creek sand specimens were prepared for measurement of the SWCCs. One of the preparation procedures for the sand specimens where the drying SWCC was measured in suction ranges from 0 to 1500 kPa was as follows:

1- 2000 grams of air-dried Beaver Creek sand was mixed with 340 grams of distilled water to produce a gravimetric water content of 17%.

2- The soil sample was left in a plastic container with a tight lid cover for one day.

3- The moist soil was placed into a Plexiglass column 180 mm in height and 70 mm in diameter with an extension tube. The column was placed on a circular thick steel plate. It should be noted that this column was later used as the *primary evaporation soil column*. The details on the design of the column will be later described in section 4.6.1.2.

4- A vertical force of 14.25 kN was applied to the top of the soil through a load cap using a high-pressure consolidation load frame.

5- The extension tube was removed and extra soil was carefully trimmed from the top of the column.
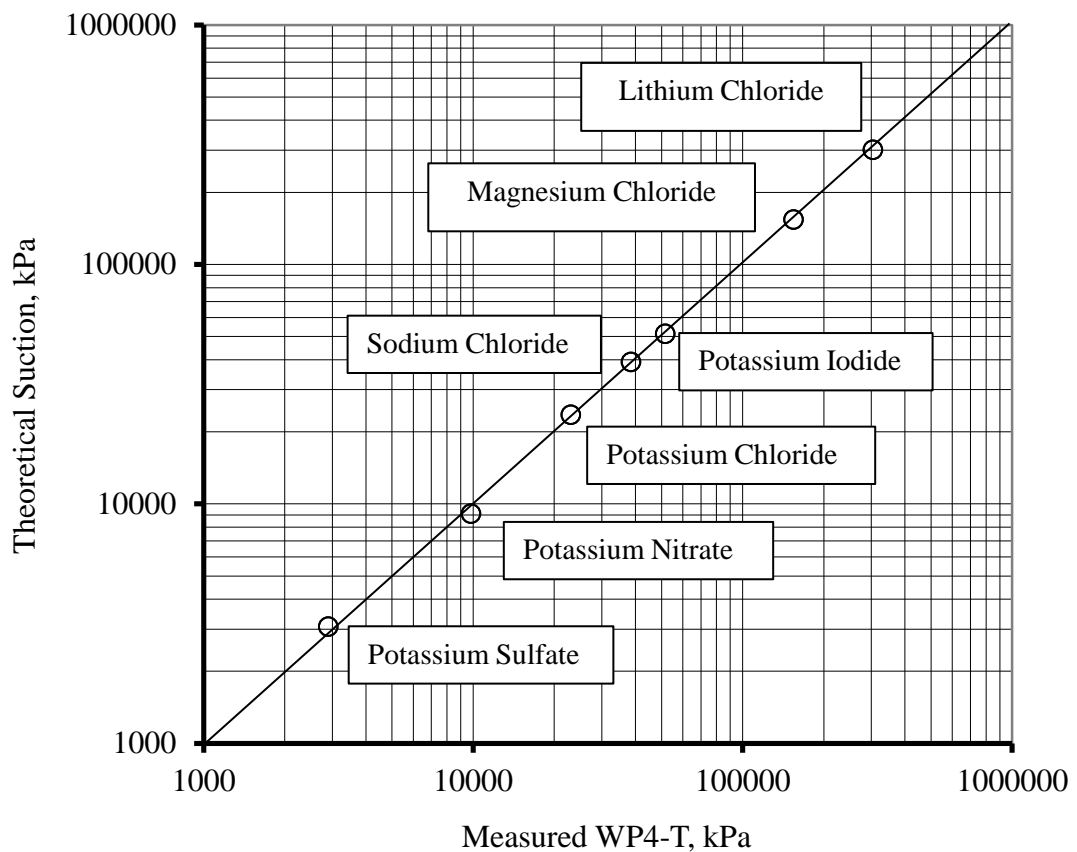


Figure 4.8 Theoretical and measured suction values using WP4-T for the selected saturated salt solutions

Four soil specimens were extruded from the soil column into stainless steel specimen holders. A piston was inserted from the bottom of the soil column to push the soil out of the column. A soil sample holder was pushed into the soil from the top of the soil column. The soil inside the specimen holder was then separated from the remaining soil inside the column using a fine fish line. The soil on the both sides of the specimen holder was trimmed carefully. This procedure was repeated until four soil specimens were prepared. Hereafter, the prepared soil specimens will be referred to as S1-1, S2-1, S3-1, and S4-1.

Using a similar procedure explained in the previous paragraphs, another set of four specimens of Beaver Creek sand were prepared. Hereafter, these specimens will be referred as S1-2, S2-2, S3-2, and S4-2. Some of the extruded specimens from the consolidation cells were broken during sampling or during setting up the SWCC test. Four out of 8 samples (i.e., S1-1, S3-1, S3-2, and S4-2) were successfully transferred to the SWCC measurement apparatuses. The volume-mass properties of Specimen S4-1 at the end of the consolidation test were used to estimate the initial volume-mass properties of the soil specimens (i.e., water content, dry density, and void ratio). The volume-mass relation of the SWCC specimens was also determined after completion of the SWCC tests.

Another Beaver Creek sand specimen was prepared to use for SWCC measurement (MS1). Specimen MS1 was extruded from the cell that was used for the consolidation and coefficient of permeability test. The specimen was consolidated to the maximum vertical pressure of 200 kPa (see section 4.4.2).

Table 4.3 summarizes all of the Beaver Creek sand specimens and their positions within the consolidometer cells in the preparation procedure used for SWCC testing.

### 4.5.2.2 Preparation Procedures of the Botkin Silt Specimens for the SWCC Measurement

A total of 7 Botkin silt specimens for the measurement of the SWCCs were prepared. One of the preparation procedures for the Botkin silt specimens where the drying SWCC was measured in suction ranges from 0 to 1500 kPa was as follows:

1- 3,000 grams of air-dried Botkin silt soil was mixed with 1,020 grams of distilled water to make saturated slurry with 34% gravimetric water content. This slurry

was placed in a Plexiglass column with a height of 208 mm and a diameter of 113 mm (Figure 4.9), and the column was placed on a pedestal. The column had a porous stone at the bottom and top.

2- Over the top porous stone a stainless steel loading cap was placed. The soil column was placed into a loading frame for consolidation.

3- The soil was consolidated to a maximum vertical pressure of 19 kPa.

4- After consolidation of the soil was complete (i.e., after about one week), four soil specimens were extruded into stainless steel specimen holders. Hereafter, the prepared specimens will be referred to as CS1-1, CS2-1, CS3-1, and CS4-1. Three of the soil specimens (i.e., CS1-1, CS2-1, and CS3-1) were transferred to the SWCC measurement apparatuses. The mass-volume properties of Specimen CS4-1 at the end of the consolidation test were taken as initial volume-mass properties of the SWCC specimens (i.e., gravimetric water content, dry density, and void ratio). The volume-mass relation of the SWCC specimens was also determined after completion of the SWCC tests.
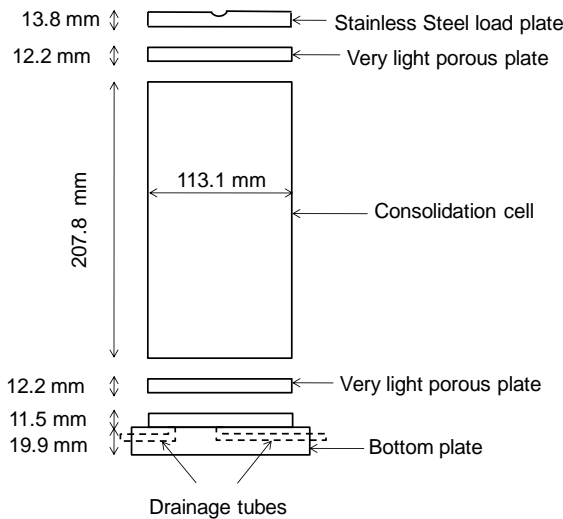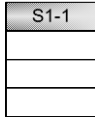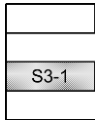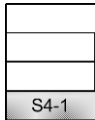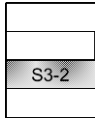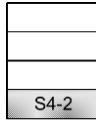


Figure 4.9 A schematic diagram of the consolidation column
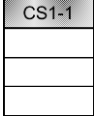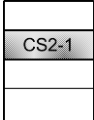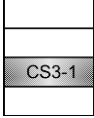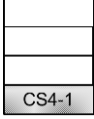
The saturated slurry in step one above was used to prepare two more Botkin silt specimens for the SWCC measurements. Hereafter, these two specimens will be referred to as CS01 and CS02.

Table 4.3 Specimens used for the SWCC measurement of the Beaver Creek sand in the
suction ranges from 0 to 1500 kPa

| Specimen | Testing | Specimen Position |
|---|---|---|
| S1-1 | SWCC | From consolidation cell No. 1 |
| S3-1 | SWCC | From consolidation cell No. 1 |
| S4-1 | Initial Properties | From consolidation cell No. 1 |
| S3-2 | SWCC | From consolidation cell No. 2 |
| S4-2 | SWCC | From consolidation cell No. 2 |
| MS1 | SWCC | From consolidation and k-test cell |

Specimen MCS was another SWCC Botkin silt specimen initially consolidated to a maximum vertical pressure of 50 kPa, using the consolidation cell that was used for the consolidation and coefficient of permeability test (section 4.4.2). Table 4.4 summarizes the Botkin silt specimens and their placement in the preparation procedure used for SWCC.

Table 4.4 Specimens used for the SWCC measurement of the Botkin silt in the suction
ranges from 0 to 1500 kPa

| Specimen | Testing | Specimen Position |
| --- | --- | --- |
| CS1-1 | SWCC | From consolidation cell |
| CS2-1 | SWCC | From consolidation cell |
| CS3-1 | SWCC | From consolidation cell |
| CS4-1 | Initial Properties | From consolidation cell |
| CS01 | SWCC | From saturated slurry |
| CS02 | SWCC | From saturated slurry |
| MCS | SWCC | From consolidation and k-test cell |

### 4.5.3 Laboratory Testing Procedures for the Measurement of SWCCs

The hanging-column and axis-translation techniques are used in soil suction ranges from 0 to 1500 kPa. For high suction ranges (i.e., 1,500 to 300,000 kPa), chemical energy is used to provide a constant vapour pressure environment in which the soil samples were allowed to equalize. Sections 4.5.3.1 and 4.5.3.2 describe the testing procedure used to measure SWCCs of the selected soils in suction ranges from 0 to 1500 kPa and high suction ranges from 1500 kPa to 300,000, respectively.

**4.5.3.1 Laboratory Test Procedure for the Measurement of the SWCC in Soil Suction Ranges from 0 to 1500 kPa**

A combination of the hanging-column and axis-translation techniques (Hilf, 1956) was used to measure the soil-water characteristic curve for the prepared Beaver Creek sand and Botkin silt soil specimens in suction ranges from 0 to 1500 kPa. The University of Saskatchewan Pressure Plate Cell and GCTS SWC 100 apparatuses were used for this purpose. Tables 4.5 and 4.6 show types of the SWCC testing apparatuses used for the measurement of the SWCC for the Beaver Creek sand (S) and the Botkin silt or clayey silt (CS) specimens, respectively.

Table 4.5 SWCC experiments conducted on the Beaver Creek sand specimens tested for applied suctions from 0 to 1500 kPa

| Specimen | Initial Condition | Testing Equipment |
|---|---|---|
| S1-1 | Compressed to 3870 kPa | U of S Pressure Plate  (0-10) kPa |
| S3-1 | Compressed to 3870 kPa | GCTS SWC 100 (100-1500) kPa |
| S3-2 | Compressed to 3870 kPa | U of S Pressure Plate (10–100) kPa |
| S4-2 | Compressed to 3870 kPa | U of S Pressure Plate (100-500) kPa |
| MS1 | Consolidated to 200 kPa | GCTS SWC 100 (0 – 1500 kPa) |

Porous plates with air-entry values of 1-bar and 5-bar were used during the measurement of the soil-water characteristic curve using a U of S Pressure Plate cell. The porous plates were saturated by placing them in distilled water for at least 24 hours. Before installing the saturated porous plate in the apparatus, the mass of the porous plate was measured. When the porous plate was replaced or the test was completed, the mass of the plate was again measured. The difference between the initial and final masses should be negligible.

The masses of the prepared soil specimen (i.e., S1-1, S3-2, S4-2, CS1-1, CS2-1, CS01, or CS02) and the specimen holder were measured and transferred onto the saturated porous plate. A thin layer of distilled water was provided on the surface of the porous plate before transferring the specimen to ensure good hydraulic connectivity between the bottom of the soil specimen and the porous plate. A Plexiglass tube was

attached to the pedestal. The top cap of the apparatus was placed into its designated place (see Figure 4.10). An O-ring was used to prevent the air leakage between the cell and top cap. There was a hole in the middle of the cap which allowed the specimen to remain at atmospheric pressure during the hanging-column portion of the test. Later it was possible to apply air pressure to the inside of the apparatus during the axis-translation portion of the test.

Table 4.6 SWCC experiments conducted on the Botkin Silt specimens tested for applied suctions from 0 to 1500 kPa

| Specimen | Initial Condition | Testing Equipment |
| --- | --- | --- |
| CS1-1 | Consolidated to 19 kPa | U of S Pressure Plate Cell and GCTS SWC 100 |
| CS2-1 | Consolidated to 19 kPa | U of S Pressure Plate Cell (0-500 kPa) |
| CS3-1 | Consolidated to 19 kPa | GCTS SWC 100 (10-1500 kPa) |
| CS01 | Saturated Slurry | U of S Pressure Plate Cell (0-500 kPa) |
| CS02 | Saturated Slurry | U of S Pressure Plate Cell (0-500 kPa) |
| MCS | Consolidated to 50 kPa | GCTS SWC 100 (100 – 1500 kPa) |

The soil-water characteristic curve was measured using the hanging-column technique for the low suction range (i.e., 0 – 10 kPa). Figure 4.10 shows a schematic set-up of the hanging-column apparatus using the U of S Pressure Plate Cell. The soil was saturated by applying water to the bottom of the specimen. The suction was set at 0 for about 48 hours in order to allow equilibrium conditions to be established. The zero level was referenced at the bottom of the soil specimen. Then a suction head, h, was applied. The smallest applied suction was 0.5 kPa (i.e., h = 50 mm). The mass of the U of S Pressure Plate cell along with the specimen was recorded at each suction level including zero suction conditions after equilibrium. The water that drained from the soil specimen was collected inside a small glass bottle. Water flowed from a needle that was attached to the end of a flexible tube.

After the equilibrium suction of 10 kPa was established, mass of the entire cell was measured and the technique of the water extraction from the specimen was changed from the hanging-column to the axis-translation method. During the axis-translation

method, air pressure was applied to the top of the soil to further remove water from the soil specimen (see Figure 4.11). The first air pressure applied to the soil specimen was equal to the maximum suction applied using the hanging-column test (i.e., 10 kPa). This duplication was useful in back-calculating the water content of the specimen at the end of the test. Air pressures of 20, 50, and 100 kPa were applied to the soil specimen before changing the ceramic porous plate at the bottom of the sample. After reaching an applied air pressure near 100 kPa, the 1-bar ceramic porous plate was changed. A 5-bar porous plate was then placed into the Pressure Plate apparatus. The following procedure was used when changing the porous plates.
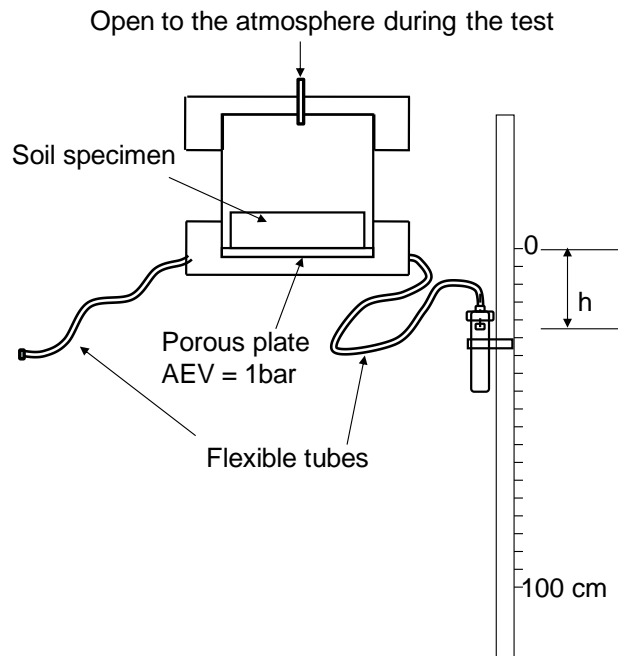


Figure 4.10 A schematic set-up for the hanging-column technique using a U of S Pressure Plate Cell

The mass of a 5-bar pre-saturated porous plate was measured. The U of S Pressure Plate cell was opened. The mass of the soil specimen along with the specimen holder was measured. The mass of the 1-bar porous plate was also measured. The 5-bar porous plate was placed onto the grooved pedestal and a thin layer of water was poured on the plate. Two O-rings were placed between the pedestal and steel ring of the porous plate and between the cell wall and the steel ring of the porous plate. The sample was placed

on top of the porous plate. The device was re-assembled using a similar procedure to that explained earlier for the 1-bar porous plate. Air pressure of 100 kPa was applied to the system and time was allowed for equalization of the water content. The procedure was carried out similarly by applying 150, 300, and 450 kPa air pressures.
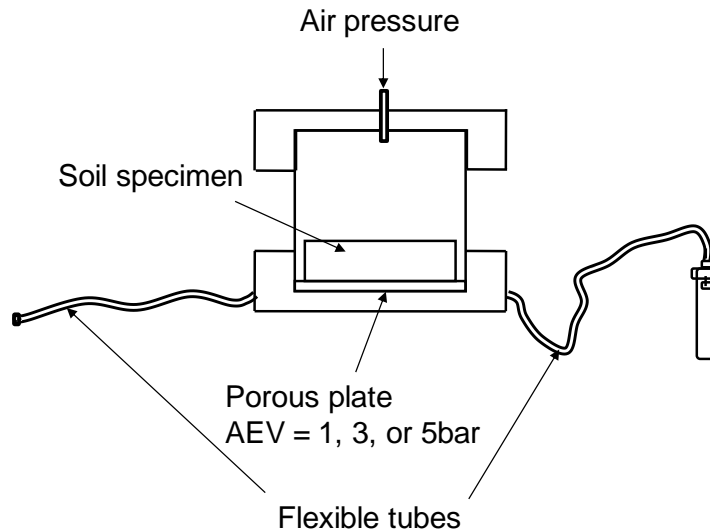


Figure 4.11 A schematic set-up for axis-translation technique using U of S Pressure Plate Cell

As the pressure was increased, air bubbles began to accumulate at the bottom of the pedestal. The air bubbles can create a substantial error during the back-calculations of the water contents of the soil. Therefore, by passing a small flow of water through the flexible tubes attached to two sides of the pedestal, the air bubbles were replaced with water before measuring mass of the cell.

At the end of the test the soil specimen was carefully removed from the cell. The gravimetric water content of the specimen was measured by oven-drying the soil. The mass of the 5-bar plate was also measured. The specimen holder and soil of Specimen CS1-1 was transferred to the GCTS SWC 100 device in order to apply higher air pressures. The experimental procedure used for the GCTS SWC 100 device will be described later in this section.

The SWCC of two Beaver Creek sand specimens (S3-1 and MS1) and three Botkin silt (clayey silt) specimens (CS1-1, CS3-1 and MCS) was measured using GCTS SWC

117

100 device. Two of the five specimens were transferred to the GCTS SWC 100 device after saturating using hanging-column technique (i.e., specimens S3-1 and CS3-1). Specimen CS1-1 was transferred from U of S Pressure Plate apparatus to the GCTS SWC 100 equipment after reaching the equilibrium under an applied pressure of 500 kPa. The applied pressure was increased to 1000 kPa when the specimen was placed in the GCTS SWCC 100 equipment.

The GCTS SWC 100 device cell was composed of two walls, a bottom plate, and a top plate. The bottom plate was grooved in order to collect and direct drained water from the specimen to the flexible tubes and finally to the volume tubes.

Ceramic porous plates with air-entry values of 1, 5, and 15 bars can be used depending on the maximum desired air pressure. These plates needed to be saturated prior to the start of the test. This procedure is similar to that used for the U of S Pressure Plate cell. The mass of the saturated porous plates was measured at the beginning and the end of the test.

The procedure for the laboratory test with the GCTS SWC 100 equipment was as follows:

1- The specimen was slowly removed from the U of S Pressure Plate cell and after being weighed, it was placed onto the saturated porous plate of the GCTS SWC 100 device. The saturated porous plate was already in place at the bottom of the device. If started from the saturated condition, the soil specimen inside the specimen holder was saturated by applying the water from the bottom of the sample or by placing it in a water container. After measuring the mass, the soil specimen was placed onto the saturated porous plate of the GCTS SWC 100 device. The walls of the cell were installed and then the top plate was attached to the cell.

2- The cell was fastened using four bolts and nuts.

3- The valves attached to the glass volume tubes were opened.

4- The required air pressure was applied into the cell.

5- After equilibrium, the readings on the volume tubes were taken.

6- The applied air pressure was increased and readings of the water level were taken.

7- After equilibrium under the highest applied air pressure, the specimen was dismantled and water content of the specimen was measured.

8- The water content values corresponding to the applied suction or air-pressure values were back-calculated using recorded masses during the test.

### 4.5.3.2 Laboratory Test Procedure for the Measurement of the SWCC in Soil Suction Ranges from 1,500 to 300,000 kPa

The main objectives of the tests in this section were:

1- to measure drying and wetting soil-water characteristic curves for the selected soils in the high suction range in order to establish the SWCC beyond suction values of 1500 kPa,

2- to evaluate the performance of the WP4-T apparatus used throughout the entire laboratory testing program for this research, and

3- to assess the significance of the hysteresis in high suction ranges for Botkin silt and Regina clay soil samples.

Two pieces of equipment were used to measure the drying and wetting SWCCs of the soils in high suction ranges: the Air Tight Chamber (ATC) and the dew-point Water PotentiaMeter (WP4-T). The data from the ATC were used as a benchmark to evaluate the performance of the WP4-T device. The testing procedures using these apparatuses are explained in this section.

The experimental tests were conducted in an environmentally-controlled room with a constant temperature in the range of 25–26 $^{\circ}$C. Details of the room will be described in section 4.6.1.1. Seven different saturated salt solutions with known osmotic suction values, selected from ASTM E 104-85, 1998 and E104-02, 2003, were made and placed at the bottom of the various air-tight chambers. The expected constant relative humidity values and the corresponding suctions from each solution are given in Table 4.7. According to ASTM standards, these salts can be used for an entire year (ASTM E 104-02, 2003).

Small soil samples were placed inside an air-tight chamber, where an environment of a known relative humidity was created through use of a saturated salt solution. The soil samples were kept in this environment until equilibrium was reached. At equilibrium, the relative humidity and temperature inside the chamber become the same

as in the soil pores. The relative humidity inside the chamber remains constant and is determined by the saturated salt solution inside the chamber. To confirm that the expected relative humidity value given in Table 4.7 was achieved, an independent measurement of the relative humidity inside the ATC was taken using a portable Traceable Hygrometer. After equilibrium was achieved, the gravimetrical water content of the soil samples was measured. The soil-water characteristic curve could be determined since the water contents and corresponding soil suctions were known. The resulting soil-water characteristic curve corresponded to the drying curve when the soil samples were initially in a saturated condition. The results represent the wetting curve when the soil samples were initially dry. The number of the selected points on the SWCC determined the required number of various salt solutions that needed to be prepared.

Table 4.7 The saturated salt solutions and corresponding relative humidities  (ASTM E 104-85, 1998 and E 104-02, 2003) and calculated suction values for t = 25 $^{\circ}$C

| Salt Solution | Relative Humidity, % | Suction, kPa |
| --- | --- | --- |
| Lithium Chloride | 11.3 ± 0.3 | 300008 |
| Magnesium Chloride | 32.8 ± 0.2 | 153383 |
| Potassium Iodide | 68.9 ± 0.3 | 51256 |
| Sodium Chloride | 75.3 ± 0.2 | 39034 |
| Potassium Chloride | 84.3 ± 0.3 | 23500 |
| Potassium Nitrate | 93.6 ± 0.6 | 9100 |
| Potassium Sulfate | 97.3 ± 0.5 | 3766 |

Figure 4.12 shows a schematic diagram of the set-up for the SWCC measurements of the selected soils using vapour pressure methods. Twenty-eight soil samples were prepared for each type of soil. Fourteen soil samples were saturated and the other fourteen were oven-dried. The saturated samples were used to determine the desorption SWCC and oven-dried samples were used to determine the sorption SWCC.

Eight soil samples were placed in each chamber: four Botkin silt samples and four Regina clay samples. Two of the four samples were initially oven-dried and two were

initially saturated. The mass of the soil samples inside each chamber was monitored until there was no difference in masses between two consecutive weightings on two different days.
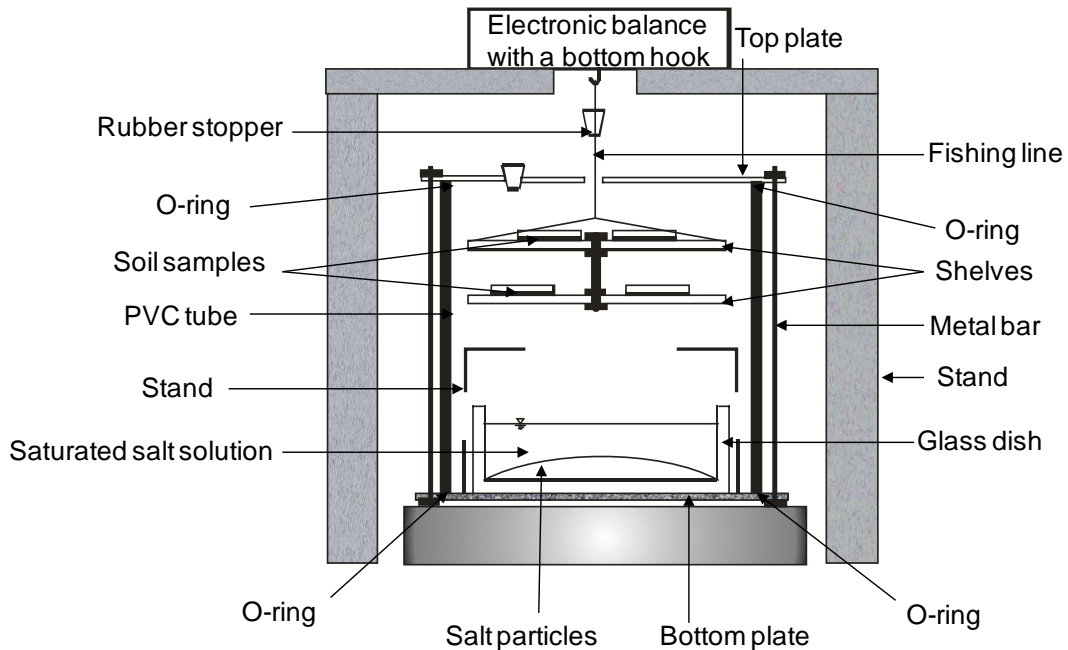


Figure 4.12 A schematic diagram of the set-up for the SWCC measurements of the selected soils using vapour pressure methods

Before placing the soil samples in each ATC, about 400–500 cc of a selected saturated salt solution of known osmotic suction was prepared and poured into a glass dish. The glass dish was placed at the bottom of the air-tight chamber. Using a pair of shelves, eight individual soil samples were placed inside the chamber on a stand. Two lengths of fishing line were attached to the top Plexiglass shelf to allow the samples to be easily lifted from the stand for weighing. The fishing lines passed through a hole made in the top plate of the chamber. The mass of the shelves along with the soil samples was monitored, without removing the soil samples from the chamber, using an electronic balance with a bottom hook (see Figure 4.12). The mass changes with time due to adsorption or desorption were recorded. An equilibrium condition was assumed to be reached when the weight stayed constant. The higher the relative humidity inside the chamber, the more time was required for equilibration. At equilibrium conditions, the relative humidity within the soil pores becomes the same as the relative humidity of the

121

environment inside the chamber created by the saturated salt solution. An independent measurement of the relative humidity inside the ATC was taken using the portable Traceable Hygrometer.

After the equilibrium conditions were reached, four soil samples (i.e., two samples of each soil type, one oven-dried and one saturated) were taken from each chamber. The gravimetrical water contents were measured. To prevent the samples from absorbing or loosing water through evaporation, immediately after the sample was taken out from the chamber the lid was put on the soil container. Each sample was weighed in a short period of time (i.e., in the order of seconds). The precision of the electronic balance for the measurement of water contents was 0.0001 g. The other four samples from each chamber were used to measure total soil suction values with the WP4-T device.

## 4.6    LABORATORY TESTING PROGRAM FOR ONE-DIMENSIONAL EVAPORATION PROCESSES

A series of evaporation column tests were conducted in an environmentally controlled room to measure the unsaturated coefficient of permeability of the selected soils around the residual-state condition. The laboratory testing equipment, design of the evaporation columns, sample preparation, instrumentation, and testing procedure are described in this section.

The main purpose of using the environmentally controlled room for conducting the evaporation tests was to have a controlled temperature and relative humidity so that a steady-state flow condition could be achieved at the end of the evaporation processes. The combination of temperature of about 25 $^\circ$C and relative humidity of about 26% were chosen to generate a suction value of about 165,000 kPa. This suction value was assumed to be large enough to establish a dry condition in the top portion of the soil. It was anticipated that at the end of the evaporation processes, water content at some locations along the soil profile would drop lower than the residual water content.

### 4.6.1   Laboratory Testing Equipment

The laboratory equipment used for the evaporation processes consisted of an environmentally controlled chamber, evaporation column, T-type thermocouples, a Campbell Scientific data logger (CR1000), Geotechnical Digital System (GDS) (i.e.,

volume/pressure controller), a Mariotte column, an Ohaus Explorer electronic balance and a balance talk software, a lamp and relay system, and a small computer fan. The following sections explain some of these components in a greater detail.

### 4.6.1.1  Environmentally Controlled Room

Constant ambient temperature and relative humidity are essential in order to reach a steady-state condition during the evaporation processes. The Controlled-Environment Facility (CEF) at the University of Saskatchewan consists of 183 environmentally controlled reach-in cabinets and walk-in rooms. Walk-in rooms (Model PGV36) were suitable for the proposed research studies. The interior dimensions of the walk-in rooms were W (226 cm) × D (245 cm) × H (203 cm).  The temperature of the room could be controlled in the ranges of 4–45 $^{\circ}$C and 10–45 $^{\circ}$C with lights off and with lights on, respectively. Most of the walk-in rooms were also capable of controlling additive humidity. In other words, the rooms had the capability of increasing the humidity inside the chamber compared to the outside ambient humidity. Only three of the walk-in rooms were equipped with dehumidifiers (Model HC300 and manufactured by Cargocaire) and had the capability of dehumidification using a chemical dryer.

At the time of starting the evaporation processes, all three chambers equipped with dehumidifiers were occupied and tests were being conducted for three years inside those chambers. Therefore, it was decided to start primary evaporation processes using one of the walk-in chambers with additive relative humidity control until a chamber with dehumidifier became available. To minimize the humidity fluctuations inside the chamber with additive humidity control, any opening into the chamber, including the vents, was covered with thick plastic sheets. Relative humidity and temperature inside the chamber were monitored for a couple of weeks.

It was observed that the relative humidity fluctuated less at higher temperatures than at lower ones. The fluctuation of relative humidity was even in the negligible range when the temperature was high. However, it was quite high for lower temperatures. The primary tests were conducted at a temperature of 30 $^{\circ}$C and a relative humidity of 40%.

After a couple of months of some primary evaporation processes inside the chamber with the additive humidity control, a chamber with a dehumidifier became available. The rest of the evaporation processes were conducted inside the new chamber. Most of

the evaporation processes, and also the SWCC measurements using the vapour pressure techniques (i.e., osmotic desiccation, Air-Tight Chamber, and WP4-T device), were conducted inside the chamber with dehumidifier at a constant temperature in the range of 25–26 $^{\circ}$C and a constant relative humidity in the range of 25–26 %.

### 4.6.1.2 Evaporation Columns

Two evaporation columns: the primary evaporation column and modified evaporation column, were designed for use as a central part of this study. The columns were made in Engineering Shops at the University of Saskatchewan, Saskatoon. The primary evaporation column was originally intended to be used for all of the evaporation processes. However, the Botkin silt specimens developed horizontal and vertical cracks during evaporation processes when the primary column was used. The modified evaporation column was designed and manufactured to resolve this problem.

Figure 4.13 shows a schematic diagram of the designed primary evaporation soil column. The column was consisted of a Plexiglass tube, a porous plate, and a grooved pedestal. The Plexiglass tube had an inside diameter of 69.8 mm and height of 159.2 mm. Eight holes were drilled along the sides of the primary column for the installation of thermocouples. Some ports were also drilled around the perimeter of the tube to retrieve soil samples for gravimetric water content and/or electrical conductivity measurements. The sampling ports in the top 40 mm of the column were smaller (5 mm in diameter), allowing sampling at closer proximities. There were three sampling ports around the perimeter of the evaporation column for each sampling layer in the top section of the column. The ports in the lower part of the column had a diameter of 10 mm. There were total of 18 sampling layers along the column. The distances from the top of the evaporation column to the center of the sampling ports are summarized in Table 4.8.

Figure 4.14 shows a schematic diagram of the modified evaporation soil column. The column consisted of a Plexiglass tube, a porous plate, and a grooved pedestal. The Plexiglass tube had an inside diameter of 69.8 mm and height of 75 mm. Five holes were drilled along the sides of the column for installing thermocouples and retrieving soil samples. The distances from center of the sampling ports along the column from top of the evaporation column are summarized in Table 4.8.

124

The sampling ports in both primary and modified evaporation columns were plugged using rubber stoppers during the evaporation processes. A heat insulation jacket (i.e., Fiberglass tube) was used around the column to prevent horizontal heat transfer during the evaporation processes. A porous plate was placed on the grooved pedestal. The Plexiglass tube was attached to the pedestal using five bolts and nuts as shown in the Figure 4.13 and 4.14. O-rings were used between the Plexiglass tube and the pedestal to prevent water leakage during the evaporation processes. Figure 4.15 shows a schematic diagram of the pedestal. The inside surface of the pedestal was grooved for even distribution of the water into the soil column.
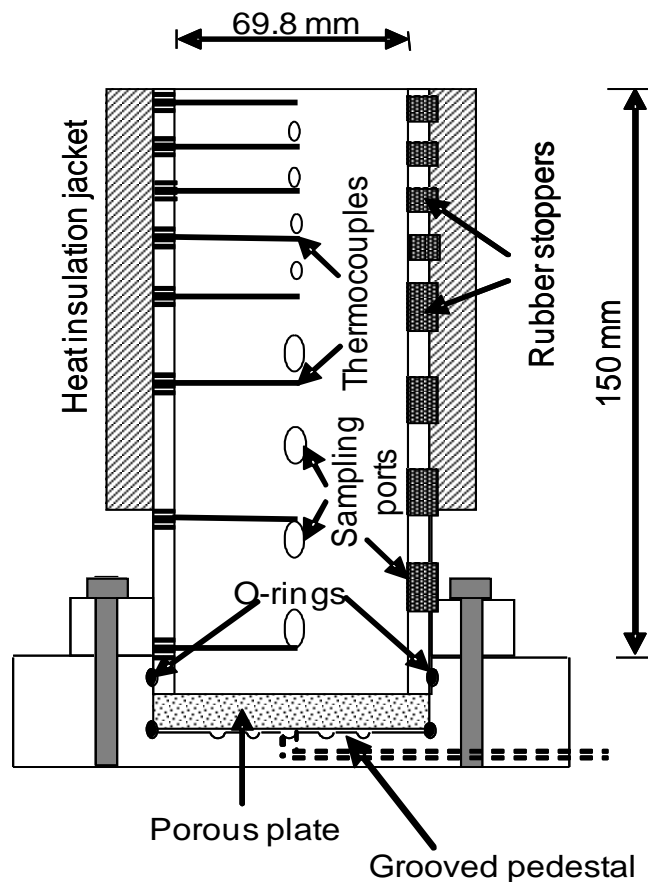


Figure 4.13 A schematic diagram of the primary evaporation column used in evaporation processes

Extension column = 40mm at top

69.8 mm

Thermocouples

75 mm

Porous plate

Grooved pedestal
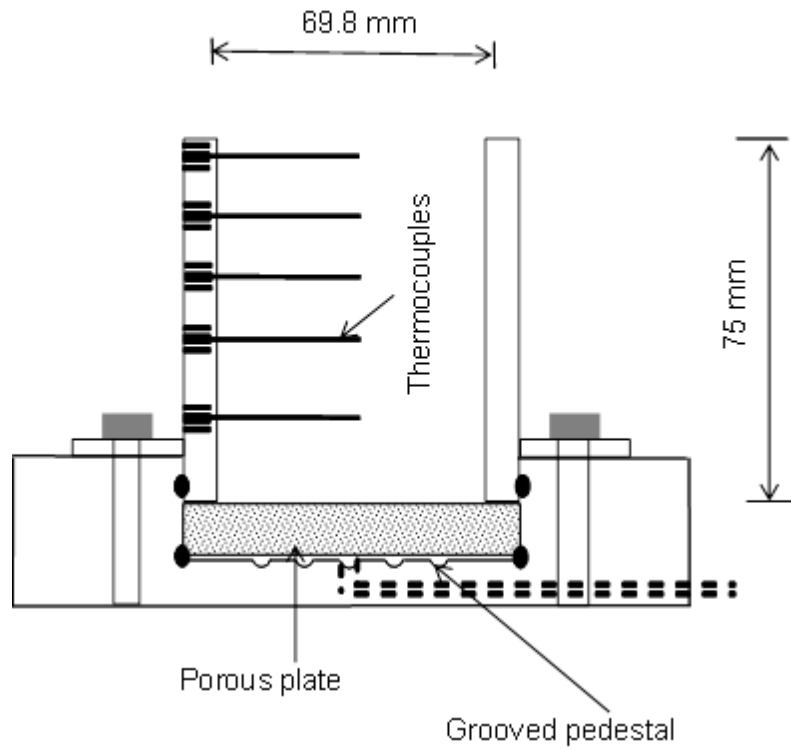
Figure 4.14 A schematic diagram of the modified evaporation column used in
evaporation processes

82

141
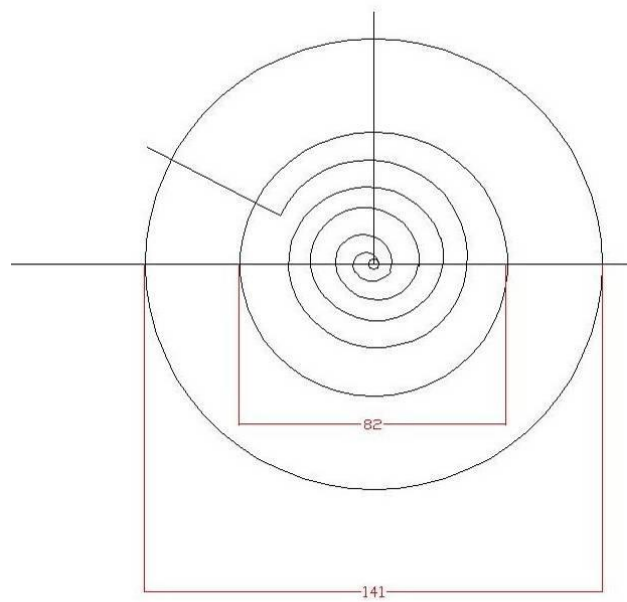
Figure 4.15 Schematic diagram of the pedestal

Table 4.8 Distance of the sampling ports from top edge of the primary and modified
     evaporation column

| Sampling Port No | Distance from top edge of the primary evaporation column, mm | Distance from top edge of the modified evaporation column, mm |
| --- | --- | --- |
| 1 | 5.2 | 5 |
| 2 | 10.3 | 15 |
| 3 | 15.4 | 25 |
| 4 | 20.5 | 35 |
| 5 | 25.6 | 50 |
| 6 | 30.7 | |
| 7 | 35.8 | |
| 8 | 40.9 | |
| 9 | 50.5 | |
| 10 | 60.4 | |
| 11 | 70.3 | |
| 12 | 80.5 | |
| 13 | 90.5 | |
| 14 | 100.5 | |
| 15 | 110.5 | |
| 16 | 120.5 | |
| 17 | 130.5 | |
| 18 | 140.5 | |

### 4.6.1.3  Thermocouples

T-type thermocouples were used to measure the temperature above and within the soils
along the evaporation columns during the evaporation processes. There were ten
thermocouples, two for the measurement of the temperature above the *primary*

*evaporation column* and eight for the measurement of the temperature within the column at different depths. The length of the thermocouples was 1,100 mm. Stainless steel pins with a diameter of 1.5 mm were attached to one end of the thermocouples in order to facilitate the insertion of the thermocouples into the soil column. The other ends of the thermocouples were attached to a Campbell Scientific data logger for automatic recording of temperatures. Details related to the data logger are explained in the next section. Distances between the center of the thermocouples from the top edge of the evaporation column are summarized in Table 4.9.

Similar thermocouples were used for measuring the temperature above and along the *modified evaporation column*. It was initially decided to use a total number of seven thermocouples, two for the measurement of the temperature above the modified evaporation column to measure the ambient temperature, and five within the modified evaporation column at different depths. The number of thermocouples used in some of the evaporation processes using the modified evaporation column was adjusted. The sampling ports along the modified evaporation column were used as thermocouple ports as well. The distances between the centers of the sampling ports (i.e., thermocouple ports) from the top edge of the modified evaporation column are summarized in Table 4.8.

Table 4.9 Distances of the center of the thermocouple ports from top edge of the primary evaporation column

| Thermocouples | Distance from surface of the column, mm |
|---|---|
| 1 | 4.5 |
| 2 | 14.5 |
| 3 | 24.5 |
| 4 | 34.5 |
| 5 | 49.4 |
| 6 | 72.1 |
| 7 | 112.5 |
| 8 | 147.0 |

### 4.6.1.4 Campbell Scientific Data Logger

A Model CR1000 Campbell Scientific data logger was used for two purposes: i) to collect readings from thermocouples placed above and within the soil column during the evaporation processes at specified time increments, and ii) to control the temperature at the surface of the soil column and keep it constant around the ambient temperature.

Figure 4.16 shows the Campbell Scientific data logger along with its compartments inside a box. The original data logger had 8 ports for attaching thermocouples. As 10 thermocouples were needed with some of evaporation processes, a multiplexer was used to extend the number of available ports. All thermocouples were referenced to a single reference temperature.

In order to control the temperature at the surface of the soil, a relay system with a bulb was installed on the data logger. The data logger was programmed so that it was possible to turn the bulb on and off based on the temperature reading at the surface of the soil.
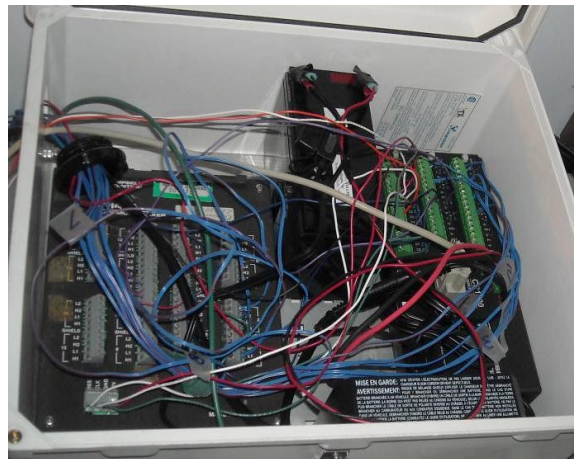


Figure 4.16 Campbell Scientific data logger (CR1000)

### 4.6.1.5 Geotechnical Digital System (GDS Volume-Pressure Controller)

To reach a steady-state condition during the evaporation process, it was necessary to accurately apply a very small and constant inflow of water to the soil column. Different syringe pumps available in the Environmental Laboratory of the Department of Civil and Geological Engineering at the University of Saskatchewan were tested for their suitability. None of them were found suitable for the purpose of the current research. A

GDS volume-pressure controller system was then tested for its suitability. It was found that the GDS system was capable of applying small and accurate constant inflow. Both pressure and water volume can be controlled during a test using a GDS system.

A GDS volume-pressure controller was located inside the environmentally controlled room and left there for 48 hours. The system was turned on and emptied of any fluid. Then the system was filled with the distilled water. The empty function pressed to remove all water along with air bubbles which were visible through the plastic tubing. A plastic connector was used to connect the GDS volume-pressure controller to the base of the soil column through flexible tubes. The ramp function was used to program the system in order to transfer a given constant water flow to the soil column. The system was programmed to operate manually. The following steps were followed in order to get a flow rate of 0.36 $cm^3$/ hr.

1- The ramp key was pressed.
2- Number 9 was pressed for the "slope CM" key to apply the unit "second" for time.
3- A "slope value" of 10 was entered.
4- A "slope value" of 10 was entered.
5- A lower value of -900,000 $mm^3$ was entered for the lower volume.
6- The value shown on the LCD screen of the GDS controller was entered as the upper value for the volume.
7- A function value of 47, defined as "volume ramp/cycle, negative slope" was entered. It should be noted that there are other function values available for different volume and pressure controls.
8- The "OK" key was entered in order to commence the discharge.

Slope value is the most important parameter when using a given outflow from the GDS volume-pressure controller. The slope value indicates the time per unit volume in s/$mm^3$. For example, a slope value of 10 means it takes 10 seconds for 1 $mm^3$ water to discharge from the system (i.e., 0.1 $mm^3$/s or 0.36 $cm^3$/hr). Table 4.10 indicates the expected discharge rates from the GDS device for different slope values from 1 to 10.

Table 4.10 Expected discharges from the GDS device for different "slope values" from 1
       to 10

| Slope value | Expected discharge from the GDS system ($cm^3$/hr) |
|---|---|
| 1 | 3.6 |
| 2 | 1.8 |
| 3 | 1.2 |
| 4 | 0.9 |
| 5 | 0.72 |
| 6 | 0.6 |
| 7 | 0.51 |
| 8 | 0.45 |
| 9 | 0.4 |
| 10 | 0.36 |

To avoid any possible errors during the evaporation processes and to evaluate the performance of the GDS volume-pressure controller used in this research, a simple procedure was carried out to check the accuracy of the device. Figure 4.17 shows the set-up for evaluating the GDS apparatus. The device was programmed to discharge distilled water at two different rates, namely, 3.6 and 0.72 $cm^3$/hr (i.e., slope values of 1 and 5). The volume of water discharged from the GDS volume-pressure controller was collected and measured using a graduated laboratory tube. The results are summarized in Tables 4.11 and 4.12 for a slope of 1 and 5, respectively. The accuracy of the readings was in the order of 0.03 $cm^3$ which could be due to error in measuring the collected volume of water.

Figure 4.17 Set-up for evaluating the performance of GDS

Table 4.11 Evaluating of the GDS for discharge rate of 3.6 cm$^3$/hr (i.e., slope value = 1)

| t (min) | Burette readings (cc) | GDS controller readings (cc) | Difference in readings from Burette (cc) | Difference in readings from GDS controller , mm$^3$  (cc) |
|---|---|---|---|---|
| 0 | 2.5 | 973937 | ---- | ---- |
| 15 | 3.4 | 973029 | 0.9 | 898 (0.898) |
| 30 | 4.3 | 972100 | 0.9 | 929 (0.929) |
| 45 | 5.2 | 971200 | 0.9 | 900 (0.900) |
| 60 | 6.10 | 970300 | 0.9 | 900 (0.900) |

**4.6.1.6  Mariotte Column**

A Mariotte column was used to control the water level within the soil at a desired constant distance from top of the soil column during evaporation process. Figure 4.18 shows the schematic diagram of the Mariotte column made in the environmental laboratory with the help of the Environmental Laboratory technician in the Department of Civil and Geological Engineering, University of Saskatchewan.

Table 4.12 Evaluating of the GDS for discharge rate of 0.72 cm$^3$/hr (i.e., slope value = 5)

| t (min) | Burette readings (cc) | GDS controller readings (mm$^3$) | Difference in readings from Burette (cc) | Difference in readings from GDS controller, mm$^3$ (cc) |
|---------|-----------------------|----------------------------------|------------------------------------------|---------------------------------------------------------|
| 0 | 1.74 | 968934 | ---- | ---- |
| 15 | 1.57 | 968754 | 0.170 | 180 (0.180) |
| 30 | 1.40 | 968573 | 0.170 | 181 (0.180) |
| 45 | 1.23 | 968393 | 0.170 | 180 (0.180) |

The Mariotte column consisted of a long tube (L =1,200 mm) with an inner diameter of 40 mm. Rubber stoppers with a hole in the middle were attached to two ends of the tube. A long glass tube with a length of about 1,150 mm was inserted through the top rubber stopper. The fit was tight enough to be air-proofed. The inner tube must be open to the atmosphere in order to create atmospheric pressure at the other end of the tube. To minimize evaporation errors, a rubber cap was installed on top of the glass tube and a needle was inserted through the rubber cap. A short glass tube (100 mm) was inserted through the bottom rubber stopper. A flexible tube was attached to the short glass tube to direct water into the bottom of the evaporation column. The main tube of the Mariotte bottle was graduated using a graduated tape in millimeters. The level of the water in the evaporation column attached to the Mariotte column is maintained at the same level as the end of the inner tube (see the location of the air bubble shown in Figure 4.18) provided the valve is open.

### 4.6.1.7   Electronic Balances and Balance Talk Software

Two electronic balances were used during the evaporation processes: the Ohaus Explorer balance and the Metler Toledo – AG204 balance. The maximum capacity of the Ohaus Explorer balance was 4,100 g with the readability of 0.01 g. The balance was mainly used to measure the mass of the evaporation soil column during evaporation processes. The balance had the capability of automatically recording the masses at specified time increments. To record the data, "balance talk" software was installed on a

computer and the balance was attached to the computer through a cable. It should be noted that although the balance cable was identical in appearance to a nine-pin computer cable, the computer cable did not work with the balance. A suitable cable was ordered through the Ohaus Company as it was not included with the balance. The balance was set to record the mass of the soil column at 10-minute increments.
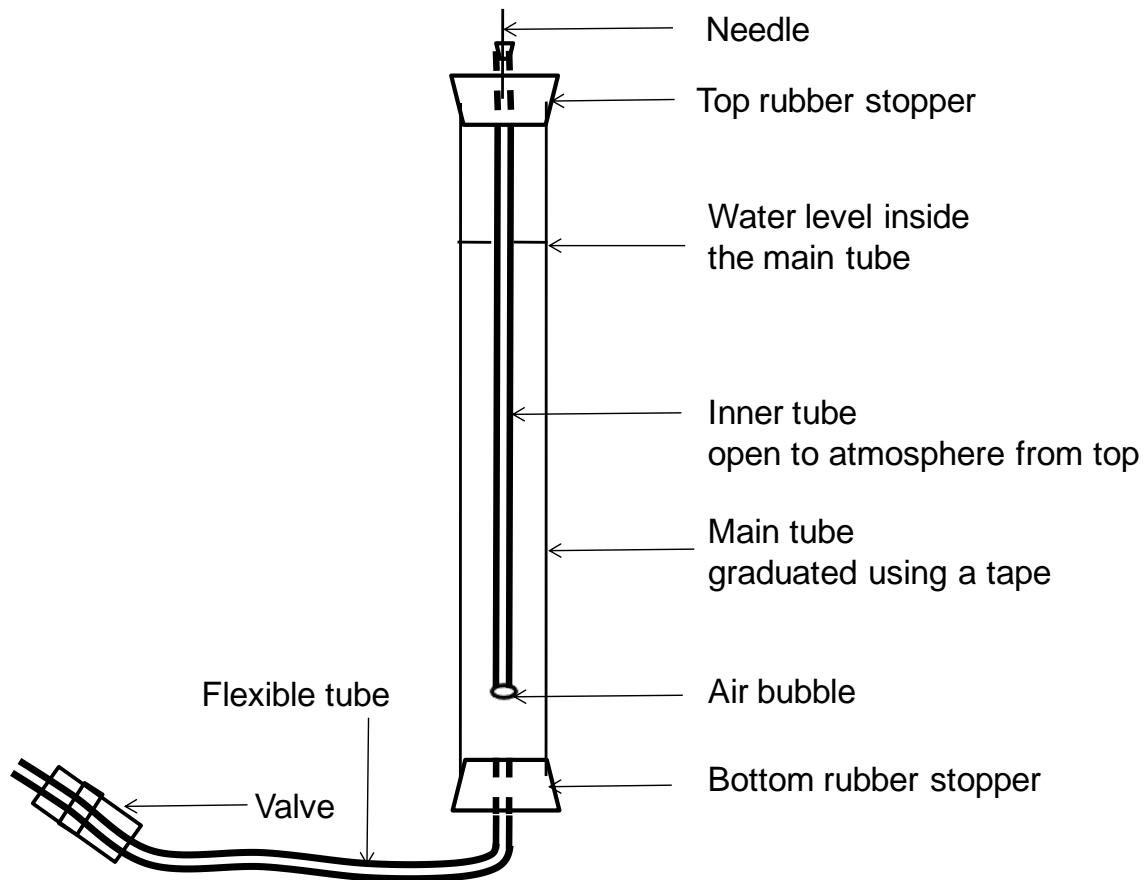


Figure 4.18 Schematic diagram of the Mariotte column

The maximum capacity of the Metler Toledo – AG204 balance was 210 g with a readability of 0.0001 g. This balance was mainly used to measure mass of the soil samples taken from the soil column at the end of the evaporation processes.

### 4.6.2   Preparation of the Soil Columns for the Evaporation Processes

Different test procedures were used for the preparation of the Beaver Creek sand and the Botkin silt evaporation soil columns. The test procedures are described in the following

sections. The letters P and M in front of the sample designations refer to the *primary* and the *modified* evaporation column, respectively.

### 4.6.2.1 Preparation of the Primary and Modified Evaporation Soil Columns for Beaver Creek Sand

Two kinds of evaporation soil columns were prepared for primary evaporation processes with Beaver Creek sand: a saturated slurry sand column and a consolidated sand column. The preparation procedures are explained in this section.

The following steps were used for preparation of the primary evaporation columns using slurry saturated soil.

1- The base of the primary evaporation column (i.e., grooved pedestal) was filled with distilled water and a pre-saturated porous plate (with an air-entry value of either 100 kPa or 1.8 kPa) was placed in the pedestal. A detail on design of the pedestal was described in section 4.6.1.2 (see Figure 4.15). O-rings were placed on top and bottom of the porous plate to prevent water leakage.

2- The Plexiglass column constructed for the evaporation process was placed on the pre-saturated plate and fastened to the pedestal using five bolts. A detail on design of the primary evaporation column was described in section 4.6.1.2 (see Figure 4.13). The thermocouple and sampling ports along the evaporation column were closed with tight rubber stoppers.

3- The evaporation column was filled with the prepared slurry sand with a gravimetric water content of 27%. The evaporation column was gently tapped a few times while it was being filled.

4- The top of the evaporation column was covered with a lid to prevent evaporation.

5- The sample was then transferred to the environmentally controlled room.

The following steps were followed for preparation of the primary evaporation column with consolidated sand:

1- 2000 g of air-dried Beaver Creek sand was mixed with 340 g of distilled water to produce a gravimetric water content of 17%.

2- The soil was left in a plastic container with a tight lid for a day, and was mixed occasionally in order to produce a soil sample of uniform water content.

3- The Plexiglass column manufactured for the primary evaporation process was extended using a small piece (i.e., 30 mm in length) of a Plexiglass tube with the same diameter as the column. The thermocouple and sampling ports along the evaporation column were closed using tight rubber stoppers.

4- The wet soil sample was poured into the evaporation column. A vertical load of 1,450 kg (i.e., vertical stress of 3870 kPa ) was applied from the top of the soil through the load cap using a high pressure consolidation load frame.

5- After consolidating the soil inside the column, the extended tube was removed. The extra soil was carefully trimmed from top of the column using a piece of fishing line.

6-  The evaporation soil column was placed on the pre-saturated plate and fastened to the pedestal using five bolts.

7-  The top of the evaporation column was covered with a tight lid.

8-  The sample was then transferred to the environmentally-controlled room.

For the modified evaporation column, the saturated Beaver Creek sand was placed inside the modified evaporation column and consolidated to 200 kPa. A detail on design of the modified evaporation column was described in section 4.6.1.2 (see Figure 4.14). An extension tube was attached to the column during consolidation. Steps 5 to 8 above were then followed.

Soil specimens for the evaporation tests and the SWCC tests were prepared using similar procedures. For the SWCC specimens, soil samples were extruded into the stainless steel sample holders after step 5 of preparation of the compressed sand column (see section 4.4.2).

### 4.6.2.2  Preparation of the Primary and Modified Evaporation Soil Columns for Botkin Silt

Two kinds of evaporation soil columns were prepared for the primary evaporation processes on the Botkin silt: the slurry Botkin silt column, and the consolidated Botkin

136

silt column. With the modified evaporation column, only the consolidated silt column was prepared.

The following steps were used for preparation of the primary evaporation column using slurry soil:

1- In a plastic container, 3,000 grams of air-dried Botkin silt soil was mixed with 1,080 grams of distilled water to produce the saturated slurry with a gravimetric water content of 36%. The lid of the plastic container was tightened and the slurry was mixed a couple of times every day in order to get rid of entrapped air bubbles and to create uniform slurry. After 72 hours, two soil samples were taken from the saturated slurry to measure the gravimetric water content of the slurry before starting the consolidation process.

2- The base of the evaporation column (i.e., grooved pedestal) was filled with distilled water, and a pre-saturated porous plate (with an air-entry value of either 100 kPa or 1.8 kPa) was placed in the pedestal. A detail on design of the pedestal was described in section 4.6.1.2 (see Figure 4.15). O-rings were placed on the top and bottom of the porous plate to prevent the water leakage.

3- The Plexiglass cell was placed on the pre-saturated plate and fastened to the pedestal through five bolts. The details of the design of the primary evaporation column were described in section 4.6.1.2 (see Figure 4.13). The thermocouple and sampling ports along the evaporation column were closed with tight rubber stoppers.

4- The evaporation column was filled with prepared slurry Botkin silt with a gravimetric water content of 36%. The soil inside the evaporation column was gently mixed with spatula a few times while the column was being filled to remove air bubbles.

5- The top of the evaporation column was covered using a tight lid.

6- The sample was then transferred to the environmentally controlled room.

For preparation of the primary evaporation column with consolidated Botkin silt the following steps were followed:

1- The slurry was poured into the consolidation cell (208 mm high and 113 mm in diameter). The consolidation cell was used for preparation of the SWCC specimens. Details on the consolidation cell and its compartments were described in section 4.5.2 (see Figure 4.9). The bottom plate was grooved and could collect the water under the consolidated sample and be directed outside the system through two attached drainage tubes. The consolidation cell was attached to the bottom plate and water proofed using an O-ring around the bottom plate. Vacuum grease was used on the O-ring to prevent possible water leakage. The slurry soil with the determined water content was poured into the consolidation cell. While the column was being filled an attempt was made to remove any air bubbles by mixing the slurry using a spatula. A porous plate, similar to the one at the bottom of the column, was placed on top of the soil. A stainless steel load plate was placed on top of the porous plate. The column was placed in a consolidation apparatus and a token load of 1,800 g was applied.

2- The vertical deflection verses elapsed time was monitored using a dial gauge. The load was increased in two steps.

3- After completion of the consolidation test, the soil specimen was transferred to the designed column for the evaporation process. The consolidation cell was carefully removed from its bottom plate. A metal column with a smaller diameter than the consolidation column was placed on the table. The soil was extracted from the cell by pushing from the bottom through the porous plate. The top porous plate was removed using a piece of fishing line.

4- The consolidated soil specimen was carefully trimmed into the primary evaporation cell (see Figure 4.19). While trimming the specimen, three soil samples from the top, middle, and bottom sections of the soil column were taken to measure the final water content of the consolidated soil. Silicon lubricant was sprayed on the inner surface of the evaporation column, to prevent soil cracking during transfer from the consolidation cell to the evaporation column and also during the evaporation process as a result of desiccation.

5- The evaporation soil column was placed on the pre-saturated plate and fastened to the pedestal using five bolts.

6- The top of the evaporation column was covered using a tight lid.

7- The sample was then transferred to the environmentally controlled room and left for 24 hours for equilibration.

For the modified evaporation column, two soil columns, hereafter referred to as MCS1 and MCS2, were prepared. For preparation of the MCS1, the Botkin silt slurry was placed directly inside the designed modified evaporation column and consolidated to 100 kPa. A detail on design of the modified evaporation column was described in Section 4.6.1.2 (see Figure 4.14). An extension tube was attached to the column during consolidation. After completing the consolidation test the extension tube was removed. The sample was trimmed from top of the modified evaporation column. Rubber stoppers were removed and replaced with five T-type thermocouples which were inserted horizontally into the soil columns. The soil column was transferred to the environmentally controlled room for evaporation process.



Figure 4.19 Transferring the consolidated soil specimen into the primary evaporation column

For preparation of Specimen MCS2, a triaxial rubber tube was placed between the inner wall of the modified evaporation column and the slurry soil. It was expected that the rubber tube would prevent the evaporation from the side surface of the sample

during evaporation process. The slurry soil was consolidated to a maximum vertical load of 50 kPa. The extra part of the rubber tube was then removed from top of the soil. The soil was trimmed and the surface of the soil was covered. The prepared evaporation soil column was transferred to the environmentally controlled room.

### 4.6.3   Procedures of the Evaporation Processes

Preparation of the evaporation specimens for Beaver Creek sand and Botkin silt soils was described in sections 4.6.2.1 and 4.6.2.2, respectively. Ten sets of evaporation processes were conducted on the prepared specimens. These evaporation processes will be referred to as PS1, PS2, PS3, PS4, PS5, and MS1 for evaporation processes conducted on Beaver Creek sand specimens, and as PCS1, PCS2, MCS1, and MCS2 for the evaporation processes conducted on Botkin silt specimens (see Table 4.13). In the specimen labeling, the letters P and M stand for Primary and Modified referring to the primary evaporation column and the modified evaporation column, respectively. The letters S and CS stand for sand and clayey silt referring to Beaver Creek sand and Botkin silt soils, respectively. The number at the end of each label refers to the specimen number.

The evaporation soil processes were conducted in the environmentally controlled room. Only one evaporation process was conducted at a time. Information on the soil and the environment conditions for the evaporation processes are summarized in Table 4.13. Both temperature and relative humidity were controlled in the environmentally controlled room. The room temperature and humidity were kept constant during the evaporation processes. The temperature was about 25–26 $^{\circ}$C and the relative humidity was about 25–26% for most of the experiments. For evaporation Process PS1, a different room temperature and relative humidity was used as the test was conducted in a different chamber which was limited to additive humidity control (see Table 4.13). To minimize the effect of radiation on evaporation, all lights were turned off during the evaporation processes. The temperature and relative humidity in the room were also recorded using two Hobo data loggers.

Figures 4.20 and 4.21 show the schematic diagrams of the evaporation processes set-ups for the primary and modified evaporation column tests, respectively. The main differences between these two set-ups are: the height of the columns (150 mm versus 75

mm) and the number of thermocouples installed along each column (8 versus 5). Additionally, the relay and bulb system was not used with the modified evaporation column.

After the evaporation soil column was prepared, it was transferred to the environmentally controlled room. The soil column was then placed on an electronic balance. The thermocouples were attached to a CR1000 Campbell Scientific data logger (section 4.6.1.4). The thermocouples were horizontally inserted into the evaporation column through the designated temperature ports. They were passed through rubber stoppers to prevent water leakage. Ambient temperature above the soil column was also monitored using one or two thermocouples.

The soil column was saturated by applying a slow flow of distilled water from the bottom of the column using the Mariotte column. After saturation, the top of the soil was covered tight with a plastic lid, which was open to the atmosphere through a small hole. The column was left in the environmentally controlled room for a few hours until thermodynamic equilibrium was achieved. The equilibration of the soil columns was determined by monitoring the temperature changes. When the temperature was the same along the entire soil column and approximately equal to the ambient temperature, thermodynamic equilibration was presumed. A fiberglass insulation tube was cut and placed around the top part of the column to prevent horizontal heat transfer. Two pieces of Velcro were used to tighten the fiberglass around the evaporation column.

The CR1000 data logger was programmed to control the temperature along the column. A system of relay and lamp was used for this purpose. A 60 or 30 Watt lamp was placed above the soil column. A relay was used to automatically switch the lamp on and off. The first thermocouple in the soil was 4 mm from the soil surface and was programmed so that when the temperature in the surface of the soil passed the air temperature by about 0.1 degree, the lamp would shut off and when temperature dropped about 0.1 degree below the ambient temperature the lamp would turn on. By so doing, the temperature was kept constant at the surface of the soil column. A program was written for the data logger in order to record the temperature data and control the temperature at the surface of the soil.

Table 4.13 Summary of evaporation processes conducted on Beaver Creek sand (PS and MS) and Botkin silt (PCS and MCS) specimens

| Experiment Number | Soil | Initial Condition | Device Used for Controlling Inflow Rate | Inflow Rate (mm/day) | Air Entry Value of Bottom Plate (kPa) | Boundary Conditions Top | Room *RH(%) | Room Temperature (°C) |
|---|---|---|---|---|---|---|---|---|
| PS1 | Sand | Slurry | GDS volume/pressure controller | Start = 11.49; End = 5.74 | 1.8 | ** "W & R" Treatment | 40 | 30 |
| PS2 | Sand | Slurry | GDS volume/pressure controller | 5.74 | 1.8 | *** "W" Treatment | 25.3 | 25.8 |
| PS3 | Sand | Slurry | GDS volume/pressure controller | 5.74 | 1.8 | "W & R" Treatment | 25.5 | 26 |
| PS4 | Sand | Compressed | GDS volume/pressure controller | 2.3 | 100 | "W" Treatment | 26 | 25 |
| PS5 | Sand | Compressed | Mariotte Bottle | Controlled by Evaporation | 1.8 | "W" Treatment | 25 | 25.5 |
| PCS1 | Silt | Slurry | GDS volume/pressure controller | 5.74 | 1.8 | "W" Treatment | 26 | 25 |
| PCS2 | Silt | Consolidated to 20 kPa | GDS volume/pressure controller | 2.3 and 11.5 | 100 | "W" Treatment | 26 | 25 |
| MS1 | Sand | Consolidated to 200 kPa | GDS volume/pressure controller | 5.7 and 4.6 | 100 | "W" Treatment | 26 | 25.5 |
| MCS1 | Silt | Consolidated to 100 kPa | GDS volume/pressure controller | 11.5 | 100 | "W" Treatment | 26 | 25.5 |
| MCS2 | Silt | Consolidated to 50 kPa | GDS volume/pressure controller | 1.13 | 100 | No "R" No "W" | 26 | 25.5 |

* Relative Humidity      ** "Wind and Radiation" Treatment      *** "Wind" Treatment
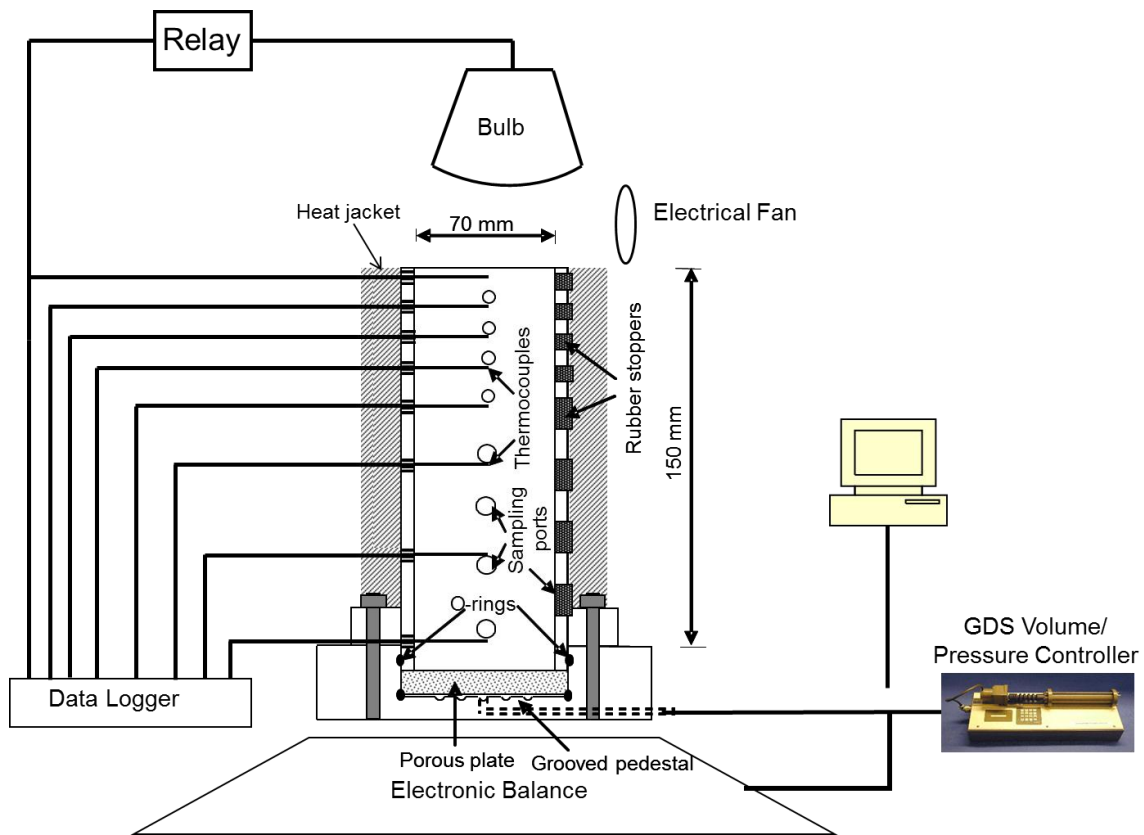
Figure 4.20 A schematic diagram of the experimental set-up for a primary evaporation
column test
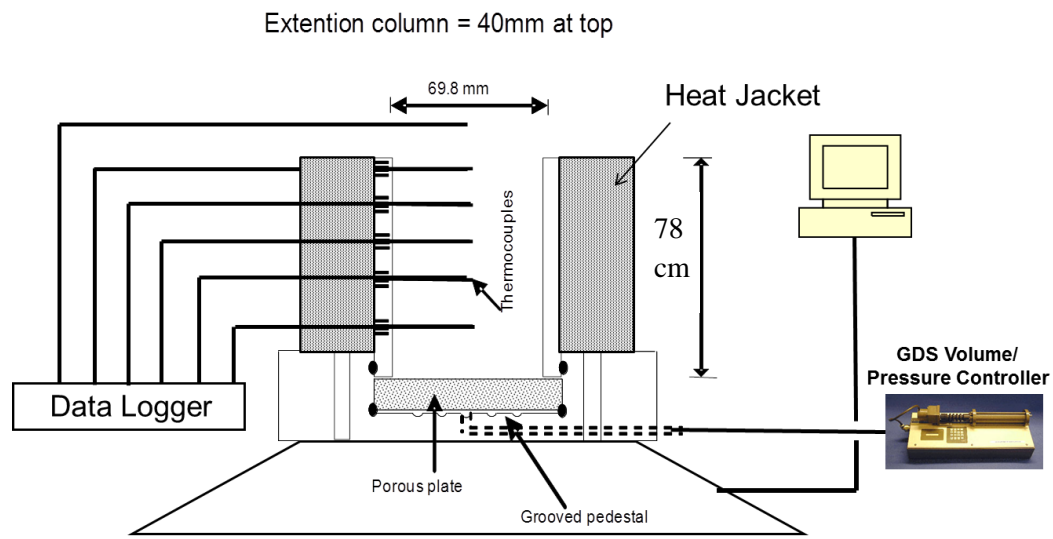


Figure 4.21 A schematic diagram of the experimental set-up for a modified evaporation
column test

The evaporation processes were conducted using three types of top boundary conditions: i) radiation and wind treatment, ii) wind treatment, or iii) no-radiation–no-wind treatment. For evaporation processes conducted under the "radiation and wind treatment", an attempt was made to keep the temperature constant and equal to the room temperature along the soil column. A system comprised of a relay and lamp was used to control the temperature of the soil surface (Figure 4.20). A small computer fan was placed above the evaporation soil column as a wind source.

A GDS volume/pressure controller (section 4.6.1.5) was attached to the column from the bottom through a plastic tube and a connector. The evaporation process was initiated by removing the lid. An electric fan was used above the column to promote evaporation. The mass of the soil column was recorded in 10-min time increments during the test (i.e., using an Ohaus electronic balance with a readability of 0.01g). The GDS volume/pressure controller was the source of pressure/volume control in all of the evaporation processes except in evaporation Process PS5. The Mariotte Bottle previously described in section 4.6.1.6 (see Figure 4.18) was replaced with the GDS volume/pressure controller for evaporation Process PS5. The GDS controller was programmed to control the inflow rate as a bottom boundary condition. At the end of the evaporation test soil samples were retrieved from different depths along the evaporation column, either through the sampling port or by sectioning the specimen, for gravimetric water content measurements.

A series of evaporation processes using the primary evaporation column filled with distilled water was conducted within the environmentally controlled room. The temperature and relative humidity of the room were set at $25^{\circ}$C and 26%, respectively. The temperature, relative humidity, and wind speed above the evaporation column were controlled to resemble environmental conditions during the actual evaporation processes. The rate of the mass change with respect to time data for the distilled water-filled column was used to calculate the potential evaporation rates. Temperature of the water at the distance of 5 mm from the surface of the column was measured using a thermocouple horizontally inserted into the water-filled column. Potential evaporation rates were measured under three different top boundary conditions: i) no-radiation–no-wind, ii) wind, and iii) wind and radiation.

# CHAPTER 5

# PRESENTATION OF THE LABORATORY TEST RESULTS

## 5.1 INTRODUCTION

This chapter presents results of the laboratory tests described in Chapter 4. Experimental results for the consolidation tests are presented in section 5.2; for the saturated coefficient of permeability tests, in section 5.3, for the soil-water characteristic curve (SWCC), in section 5.4, and for the primary and modified soil column evaporation processes, in section 5.5.

## 5.2 CONSOLIDATION TEST RESULTS

Test procedures for the consolidation and saturated coefficient of permeability were described in Chapter 4. The objectives of these tests were: i) to measure the saturated coefficient of permeability of the Beaver Creek sand and Botkin silt soils, and ii) to establish known initial conditions of the SWCC and evaporation tests specimens. For purposes of analysis in this thesis, it is necessary that the SWCC and evaporation test specimens have identical initial conditions. The SWCC and evaporation specimens were prepared using consolidation tests in order to create these conditions.

During preliminary evaporation tests, the Botkin silt specimens prepared from slurry conditions with no vertical stresses were cracked both vertically and horizontally. To help prevent the cracking problem, slurry soil samples were consolidated to different maximum vertical stresses, and the evaporation column was modified.

This section also presents deflection versus time plots for the consolidation tests during which the saturated coefficient of permeability was measured. The results of the saturated coefficient of permeability tests are presented in section 5.3.

Figures 5.1 and 5.2 show deflection versus time plots for each applied vertical pressure for specimens CS1-2 and CS2-2, respectively. Similar results were obtained for both samples to an applied pressure of 100kPa.
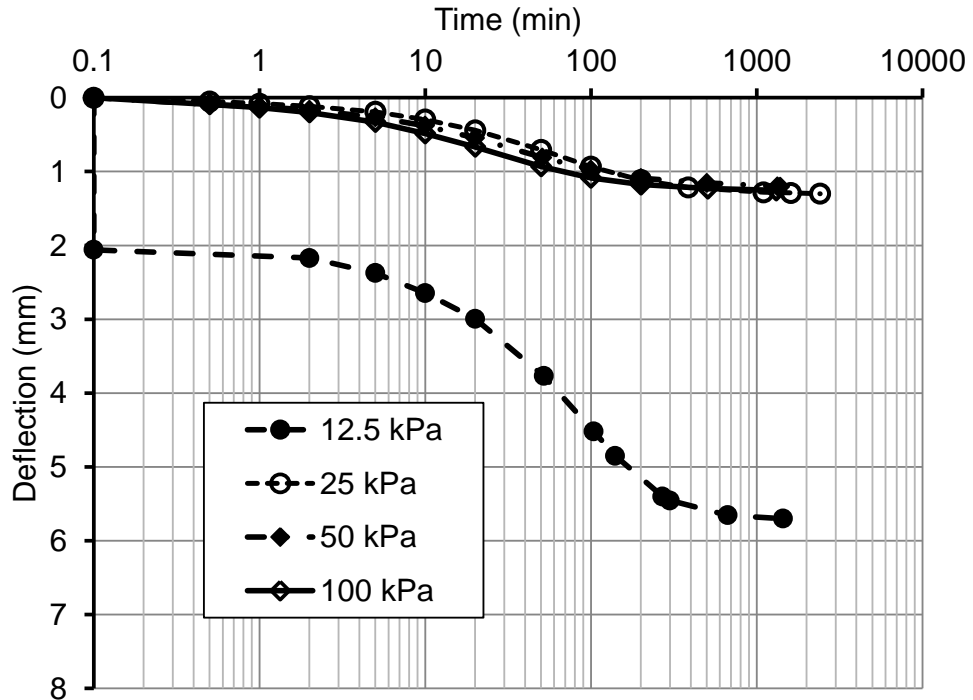


Figure 5.1 Deflection versus time for the consolidation test on Botkin silt (Specimen CS1-2)

## 5.3 SATURATED COEFFICIENT OF PERMEABILITY

The saturated coefficient of permeability was measured using the falling-head technique as described in Chapter 4, section 4.4. The falling-head procedure was conducted at the end of each vertical stress increment during consolidation tests. The purpose of the test was to determine the initial hydraulic condition (i.e., saturated coefficient of permeability) of the specimens used for the evaporation column test. This value is required for predicting the unsaturated coefficient of permeability. The consolidation/permeability tests were not intended to study the effect of volume change on the saturated coefficient of permeability.

The saturated coefficient of permeability for Beaver Creek sand was independent of applied pressure. The average value obtained was $1.27 \times 10^{-6}$ m/s.
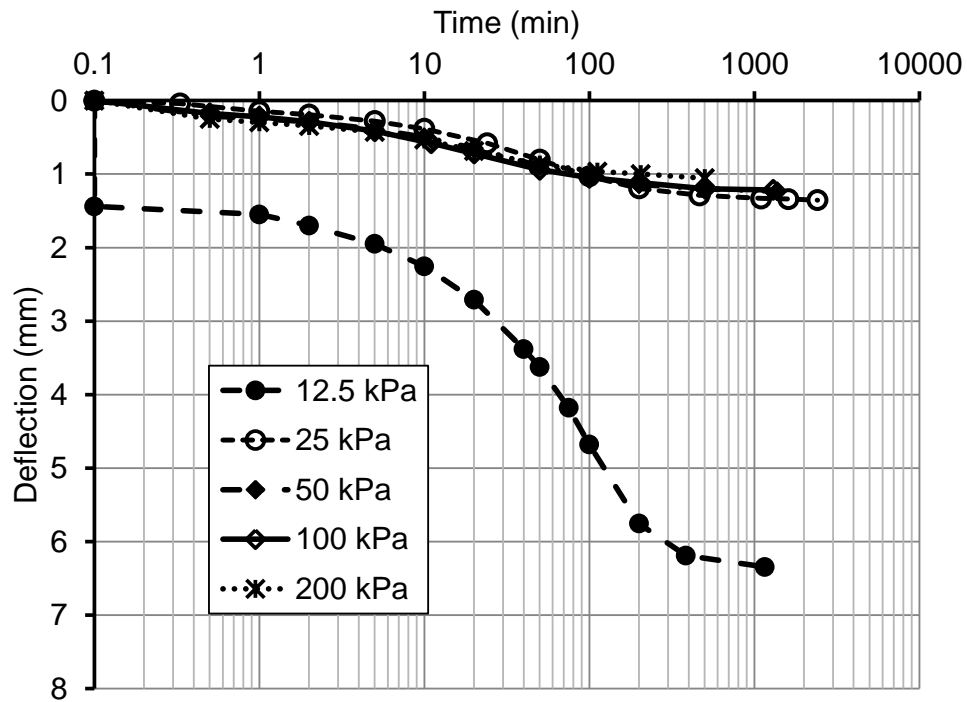
Figure 5.2 Deflection versus time for the consolidation test on Botkin silt (Specimen CS2-2)

Figure 5.3 shows measured magnitudes of the saturated coefficient of permeability versus applied pressure for Botkin silt (Specimens CS1-2 and CS2-2). The magnitude of the coefficient decreased from $3.2 \times 10^{-9}$ to $1.9 \times 10^{-9}$ m/s in response to increase in the applied pressure from 50 to 200 kPa.

The experimental data for the consolidation and k-tests are tabulated in Appendix B.

## 5.4 SOIL-WATER CHARACTERISTIC CURVES

This section presents the experimental test results for the measurement of the Soil-Water Characteristic Curves (SWCCs) for the selected soils. The results obtained from different devices (i.e., U of S Pressure Plate Cell, GCTS SWC 100, Air-Tight Chamber (ATC) and Chilled- Mirror Water-Potentia Meter (WP4-T)) are presented in three separate sections: 5.4.1, 5.4.2, and 5.4.3. The results obtained from the U of S Pressure Plate Cell and GCTS SWC 100 SWCC are presented in sections 5.4.1 and 5.4.2, respectively. The results obtained from ATC and WP4-T devices are presented in section 5.4.3. Section 5.4.4 presents the entire SWCCs of the selected soils for suction

ranges from 0 - 1,000,000 kPa. The soil suction value is assumed to be 1,000,000 kPa at oven-dry condition.

Air-tight chambers and the WP4-T device were used to measure the soil-water characteristic curves for the high suction range (i.e., 1500 – 300,000 kPa) for the Beaver Creek sand, Botkin silt, and Regina clay.
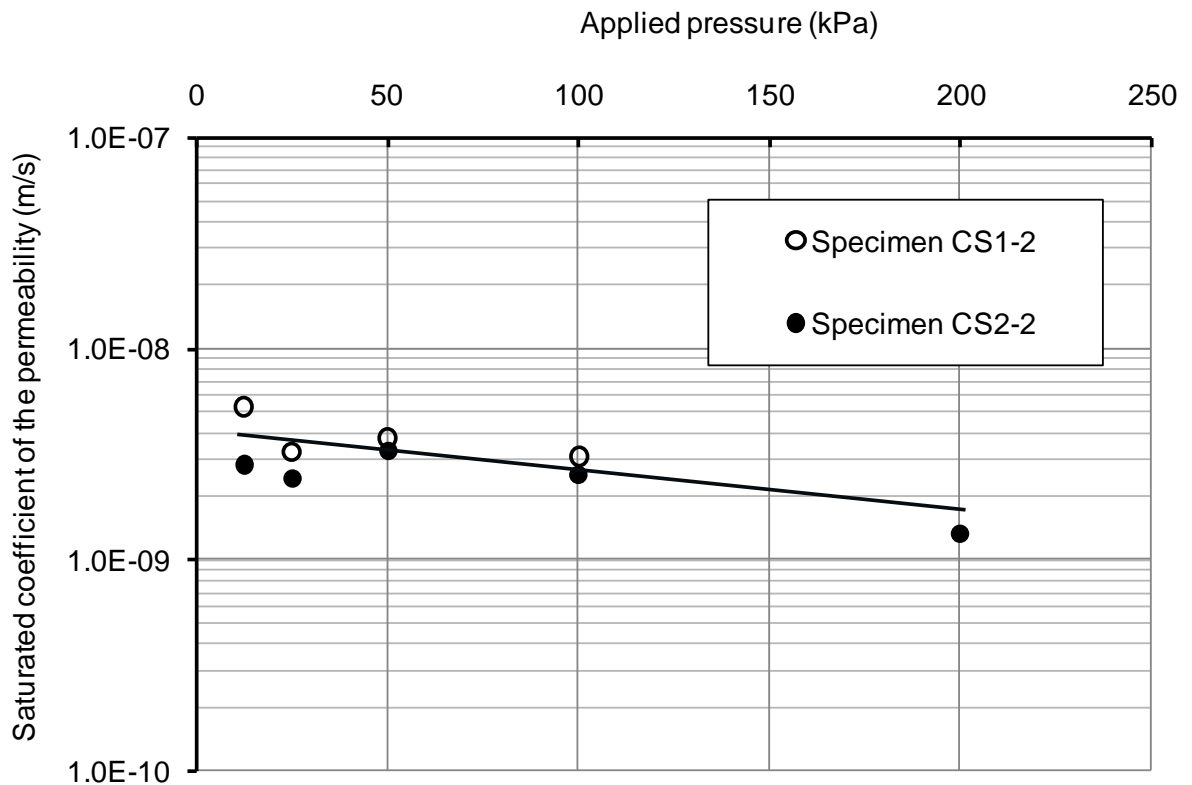


Figure 5.3 Saturated coefficient of permeability versus applied pressure for Botkin silt

In addition to the drying SWCC of the Botkin silt and Regina clay, the wetting branch of the curve was measured in the high suction ranges. Section 5.4.3 presents the resulting drying and wetting SWCCs for these two soils. The drying SWCC data are used to establish the SWCC for the high suction ranges. The drying and wetting data will be used (in Chapter 6) to assess the performance of the WP4-T device and to study the SWCC hysteresis in the high suction range.

The focus of this research was to study the hydraulic behavior of the soils around residual conditions, where the volume change of the specimen tends to become small. In

the case of Beaver Creek sand, the volume change did not appear to be important even in near-saturation condition.

Soil-water characteristic curves are presented as gravimetric water content versus soil suction curve throughout this thesis. The soil suction values are presented in kilopascal (kPa). The volumetric water content values obtained from the GCTS SWC 100 equipment were converted to the gravimetric water content using the volume-mass relations of the soil specimens. For the hanging-column techniques when using the U of S Pressure Plate Cell, applied suctions were in mm-$H_2O$. These soil suction values were converted to kPa. The Chilled-Mirror Water Potentia Meter (i.e., WP4-T) measures the soil-water potential values in MegaPascals (MPa) (i.e., negative numbers). These numbers were converted to soil suction values in kPa (i.e., positive numbers).

Five Beaver Creek sand and six Botkin silt specimens (see Chapter 4, Tables 4.5 and 4.6) were used for the measurement of the SWCC using U of S Pressure Plate Cell and GCTS SWC 100 devices. The preparation of the soil specimens and test procedures for the measurement of soil-water characteristic curves were described in Chapter 4, section 4.5.3. Tables 5.1 and 5.2 summarize the initial condition and volume-mass relations for the SWCC specimens of the Beaver Creek sand and Botkin silt soils, respectively. The volume-mass relations of the SWCC specimens were determined using the volume-mass relations at the end of the SWCC tests.

Table 5.1 Initial condition and volume-mass relations of the Beaver Creek sand SWCC specimens

| Specimen ID | Initial condition | Water content (%) | Dry density (g/cm$^3$) | Void ratio |
|---|---|---|---|---|
| S1-1 | Compressed to 3870 kPa | 24.82 | 1.46 | 0.82 |
| S3-1 | Compressed to 3870 kPa | 25.75 | 1.45 | 0.83 |
| S3-2 | Compressed to 3870 kPa | 23.01 | 1.45 | 0.83 |
| S4-2 | Compressed to 3870 kPa | 18.10 | 1.43 | 0.86 |
| MS1 | Consolidated to 200 kPa | 22.69 | 1.56 | 0.69 |

Table 5.2 Initial condition and volume-mass relations of the Botkin silt SWCC specimens

| Specimen ID | Initial condition | Water content (%) | Dry density (g/cm³) | Void ratio |
|---|---|---|---|---|
| CS1-1 | Consolidated to 19 kPa | 26.39 | 1.60 | 0.69 |
| CS2-1 | Consolidated to 19 kPa | 26.62 | 1.59 | 0.70 |
| CS3-1 | Consolidated to 19 kPa | 30.69 | 1.36 | 1.00 |
| CS01 | Saturated Slurry | 34.17 | 1.35 | 1.01 |
| CS02 | Saturated Slurry | 34.17 | 1.35 | 1.00 |
| MCS | Consolidated to 50 kPa | 24.46 | 1.63 | 0.66 |

### 5.4.1 U of S Pressure Plate Cell

Figure 5.4 shows the soil-water characteristic curve on the Beaver Creek sand specimens using the U of S Pressure Plate Cell for suctions ranging from 0 to 500 kPa. Three soil specimens: S1-1, S3-2, and S4-2, were used to complete the measurements. The hanging-column technique was applied to Specimen S1-1 to measure the SWCC for suctions ranging from 0 to 10 kPa. The axis-translation technique was applied to Specimens S3-2, and S4-2 to measure the SWCC curves for suctions ranging from 10 to 100 kPa and from 100 to 500 kPa, respectively. The test procedures for the hanging-column and axis-translation techniques using the U of S Pressure Plate Cell were described in the previous chapter (see Chapter 4, section 4.5.3). The data point corresponding to 100 kPa in Figure 5.4 were measured using two different specimens (Specimen S3-2 and Specimen S4-2).

Figure 5.5 shows results of the soil-water characteristic curve tests obtained from the U of S Pressure Plate Cell for two Botkin silt specimens with slurry initial conditions (i.e., specimens CS01 and CS02). The results obtained from tests on two specimens are similar. These results were not used for the analyses along with the evaporation test results, because the preliminary evaporation tests on the specimens with the slurry initial conditions encountered some difficulties.

Figure 5.6 shows the soil-water characteristic curve data for Botkin silt Specimen CS1-1 for suctions ranging from 0 to 1000 kPa. The soil specimen was first consolidated

to 19 kPa. A U of S Pressure Plate Cell was used to measure the soil-water characteristic curve from 0 to 500 kPa. The hanging-column technique was used for suctions ranging from 0 to 10 kPa. The axis-translation technique was used for suctions ranging from 10 to 500 kPa. The test was started using a 1-bar high air-entry ceramic plate. The 1-bar plate was then replaced with a 5-bar ceramic plate after the applied suction value reached 70 kPa.
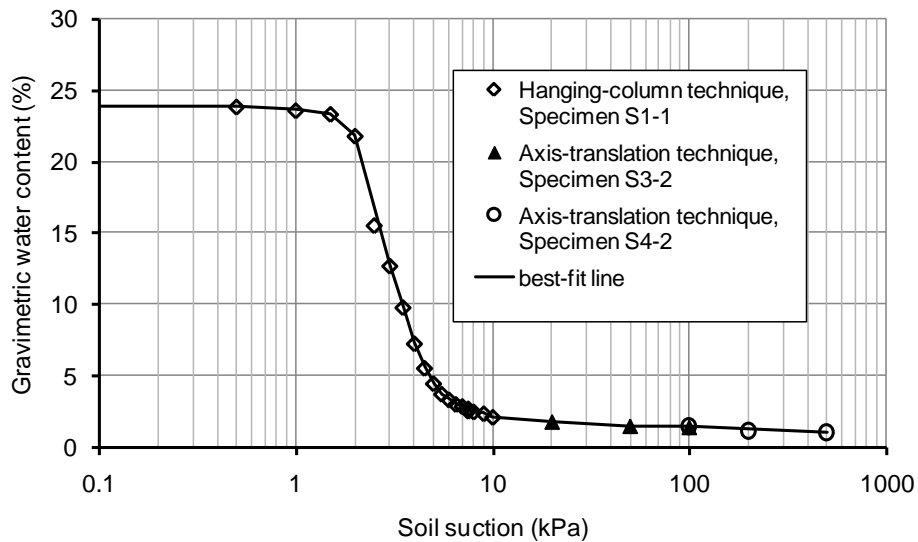


Figure 5.4 Soil-water characteristic curve data for Beaver Creek sand using the U of S Pressure Plate Cell for suctions ranging from 0 to 10 kPa (i.e., hanging column technique on Specimen S1-1 and axis-translation technique on Specimens S3-2 and S4-2)

The experimental test data obtained from GCTS SWC 100 device are presented in a separate section (i.e., Section 5.4.2). However, in order to emphasize the error that occurred when using U of S Pressure Plate Cell with the 5-bar porous plate, the data obtained for Specimen CS1-1 (i.e., GCTS SWC 100 apparatus), for suctions ranging from 500 to 1000 kPa are presented in Figure 5.6. The data point corresponding to 500 kPa in Figure 5.6 was measured using both U of S Pressure Plate Cell and GCTS SWC-100 equipment. The data points obtained using U of S Pressure Plate Cell with the 5-bar ceramic plate is shown inside a dashed circle in Figure 5.6.

An error is visible in the SWCC results obtained from the U of S Pressure Plate Cell (see Figure 5.6). The error appears to be attributable to the possible lack of a complete

hydraulic connection between the soil and saturated 5-bar ceramic plate. Similar results were obtained for Specimen CS2-1 where only a U of S Pressure Plate Cell was used to measure the SWCC for suctions ranging from 0 to 500 kPa. Soil Specimen CS2-1 was also consolidated to 19 kPa.
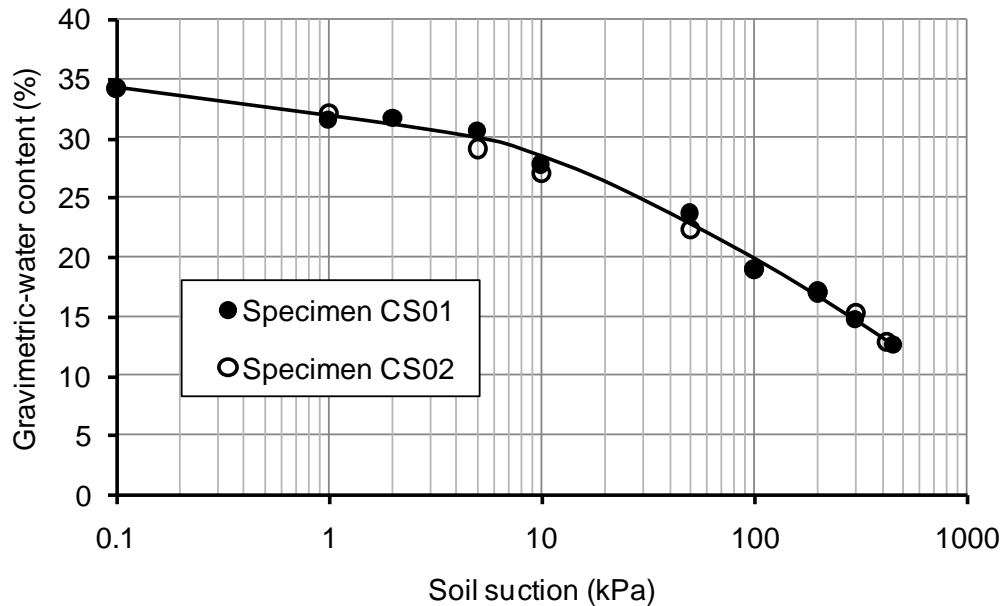


Figure 5.5 Soil-water characteristic curve data for Botkin silt using the U of S Pressure Plate Cell for suctions ranging from 0 to 500 kPa (Slurry Specimens CS01 and CS02)

### 5.4.2 GCTS SWC 100 Device

Soil-water characteristic curve data for the Beaver Creek sand and Botkin silt soils obtained from the GCTS SWC 100 apparatuses are presented in this section. Figure 5.7 shows the soil-water characteristic curve data obtained from the GCTS SWC 100 equipment on Beaver Creek sand (i.e., Specimen S3-1). The SWCC was measured for suctions ranging from 100 to 1500 kPa. The axis-translation technique was used as described in Chapter 4.

Figures 5.8 and 5.9 show SWCCs for Beaver Creek sand and Botkin silt specimens obtained from the GCTS SWC 100 equipment. The data from WP4-T device was also included for extension of the SWCC to the high suction range.
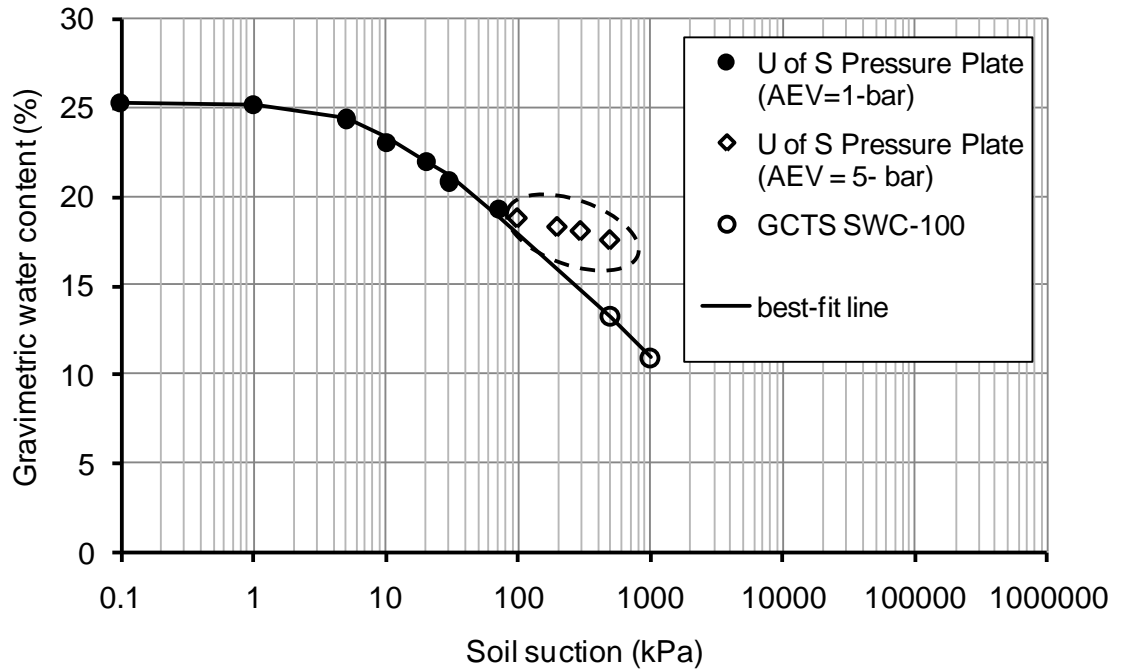
Figure 5.6 Soil-water characteristic curve data for Botkin silt using the U of S Pressure
Plate Cell and GCTS SWC 100 device for suctions ranging from 0 to 1000
kPa (Specimen CS1-1, Consolidated to 19 kPa)
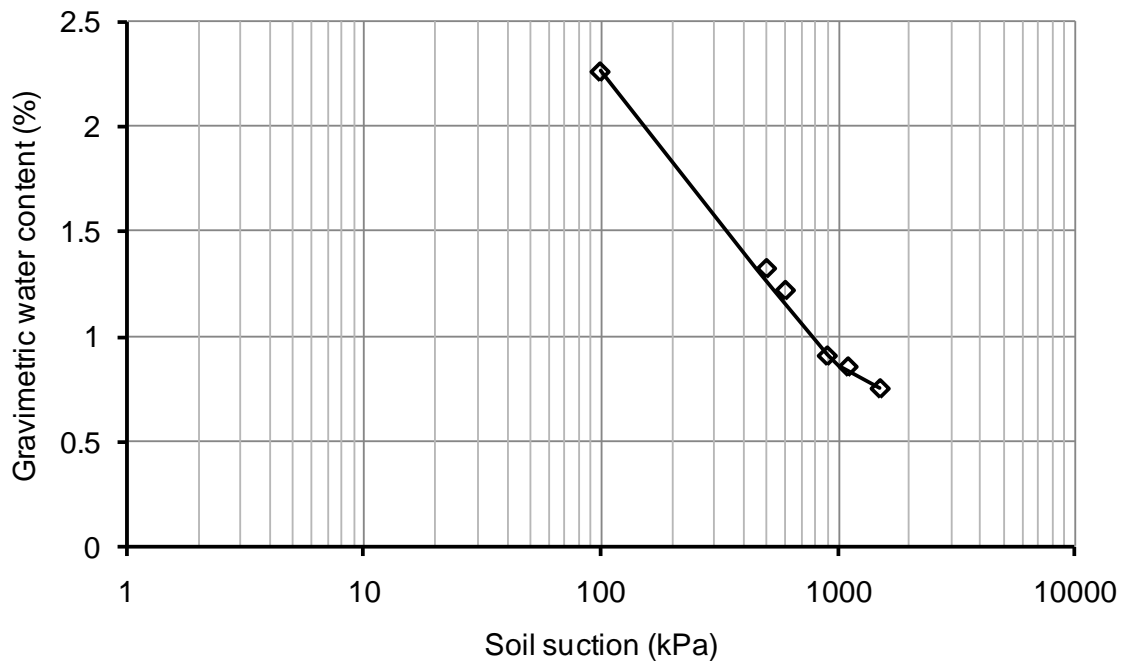


Figure 5.7 Soil-water characteristic curve data for Beaver Creek sand (Specimen S3-1)
using GCTS SWC 100 device for suctions ranging from 100 to 1500 kPa
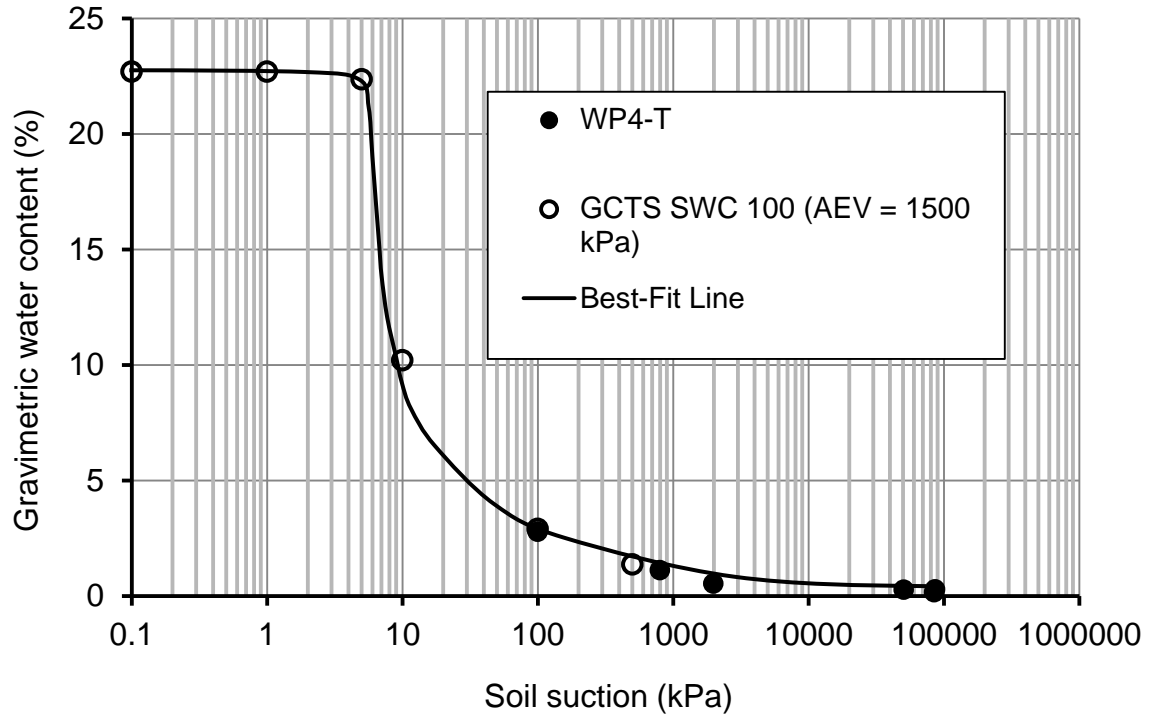
Figure 5.8 Soil-water characteristic curve data for Beaver Creek sand (Specimen MS1) using GCTS SWC 100 device for suctions ranging from 0.1 to 1500 kPa
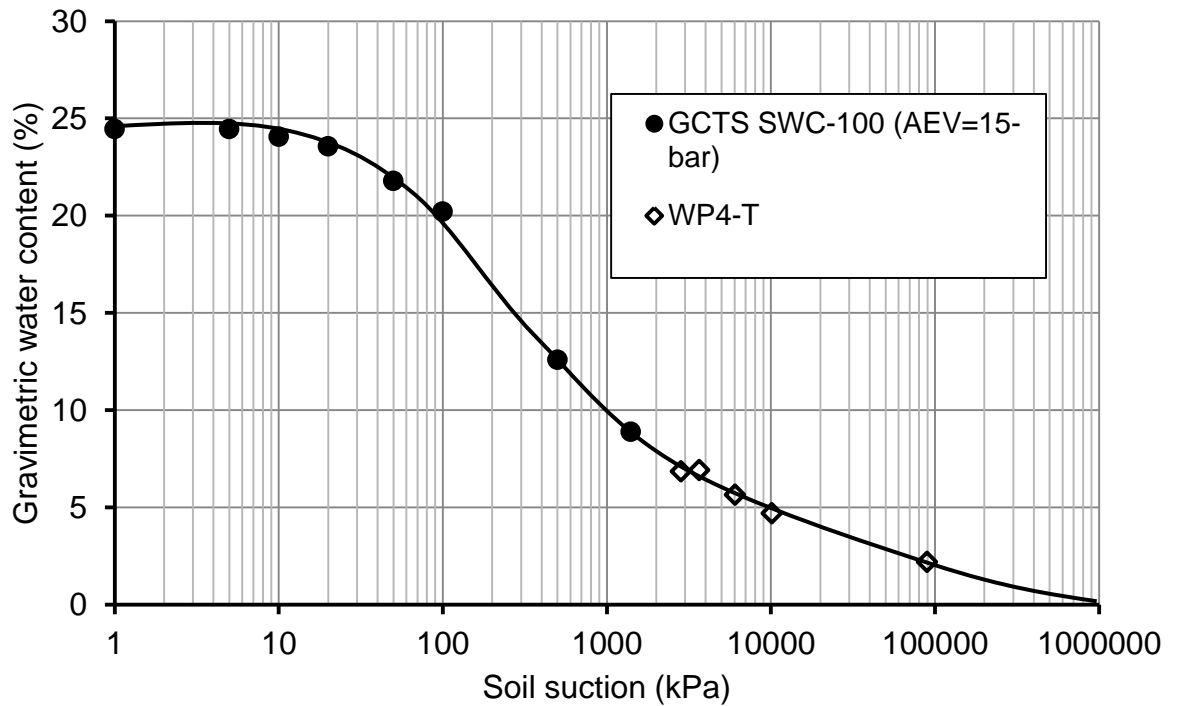


Figure 5.9 Soil-water characteristic curve data for Botkin silt (Specimen MCS) using GCTS SWC 100 device for suctions ranging from 1 to 1500 kPa

The SWCC data of the Beaver Creek sand from the GCTS SWC 100 device (see Figure 5.7) appear to be consistent with the results obtained from the U of S Pressure Plate Cell apparatus (see Figure 5.4), for suction ranges between 100 and 500 kPa. While, for suction ranges between 1 and 10 kPa, the results obtained from the GCTS SWC 100 (see Figure 5.8) do not appear to be consistent with the results obtained from the U of S Pressure Plate Cell apparatus (see Figure 5.4).

The SWCC test results on a single specimen of the Botkin silt soil (MCS)  using the GCTS SWC 100 device (see Figure 5.9) are consistent with the data obtained from the U of S Pressure Cell apparatus(see Figure 5.6), for suction ranges less than 100 kPa. It should be noted that the MCS specimen was consolidated to 50 kPa vertical stress before the commencement of the SWCC test using the GCTS SWC 100 apparatus.

### 5.4.3   Air-Tight Chambers (ATC) and Chilled-Mirror Water-Potentia Meter (i.e., WP4-T)

As described in detail in the previous chapter (Chapter 4, section 4.5.3), seven air-tight chambers (ATCs) were used to measure the soil-water characteristic curve for the selected soil samples (i.e., Botkin silt and Regina clay) in the high-suction ranges from 3,766 to 300,008 kPa. This section presents results of these measurements.

### 5.4.3.1   Equilibrium Conditions inside ATC

Equilibration conditions were assumed to have been reached when the change in the mass of the sample holders inside each ATC was zero for two consecutive measurements; that is, when the mass of the sample holders was constant. Different saturated solutions were used inside each air-tight chamber in order to achieve different relative humidity, and hence different suction values, at equilibrium.

Table 5.3 shows the results for the mass of the sample holders inside each ATC with respect to time. Mass of sample holder for each ATC is given at the start of the test (at day 0) and at days 3, 7, 25, and 34. Targeted relative humidity numbers and the corresponding suction values for each ATC are also given. The relative humidity was selected in the range between 11.3 to 97.3%, covering suction values between 3766 and 300,008 kPa.

Table 5.3 Change in the mass of soil sample holders inside the air-tight chambers with time

| Air-Tight Chamber | Saturated Solution | Relative Humidity (%) | Suction (kPa) | Elapsed Time (day) | | | | |
|---|---|---|---|---|---|---|---|---|
| | | | | 0 | 3 | 7 | 25 | 34 |
| | | | | Mass of the Sample Holders (g) | | | | |
| A | Lithium Chloride | 11.3 ± 0.3 | 300,008 | 421.1 | 418.2 | 428.7 | 428.5 | 428.5 |
| B | Magnesium Chloride | 32.8 ± 0.2 | 153,383 | 439.3 | 433.4 | 433.2 | 433.6 | 433.6 |
| C | Potassium Iodide | 68.9 ± 0.3 | 51,256 | 433.4 | 430 | 427.7 | 427.7 | 427.7 |
| D | Sodium Chloride | 75.3 ± 0.2 | 39,034 | 423.3 | 420.2 | 416.8 | 416.9 | 416.9 |
| E | Potassium Chloride | 84.3 ± 0.3 | 23,500 | 427.5 | 423.2 | 420.6 | 414.6 | 414.6 |
| F | Potassium Nitrate | 93.6 ± 0.6 | 9,100 | 405.5 | 403.8 | 407.7 | 409.3 | 409.4 |
| G | Potassium Sulfate | 97.3 ± 0.5 | 3,766 | 417.9 | 417.0 | 416.4 | 413.9 | 413.8 |

Figure 5.10 shows the change in mass of the sample holders (i.e., mass change of the group of soil samples) for each air-tight chamber with respect to time. Soil samples inside chambers A, B, C, and D reached equilibrium with the chamber environment in 25 days. The soil samples inside the chambers E, F, and G reached equilibrium conditions in about 34 days. The saturated solutions and associated target humidity values used in each of the chambers A, B, C, D, E, F, and G were given in Table 5.3.

Based on the results described in this section, it appears that the equilibrium time is a function of type of saturated salt solution placed inside the ATC and is therefore a function of the target relative humidity. It was observed that the higher the expected relative humidity, the longer the equilibrium time.

### 5.4.3.2 SWCCs of Botkin Silt and Regina Clay Soils in High Suction Ranges

After equilibrium was reached (see section 5.4.3.1), the mass of the soil samples was measured using an electronic balance with a readability of 0.0001g. The gravimetric water contents were determined after measuring the oven-dried weight of the samples.
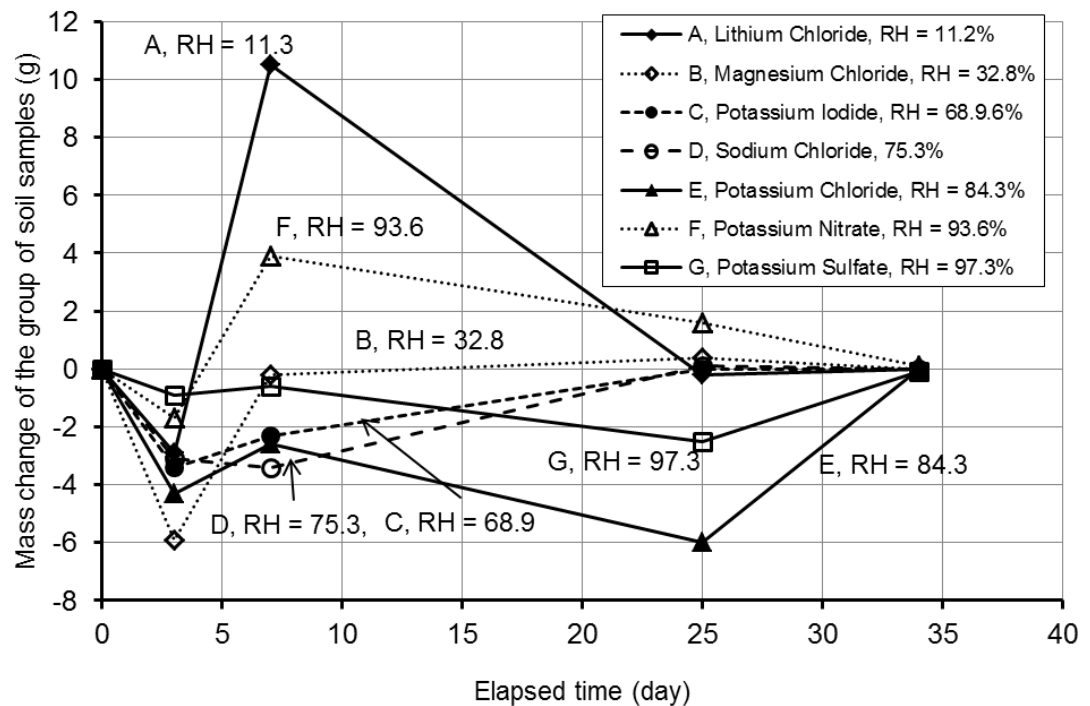


Figure 5.10 Equilibrium time for soils inside air-tight chambers with different saturated salts or different relative humidities

In addition to the values, given in Table 5.3, the relative humidity and soil suctions were determined using a Traceable Hygrometer.

The WP4-T measurements were taken after equilibrium was reached inside each ATC. Details of the test procedures were given in Chapter 4, section 4.5.3.2. The soil-water potential values in MPa (negative values) were converted to soil suction in kPa.

Figures 5.11 to 5.14 show the drying and wetting soil-water characteristic curves data measured when using the ATC and WP4-T experimental results.

Figure 5.11 and 5.12 show the drying and wetting curves for Botkin silt and Regina clay, measured using the air-tight chambers (i.e., equilibration of soil samples over salt solutions of known osmotic suction). The difference between drying and wetting SWCCs (i.e., hysteresis) is greater for Regina clay soil than for Botkin silt.

Figure 5.13 and 5.14 show the drying and wetting curves for Botkin silt and Regina clay measured using the Chilled-Mirror Water PotentiaMeter (i.e., WP4-T) device. The results are similar to the results obtained from the air-tight chambers (see Figure 5.11 and 5.12). The hysteresis is more visible for Regina clay than for Botkin silt.
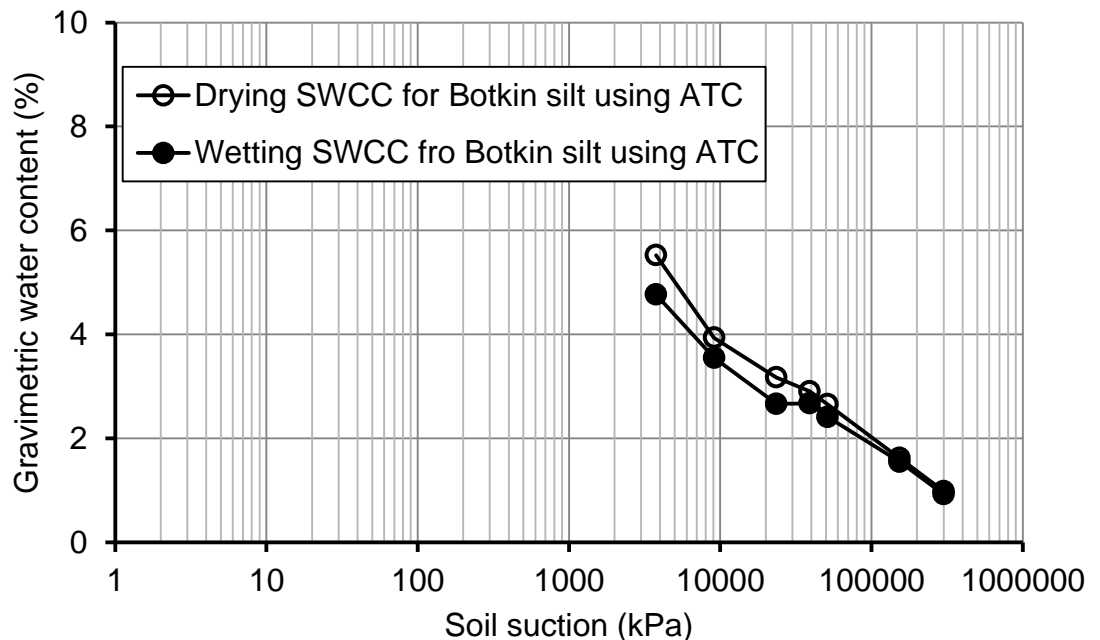


Figure 5.11 Drying and wetting soil-water characteristic curves data using ATC apparatus in the environmentally-controlled room for Botkin silt in the high suction ranges
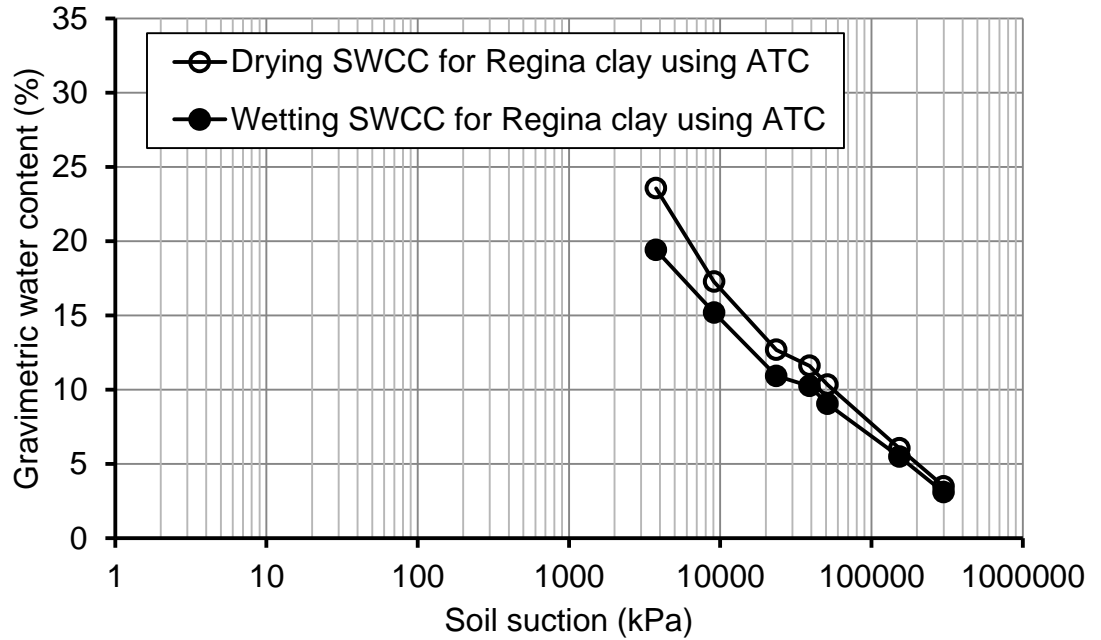
Figure 5.12 Drying and wetting soil-water characteristic curves data using ATC
apparatus in the environmentally-controlled room for Regina clay in the high
suction range
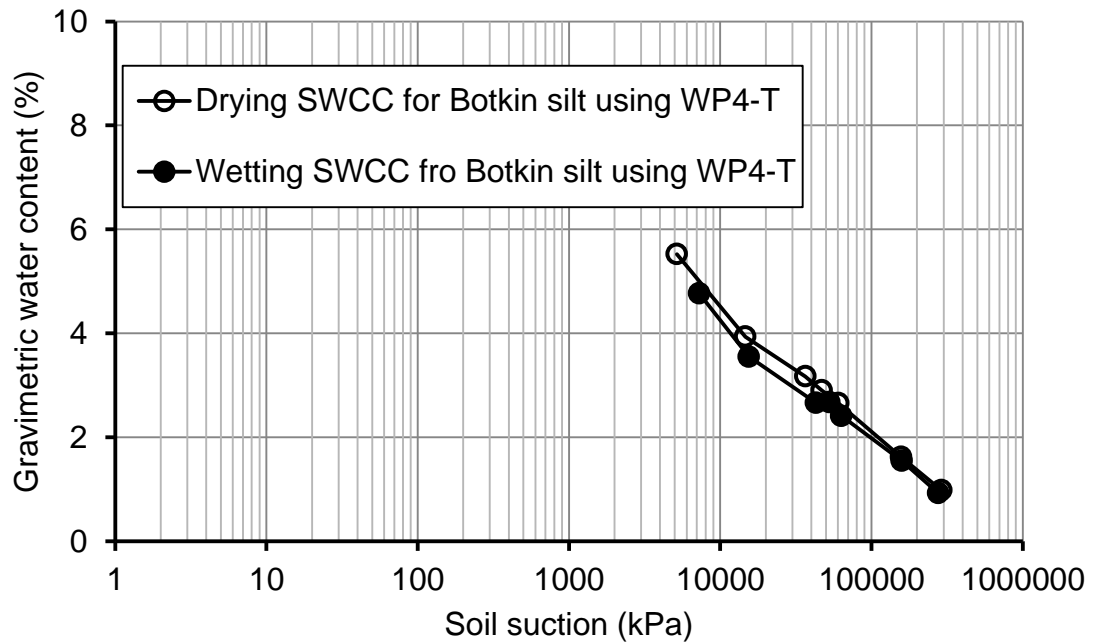


Figure 5.13 Drying and wetting soil-water characteristic curves data using WP4-T
device in the environmentally-controlled room for Botkin silt in the high
suction ranges
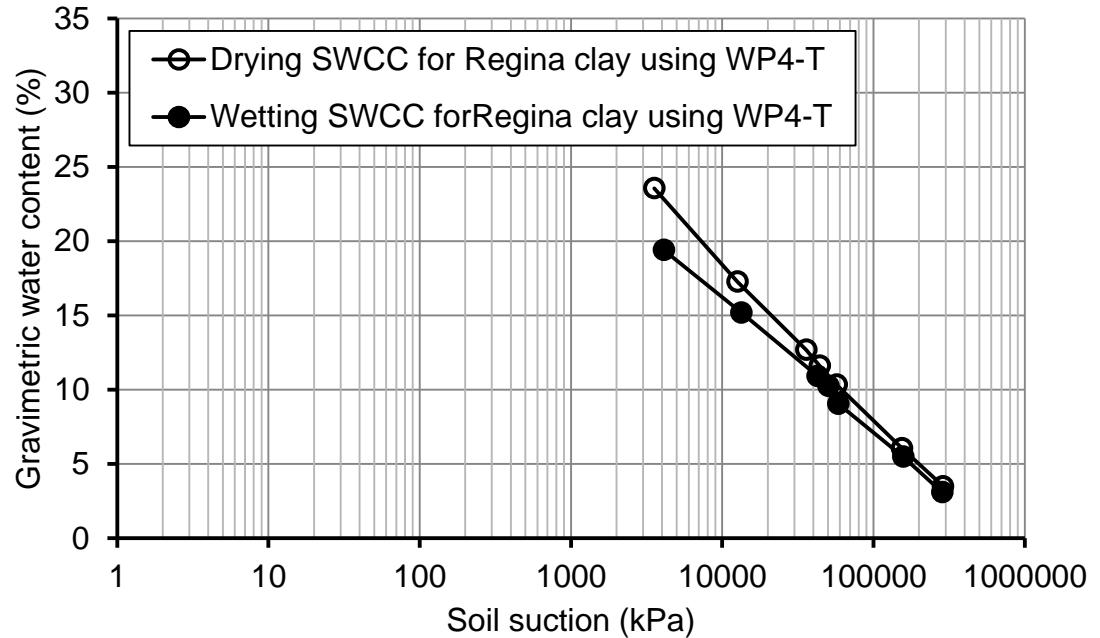
Figure 5.14 Drying and wetting soil-water characteristic curves data using WP4-T device in the environmentally-controlled room for Regina clay in the high suction ranges

### 5.4.4 Difficulties Associated with the SWCC Tests

This section discusses some difficulties related to the SWCC testing and the associated solutions used to resolve these issues.

### 5.4.4.1 U of S Pressure Plate Cell and GCTS SWC 100

To accelerate the testing procedure, ceramic plates with different air-entry values were used with U of S Pressure Plate Cell apparatuses (see Chapter 4, section 4.5.3). For example, during the SWCC measurement on specimen CS1-1 of Botkin silt, a ceramic plate with 100 kPa air-entry value was replaced with a ceramic plate with 500 kPa air-entry value. The sample was then transferred to GCTS SWC 100 device for applying higher suction values, where a ceramic plate with air-entry value of 1000 kPa was used. The results for this SWCC measurement were presented in Figure 5.6. A difference was observed between the water-content values at 500 kPa suction obtained from U of S Pressure Plate apparatus with 500 kPa air-entry value ceramic plate and from GCTS SWC 100 apparatus with 1500 kPa air-entry value ceramic plate. The water-content value at 500 kPa was about 3% (in gravimetric water content) higher for the U of S

Pressure Plate Cell than that for the GCTS SWC 100. The higher water content for the U of S Pressure Plate Cell might be attributed to the lack of a complete hydraulic connectivity between the porous plate and the sample during exchange of the ceramic plates. A similar problem was observed on the results obtained from the U of S Pressure Plate Cell for Specimen CS2-1.

Figure 5.15 compares the SWCC data for Beaver Creek sand Specimen MS1 from GCTS SWC 100 device using a ceramic plate with 1500 kPa air-entry value, with the data for Beaver Creek sand Specimen S1-1 from U of S Pressure Plate Cell using a ceramic plate with 100 kPa air-entry value. In the soil suction range from about 2 to 10 kPa, the water content values remained higher when a ceramic plate with 1500 kPa air-entry value was used. For example, gravimetric water content values at 10 kPa soil suction are about 2% and 10% for the ceramic plates with associated air-entry values of 100 kPa and 1500 kPa, respectively. It appears that using a ceramic plate with a high air-entry value of 1500 kPa did not create reasonable SWCC data. The hanging-column technique using a ceramic plate with a lower air-entry value of 100 kPa, appears to result in more reasonable data.

### 5.4.4.2  Problem Associated with Diffused Air

Another difficulty in measuring the SWCC was the issue of diffused air through ceramic plates. Diffused air may cause errors in the mass readings for the U of S Pressure Plate Cell or for the volume readings for the GCTS SWC 100 device. This is particularly true in the high air pressure range where the amount of diffused air is usually greater. A common solution for reducing this error is to periodically flush the diffused air from beneath the ceramic plate by water flow.

Diffused air was flushed by applying water flow and pushing the air out from beneath the ceramic plate of the U of S Pressure Plate Cell. An air squeezer was used to force water to flow back and forth repeatedly through the bottom of the ceramic plate and between two tubes on the sides of the GCTS SWC 100 device. This procedure was continued until all diffused air accumulated beneath the plate flowed out of the compartment below the high air-entry value plate.
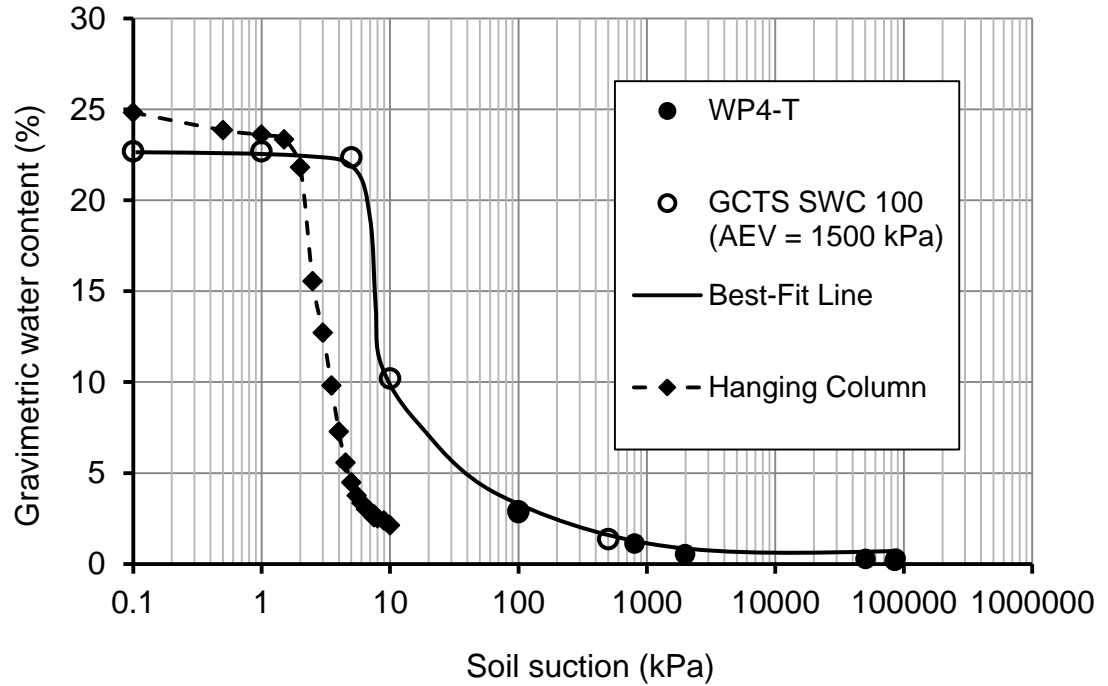
Figure 5.15 Comparison of the SWCC curves for the Beaver Creek sand obtained using a ceramic disk with AEV = 100 kPa on Specimen S1-1 and a ceramic disk with AEV = 1500 kPa on Specimen MS1

The amount of diffused air was measurable when the GCTS SWC 100 apparatus was used. At the end of each air pressure increment, two readings were taken for the water level, one reading before and another one after the diffused air was removed. The diffused air was quantified using the difference between the readings before and after the removal of the diffused air.

Figure 5.16 shows the soil-water characteristic curve data resulting from the GCTS SWC 100 equipment on the Botkin silt Specimen CS3-1. The soil-water characteristic curve was measured for soil suctions ranging from 10 to 1500 kPa. The water content of the soil specimen did not change significantly for 6 days after the applied air pressure was increased from 1000 kPa to 1500 kPa. The 15-bar ceramic plate could not withstand the air when the applied pressure was greater than 800 kPa. During the test with an applied pressure of 1500 kPa, the amount of diffused air passing through the 15-bar ceramic plate was so great that the diffused air required to be flushed at least 5 times a day. The SWCC of CS3-1 has been shown for discussion purposes only and will not be used in data analyses.
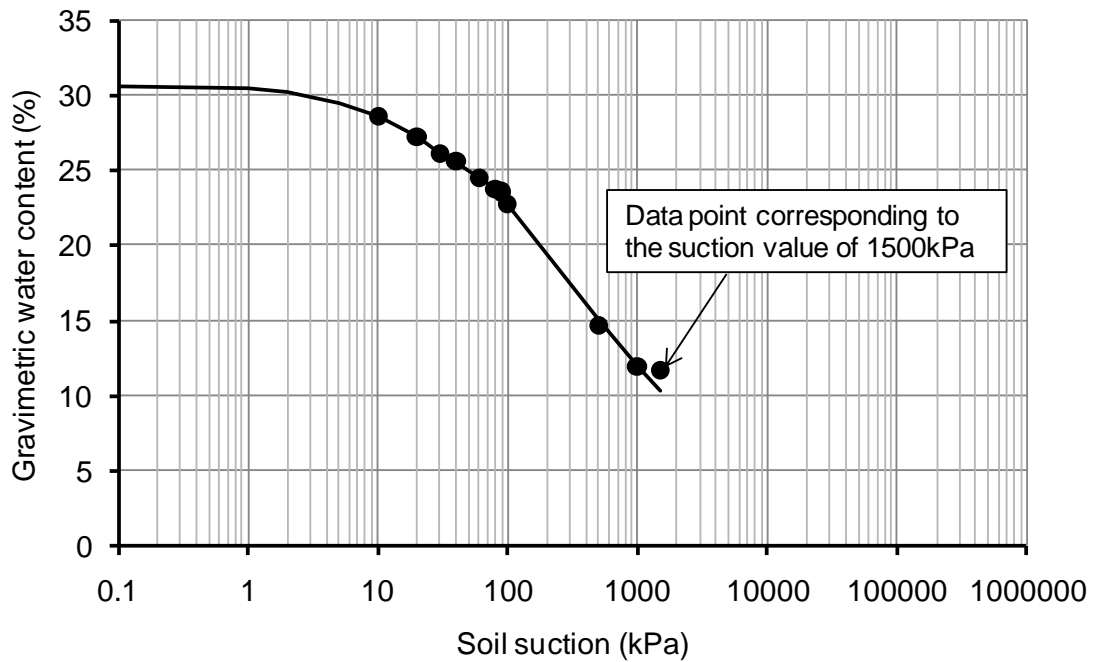
Figure 5.16 Soil-water characteristic curve data for Botkin silt (Specimen CS3-1) using GCTS SWC 100 device for suctions ranging from 10 to 1500 kPa

Figures 5.17 shows photos of the ceramic plate with an air entry value of 1500 kPa used to obtain the SWCC data on Botkin silt Specimen CS3-1 (see Figure 5.16). Damage was observed on both front and back sides of the ceramic plate.

### 5.4.4.3 Solution to the Problem Associated with Diffused Air

To make it possible to measure a reliable set of SWCC data for suction ranges between 500 and 1500 kPa, the problem associated with the 1500 ceramic plate had to be resolved. Three ceramic plates were purchased and mounted on three steel rings using an epoxy from Engineering Shops at the University of Saskatchewan. Care was given to reduce the amount of the air bubbles during the process of applying the epoxy between the ceramic plates and the rings. Figures 5.18a and 5.18b show the front and back view of one of the ceramic plates mounted within a steel ring.
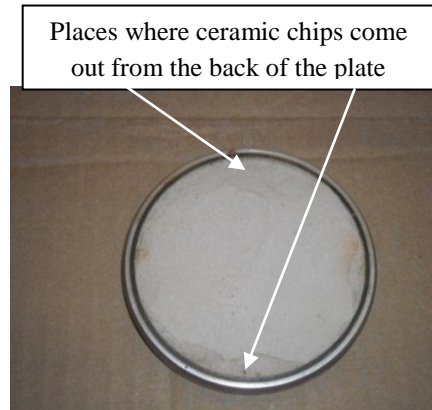
a)   Back view of the 15-bar ceramic plate after SWCC testing
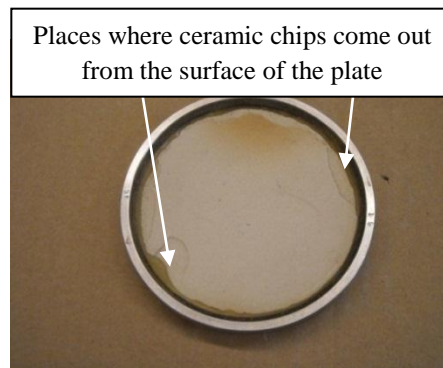


b)   Front view of the15-bar ceramic plate after SWCC testing

Figure 5.17 Photos of the back and front view of the used 15-bar ceramic plate after the SWCC testing for Specimen CS3-1

Two out of three ceramic plates functioned properly, while the issue of air leakage was observed with one of the plates during testing. The air leakage with the latter ceramic plate remained even after a few attempts to solve the problem. It was concluded that precise care must be taken when mounting a 15-bar ceramic plate within a steel ring in order to avoid air leakage during the measurement of the SWCC.

The set of apparently reasonable SWCC data for Botkin silt Specimen MCS, shown on Figure 5.9, were obtained using the modified ceramic plate with an air-entry value of 1500 kPa. The amount of diffused air during the test was lower and the diffused air required flushing once a day.

a) Back view of the new 15-bar plate mounted on a steel ring in the Engineering Shops, U of S



b) Front view of the new 15-bar plate mounted on a steel ring in the Engineering Shops, U of S

Figure 5.18 Photos of the back and front view of the 15-bar ceramic plate mounted on a steel ring in the Engineering Shops, U of S

A comparison of the water content value at 1500 kPa presented in Figure 5.16 (obtained using the ceramic plate shown in Figure 5.17) with that in Figure 5.9 (obtained using the ceramic plate shown in Figure 5.18) reveals that the problem associated with the air diffusion was resolved with the latter.

### 5.4.5   Entire Drying SWCCs for Beaver Creek sand and Botkin silt soils

The entire drying soil-water characteristic curves are presented in Figures 5.19 and 5.20 for the Beaver Creek sand and Botkin silt specimens, respectively. The device or technique used to establish the soil-water characteristic curve in each suction range is presented on the graphs.

Figure 5.19 presents drying soil-water characteristic curves of the initially compressed obtained from U of S Pressure Plate, GCTS SWC 100, and WP4-T devices,

loose (prepared from saturated slurry with zero vertical stress) obtained from U of S Pressure Plate Cell; and consolidated Beaver Creek sand specimens obtained from GCTS SWC 100 and WP4-T. It can be seen from the results that the SWCC of the compressed and loose specimens are almost identical. For the suction ranges between 2 and 10 kPa, the points from the GCTS SWC 100 device (empty circles) are not consistent with the other results. As mentioned before (see section 5.4.4.1), this inconsistency can be attributed to the use of a ceramic disk with an air-entry value of 1500 kPa.

Figure 5.20 presents drying soil-water characteristic curves of the Botkin silt specimens initially consolidated to maximum vertical pressures of 19 and 50 kPa. It also presents drying SWCC data for the specimens prepared in a saturated slurry condition with no vertical stress at the top. The soil-water characteristic curves of the specimens are almost identical for suction ranges beyond 200 kPa, regardless of the initial condition of each sample. This finding is important because it indicates that any of these soil-water characteristic curves can be used along with the evaporation data for determination of the unsaturated coefficient of permeability around the residual-state condition.
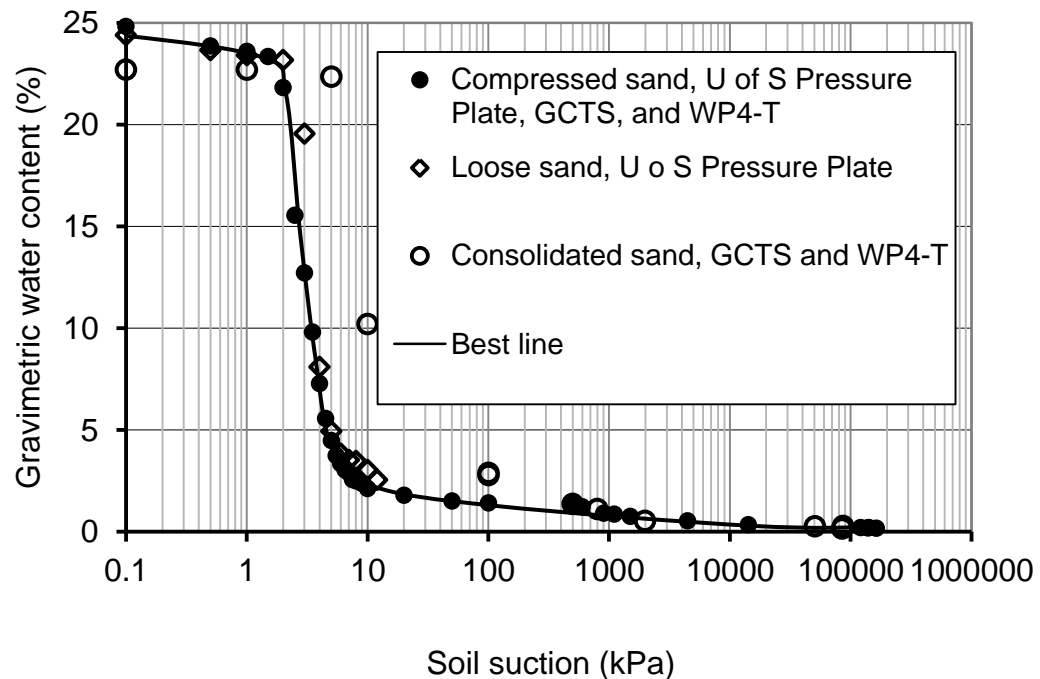


Figure 5.19 Soil-water characteristic curves for Beaver Creek sand specimens
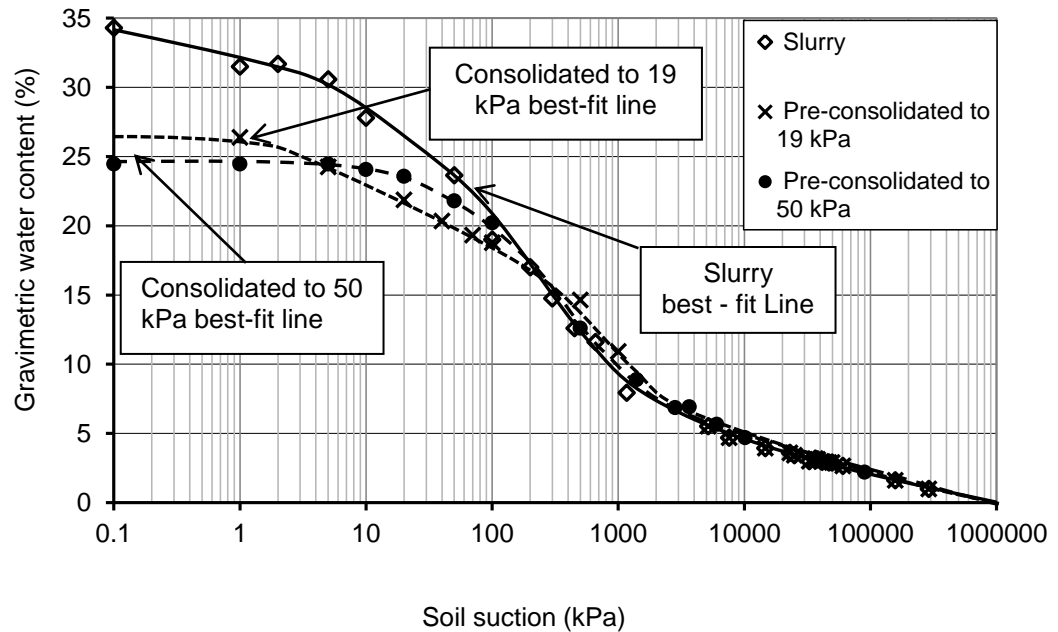
Figure 5.20 Soil-water characteristic curves for Botkin silt specimens

## 5.5 EVAPORATION TEST RESULTS

A total of ten evaporation processes were conducted on the Beaver Creek sand and Botkin silt specimens: 6 on Beaver Creek sand and 4 on Botkin silt (Chapter 4, Table 4.13). The details on evaporation processes were described in Chapter 4, section 4.6.3 (Table 4.13). This section presents the experimental results obtained during the evaporation processes. The results include potential (section 5.5.1) and actual (section 5.5.2) evaporation rates, temperature changes with time (section 5.5.3), and the gravimetric water content profiles at the end of the evaporation tests (section 5.5.4). Experimental data for evaporation processes are tabulated in Appendix D.

The relative humidity and temperature were controlled inside the environmentally controlled room where independent evaporation processes were conducted. The relative humidity and temperature in the room were recorded using two Hobo data loggers during evaporation processes. The data obtained from two different data loggers for relative humidity and temperature were comparable, and the average numbers were used in the analysis.

Figure 5.21 and 5.22 show temperature and relative humidity with respect to time in the environmentally controlled room for evaporation Process PS3. Both temperature and

relative humidity show approximately constant values with small fluctuations. The temperature and relative humidity of the room were assumed to be constant and equal to the average values of approximately 25 $^{o}$C and 26% during the evaporation process. Similar results were obtained for other evaporation processes with slightly different temperature and relative humidity values.

Evaporation Process PS1 was conducted in a different chamber (an additive humidity chamber; see Chapter 4, section 4.6.1.1). The relative humidity and temperature values for Test PS1 were based on the values recorded by a built-in data acquisition system used to control the chamber environment. The relative humidity and temperature measurements were not recorded by an individual data logger.
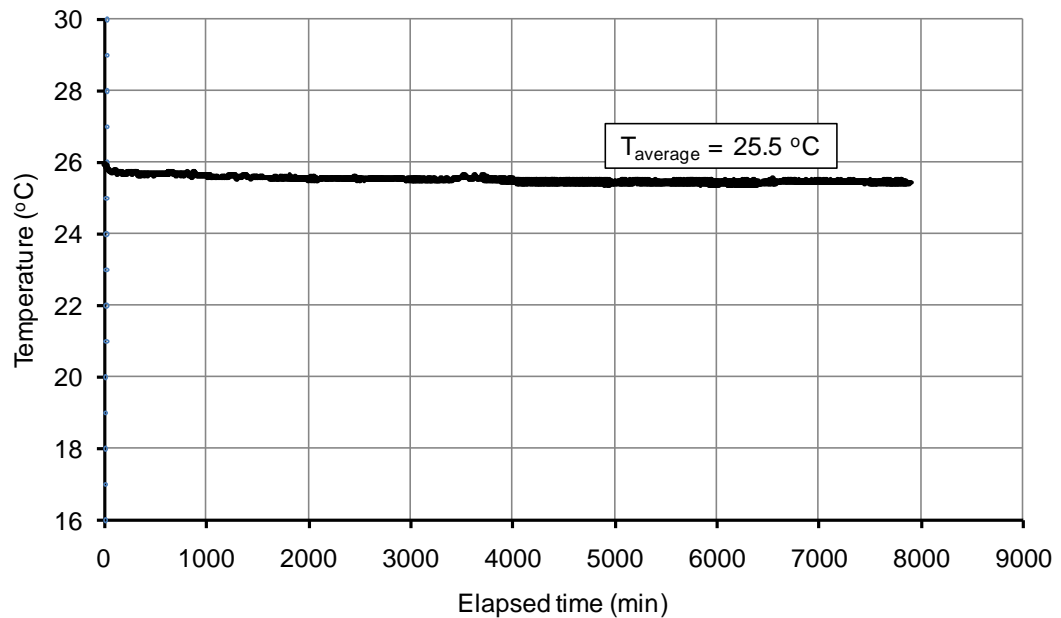


Figure 5.21 Temperature changes inside the environmentally-controlled room during evaporation Process PS3

### 5.5.1 Potential Evaporation Rates

Figure 5.23 shows the potential evaporation rate for a no-radiation–no-wind condition within the environmentally controlled room. Figure 5.24 shows the change in temperature of the water with respect to time during potential evaporation process. Water temperature decreased while the evaporation rate increased. The evaporation rate

reached the maximum value of about 8 mm/d when the water temperature at the surface of the water was 23.7 $^{o}$C.

The temperature showed a sudden drop and rise between the elapsed times of approximately 934 to 953 minutes. The sudden change in the temperature was due to the downward movement of the water surface as a result of evaporation. The thermocouple measured the air temperature above the water surface when the elapsed time was greater than 935 minutes. A difference of about 1.5 $^{o}$C between water and air temperatures was observed (see Figure 5.20).
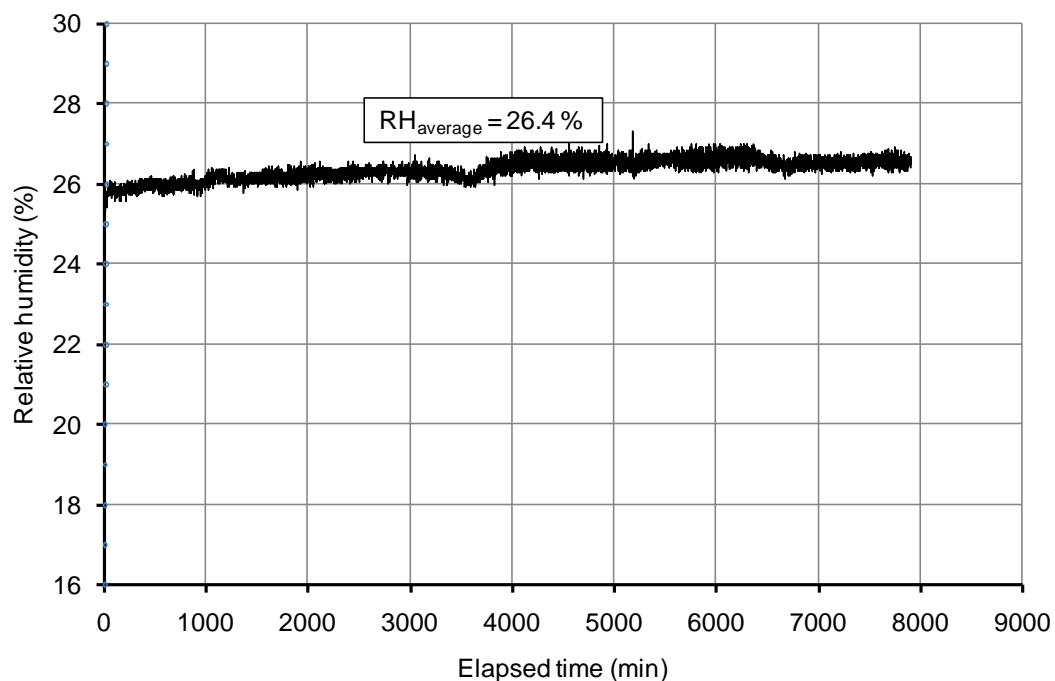


Figure 5.22 Relative humidity changes inside the environmentally-controlled room during evaporation Process PS3

Figure 5.25 and Figure 5.26 show the potential evaporation values for "wind" and "wind and radiation" treatments, respectively. As the water surface moved downward into the evaporation column, the evaporation rate decreased as a result of reduction in the effect of the wind. Maximum evaporation rates of about 25 and 35 mm/d were measured for the "wind" and "wind and radiation" treatments, respectively.

169
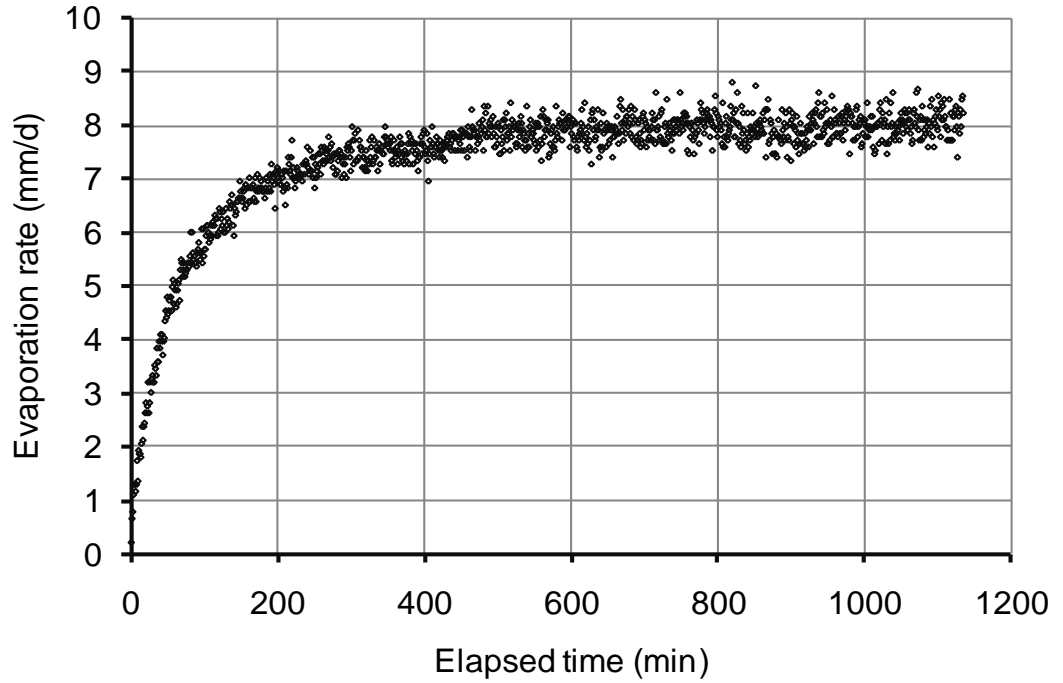
Figure 5.23 Evaporation rate versus time for "without wind" treatment (an environmental condition of RH = 26 % and T = 25.5 $^{\circ}$C)
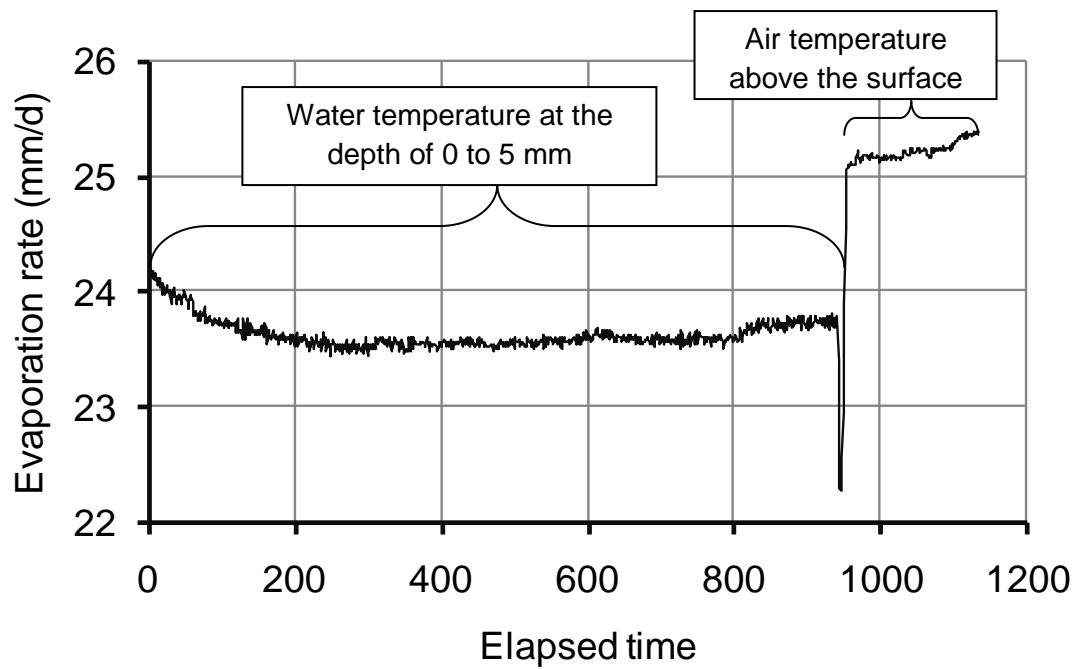


Figure 5.24 Temperature versus elapsed time at 5 mm from the top edge of the evaporation column during measurement of the potential evaporation

170
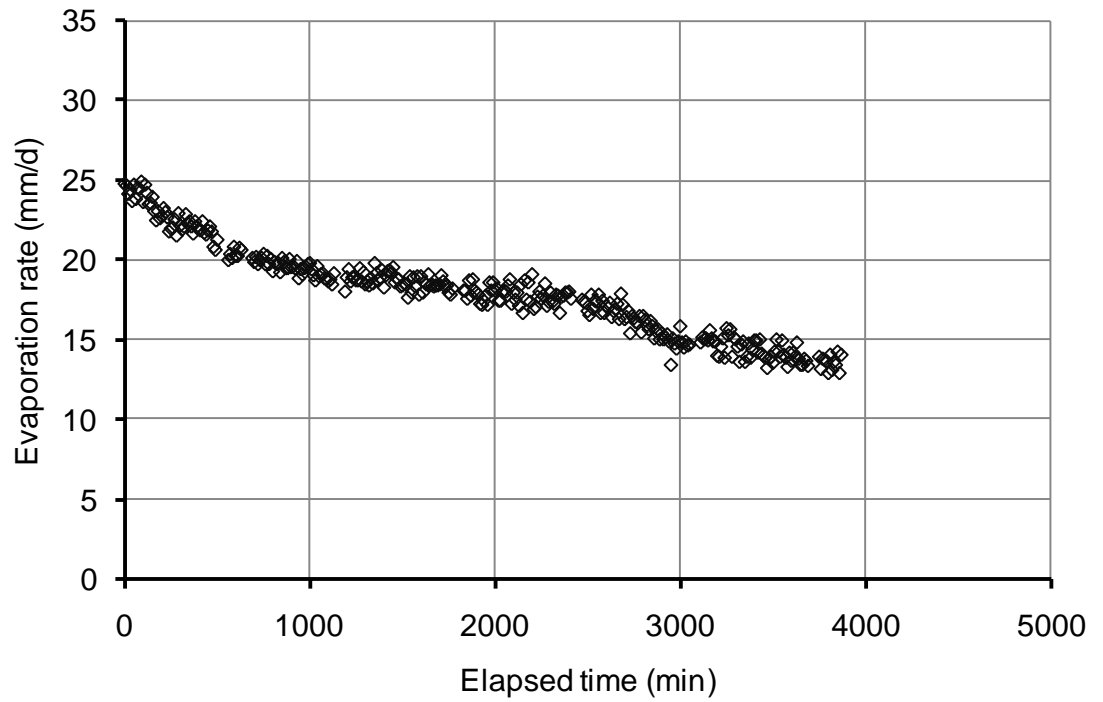
Figure 5.25 Evaporation rate versus elapsed time for "wind" treatment
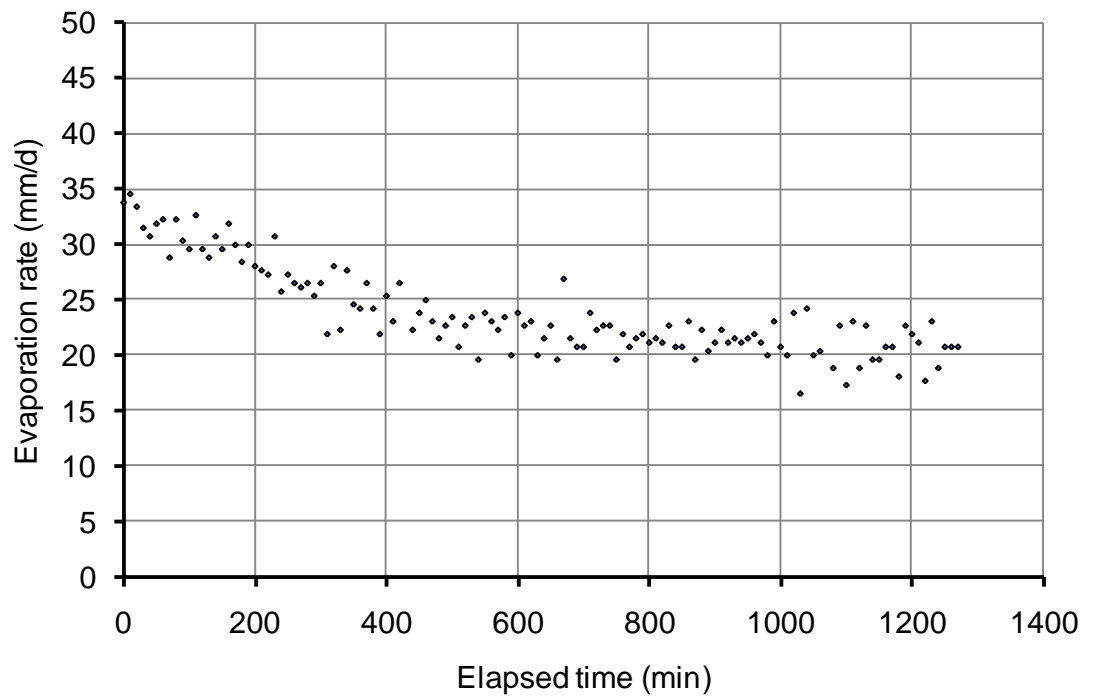


Figure 5.26 Evaporation rate versus elapsed time for "wind and radiation" treatment

171

### 5.5.2 Actual Evaporation Rates

The mass of the soil-filled evaporation columns was measured during the evaporation processes by means of an electronic balance (Ohaus Explorer) with a readability of 0.01g. The mass values fluctuated slightly (± 0.05g) because of air circulation within the environmentally controlled room. The mass was automatically recorded with time increments of 10 min for all evaporation processes except evaporation process PS1, for which the data were recorded manually.

The actual evaporation rate at a given elapsed time was estimated as the slope of the change in the soil column mass versus time plot, plus the constant inflow rate applied to the soil column through the GDS volume and pressure control system. Since the mass values were recorded at 10-minute increments, the actual evaporation rates could be calculated based on the mass changes in 10 minutes. At the early stages of evaporation when the rate was high, the actual evaporation could be calculated using the change in mass data within shorter time increments. At the later stages of the evaporation, the changes in mass of the soil columns within 10-minute increments were too small to be used in the calculation of the evaporation rates, as there could be substantial errors.

The evaporation rates are calculated using 1-hour, 6-hour and 24-hour based data. To calculate 1-hour based data for instance, the mass reduction of the evaporation column in the first hour was calculated. The constant inflow rate applied to the soil column through the GDS volume and pressure control system for the first hour was added to the difference in the column mass. The summation was then divided by the elapsed time (60 min) and the evaporation rate was calculated in mm/d. The calculated evaporation rate is shown on the graph at 60 min. This calculation was repeated for the second set of data, starting from 10 min of the initiation of evaporation tests. The calculated evaporation from the second sets of data is shown at 70 min on the graph. These calculations were repeated for the following sets of data. The data are shown as "based on 1-hour data" on evaporation versus elapsed time plots.

The calculations were repeated based on first 6 hour data at the beginning of the evaporation test. The first calculated evaporation rate was shown on the plot at 6-hour elapsed time (360 min). The time lag of 360 min can be seen on the graph for 6-hour

172

based data as a result of these data analysis. The time lag for 24-hour based data is 1440 minutes.

Plots of actual evaporation rates with respect to time for the primary and for the modified evaporation column tests are presented in the following sections. Sections 5.5.2.1 and 5.5.2.2 present results for the Beaver Creek sand specimens for primary and modified evaporation processes, respectively. Sections 5.5.2.3 and 5.5.2.4 present the results for Botkin silt specimens for primary and modified evaporation processes, respectively.

Wind and/or radiation with some of the evaporation tests were exclusively considered to accelerate evaporation at the beginning of the tests (Chapter 4, table 4.13). The speed of wind and the quantity of radiation are not considered in the analysis.

At the end of the evaporation tests, whenever possible the soil samples were taken from different depths in order to measure the gravimetric water content. These results are presented in section 5.5.4.

### 5.5.2.1 Actual Evaporation Rates for Beaver Creek Sand Specimens for the Primary Soil Column Evaporation Processes

Figures 5.27 to 5.31 show the actual evaporation rate for evaporation processes using the primary evaporation column on the Beaver Creek sand specimens.

Figure 5.27 shows the change in actual evaporation rate for evaporation Process PS1. The test was conducted in a chamber with additive relative humidity control. The temperature and relative humidity of the chamber were set at 30 $^\circ$C and 40% during the evaporation test. Out of ten evaporation tests, the test PS1 was the only one conducted in this chamber. The remaining tests were conducted in a room equipped with a dehumidifier system (see Chapter 4, section 4.6.1.1). The initial soil was in slurry condition when the specimen for evaporation process PS1 was prepared (see Chapter 4, section 4.6.2.1). A porous stone with air-entry value of 1.8 kPa was placed at the bottom of the specimen. The GDS volume/pressure controller was used to control the inflow rate. The inflow rate at the start of the test was set at 11.49 mm/d. The evaporation rate began to decrease and became constant at elapsed time corresponding to about 3,000 minutes.

At an elapsed time corresponding to 4,500 minutes, the mass of the soil column had a tendency to increase. It was reasoned that this increase in mass might be due to the high inflow rate applied at the bottom of the soil column; therefore, the inflow rate was reduced to one half of its initial value (i.e., 5.74 mm/d). The evaporation rate bagan to decrease and became constant at an elapsed time corresponding to about 6,500 minutes. The mass of the column began to increase again at an elapsed time corresponding to 8,600 minutes. The evaporation process ended at an elapsed time of 9,700 minutes.
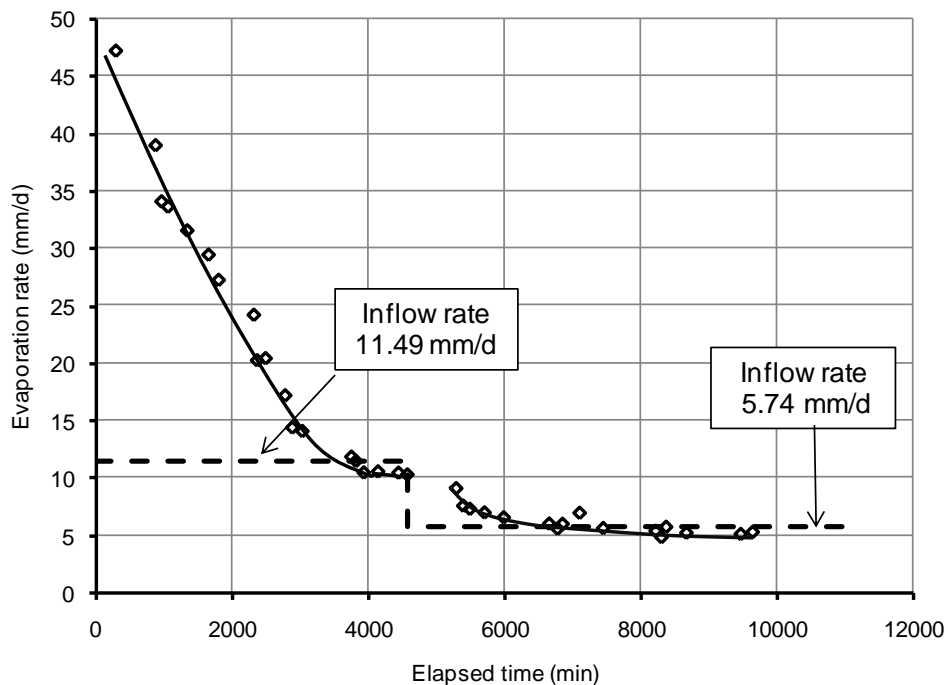


Figure 5.27 Actual evaporation rate versus time data for evaporation Process PS1(Beaver Creek sand, wind and radiation treatment)

Evaporation process PS2 was also conducted on Beaver Creek sand. The evaporation process was conducted in the environmentally controlled room 2- 47, where the chamber was equipped to a de-humidifier allowing for the constant lower relative humidity. The test conditions were similar to evaporation process PS1, except that the test was conducted in an environmentally controlled room with relative humidity and temperature of approximately 25% and 26 $^\circ$C, respectively, and that the evaporation process was accelerated only with wind. The soil column was prepared with the same

initial condition as Test PS1. The inflow rate for the evaporation Process PS2 was set at 5.74 mm/d and remained constant throughout the test.

Figure 5.28 shows the actual evaporation rate versus elapsed time for evaporation Process PS2. The actual evaporation rates are presented based on 1-hour data and 24-hour data. Likewise, the evaporation process for Test PS1 showed that the mass of the column had a tendency to rise at an elapsed time corresponding to 6,200 min. The increase in the mass of the column is not clearly reflected in evaporation rate graphs.
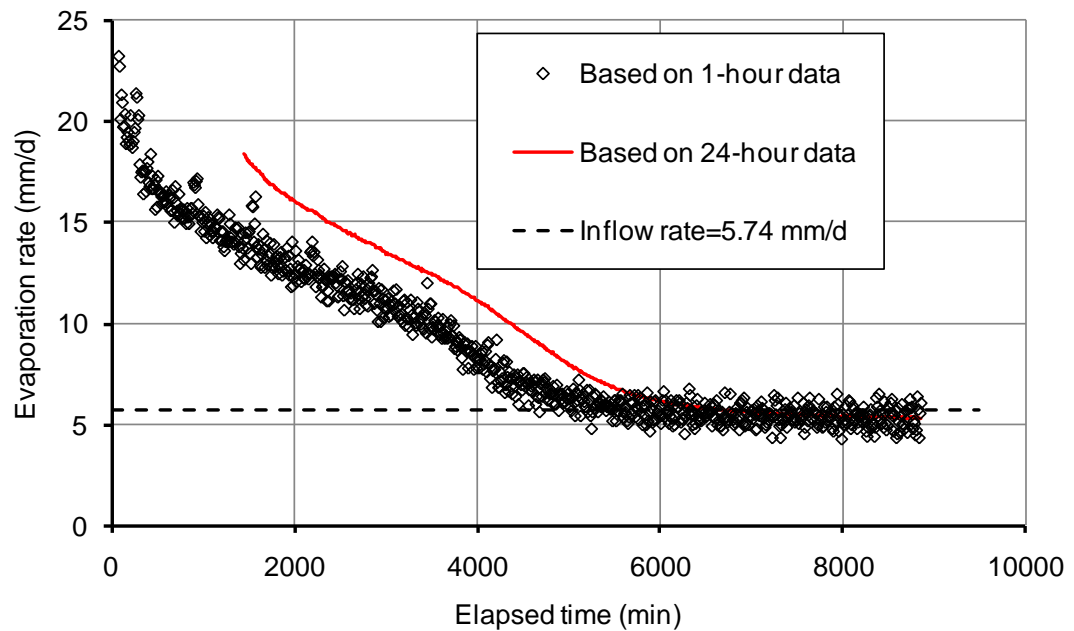


Figure 5.28 Actual evaporation rate versus time data for evaporation Process PS2 (Beaver Creek sand, wind treatment)

Evaporation Process PS3 was also conducted on a Beaver Creek sand specimen. All test conditions were the same as for Test. PS2, except that the top boundary condition had a 30 Watt bulb installed at 40 cm above the soil surface to control the temperature at the surface of the soil (described in Chapter 4, section 4.6.3 for wind and radiation treatment).

Figure 5.29 shows evaporation rate versus time data for Test PS3. The evaporation process was ended a day after reaching the point that appears to represent steady-state flow conditions.
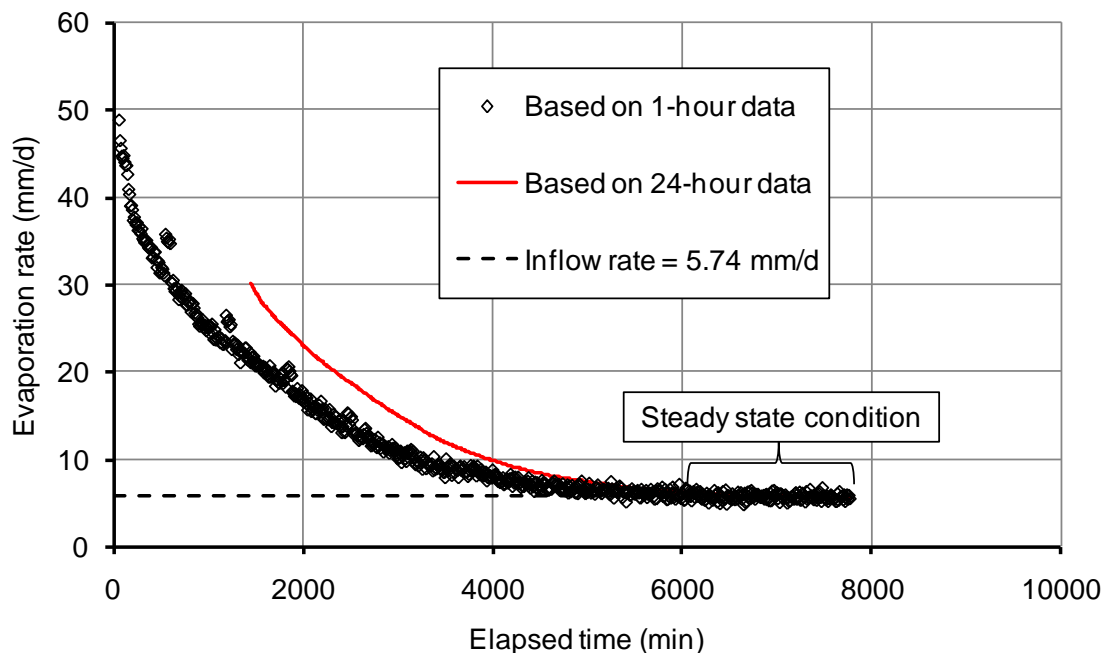
Figure 5.29 Actual evaporation rate versus time data for evaporation Process PS3
(Beaver Creek sand, wind and radiation treatment)

Evaporation Process PS4 was also conducted on the Beaver Creek sand. Some modifications were applied in an attempt to avoid the shortcomings from the earlier tests. The sand was compressed as described in Chapter 4, section 4.6.2.1. The "wind" boundary condition was applied at the top of the soil column. The wind speed was slow at the beginning of the evaporation process and changed to a higher speed at an elapsed time of t = 6,150 min. A ceramic porous plate with a high air entry value (AEV = 1 bar) was placed at the bottom of the soil column between soil and the grooved pedestal. The GDS volume/pressure controller was used to control the inflow rate from the bottom of the soil column at 2.3 mm/day.

Figure 5.30 shows the results of actual evaporation rates versus time for the primary evaporation process associated with Test PS4. The evaporation rate increased during the early stages of evaporation. The increase in the rate of actual evaporation might be attributable to the possibility that the soil column was not fully saturated at the beginning of the test. At the elapsed time of 6,150 min, the evaporation rate was further promoted by changing the wind speed from slow to high. The effect of an increase in wind speed resulted in an increase in the rate of evaporation (see Figure 5.30). The

176

increased evaporation rate reduced the inflow rate with time as a result of the further drying of the soil at the surface. The process was ended when the evaporation rate became equal to the inflow rate suggesting that steady-state flow conditions had been achieved.
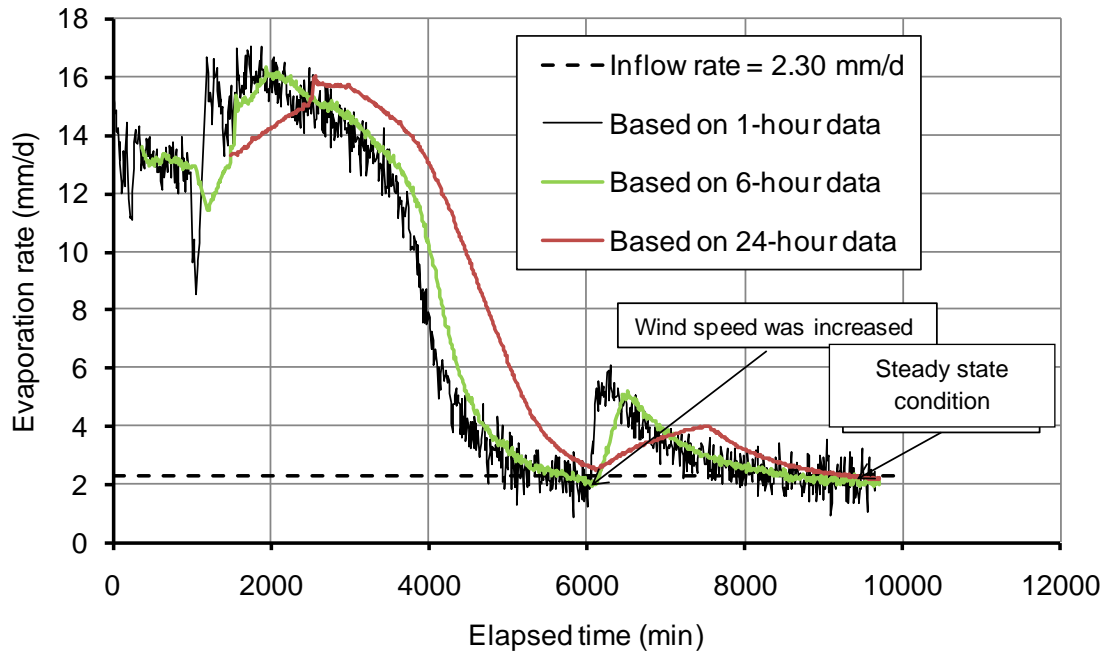


Figure 5.30 Actual evaporation rate versus time data for evaporation Process PS4
(Beaver Creek sand, wind treatment)

For evaporation Process PS5, the sample was compressed, and a porous plate with air-entry value of 1.8 kPa was used at the bottom of the soil column. Water was applied from the bottom of the sample through a water reservoir (Mariotte bottle). The bottle used for this purpose was described in Chapter 4, section 4.6.1.6. The Mariotte bottle was also used to keep the water table at a constant level inside the sample (at the depth of 140 mm). The fan was placed closer to the sample (40 mm from the edge of the soil column) to promote a higher rate of evaporation.

Figure 5.31 shows the rate of evaporation versus elapsed time for evaporation Process PS5. An extremely high evaporation rate at the start of the evaporation (about 75 mm/d) was measured. The water table was placed at a shallow depth (140 mm) to provide the required water for evaporation. The actual evaporation rate results showed a

sharp drop during the early stages of the process, followed by a slow rate. The evaporation rate remained high after about 18 days, when the test was terminated.
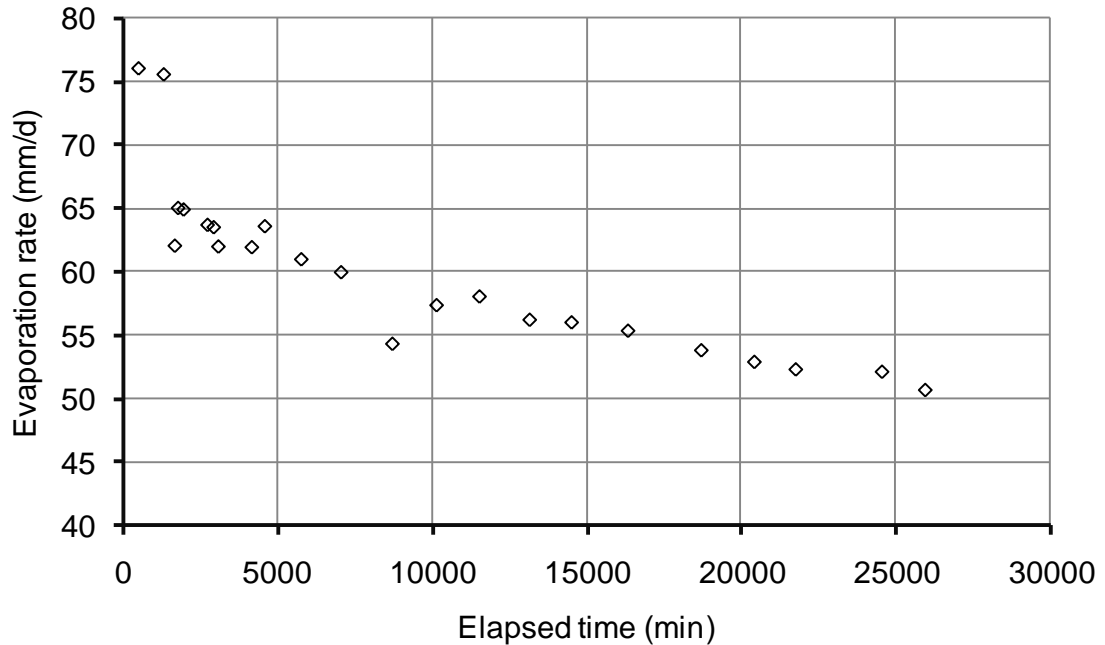


Figure 5.31 Actual evaporation rate versus time data for evaporation Process PS5
(Beaver Creek sand, wind treatment)

## 5.5.2.2 Actual Evaporation Rate for Beaver Creek Sand Specimens for Modified Column Evaporation Processes

This section presents the actual evaporation rate versus time data for the Beaver Creek sand specimens subjected to the modified evaporation process. The evaporation process was conducted in the environmentally controlled room with a relative humidity of 26% and temperature of 25 $^{\circ}$C. The soil specimen was consolidated to 200 kPa before the evaporation process. The top boundary condition consisted of a slow wind speed treatment. The ceramic porous plate with an air-entry value of 1 bar was placed at the bottom of the soil specimen. The lower boundary condition consisted of a constant flow rate of 5.74 mm/d controlled by the GDS volume/pressure controller.

Figure 5.32 shows the results of evaporation Process MS1. During the test, actual evaporation rates versus time plots were plotted and monitored. The necessary adjustments in boundary conditions were made based on the plotted results to reach flow

178

steady-state conditions. The actual evaporation rate decreased with time. It was expected that the actual evaporation rate would decrease to the inflow rate and become constant. However, the evaporation rate fell below the inflow rate and then stayed constant. There was a difference about 0.8 mm/d between actual evaporation rate and inflow rate.
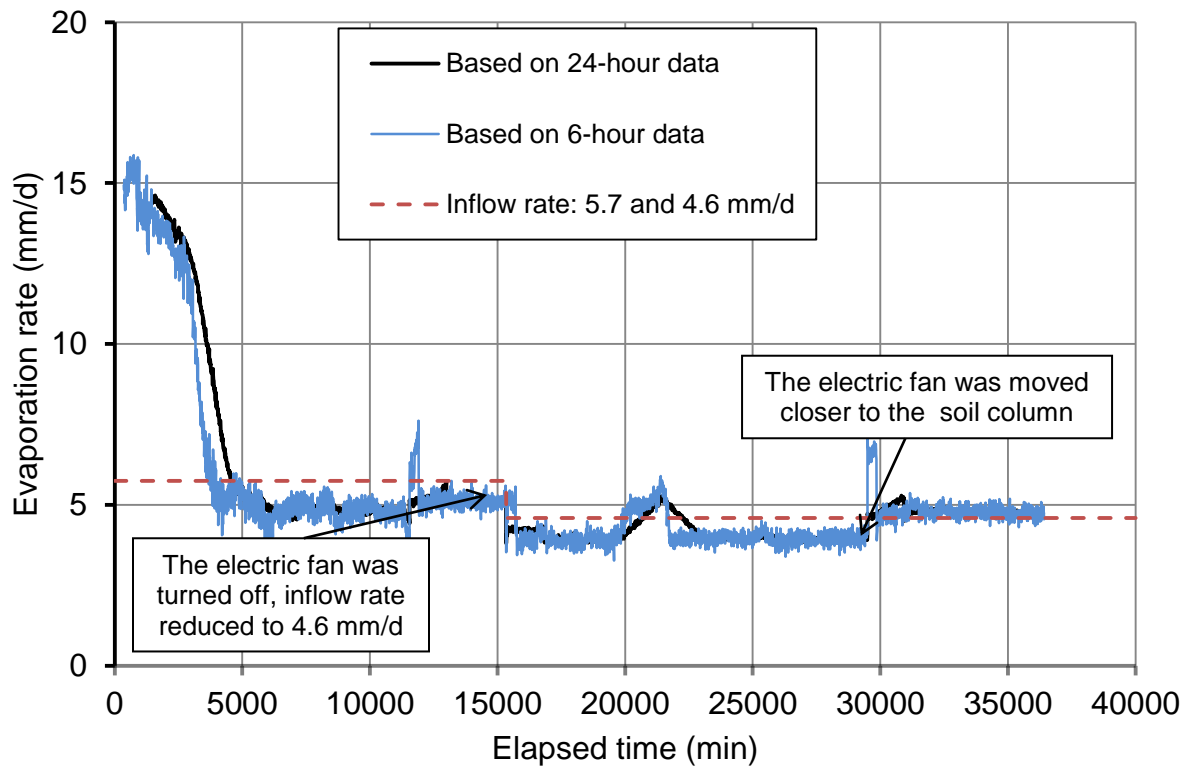


Figure 5.32 Actual evaporation rate versus elapsed time for evaporation Process
        MS1(Beaver Creek sand, wind treatment)

To achieve the steady-state condition, two options were available: i) to increase the evaporation rate, or ii) to decrease the inflow rate. The evaporation rate could be increased in one of three possible ways: first, by increasing the temperature of the room; second, by decreasing the relative humidity of the room; and third, by increasing the wind speed above the soil surface. The latter action was performed by moving the fan closer to the edge of the soil column (80 mm). The fan was initially at a distance of 122 mm from the soil column. The change was made at an elapsed time of 11,560 min as shown in Figure 5.28. In a relatively short time (about 200 min) after the adjustments

were made, the evaporation rate increased to a magnitude of 5.3 mm/d. It appeared that the steady-state flow condition was achieved.

### 5.5.2.3  Actual Evaporation Rate for Botkin Silt Specimens for the Primary Column Evaporation Processes

The first primary evaporation process on the Botkin silt (i.e., Test PCS1) was performed on a saturated slurry specimen. The sample was prepared using the saturated slurry soil with no consolidation (Chapter 4, section 4.6.2.2). Evaporation at top of the sample was accelerated using wind treatment. The relative humidity and temperature of the environmentally controlled room were 26% and 25 $^{o}$C, respectively. A porous stone with air-entry value of 1.8 kPa was used at the bottom of the column. The GDS volume/pressure controller was used to control the inflow rate at 5.74 mm/d. During the evaporation process, deep cracks appeared both horizontally and vertically in the soil specimen. The soil also shrank, resulting in a gap between the soil and the column.

Figure 5.33 shows the actual evaporation rate for Botkin silt Specimen PCS1 determined based on 1-hour, 6-hour and 24-hour data. Based on the results, the steady-state flow condition reached at about 6,000 min; however, due to cracking and shrinking, the results of this evaporation process have been discarded from further analysis.

To prevent shrinking of the soil and the formation of desiccation cracks along the soil column during evaporation, the Botkin silt Specimen PCS2 was consolidated to 20 kPa before the beginning of the evaporation process. Details on the preparation of the soil specimen were described in Chapter 4, section 4.6.2.2. Evaporation at top of the sample was accelerated using wind treatment. The relative humidity and temperature of the environmentally controlled room were 26% and 25 $^{o}$C, respectively. A ceramic plate with air-entry value of 100 kPa was used at the bottom of the column. The GDS volume/pressure controller was used to control the inflow rate at 2.3 mm/d.
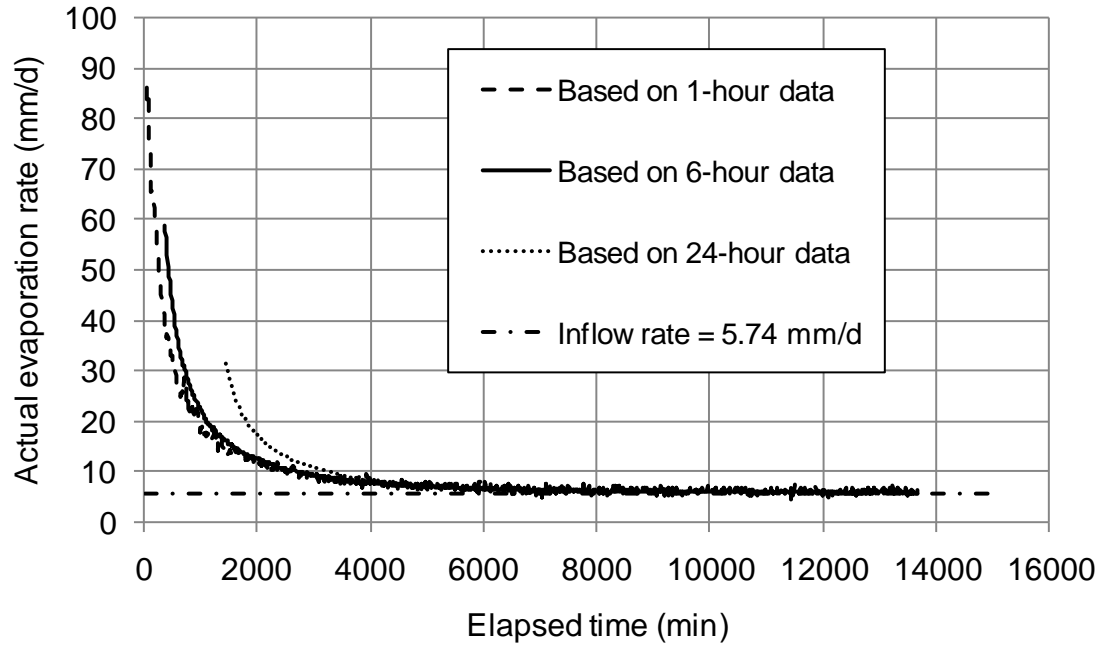
Figure 5.33 Actual evaporation rates versus time data for evaporation Process
　　　　　PCS1(Botkin silt, wind treatment)

Figures 5.34 shows the actual evaporation rate versus time data for Botkin silt
Specimen PCS2 using the primary evaporation column. The evaporation rate started at
about 26 mm/day at the beginning of the test. The rate of evaporation decreased to about
5 mm/day at t = 8,250 min. The inflow rate was 2.30 mm/d throughout the test. At t =
8,260 shrinkage cracks appeared on the surface of the soil and a vertical crack developed
from the specimen surface to a depth of about 30 to 40 mm. The heat jacket was opened
to further investigate the soil column. Horizontal and vertical cracks along the soil
column were observed (Figure 5.35)

After the shrinkage that had developed during the evaporation process on Specimen
PCS2 was observed, the specimen was again saturated. During the saturation process
(between elapsed times of 8,260 and 11,720 min) the soil surface was covered and an
inflow rate of 22.97 mm/d was applied (see Figure 5.34). After saturation, the soil
swelled and the crack opening closed.
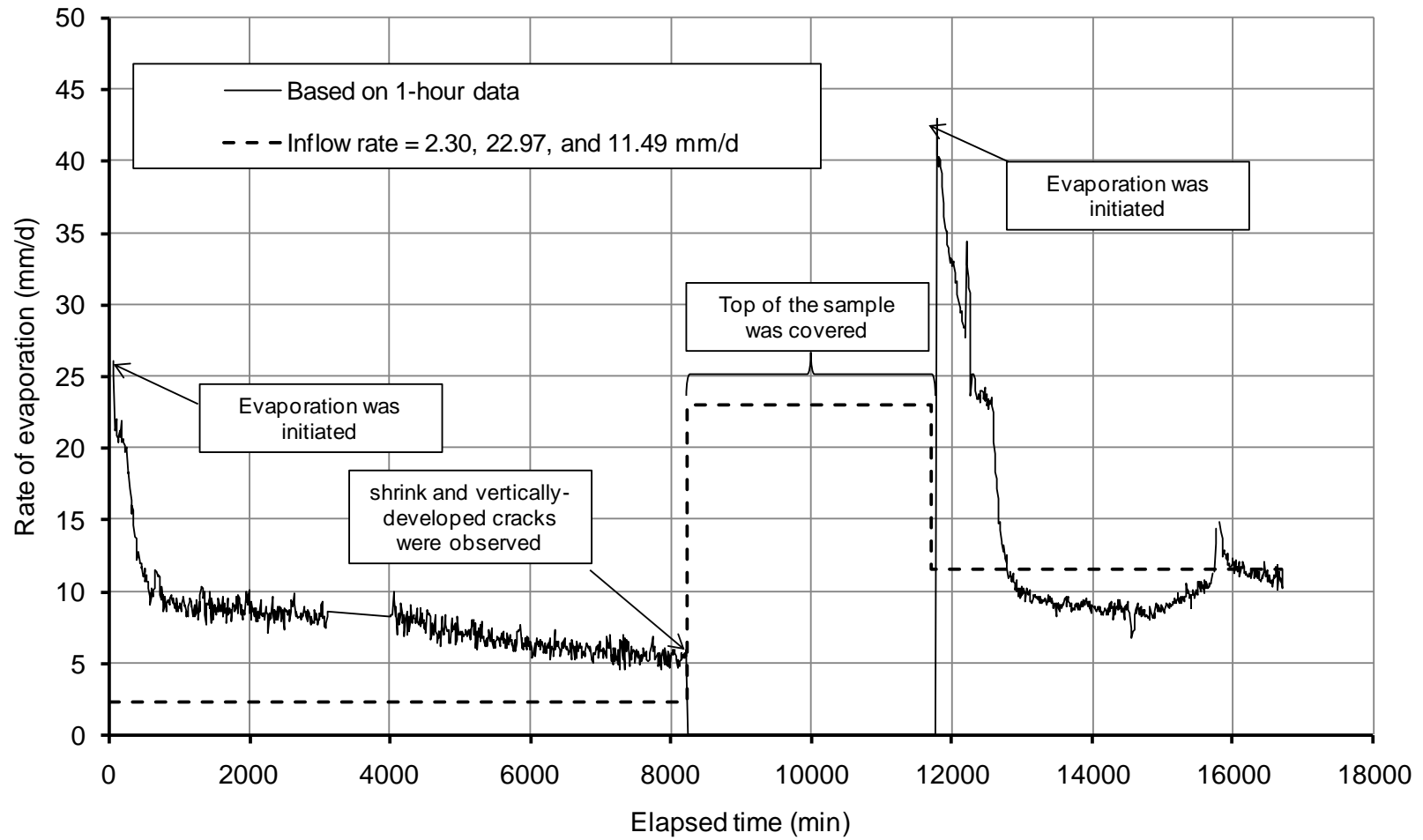
Figure 5.34 Actual evaporation rates versus time data for evaporation Process PCS2 (Botkin silt, wind treatment)
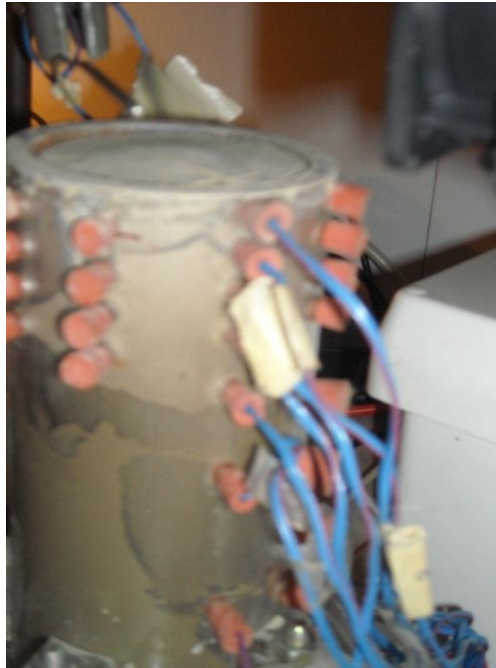
Figure 5.35 Development of the horizontal and vertical cracks along Specimen PCS2 (Botkin silt) during evaporation process

At t = 11,720 min (after saturation of the soil specimen), the evaporation process was resumed. The cover was removed from the top of the soil and the inflow rate was changed to 11.49 mm/d (Figure 5.34). Since the inflow rate was high, the evaporation reached the inflow rate (11.49 mm/d) in a relatively short time (2 to 3 days). The soil samples were not retrieved for gravimetric water content measurement from this test, since the soil was not sufficiently dry to create an acceptable water content profile for measurement of the unsaturated coefficient of permeability at lower water contents.

### 5.5.2.4   Actual evaporation rate versus time for Botkin Silt Specimens for the Modified Column Evaporation Processes

This section presents the actual evaporation rate versus time data for the evaporation processes on Botkin silt specimens MCS1 and MCS2 with the modified column evaporation process. The specimens were consolidated to 100 kPa and 50 kPa, respectively, in an attempt to overcome the problem of specimen cracking during the evaporation process. The details of the soil column preparations and evaporation procedure were described in Chapter 4, sections 4.6.2.2 and 4.6.3, respectively.

The "wind" treatment was used as the top boundary condition during the evaporation process on Specimen MCS1. The evaporation started with higher inflow rate of 11.49 mm/d. Figure 5.36 shows the evaporation rate versus time data for Specimen MCS1. The evaporation rate dropped below inflow rate beyond 2,300 minutes. The reduction in evaporation rate below the inflow rate resulted in an increase in the soil column mass. At t = 3,000 min the mass of the column increased sharply.

At t = 5,740 minutes, the heat jacket was removed and the soil column was investigated. Vertical cracks were not observed; however, there was shrinkage along the soil column, starting with about a 2 mm gap between the soil and the cell at the surface and decreasing throughout the depth of the soil column. The surface of the soil was dried. The side of the soil was also dried to a depth of about 30 mm. Water was observed in the gap between the soil and the cell below the dry surface.

After investigation of the soil column, the heat jacket was put back in place and the evaporation process was resumed for another couple of days. An attempt was made to inject wax around the gap. The injection of wax was not successful due to the small size of the gap, and needle became clogged with wax during injection. After about 6,800 minutes from the beginning of the evaporation process, the inflow rate was still greater than the rate of the evaporation; therefore, the mass of the column was still slowly increasing.

It appeared that near steady-state condition for the Specimen MCS1 were reached at an elapsed time around 7,500 min. Soil samples were taken through the thermocouple ports in order to measure the gravimetric water content of the soil. The evaporation column was then dismantled. There were no cracks observed on the soil specimen. The diameter of the soil specimen was measured in different heights. The specimen had shrunk about 2 mm at the top, 1 mm at the mid-height and 0 mm at the bottom.

From results of the evaporation process on Specimen MCS1 it was concluded that modification of the evaporation column and consolidation of the specimen to 100 kPa had helped to prevent the specimen cracking. However, it was not clear whether consolidation or shortening the evaporation column had prevented cracking of the specimen. The shrinkage or evaporation from side walls was still an issue.
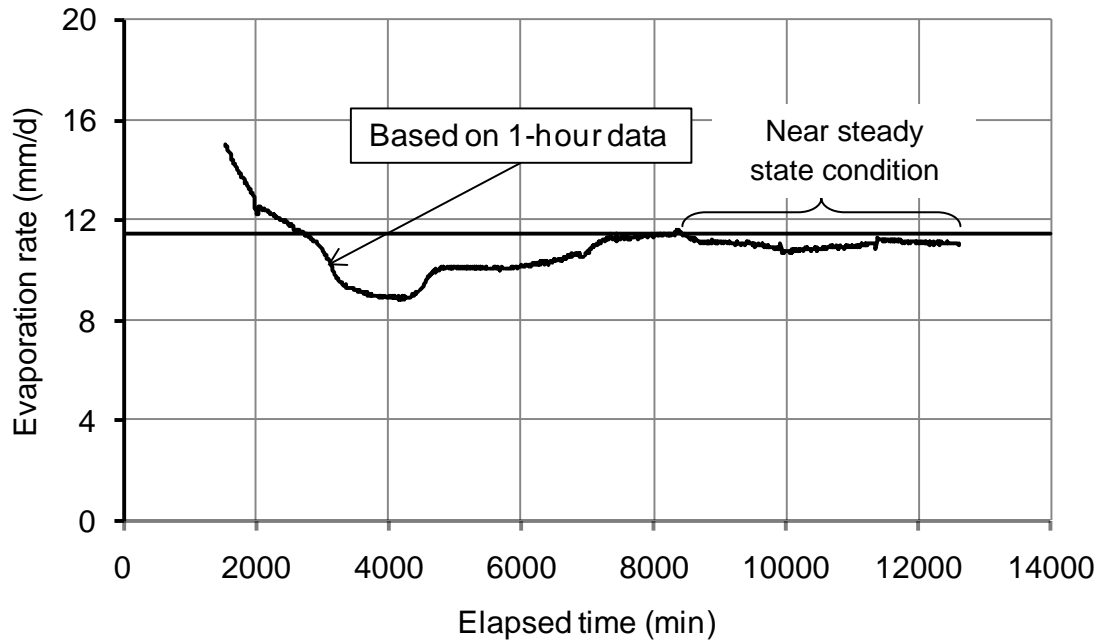
Figure 5.36 Actual evaporation rate versus time data during evaporation Process MCS1
(Botkin silt, wind treatment)

Specimen MCS2 was consolidated to a maximum vertical pressure of 50 kPa before the beginning of the evaporation process. In order to prevent evaporation from the side surface of the specimen during evaporation, the specimen was confined with a triaxial membrane during both consolidation and evaporation processes. Details of the preparation were described in Chapter 4, section 4.6.2.2. The "no-radiation–no-wind" treatment was used as the top boundary condition at initiation of the evaporation process on specimen MCS2. In other words, the evaporation started without an attempt to accelerate the rate of evaporation by use of an electronic fan or a bulb above the soil column. The inflow rate at the start of evaporation was 1.13 mm/day and remained constant throughout the evaporation process.

Figure 5.37 shows the evaporation rate versus time data for Specimen MCS2. The evaporation rate increased at the beginning of the test, stayed constant from 300 to 3,000 min and then decreased towards a constant value equal to the inflow rate. The evaporation rate became equal to the inflow rate at about 13,500 min and remained constant (steady-state flow condition) until the test was terminated.
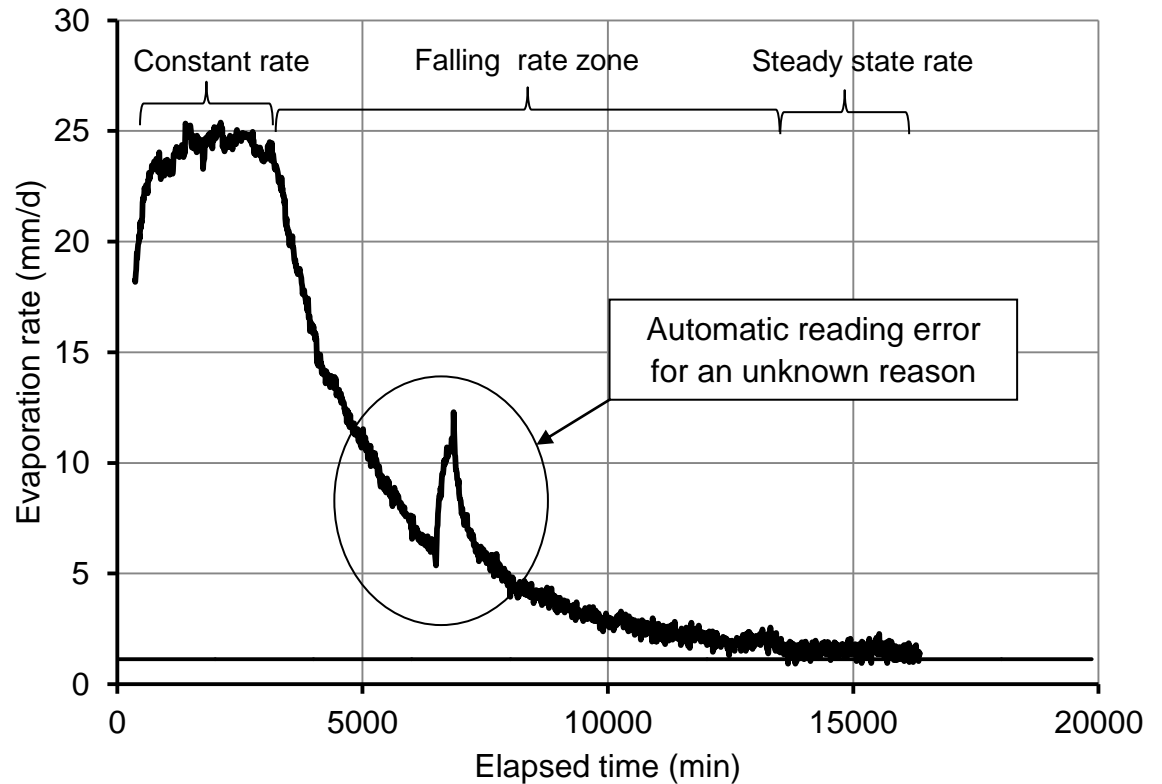
Figure 5.37 Actual evaporation rate versus time data during evaporation Process MCS2
(Botkin silt, no-wind –no-radiation treatment)

### 5.5.3   Temperature Measurements

Soil temperature data at selected depths along the soil column were recorded using T-type thermocouples attached to a Campbell Scientific data logger (CR1000). There were 8 selected depths for thermocouples along the column for the primary evaporation column tests. For the modified evaporation processes, thermocouples were placed at 5 selected depths along the column. For the last evaporation process on a Botkin silt soil column (MCS2), the temperature was measured only at the surface of the soil. A time increment of 10 minutes was chosen for the measurement of the soil temperature.

In addition to the thermocouples used for recording the soil temperature, air temperature above the surface of the soil was also measured using 1 or 2 thermocouples for some of the evaporation processes. Temperature in the room was also recorded using two Hobo data loggers.

The following sections present the results of temperature measurements including soil temperature for the selected depths along the evaporation columns and air temperature during evaporation.

### 5.5.3.1 Change in Temperature along and above the Beaver Creek Sand Specimens for the Primary Evaporation Column Tests

This section presents temperature changes with respect to time at the selected depths along the primary evaporation column for Beaver Creek sand specimens PS1 to PS5 (Figures 5.38 to 5.42).

Figure 5.38 shows the change in temperature versus time data for primary evaporation process for Beaver Creek sand Specimen PS1. The "wind and radiation" treatment was used as the top boundary condition. An attempt was made to control the temperature of the soil surface through thermocouple T1, which was placed at a depth of 4.5 mm from the surface of the soil. The temperature was maintained at a constant value of $30 \pm 0.1\ ^{o}C$ by switching on and off a 60 Watt bulb above soil surface.

At the beginning of the evaporation process, the rate of evaporation was high. This demanded high radiation energy from the bulb in order to maintain the temperature at the given constant value $(30 \pm 0.1\ ^{o}C)$. This required a longer "turned on" status for the bulb during the early stages of evaporation. A portion of the radiation energy, in addition to the portion required for latent heat, was transferred to the lower layers of the soil through conduction. The energy transfer increased temperature in the lower layers of the soil column at the early stages of the test (see Figure 5.38, T2 to T8).

As the soil surface became drier, the rate of evaporation decreased. Reduction in the rate of evaporation resulted in a lower required latent heat, and hence a shorter time for the bulb to be turned on. The time duration in which the bulb was turned on was not measured. The conduction heat transfer from lower layers to the surface of the soil caused reduction in temperature of the lower layers (see Figure 5.38, t = 300 to 6,000 min). For later times during the evaporation process (i.e., t > 6,500 min), temperature curves remained fairly constant. The elapsed time t = 6,500 min is coincident with the time when the actual evaporation rate became equal to the inflow rate (i.e., 5.74 mm/d) (see Figure 5.27).

Figure 5.39 shows results of the temperature change with time for primary evaporation Process PS2. The top boundary condition for this test was "wind" treatment. As the evaporation process initiated, the temperature at the surface of the soil reduced due to latent heat. A portion of the required energy for evaporation was supplied from lower layers of the soil. In other words, as soil temperature at the surface decreased because of evaporation, conduction heat was transferred from lower layers to the top resulting in reduction of the temperature at lower layers of the soil column. With time, the rate of the evaporation decreased and so did the required amount of latent heat. This in turn reduced the amount of heat transfer from lower layers to the top of the soil column, resulting in an increase in the temperature. As the evaporation rate became closer to the constant flow rate, the rate of temperature rise decreased. At near steady-state flow conditions the temperatures became near constant for all depths of the soil.

Figure 5.40 shows the results of changes in temperature with time for the primary evaporation Process PS3. Boundary conditions at the top of the soil column were similar to evaporation Process PS1 ("wind and radiation" treatment). A 30 Watt bulb used to supply radiation energy for this test. At the beginning of the test, radiation from the bulb did not supply sufficient additional energy to the soil surface to overcome the latent heat of evaporation. Therefore, temperatures of the lower layers decreased as a result of conduction heat transfer to the evaporation surface.

Figure 5.41 shows the results of temperature measurements with respect to time for the selected depths for the primary evaporation process in Specimen PS4. The temperature at the surface of the soil column decreased at the beginning of the evaporation process due to the latent heat required for the evaporation. The reduction in temperature at the surface of the soil resulted in conductive heat transfer from the lower layers. This conductive heat transfer caused a temperature reduction in the lower layers. As the soil surface became drier, the required latent heat for evaporation was reduced. This resulted in an increase in the temperatures along the soil column. The rate of change in temperature along the soil column was closely related to the rate of change in actual evaporation (Figure 5.41 and Figure 5.30).

Figure 5.42 shows the results of temperature measurements with respect to time for the selected depths for the primary evaporation process PS5. The water table was kept at

a constant depth (d = 140 mm) within the Beaver Creek sand column using a Mariotte bottle connected to the column as a water reservoir. As evaporation began at t = 530 min, the temperature dropped from 25.4 $^{o}$C to 17 $^{o}$C at the soil surface in a short period of time. Following this decrease in temperature at the surface, the temperature at lower depths of the soil column decreased due to conductive heat transfer from lower layers to the surface. The rate of evaporation remained high (see Figure 5.31) due to continuous availability of water at the soil surface. After the minimum evaporation rate had been reached, the temperature remained around 17 $^{o}$C (8.4 $^{o}$C less than room temperature) at the surface of the soil.

### 5.5.3.2 Change in Temperature along and above the Beaver Creek Sand Specimens for the Modified Evaporation Column Tests

Modified evaporation column tests were conducted on the Beaver Creek sand specimens. Six thermocouples were inserted in the soil column at different depths. Five of them were inserted through sampling ports; one was buried at the surface of the soil from the top. In addition to six thermocouples attached to the soil column, one was placed above the soil column at a height of 50-60 cm for measurement of air temperature. Two Hobo data loggers were placed above the soil surface at 2.5 and 6 cm distance from surface of the soil, respectively. The data loggers measured relative humidity and temperature values at 10-min time increments.

Figure 5.43 shows the change in temperature versus time data for the modified evaporation process in Specimen MS1. The temperature decreased at the beginning of evaporation due to latent heat. With time as the surface of the soil became drier and the suction value at the soil surface increased, the rate of evaporation decreased. The decrease in the rate of evaporation reduced the amount of energy required for latent heat. This change in turn increased the temperature at the surface of the soil. The rate of heat transfer from lower layers to the surface of the soil decreased accordingly. The outcome of these changes appeared in the form of changes in temperature. For elapsed times of 400 min to about 2,800 min, the rate of change in temperature was almost constant. After 2,800 min the temperature began to rise rapidly. This rapid rise in temperature may be attributed to the sudden decrease in evaporation rate at the surface of the soil during the same time period (see Figure 5.32).

189
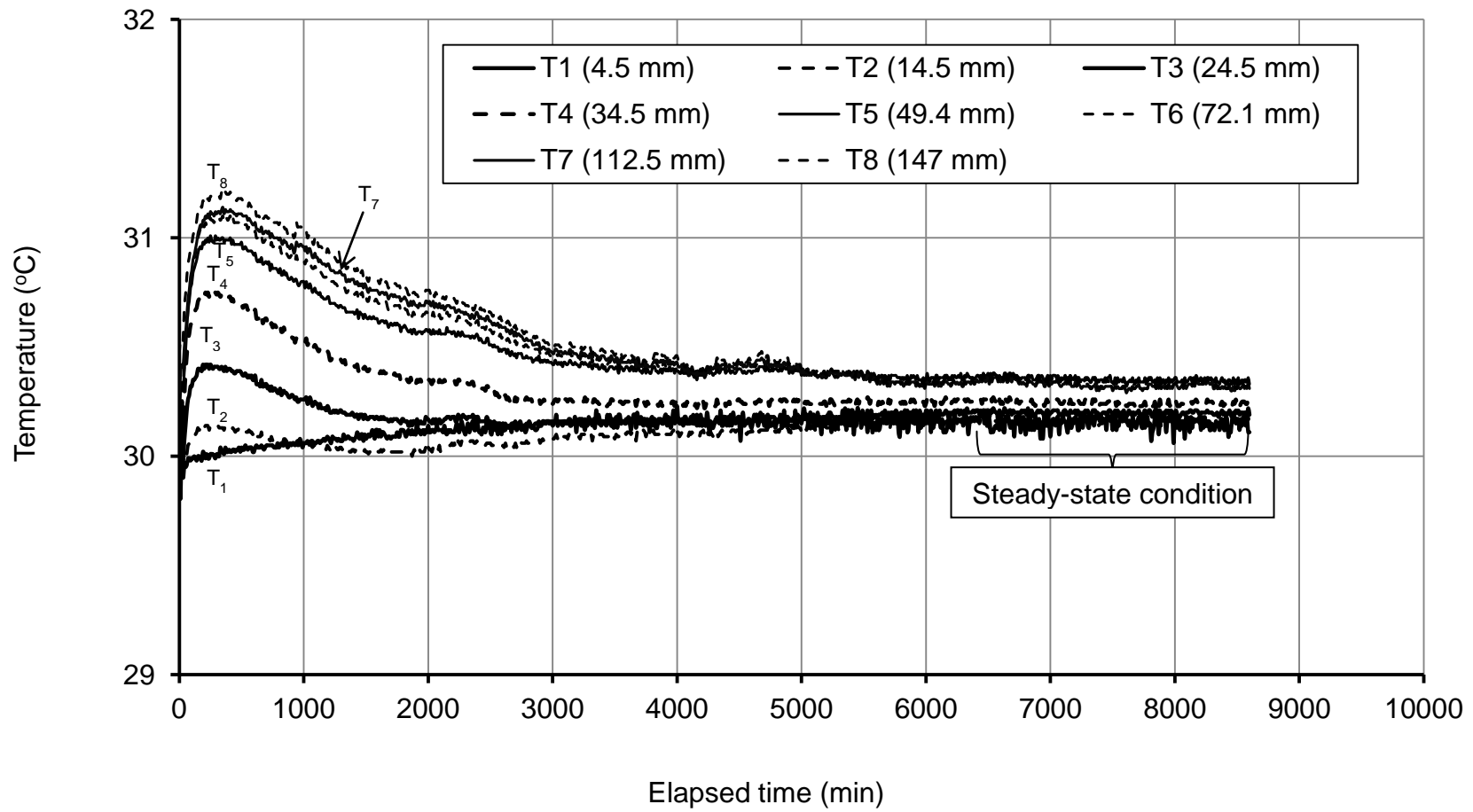
Figure 5.38 Temperature changes with respect to time along the column during evaporation Process PS1 (Beaver Creek sand)
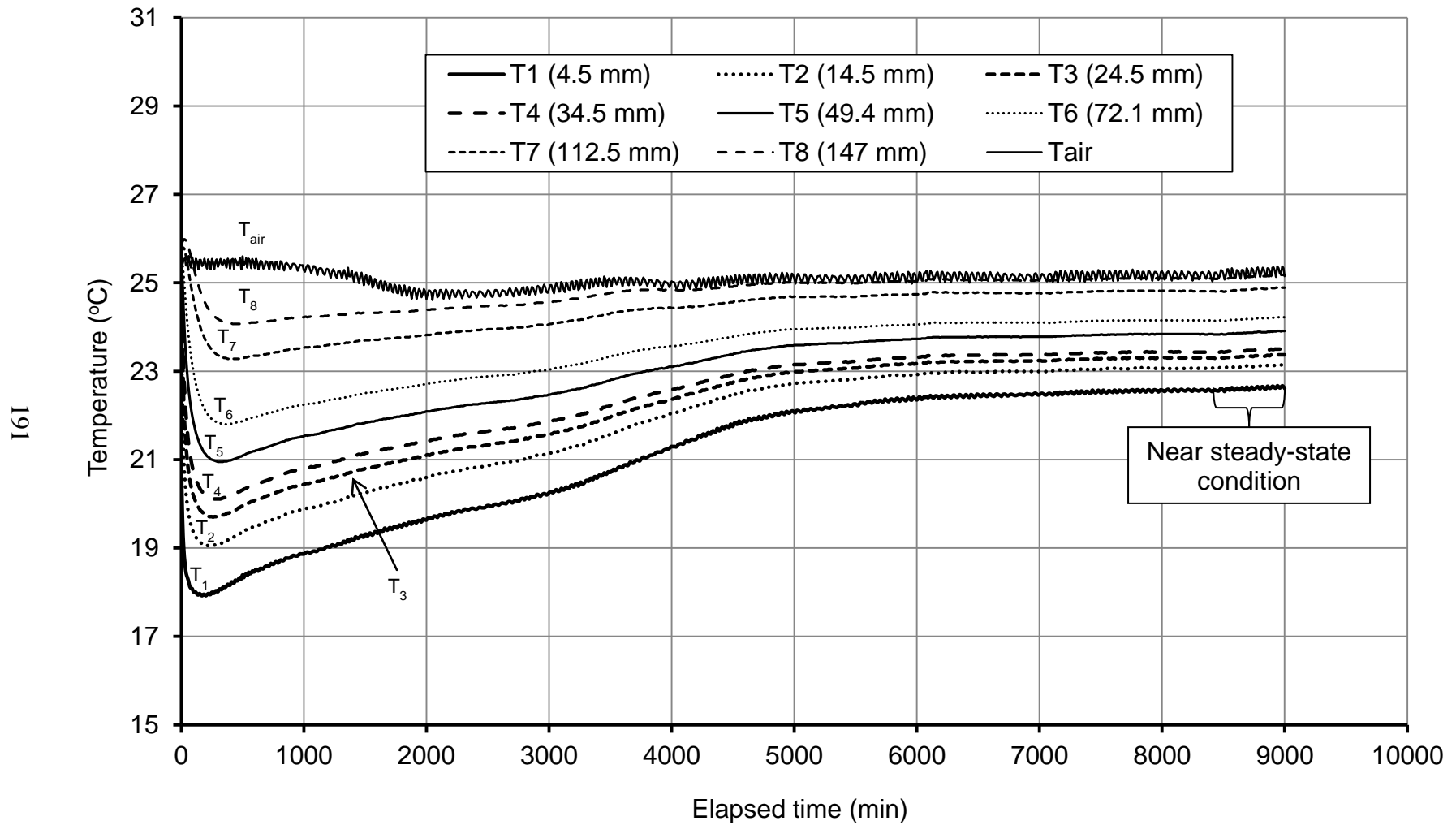
Figure 5.39 Temperature changes with respect to time along the column during evaporation Process PS2 (Beaver Creek sand)
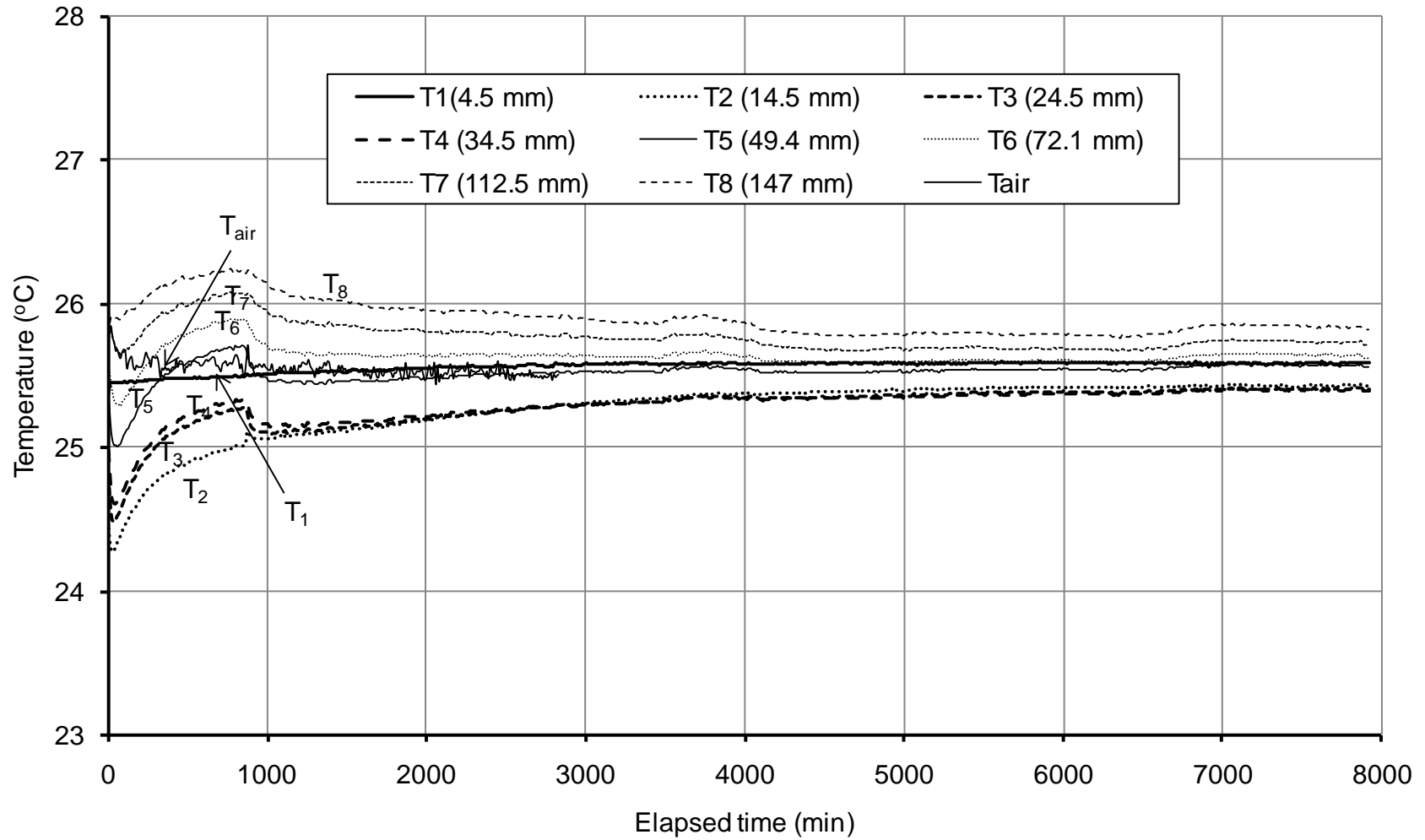
Figure 5.40 Temperature changes with respect to time along the column during evaporation Process PS3 (Beaver Creek sand)
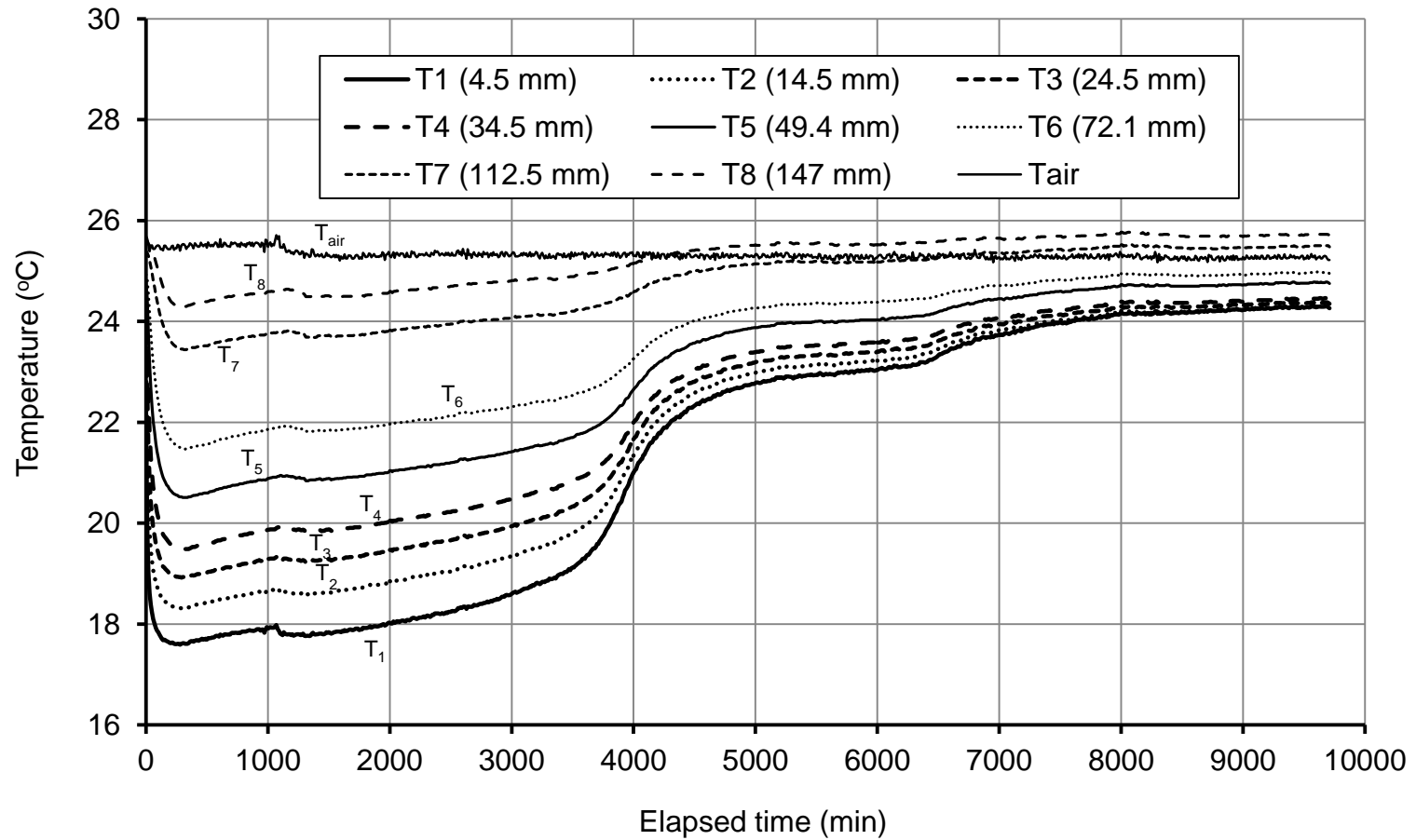
Figure 5.41 Temperature changes with respect to time along the column during evaporation Process PS4 (Beaver Creek sand)
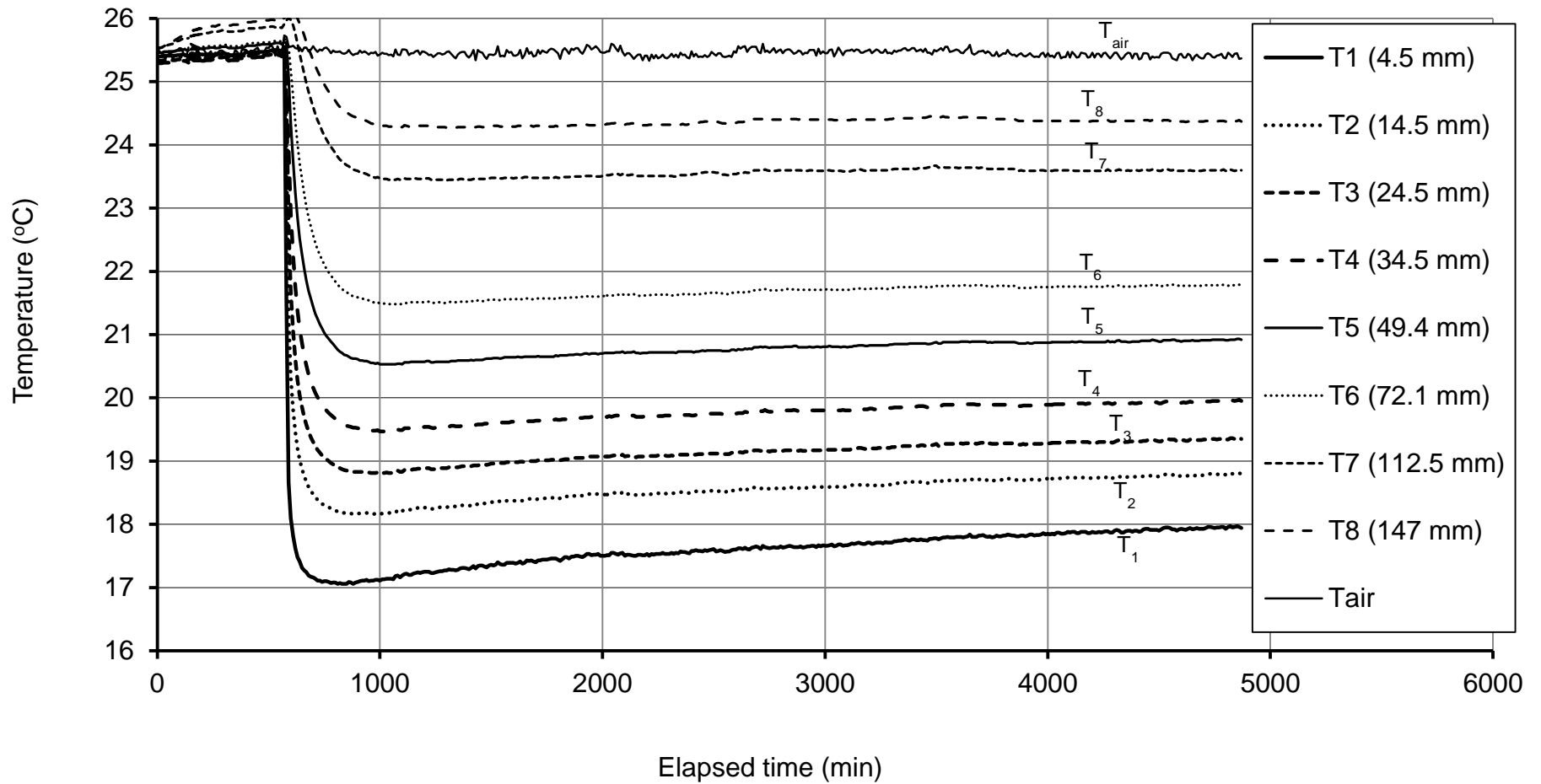
Figure 5.42 Temperature changes with respect to time along the column during evaporation Process PS5 (Beaver Creek sand)
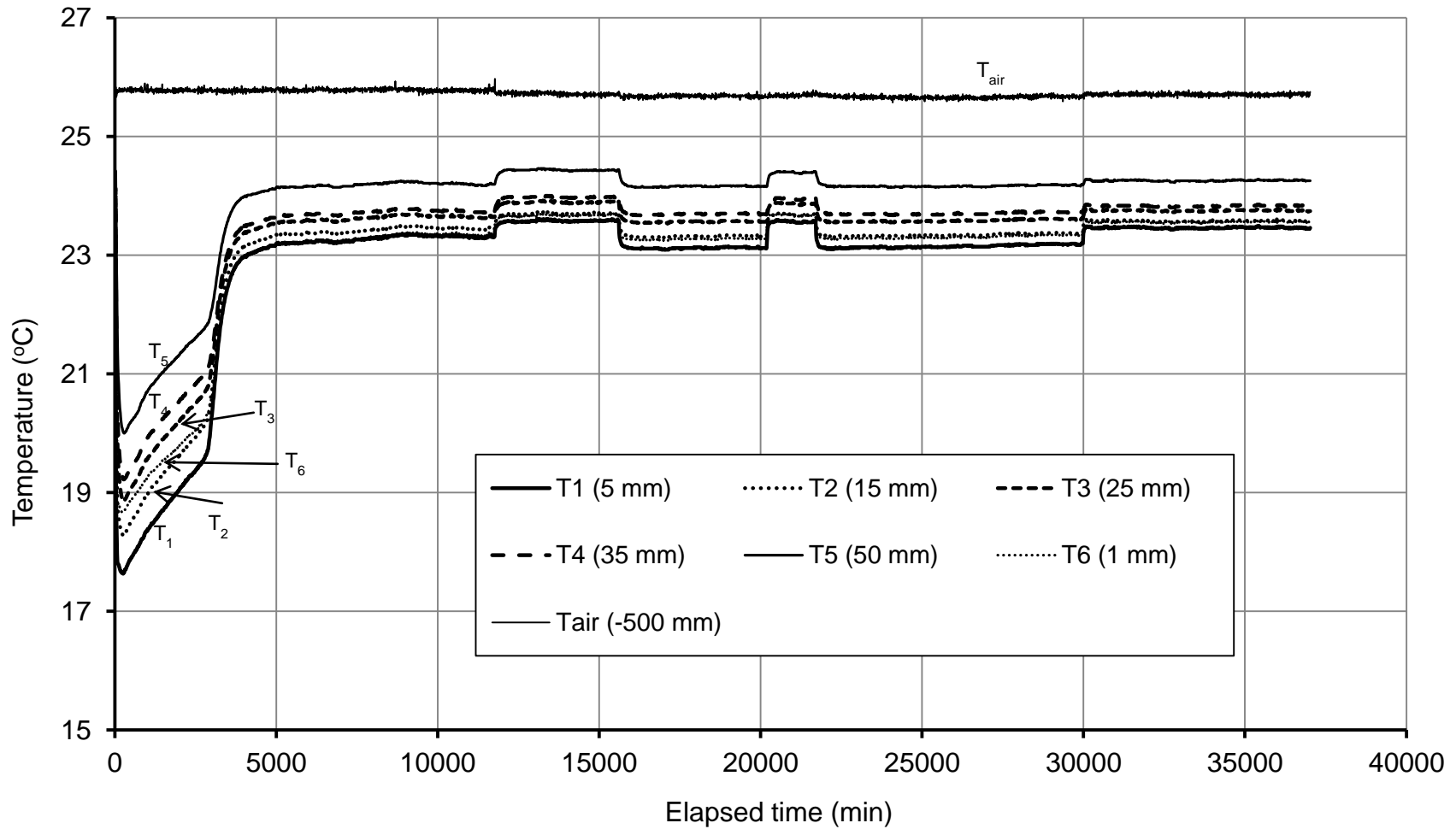
Figure 5.43 Temperature changes with respect to time along the soil column during evaporation Process MS1 (Beaver Creek sand)

### 5.5.3.3 Change in Temperature along and above the Botkin Silt Specimens for the Primary Evaporation Column Tests

Figure 5.44 shows temperature measurement results with respect to time for the selected depths during primary evaporation column Test PCS1. Temperature near the surface of the soil (i.e., T1) remained essentially constant throughout the test.

Figure 5.45 shows temperature changes with respect to time along the soil column during evaporation Process PCS2. The results are presented in the form of three processes along the elapsed time axis: first the evaporation process, the saturating process, and the subsequent evaporation process. During the first evaporation process, the soil shrank and cracks developed. This resulted in an abnormal trend for the temperature measurements with time. During the saturation process, the temperature of the soil along the column increased and approached air temperature. During the subsequent evaporation process the temperatures indicated a normal trend.

Although the temperature data at the end of both tests (PCS1 and PCS2) suggest that the steady-state flow condition had been reached, these tests were discarded from further analysis because of cracks and shrinkage observed during the evaporation tests (see section 5.5.2.3).

### 5.5.3.4 Change in Temperature along and above the Botkin Silt Specimens for the Modified Evaporation Column Tests

Figure 5.46 shows change in temperature along the soil column during the evaporation process on the Botkin silt specimen for Test MCS1. Lines T1 to T5 show the temperature change with time from top to the bottom of the soil column. $T_6$ and $T_7$ show air temperature at a distance of 20 and 50 mm above the surface of the soil. As the evaporation process was started, the temperature at the surface of the soil column decreased, and heat was transferred from the lower layers to the top layers of the soil, causing decrease in temperature of the lower layers. After the maximum evaporation rate was reached, soil began to dry at the surface, causing a decrease in the amount of evaporation. Hence, there was a decrease in the amount of heat required for evaporation from lower layers of the soil. This in turn resulted in an increase in temperatures along the soil column.

In spite of an apparent steady-state flow condition at the end of the test, evaporation test results on the Botkin silt Specimen MCS1 was discarded from further analysis because of observed shrinkage and evaporation from the side surface of the specimen (see section 5.5.2.4).

Figure 5.47 shows changes in temperature at the soil surface and temperature of the air above the soil surface with time for evaporation Process MCS2. A triaxial rubber membrane was used to minimize the amount of evaporation from the perimeter of the specimen during evaporation. To prevent any damage to the rubber membrane that installation of the thermocouples might have caused, temperature was monitored only at the surface of the soil. A thermocouple was installed at the surface of the soil from the top. The same pattern of temperature change at the surface of the specimen that occurred in Test MCS1 (Figure 5.46, $T_1$) was observed in evaporation Process MCS2 (Figure 5.47, $T_{soil\ surface}$). As evaporation started, the temperature at the surface of soil specimen decreased. The temperature remained constant during the constant evaporation rate. The soil began to dry at the surface causing a decrease in the amount of evaporation; hence, there was a decrease in the amount of heat required for evaporation from lower layers of the soil specimen. This, in turn resulted in an increase in temperatures at the surface of the specimen.

The modified evaporation process on Botkin silt Specimen MCS2 produced proper results that could be used in data analysis.

### 5.5.4 Gravimetric Water-Content Profile

At the end of the evaporation column tests, measurements of gravimetric water-contents were carried out at selected depths along the soil column. Details of these measurements were described in Chapter 4. The following sections present the results of the water-content measurements versus depth (i.e., gravimetric water-content profiles) along the soil column for evaporation processes.
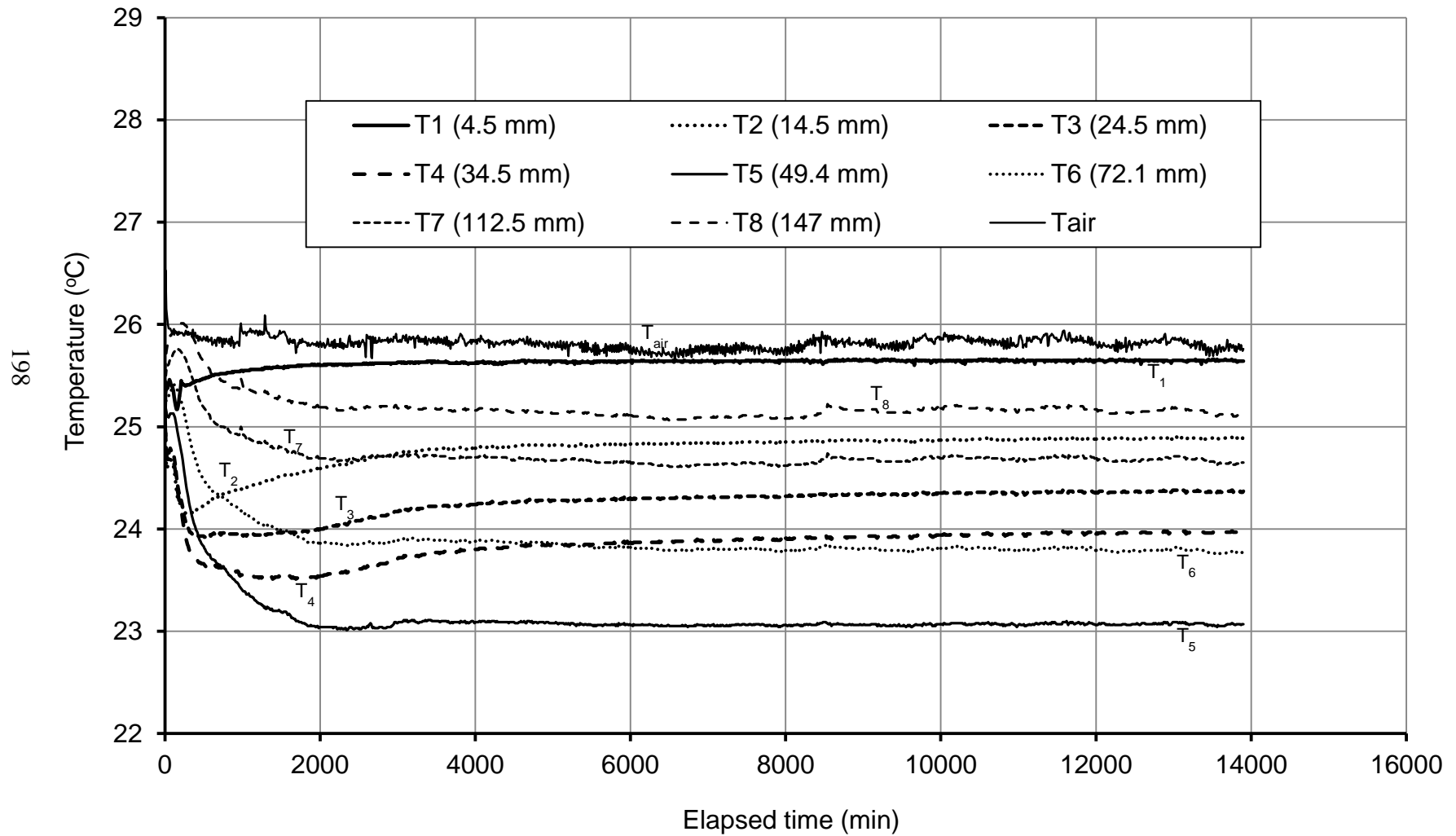
Figure 5.44 Temperature changes with respect to time along the soil column during evaporation Process PCS1 (Botkin silt)
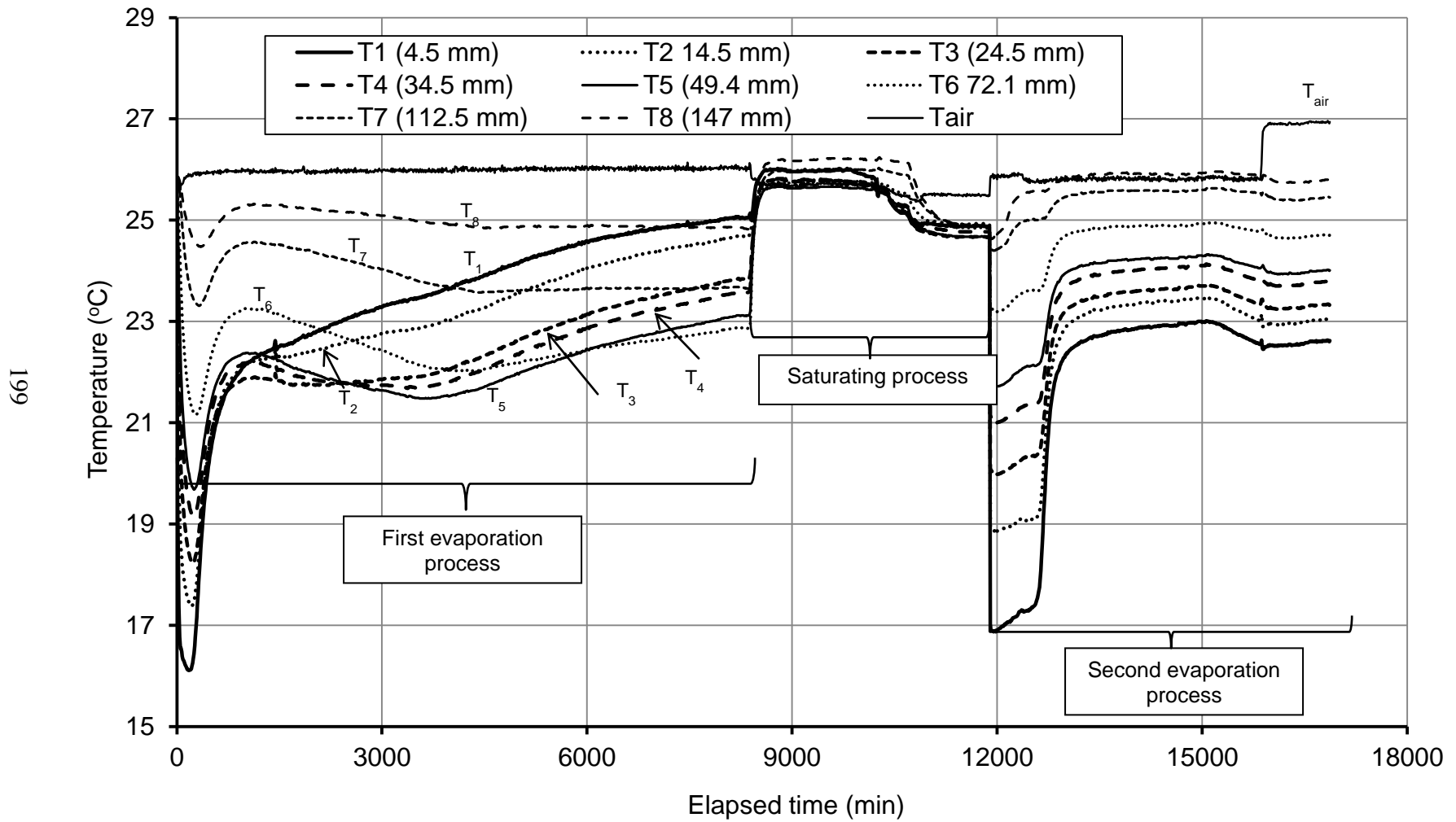
Figure 5.45 Temperature changes with respect to time along the soil column during evaporation Process PCS2 (Botkin silt)
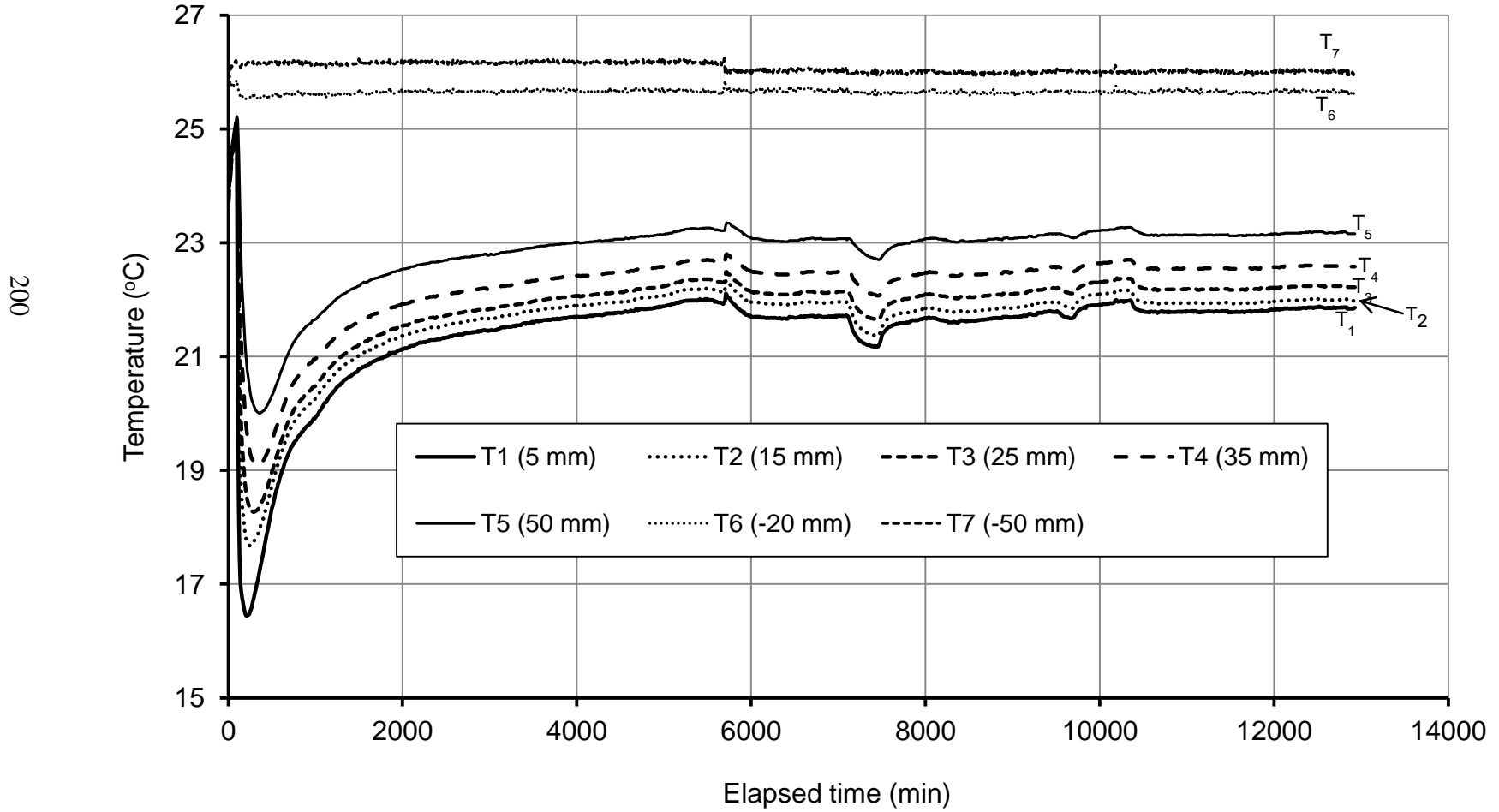
Figure 5.46 Temperature changes with time along the column during evaporation Process MCS1 (Botkin silt)
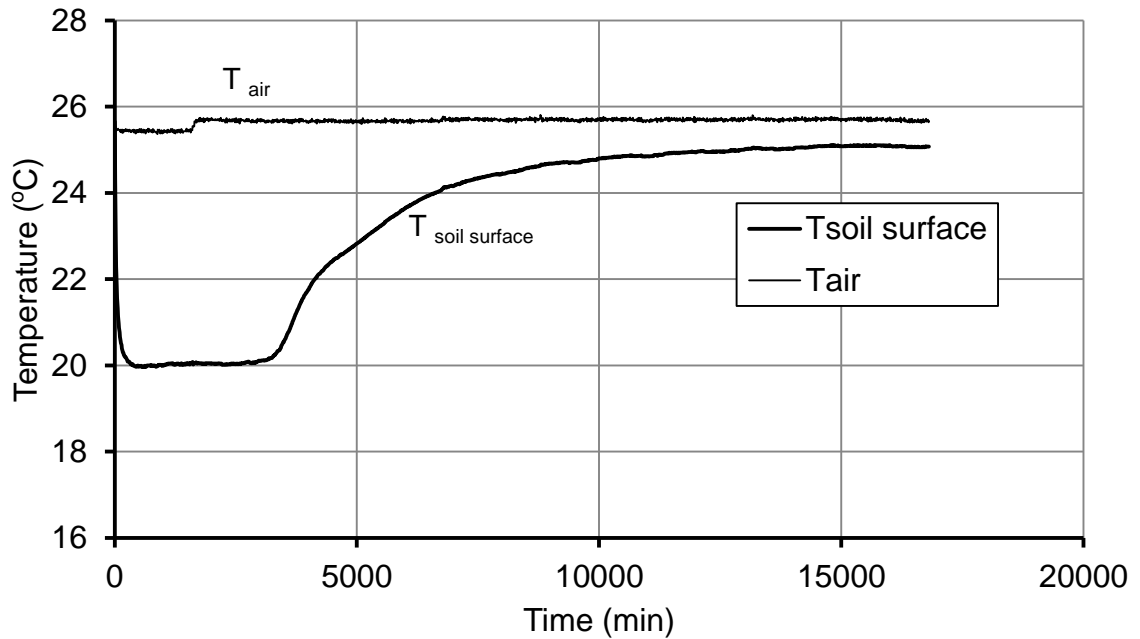
Figure 5.47 Temperature changes with time at the soil surface and the air above for evaporation Process MCS2 (Botkin silt)

### 5.5.4.1 Water-Content Profiles of the Beaver Creek Sand Specimens for the Primary Evaporation Column Tests

Figures 5.48 to 5.52 present the gravimetric water-content profiles for the Beaver Creek sand specimens at the end of the primary evaporation process.

Figure 5.48 shows the gravimetric water-content profile for evaporation Process PS1. The water content in the top 20 mm remained almost constant at approximately 3.8 %. The water-content values were larger at lower layers of the soil column. The points on the graph cannot be represented as a smooth curve. In other words, the water content at some depths indicates lower values when compared to the water content values in the upper portion (e.g., point 9 compared to point 8 on Figure 5.44). This variation may be due to non-uniform distribution of the water at the bottom of the soil column where the water was entering. Figure 5.48 shows that at the end of the evaporation process, the gravimetric water content of the sand at the bottom of the column was around 10%. The corresponding suction value of 10% gravimetric water content is about 4 kPa (see Figure

5.4). This suction value is higher than the air-entry value of the porous stone at the bottom of the column (i.e., AEV=1.8 kPa) and could withdraw water from the stone.
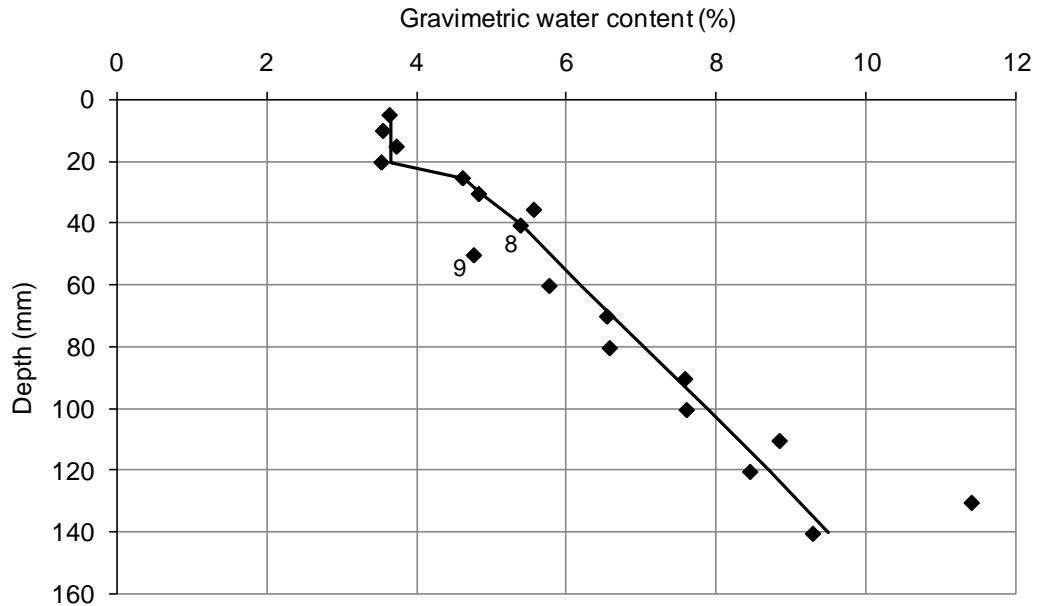


Figure 5.48 Gravimetric-water content profile at the end of evaporation Process PS1 (Beaver Creek sand)

Figure 5.49 shows the gravimetric water-content profile at the end of evaporation Process PS2. Water contents increased toward the bottom plate. The water content at the bottom of the soil column for this process was high compared to the water content at the bottom of the soil column for evaporation Process PS1. This variation appears to be mainly due to the lower potential evaporation rate for evaporation Process PS2 ("wind" treatment). Similar to evaporation Test PS1, the results of evaporation Process PS2 show that the water content at some depths was lower than that the upper portion of the column. A piece of filter paper was placed on top of the stone plate to create a uniform distribution of the water supplied at the bottom of the soil column for evaporation Process PS2. However, this procedure did not improve the test results.

Figure 5.50 shows the gravimetric water-content measurements at the end of evaporation Process PS3. The results for this test are comparable to the results obtained for evaporation Process PS1 (Figure 5.44). In both cases, the top boundary condition was "wind and radiation" treatment.

202
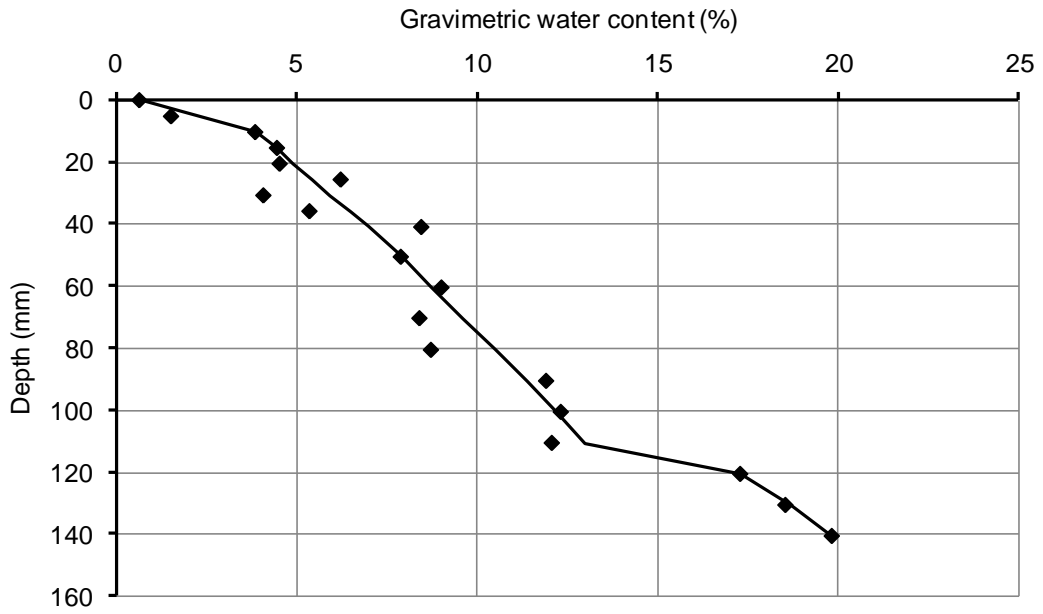
Figure 5.49 Gravimetric-water content profile at the end of evaporation Process PS2
(Beaver Creek sand)
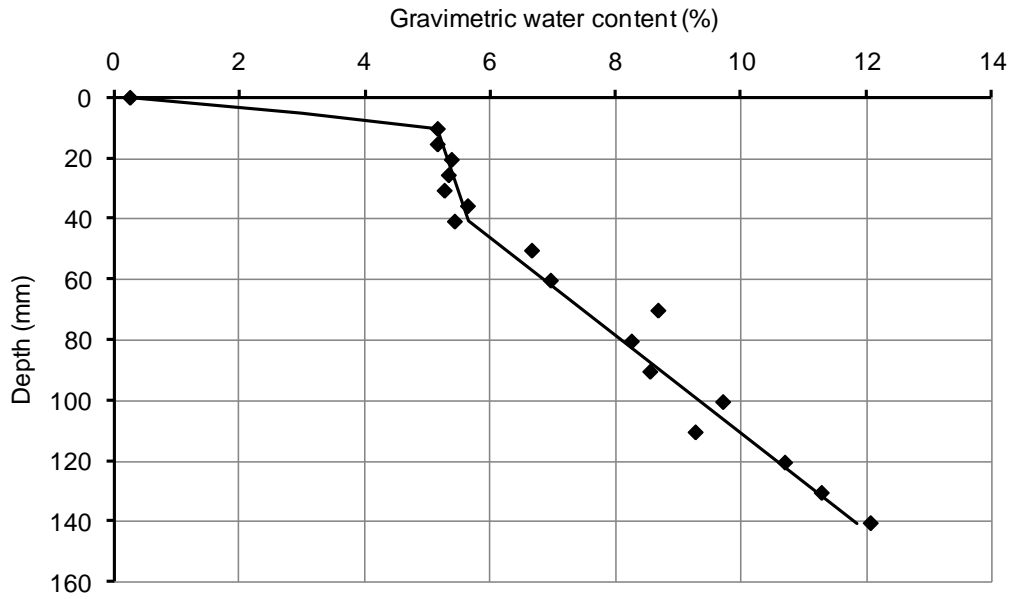


Figure 5.50 Gravimetric-water content profile at the end of evaporation Process PS3
(Beaver Creek sand)

Figure 5.51 shows the gravimetric-water content measurements at the end of evaporation Process PS4. The results of the gravimetric-water content versus depth created a smoother curve than observed in the three previous evaporation processes (i.e., Tests PS1, PS2, and PS3), mainly because of replacing a high air-entry value ceramic plate (AEV = 100 kPa) with the porous plate (AEV = 1.8 kPa).
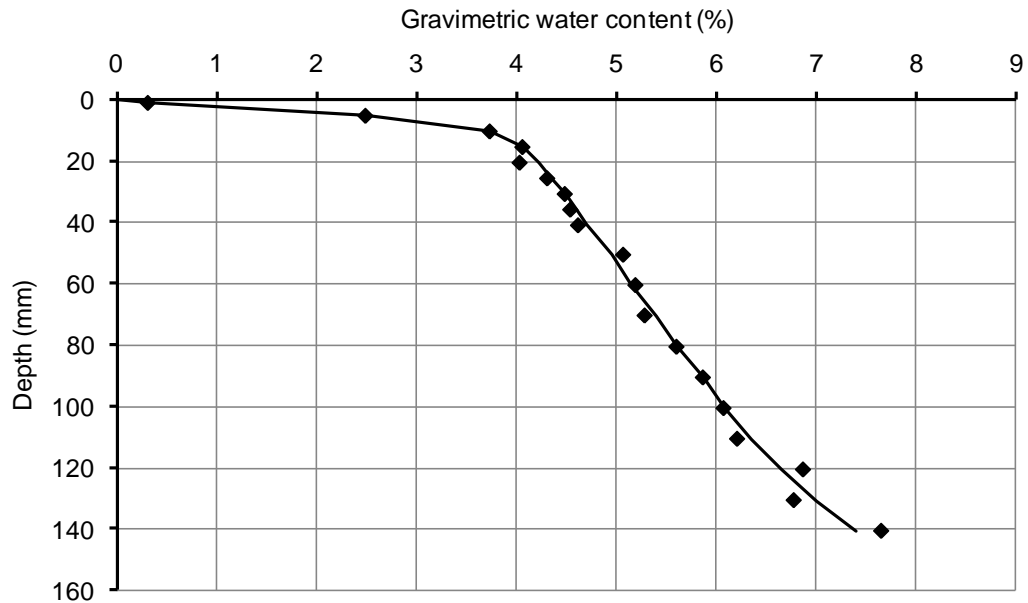


Figure 5.51 Gravimetric-water content profile at the end of evaporation Process PS4 (Beaver Creek sand)

Figure 5.52 shows gravimetric water-content measurements at the end of evaporation Process PS5. For all depths, except for the thin layer (i.e., thickness of 1 mm) at the soil surface, the water content remained high (between 22 to 26%) and close to the gravimetric water content at near-zero suction (26%). Presence of the water table at a depth of 140 mm for evaporation Process PS5 was the main reason for observation of a relatively constant water-content profile along the column. The data for this test were not suitable for the purpose of this thesis, which was the study of the hydraulic behavior of the soil around the residual-residual conditions. The water content remained high along the evaporation column and was close to the saturated water content.
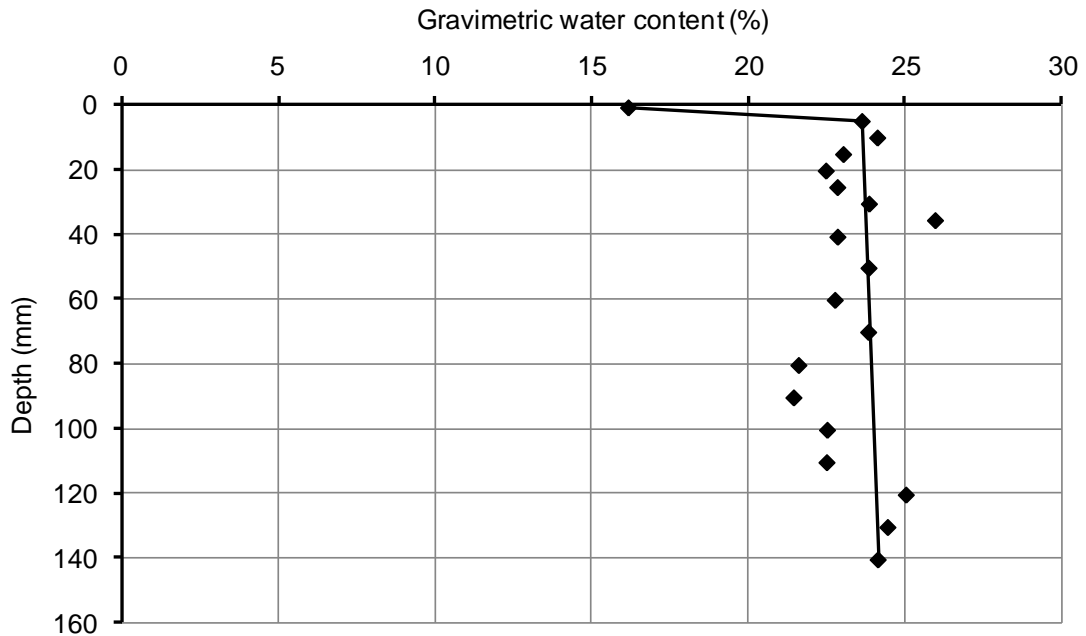
Figure 5.52 Gravimetric-water content profile at the end of evaporation Process PS5
(Beaver Creek sand)

### 5.5.4.2   Water-Content Profiles of a Beaver Creek Sand Specimen for the Modified Evaporation Column Tests

This section presents results of the gravimetric water-content measurements at the end of the modified evaporation Process MS1.

Figure 5.53 shows the gravimetric water-content profile at the end of evaporation Process MS1. Two sets of data are shown on the figure. Open circles are data associated with the soil samples retrieved from thermocouple ports. The diamonds are data associated with the soil samples retrieved through sectioning the soil column at the end of the evaporation process. The soil samples from the thermocouple ports indicated lower water contents when compared to the other group of data. These discrepancies between two groups of soil samples may be due to higher density of the soil samples retrieved from the thermocouple ports. These samples were taken after the temperature probes were pulled out from the ports.
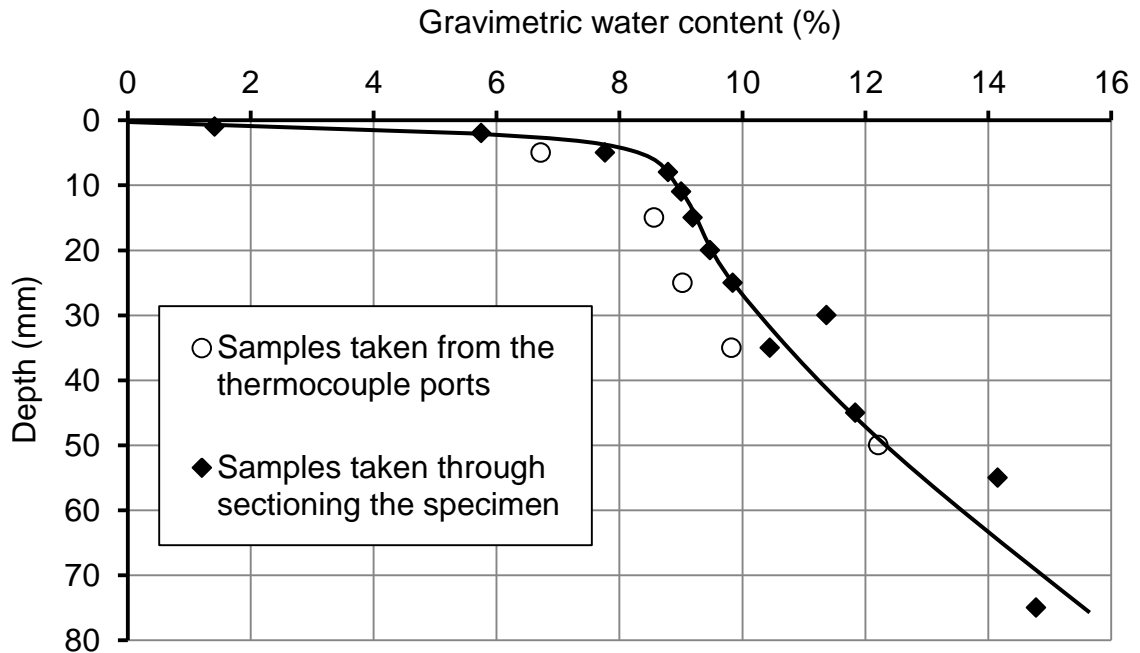
Figure 5.53 Gravimetric-water content profile at the end of evaporation Process MS1
(Beaver Creek sand)

### 5.5.4.3 Water-Content Profiles of the Botkin Silt Specimens for the Modified Evaporation Column Tests

This section presents results of the gravimetric water-content measurements at the end of the modified evaporation Processes MCS1, MCS2.

Figure 5.54 shows the gravimetric water-content measurements at the end of evaporation Process MCS1. The soil samples were retrieved through the sampling ports on the side of the evaporation column. Although the gravimetric water-content profile at the end of the test showed an expected form, the data from this test were discarded from the analysis because of shrinkage observed during the evaporation test.

Figure 5.55 shows the gravimetric water-content measurements at the end of evaporation Process MCS2. Soil samples for this test were retrieved through sectioning the soil column at the end of the evaporation process. The data from this test appear to be suitable for analysis.
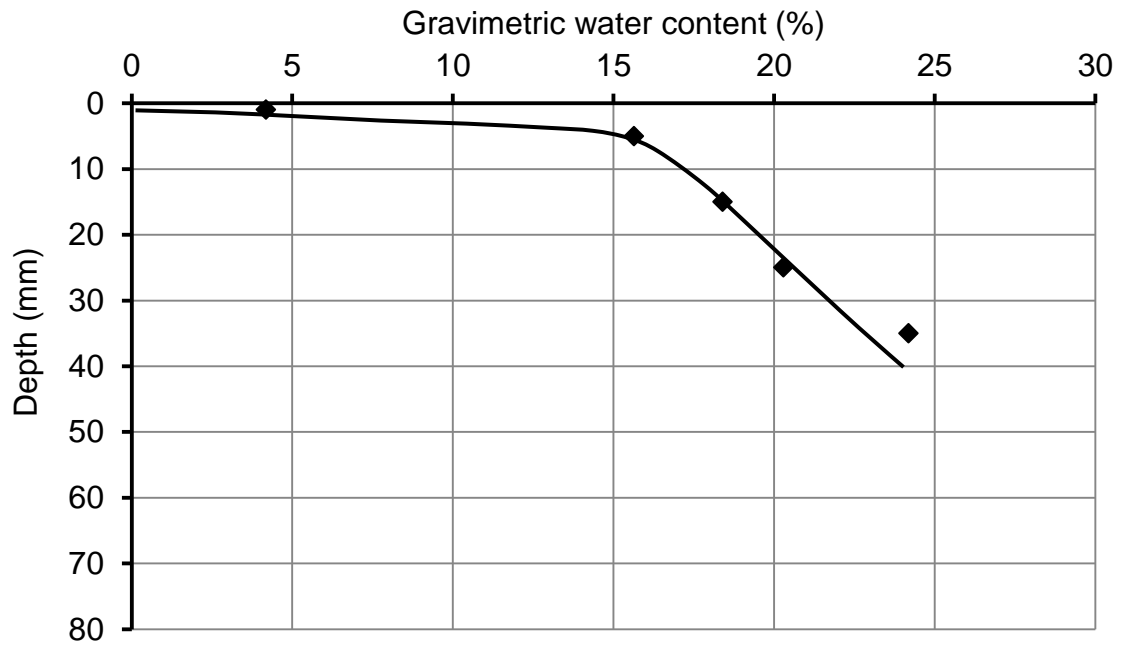
Figure 5.54 Gravimetric-water content profile at the end of evaporation Process MCS1
(Beaver Creek sand)
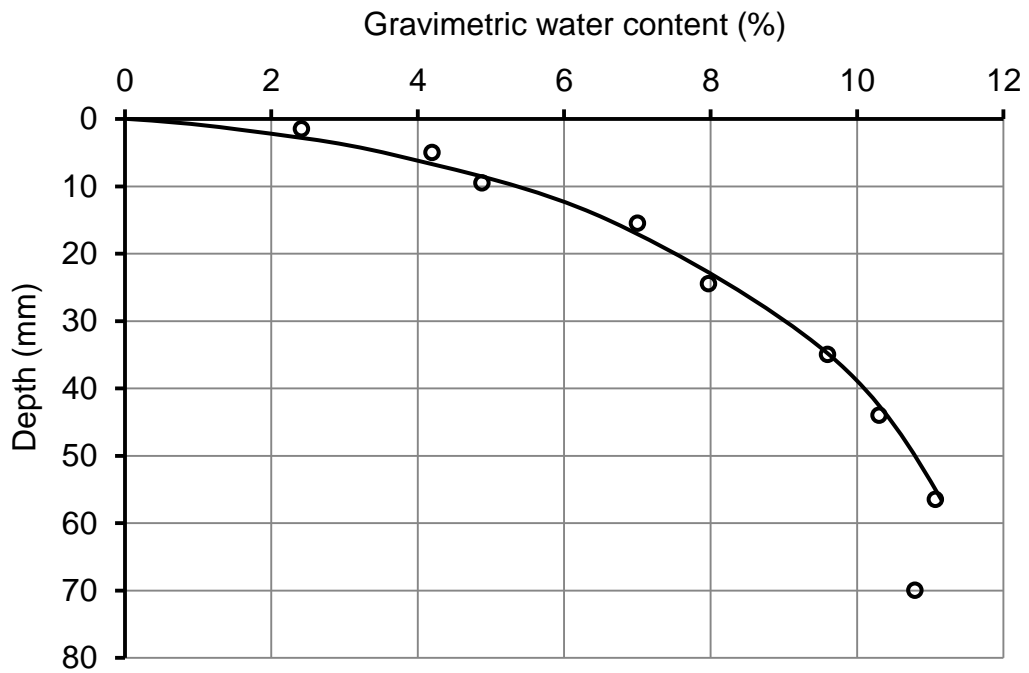


Figure 5.55 Gravimetric-water content profile at the end of evaporation Process MCS2
(Beaver Creek sand)

207

The evaporation test results, presented in this chapter, were considered as successful if they met all the following conditions:

1- The evaporation rate becomes equal to the controlled inflow rate at the end of the test (steady-state flow condition).

2- The water-content profile at the end of the test consists of water-content values around the residual water content.

3- Evaporation occurs exclusively through the top surface of the specimen (not from the side surface of the specimen because of shrinkage).

4- Cracks are not developed vertically or horizontally.

Plots of evaporation rate and temperature changes with time, as presented in this chapter, suggest that most of the evaporation tests had reached steady-state flow conditions at the end of the test before the soil samples were retrieved for the gravimetric water-content measurement. However, some of the evaporation tests could not satisfy all of the required conditions.

The required conditions were met by 5 out of 6 Beaver Creek sand specimens used in the evaporation tests: PS1, PS2, PS3, PS4, and MS1. Specimen PS5, which failed to satisfy condition 2, was discarded from the analysis. These conditions were met by 1 out of 4 Botkin silt specimens (MCS2). Results of the successful tests are used for the analysis in Chapter 6.

Along with the evaporation test results, the soil-water characteristic curve and saturated coefficient of permeability for the Beaver Creek sand and Botkin silt specimens were also required for the analysis.

The SWCC test results, as presented in section 5.4, will be used to establish a suitable SWCC for the analysis along with the selected evaporation tests. The problematic SWCC test data will not be considered for

The saturated coefficient of permeability for the Botkin silt was measured at different loads during consolidation tests. The saturated coefficient of permeability at 50 kPa will be used in the analysis. This value was chosen because the Specimen MCS2 from evaporation tests chosen for the analysis had a similar initial condition (consolidated to 50 kPa).

CHAPTER 6

**INTERPRETATION OF THE EXPERIMENTAL TEST RESULTS, DATA
ANALYSIS, AND DISCUSSION**

## 6.1 INTRODUCTION

This chapter presents interpretations of the laboratory test results, reported in Chapter 5, with data analysis, and discussion. As described in chapter 4, a total of 10 evaporation tests were conducted: 6 on the Beaver Creek sand and 4 on the Botkin silt specimens. The results of 5 evaporation tests on Beaver Creek sand (PS1, PS2, PS3, PS4, and MS1) and 1 test on Botkin silt are considered for the analysis in this chapter. The SWCC and the saturated coefficient of permeability test results selected for the analysis are also discussed.

Section 6.2 discusses the results from the consolidation and saturated coefficient of permeability tests on the Botkin silt and Beaver Creek sand specimens.

In section 6.3 the performance of the WP4-T device which was used throughout the laboratory testing program is assessed.

Section 6.4 discusses the SWCC hysteresis in the high suction range.

In section 6.5, the entire SWCC in suction ranges from near 0 to 1,000,000 kPa are established for Beaver Creek sand and Botkin silt soils.

In section 6.6, the residual-state condition is estimated using the SWCC of Beaver Creek sand and Botkin silt soils. The residual-state condition is estimated based on the new procedure developed in Chapter 3, section 3.5. The residual-state condition is also determined as a designated point on the SWCC based on the commonly used methods described in Chapter 2, section 2.3.

Section 6.7 discusses the steady-state flow conditions in evaporation processes.

In section 6.8, the transition zone of the soil suction profile is estimated by analysis of the results obtained from the evaporation processes.

In section 6.9, the residual-state condition for the Beaver Creek sand and Botkin silt specimens are compared with upper and lower limits of the transition zone of the soil suction profile.

Section 6.10 presents an analysis of the steady-state evaporation processes results in order to establish experimental data for the liquid-phase coefficient of permeability function. The equations developed in Chapter 3 were used for the data analysis.

In section 6.11, the equations developed in Chapter 3 along with the data obtained from the evaporation processes are used to determine the vapour coefficient of permeability function for the Beaver Creek sand and Botkin silt.

In section 6.12, the method for predicting the liquid-phase coefficient of permeability function, which was proposed in Chapter 3 is assessed through the experimental data from sections 6.10 and 6.11.

## 6.2 CONSOLIDATION AND THE SATURATED COEFFICIENT OF PERMEABILITY

The falling head test was used for the measuring the saturated coefficient of permeability. The testing procedure and the results of the tests were presented in Chapters 4 and 5, respectively. The saturated coefficient of permeability ($k_s$) has been shown to be a function of void-ratio or effective stress. The volume change of Beaver creek sand during consolidation tests was not substantial, and as a result, the saturated coefficient of permeability ($k_s$) remained practically constant for various applied pressures during consolidation. The saturated coefficient of permeability for Beaver Creek sand was found to be $k_s = 1.27 \times 10^{-6}$ m/s under various applied pressures. Beaver Creek sand is considered to be a non-volume-changing material throughout this study.

The results of the saturated coefficient of permeability were presented in chapter 5 (see Figure 5.3). The saturated coefficient of permeability data were plotted versus applied pressure (effective stress) for the Botkin silt specimens. The saturated coefficient of permeability decreased from $4 \times 10^{-9}$ to $1.8 \times 10^{-9}$ m/s as the applied pressure changed from near 0 to 200 kPa. Results on Specimen MCS, initially consolidated to 50 kPa, are used in data analysis. Little volume change was observed during the evaporation tests, because the Botkin silt specimen was consolidated to 50 kPa ($e = 0.66$) before the evaporation test started, The volume change is not considered in the

analysis since the focus of this research is on the hydraulic behavior of the soil around the residual-state condition, where the volume change becomes practically insignificant.

The saturated coefficients of permeability for the selected soils were used in sections 6.10, 6.11, and 6.12 for establishing the unsaturated coefficient of permeability function for the selected soils.

## 6.3 ASSESSMENT OF THE CHILLED-MIRROR WATER-POTENTIA METER (WP4-T)

A Chilled-Mirror Water-Potentia Meter (WP4-T) was used to measure the total soil suction in the high suction range of the SWCC. The device was also used to measure the suction profile after a steady-state condition on the evaporation columns was reached. Features of the device and the experimental testing procedures were previously described in Chapter 4, section 4.5 and Chapter 5, section 5.4, respectively.

In this section, the accuracy of the Chilled-Mirror Water-Potentia Meter (WP4-T) is assessed using the experimental data presented in Chapter 5. Results from a traditional vapour pressure equilibrium method (air-tight chamber method, ATC) were intended to be used as a benchmark to assess the performance of the WP4-T device. Independent measurement of relative humidity using the Traceable Hygrometer did not match with the targeted relative humidity values in high range of suctions. It could not conclusively be determined whether the discrepancies were due to error in the measurement of relative humidity values using the Traceable Hygrometer, or whether the targeted relative humidity was not achieved within the chamber.

The data from the WP4-T device are compared with the data from the ATCs (section 6.3.1) and with the data from the Traceable Hygrometer (section 6.3.2).

### 6.3.1 Comparison of the Results Obtained From the Air-Tight Chamber (ATC) and the Chilled-Mirror Water-Potentia Meter (WP4-T)

Figures 6.1 and 6.2 compare the suction values for drying and wetting curves obtained from the ATC and the WP4-T devices for Botkin silt and Regina clay, respectively. There is close agreement between suction values in the high suction range (i.e., suction values greater than 50,000 kPa). In the range of suctions less than 50,000 kPa, with the exception of the lowest measured suctions for Regina clay, there was not good agreement between suction values obtained using the WP4-T and the ATC. The WP4-T

method resulted in higher suction values compared to those measured using the ATC method.
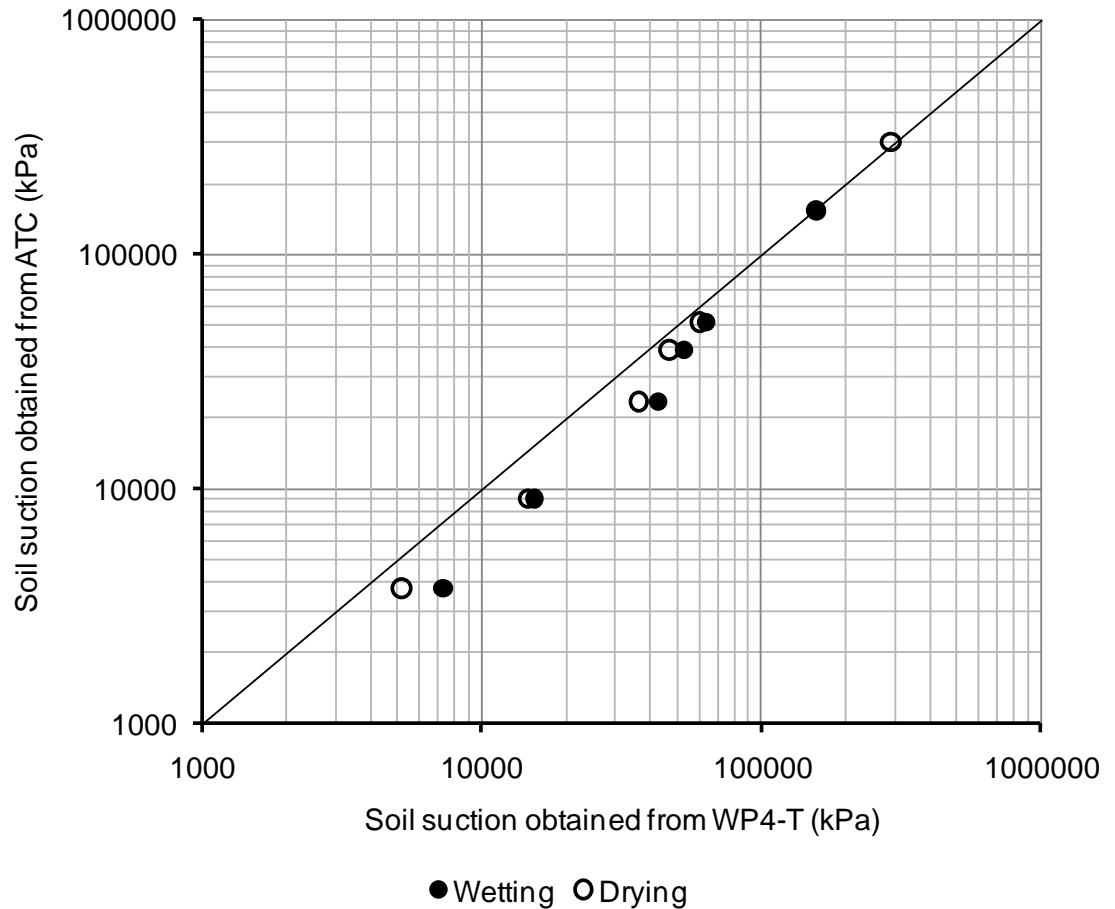


Figure 6.1 Comparison of soil suction results obtained from WP4-T and from ATC for Botkin silt

### 6.3.2 Comparison of Data Obtained from a Hygrometer and the WP4-T

The relative humidity created inside the air-tight chambers using various saturated salt solutions was measured through an access hole in the top plate (see Chapter 4, Figure 4.7) using the Traceable Hygrometer. These relative humidity values were converted to total suction values, which were then plotted against those obtained from the WP4-T device for Botkin Silt and Regina clay soils in Figures 6.3 and 6.4, respectively. The results for both soils indicate close agreement between the two methods of suction measurements: the Traceable Hygrometer and the WP4-T device.
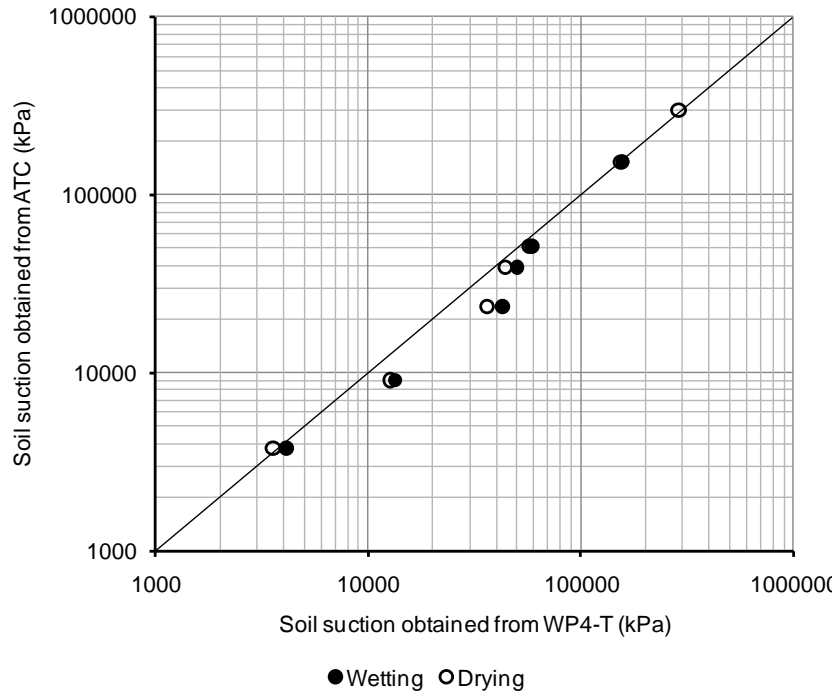
Figure 6.2 Comparison of soil suction results obtained from WP4-T and from ATC for Regina clay
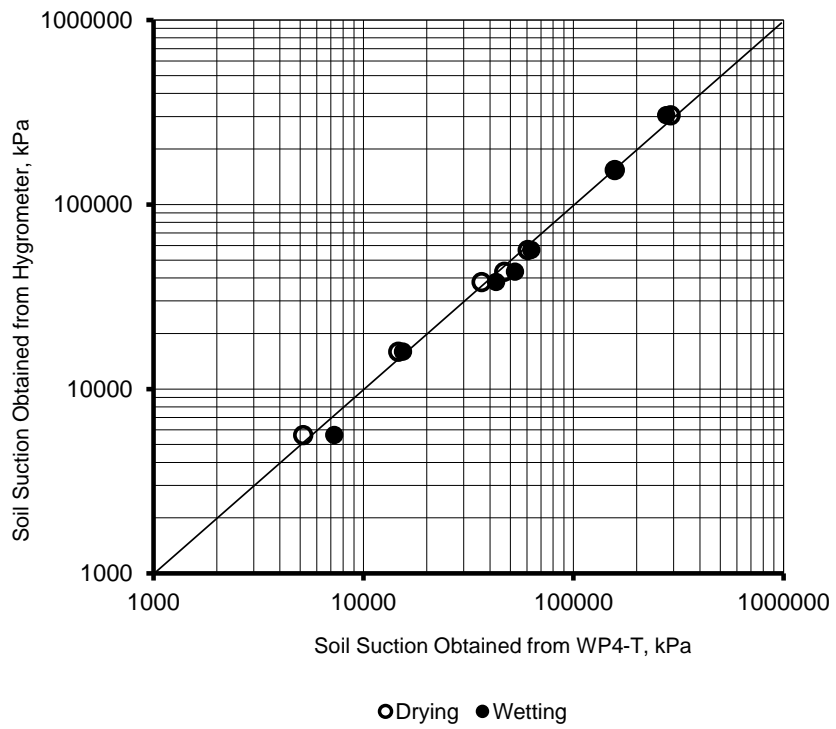


Figure 6.3 Comparison of results obtained from WP4-T and from Hygrometer for Botkin silt

It can be concluded from the results presented in sections 6.3.1 and 6.3.2 that the difference between suction values obtained from the ATC and the WP4-T devices for the suction range less than 50,000 kPa may be attributed to slightly lower than expected relative humidity at equilibrium inside some of the chambers. The lower relative humidity may be due to: i) the relatively large volume of the chamber, ii) inability of the saturated chemical to create the targeted relative humidity, and/or iii) lack of air circulation inside the chamber and air stratification.
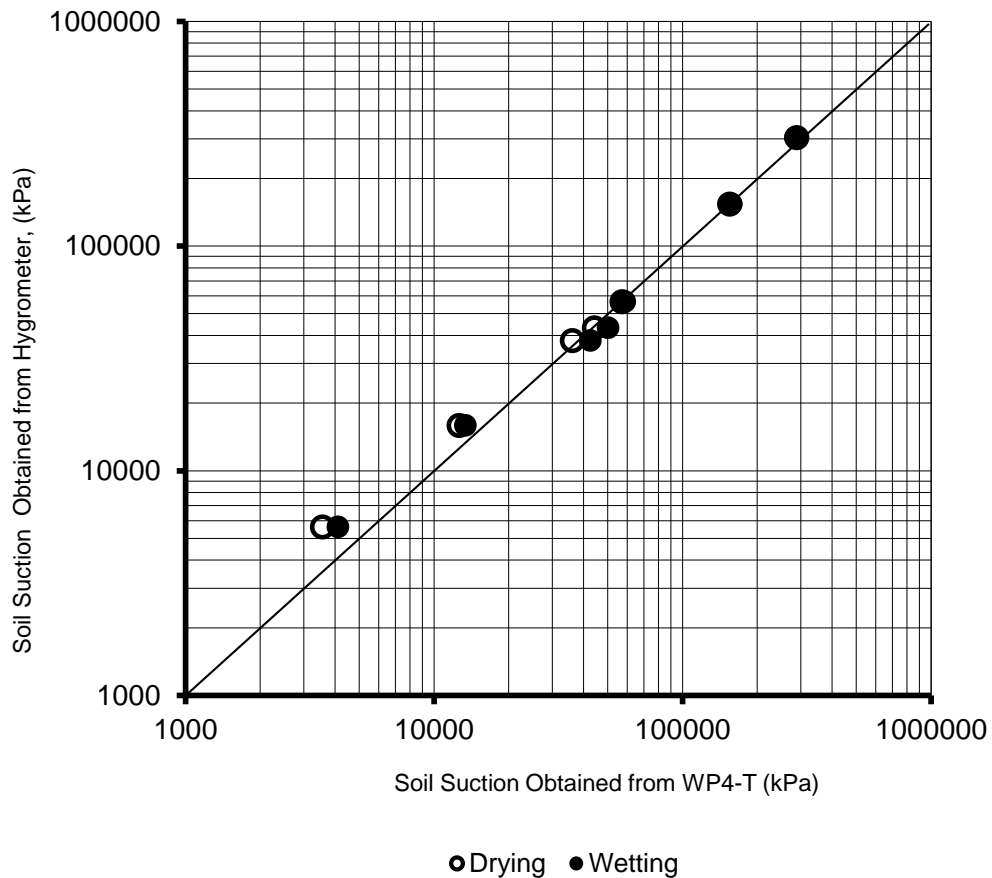


Figure 6.4 Comparison of results obtained from WP4-T and from Hygrometer for Regina clay

### 6.3.3   Comparison of the Suction Values Obtained from WP4-T with Published Suction Values for Saturated Salt Solutions

The suction values for the saturated salt solutions, measured using the WP4-T device (see Chapter 4, section 4.5.1.4, Figure 4.8), are given in Table 6.1. For comparison,

published relative humidity values for the saturated salt solutions are also given in Table 6.1. There is a good agreement between these two sets of suction values. It is concluded that the saturated salt solutions were capable of creating targeted relative humidity values in an environment with small volume (the chamber within WP4-T is small). It can also be concluded that WP4-T was capable of accurately measuring the suction values of the saturated salt solutions.

Table 6.1 Suction values for different saturated salt solutions obtained using WP4-T and calculated suction values using known relative humidities published in ASTM E 104-85, 1998 and E 104-02, 2003

| Salt Solution | Suction Measured Using WP4-T, kPa | Relative Humidity, % | Calculated Suction, kPa |
|---|---|---|---|
| Lithium Chloride | 304330 | 11.3 ± 0.3 | 300008 |
| Magnesium Chloride | 154660 | 32.8 ± 0.2 | 153383 |
| Potassium Iodide | 51680 | 68.9 ± 0.3 | 51256 |
| Sodium Chloride | 38610 | 75.3 ± 0.2 | 39034 |
| Potassium Chloride | 23050 | 84.3 ± 0.3 | 23500 |
| Potassium Nitrate | 9840 | 93.6 ± 0.6 | 9100 |
| Potassium Sulfate | 2900 | 97.3 ± 0.5 | 3766 |

The discussions in this section show that:

i)      The targeted relative humidity values were not achieved in some of the air-tight chambers due to the large volume of the chamber and/or air stratification.

ii)     Measurement of the soil suction using the WP4-T device is reliable.

## 6.4   SWCC HYSTERESIS IN THE HIGH SUCTION RANGE

The experimental program and test results for measurements of the SWCC in the high suction range using WP4-T and ATC were presented in Chapters 4 and 5, respectively. This section studies the presence of SWCC hysteresis for Botkin silt and Regina clay in high suction ranges. Results for Regina clay published by Fredlund (1964) are also

presented for comparison. Since hysteresis is assumed to be negligible for Beaver Creek sand, it is not considered for this analysis.

### 6.4.1 Drying and Wetting SWCCs Using Chilled-Mirror Water PotentiaMeter (WP4-T)

Figure 6.5 shows drying and wetting curves for Botkin silt and Regina clay measured using the Chilled-Mirror Water PotentiaMeter (WP4-T) and the ATC device. The hysteresis is more obvious for the clay than for the silt. The meeting point of the drying and wetting curves for Regina clay is located at a soil suction value approaching 300,000 kPa.
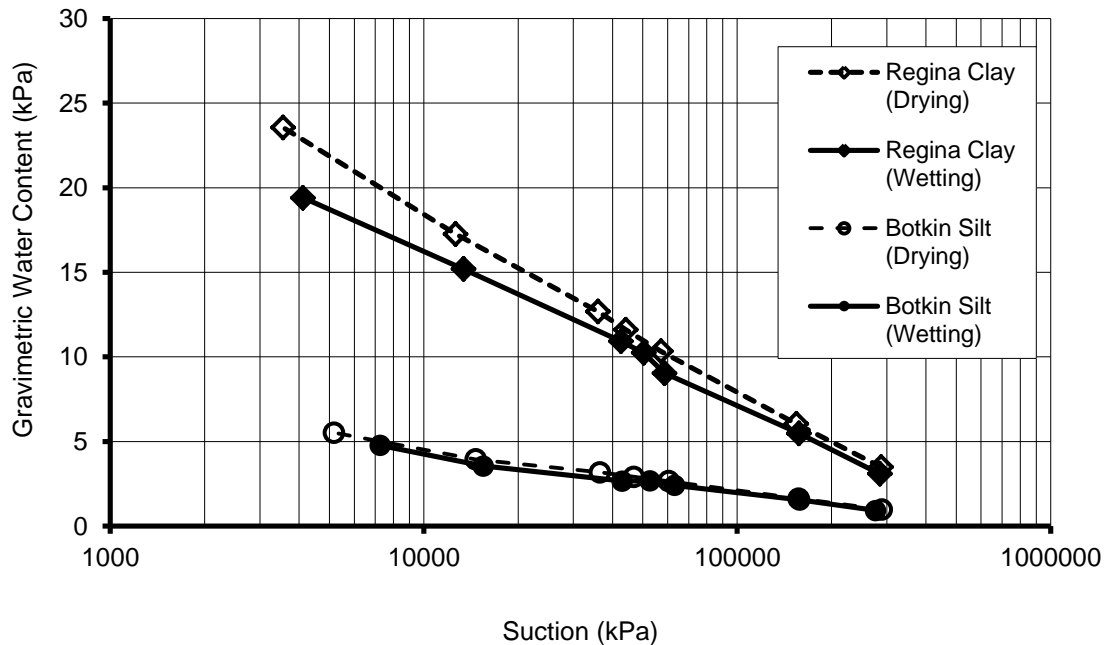


Figure 6.5 SWCC hysteresis obtained from the WP4-T device on Botkin silt and Regina clay

### 6.4.2 Drying and Wetting SWCCs Using ATC

Figure 6.6 shows drying and wetting curves for Botkin silt and Regina clay measured using air-tight chambers (equilibration of soil samples over salt solutions of known osmotic suction). The difference between drying and wetting SWCCs (hysteresis) increases from high to low suction values in both soils. The difference between drying and wetting curves is greater for the clay than for the silt. The meeting point of the

drying and wetting curves for Regina clay is located at a soil suction value approaching 300,000 kPa.
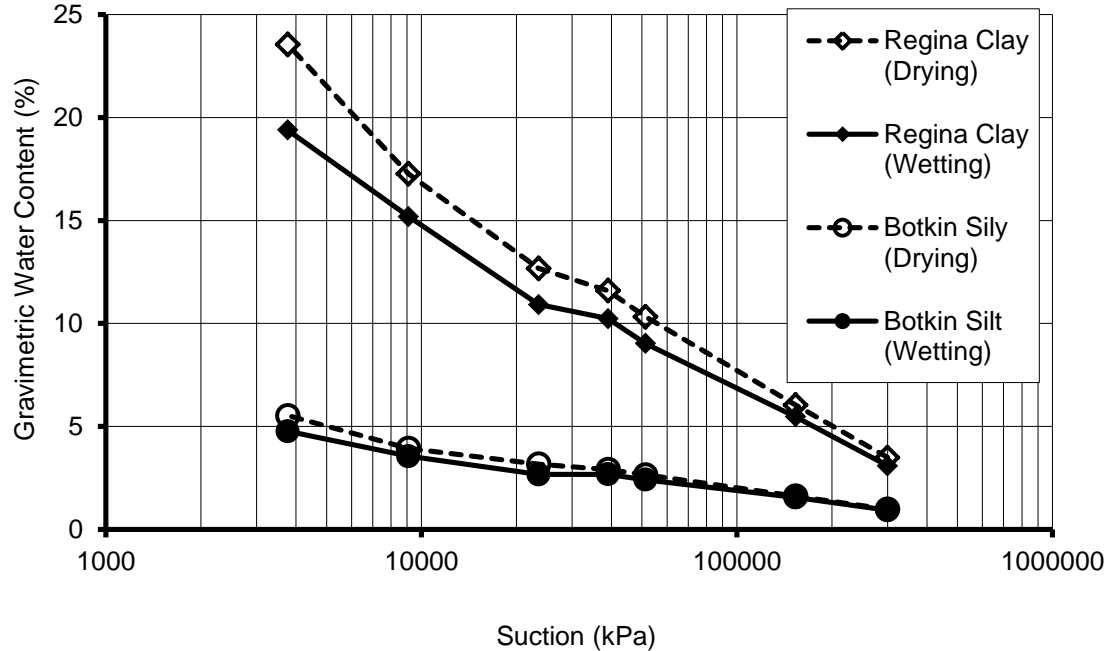


Figure 6.6 SWCC hysteresis obtained from the ATC method for Botkin silt and Regina clay

### 6.4.3   Comparison of the Hysteresis Results for Regina Clay

Fredlund (1964) conducted an experimental test on Regina clay using the equilibration of a small soil sample placed over saturated salt solutions. The procedure was similar to the air-tight chamber method in this research, except that the desiccators were used as air-tight containers. The data obtained using the Chilled-Mirror Water PotentiaMeter for a Regina clay sample are plotted along with data obtained from Fredlund (1964) on the same scale in Figure 6.7. Both data sets show hysteresis in Regina clay.

A discrepancy between the curves in Figure 6.7 was anticipated, as the soil properties of the Regina clay samples used by Fredlund (1964) and of the sample used in this thesis (i.e., with the WP4-T device) were not quite the same. For example, the percentage of clay particles for the Regina clay sample tested by Fredlund (1964) was less than that tested in this research (i.e., 51% versus 74%). For given water content values, both drying and wetting curves for the Regina clay tested in this research show

higher suction values than those for the Regina clay tested by Fredlund (1964). The drying curves of both samples overlapped at about 300,000 kPa.
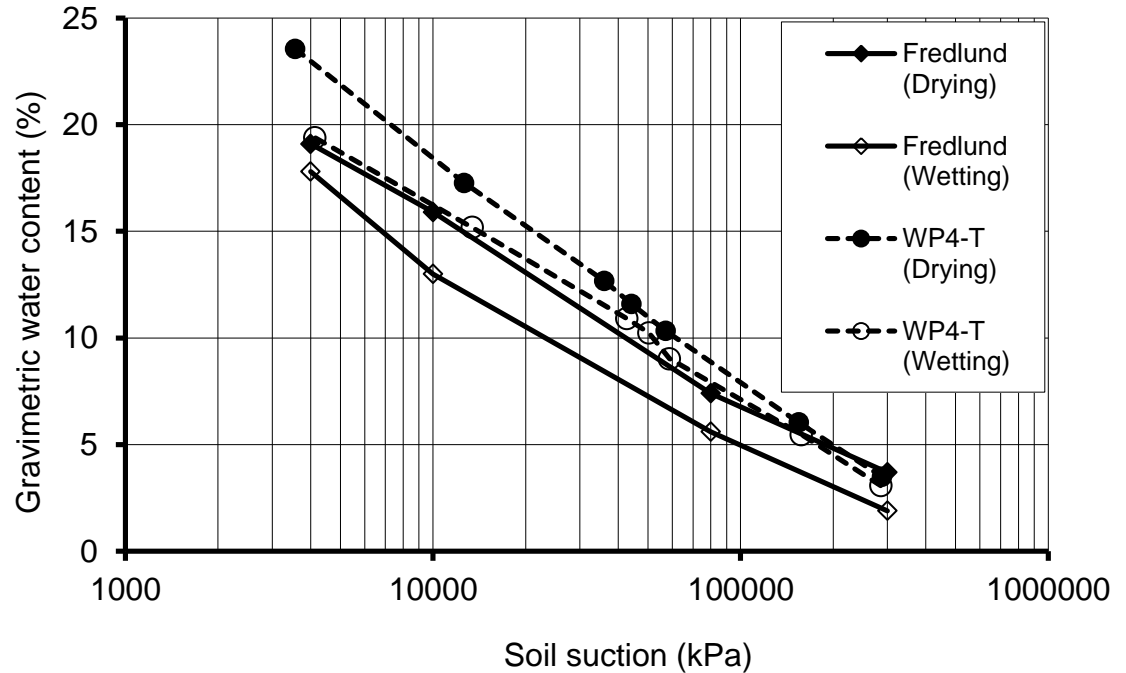


Figure 6.7 SWCC hysteresis obtained from the WP4-T device and by Fredlund (1964) for Regina clay

## 6.5 SOIL-WATER CHARACTERISTIC CURVES

The SWCC test results (presented in Chapter 5, section 5.4) are used to establish a suitable SWCC for analysis along with the selected evaporation tests. Tests with problematic results (see Chapter 5, section 5.4.4) are excluded from the analysis. Two complete SWCCs, one for Beaver Creek sand and one for Botkin silt, are used in the analysis in this chapter.

Figures 6.8 and 6.9 show the soil-water characteristic curves for Beaver Creek sand and Botkin silt samples for entire soil suction ranges from near 0 to near 1,000,000 kPa. Suitability of the SWCC for analysis along with the evaporation tests was a key factor in establishing the SWCCs. Water content of the samples assumed to be zero at suction value of 1000,000 kPa.
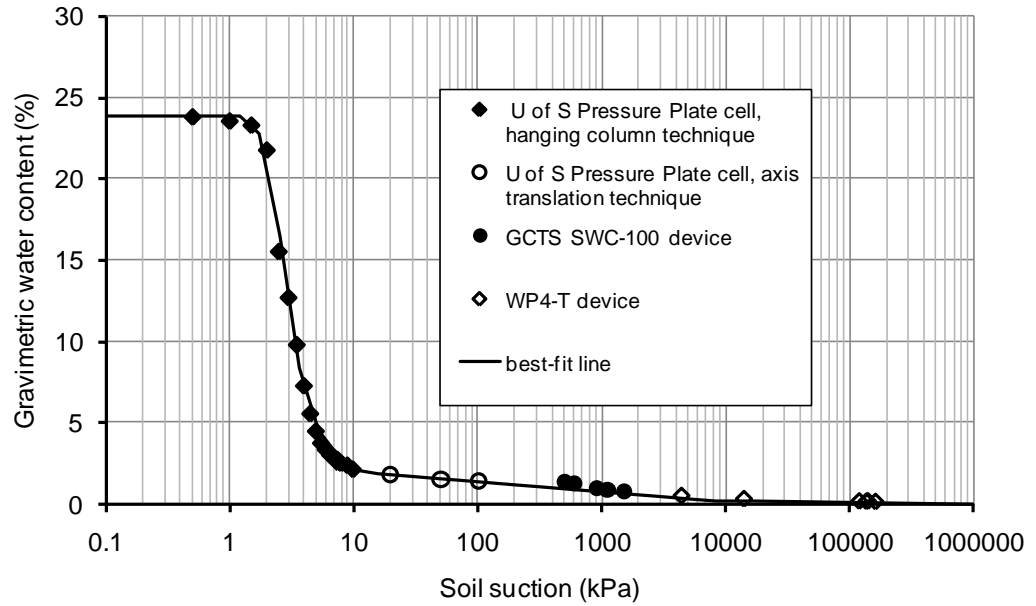
Figure 6.8 Entire soil-water characteristic curve for Beaver Creek sand (suction ranges from 0 to 1,000,000 kPa)
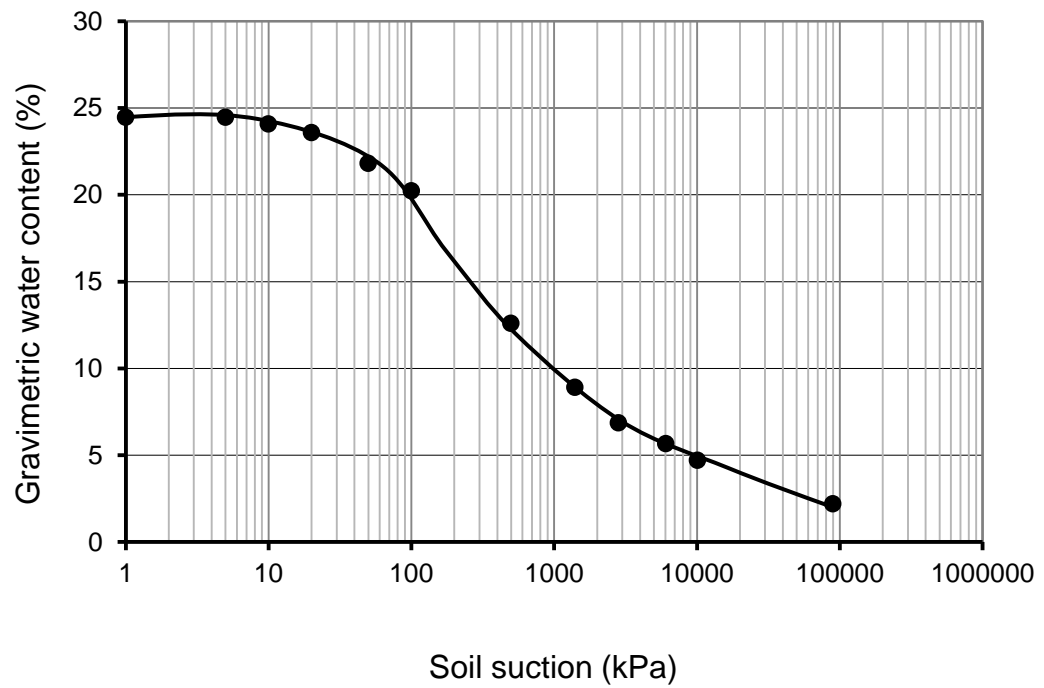


Figure 6.9 Entire soil-water characteristic curves for Botkin silt from the specimen initially consolidated to 50 kPa

## 6.6 DETERMINATION OF THE RESIDUAL-STATE CONDITION (RSC)

The method proposed in the theory chapter (Chapter 3, section 3.5) is used in this section to estimate the residual-state condition for Beaver Creek sand and Botkin silt soils. The residual-state condition is considered as a designated zone on the soil-water characteristic curve. For comparison, the residual-state condition of the soil samples is also estimated by conventionally used methods presented in the literature review (see Chapter 2, section 2.3). The residual-state condition has been considered as a definite point when the conventional methods are used for estimations.

Table 6.2 summarizes the methods considered in this section in order to determine the residual condition (i.e., water-content and soil-suction values at the residual state) for Beaver Creek sand and Botkin silt soils. The residual-state condition is estimated using soil-water characteristic curves presented in section 6.5. Whenever required, the gravimetric water content is converted to volumetric water content or degree of saturation using volume-mass properties of specimens (Chapter 5, section 5.4). The volume change is assumed to be negligible.

Table 6.2 Methods used for determination of the residual state conditions, RSCs

| Method | Reference | Description |
|---|---|---|
| Brooks and Corey | Brooks and Corey (1964) | Single point |
| Mualem | Mualem (1976) | Single point |
| van Genuchten | van Genuchten (1980) | Single point |
| Vanapalli | Vanapalli (1994) | Single point |
| Proposed method | Chapter 3 | Zone |

### 6.6.1 Brooks and Corey Method

To determine the residual-state condition of a soil sample using Brooks and Corey (1964) method, the first step is to plot the soil suction ($\psi$) versus the degree of saturation (S). Figures 6.10 and 6.11 show plots of soil suction versus the degree of saturation values for the Beaver Creek sand and Botkin silt soil specimens, respectively.

The residual degree of saturation is determined using the effective degree of saturation ($S_e$) versus soil suction ($\psi$) plots for Beaver Creek sand (Figure 6.12) and Botkin silt (Figure 6.13), respectively. The residual degrees of saturation using the Brooks and Corey method (1964) for Beaver Creek sand and Botkin silt specimens are 4% and 3%, respectively.

The pore-size index ($\lambda$) for the Beaver Creek sand and Botkin silt specimens (Figures 6.12 and 6.13) is also determined. This parameter ($\lambda$) is generally expected to be larger for sands than for clayey silts (Brooks and Corey, 1966). The pore-size index values determined for the Beaver Creek sand and Botkin silt soils (1.73 and 0.42) are consistent with the Brooks and Corey (1966) findings.
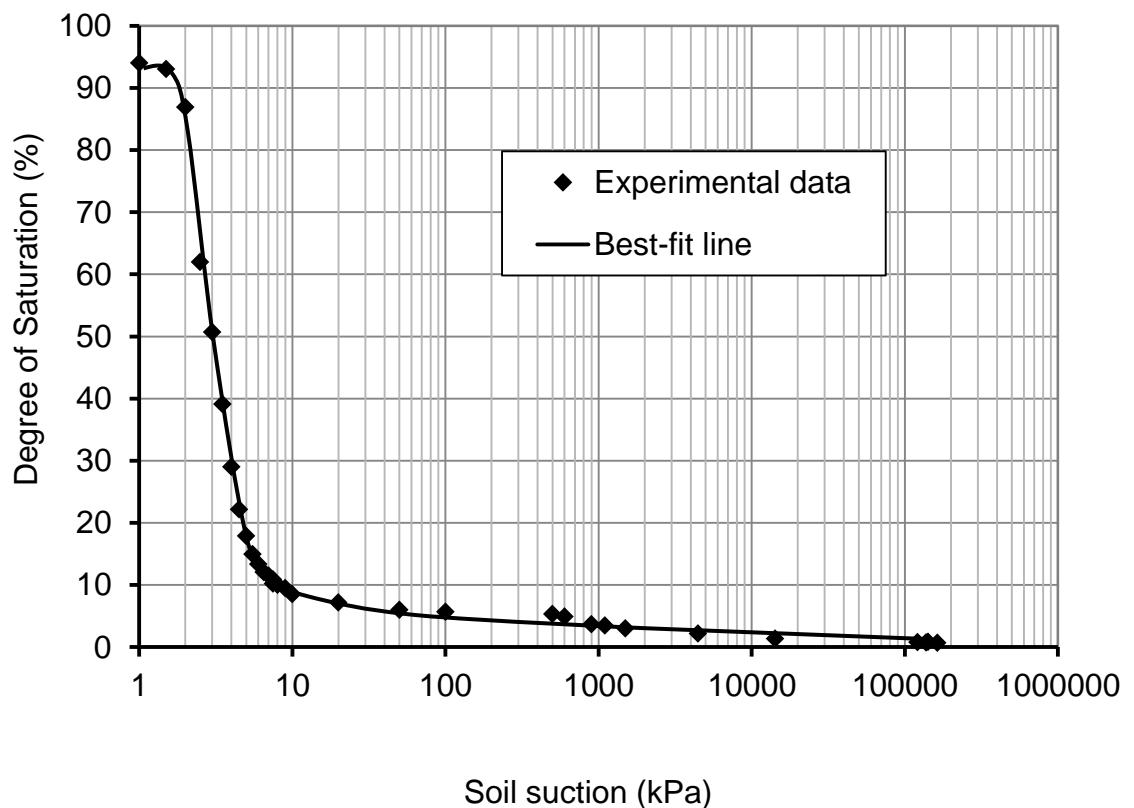


Figure 6.10 Degree of saturation versus soil suction plot for Beaver Creek sand specimen
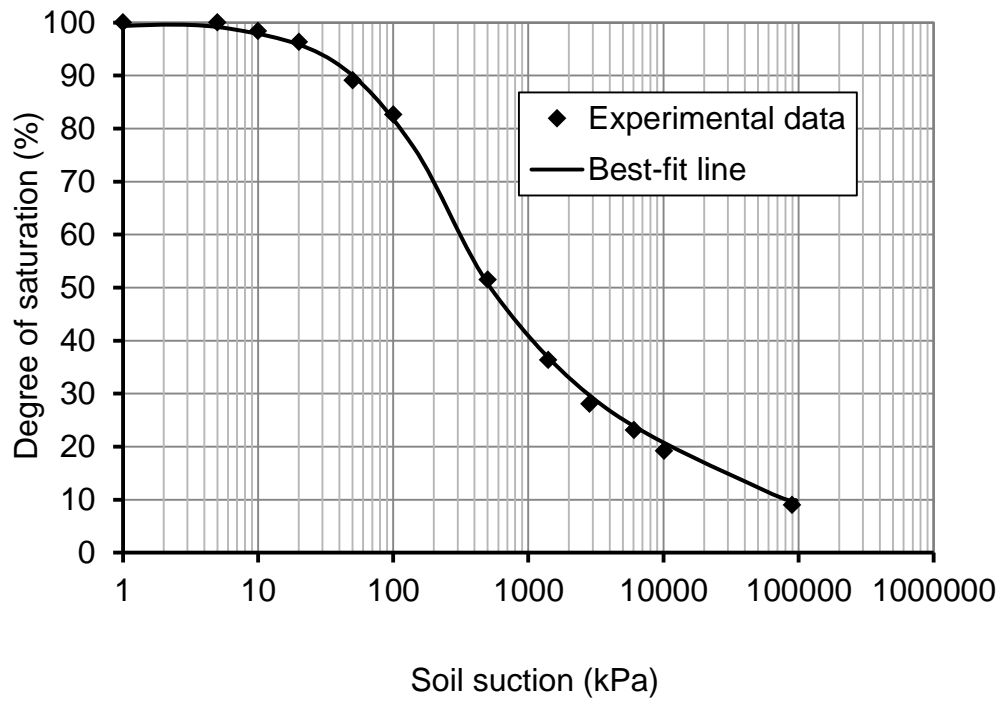
Figure 6.11 Degree of saturation versus soil suction plot for Botkin Silt specimen
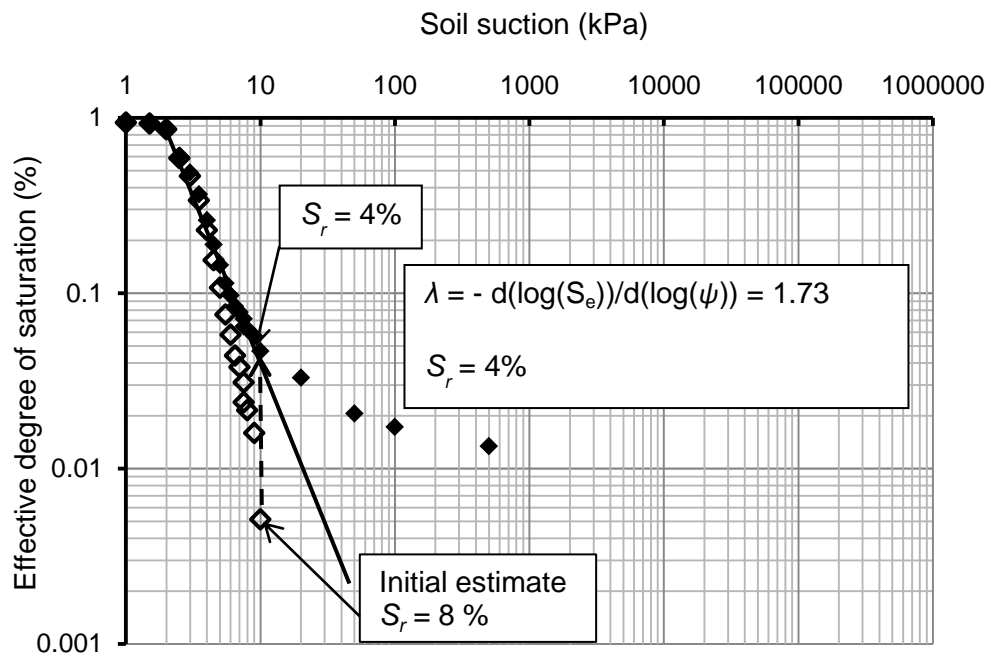


Figure 6.12 Determination of the residual degree of saturation for Beaver Creek sand
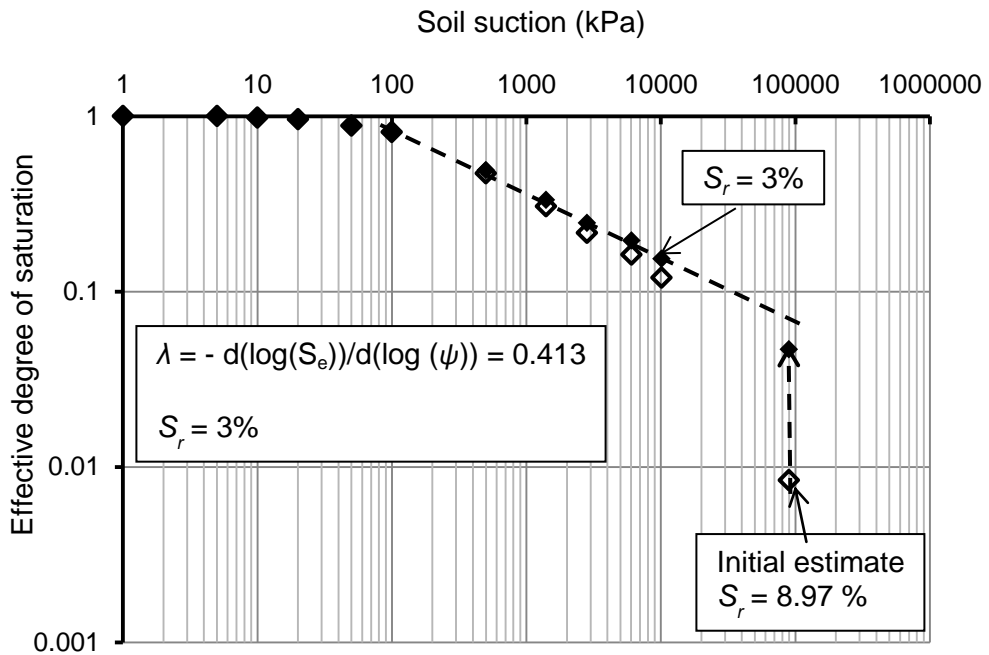
Figure 6.13 Determination of the residual degree of saturation for Botkin silt soil

### 6.6.2 Mualem (1976c) Method

The method proposed by Mualem (1976c) was used to determine the residual-water content for the Beaver Creek sand and Botkin silt soils. The method required the SWCC for the soil in the form of volumetric water content versus soil suction. Figures 6.14 and 6.15 show the soil-water characteristic curves as volumetric water content versus soil suction for Beaver Creek sand and Botkin silt soils, respectively.

Data analysis was conducted in an Excel spreadsheet in order to determine the values of the volumetric water contents. Mathematical equations proposed by Mualem (1967c) were used in the data analysis. The residual-water content values in the volumetric form based on Mualem (1967c) method were 0 and 1% for the Beaver Creek sand and Botkin silt soils, respectively.

### 6.6.3 Construction Method, Vanapalli (1994)

The construction method proposed by Vanapalli (1994) for determination of the residual-state condition (see Chapter 2, section 2.3.2) is used in this section to determine the residual-state condition for Beaver Creek sand and Botkin silt as shown in Figures

223

6.16 and 6.17. The gravimetric water content and soil suction values at the residual-state condition are 2% and 5 kPa for Beaver Creek sand and 7% and 1,800 kPa for Botkin silt.
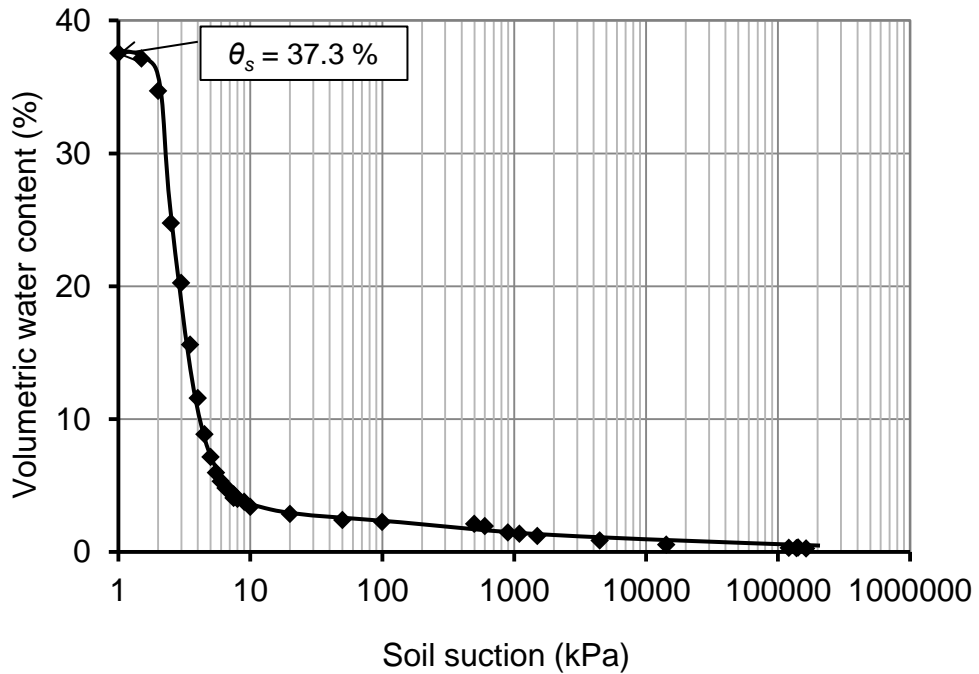


Figure 6.14 Soil-water characteristic curve for Beaver Creek sand
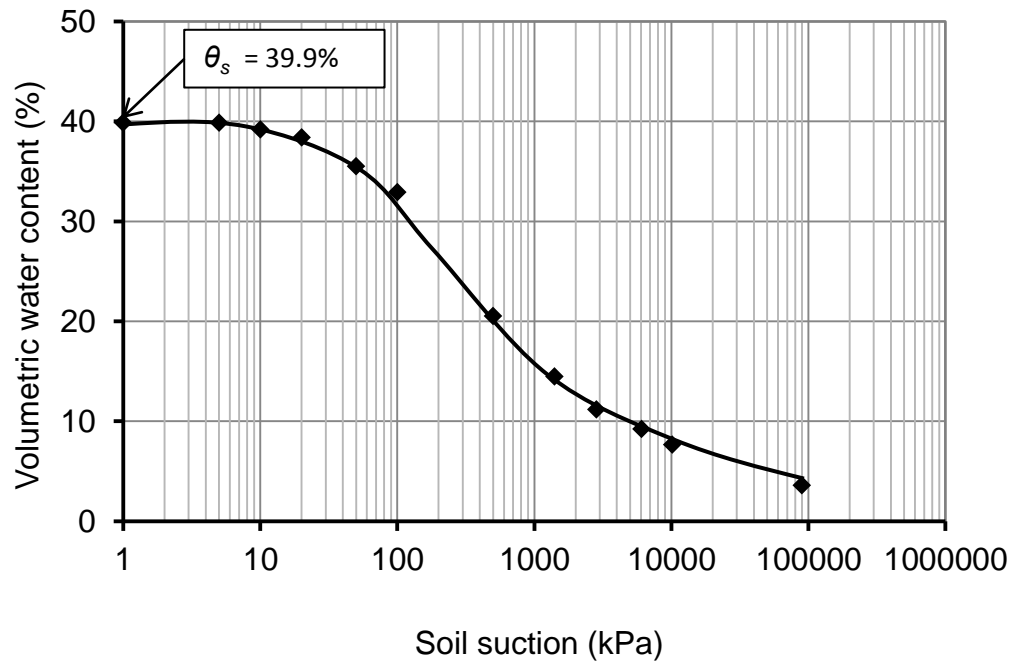


Figure 6.15 Soil-water characteristic curve for Botkin silt
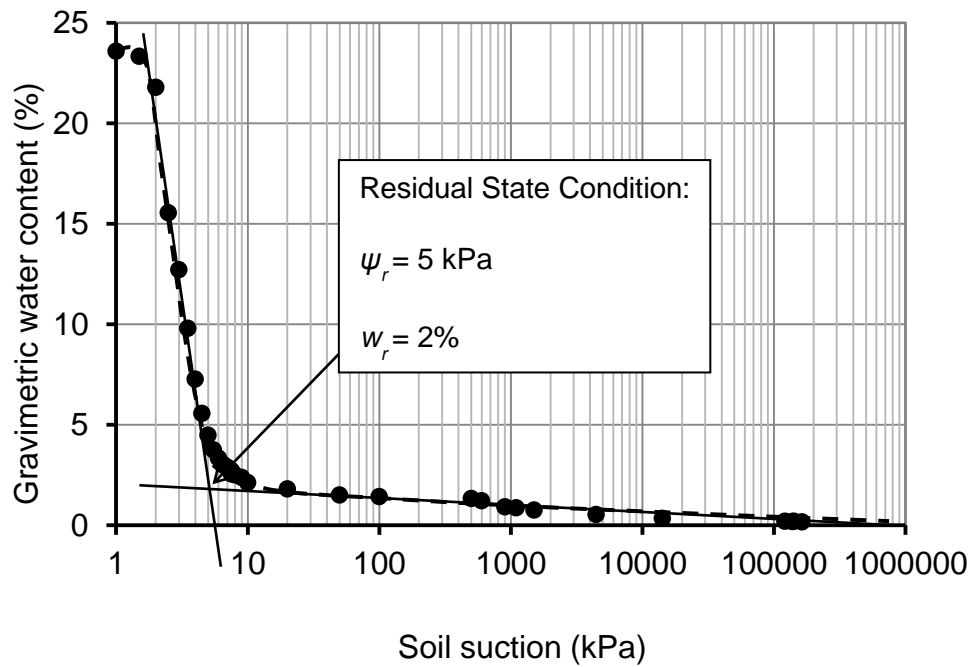
Figure 6.16 Construction method (Vanapalli, 1994) for determination of the residual
conditions for the Beaver Creek sand
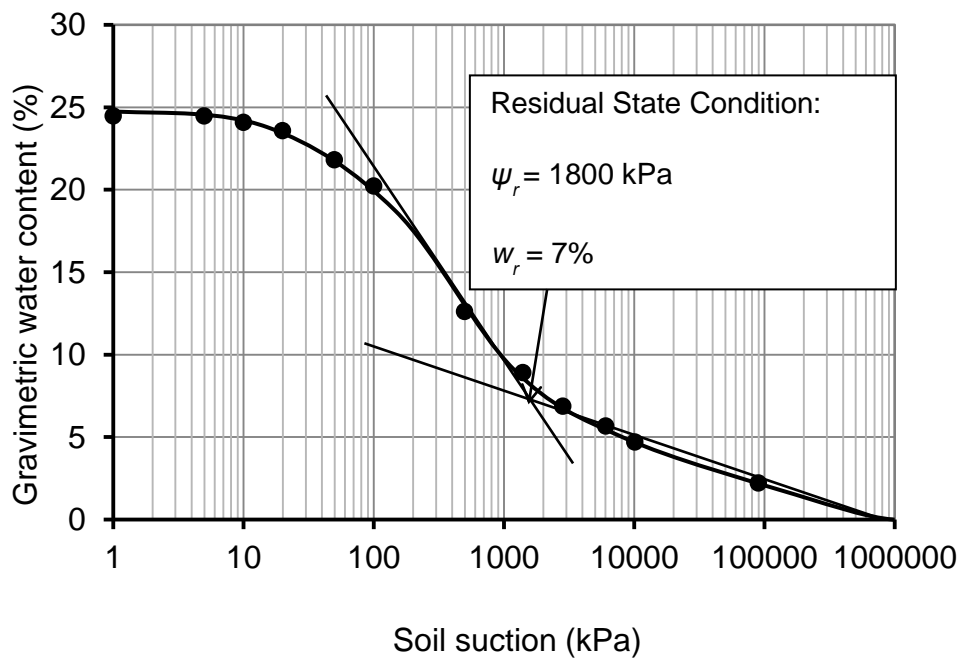


Figure 6.17 Construction method (Vanapalli, 1994) for determination of the residual
condition for Botkin silt

### 6.6.4  Van Genuchten (1980) Method

Van Genuchten (1980) suggested that the residual water content is the water content value at a high suction. The permanent wilting point for plants was suggested as the suction value at the residual condition. The soil-suction value at the residual-state condition was taken as 1,500 kPa. The corresponding gravimetric water contents to the suction value of 1,500 kPa are 0.2% and 8% for the Beaver Creek sand and Botkin silt soils, respectively.

Many research papers have used the residual-water content as a fitting parameter in the van Genuchten equation for the SWCC. Table 6.3 summarizes parameters of the van Genuchten SWCC equation for the Beaver Creek sand and Botkin silt soils. These parameters were defined in Chapter 2, sections 2.2.4 and 2.6.2.2. Figures 6.18 and 6.19 show the SWCCs represented by van Genuchten equations, along with experimental data for Beaver Creek sand and Botkin silt, respectively. Considering the residual-water content as a fitting parameter during analysis for the Botkin silt soil, a negative value was obtained for the water content at the residual-state condition (i.e., $w_r = -0.01$). Since the negative value was not an acceptable one for the water content, a constraint of $w_r \geq 0$ was applied. A value of zero for the residual-water content was the result when a constraint of $w_r \geq 0$ was used in the analysis (Table 6.3).

Table 6.3 Van Genuchten SWCC equation parameters for Beaver Creek sand and Botkin silt

| Soil Type | SWCC Equation | Residual Water Content ($w_r$) % | $\alpha$ | $n$ |
|---|---|---|---|---|
| Beaver Creek Sand | van Genuchten-Mualem (1980) | 1.7 | 0.376 | 4.237 |
| | van Genuchten-Burdine (1980) | 0.8 | 0.416 | 4.420 |
| Botkin Silt | van Genuchten-Mualem (1980) | 0.5 | 0.011 | 1.375 |
| | van Genuchten-Burdine (1980) | 0 | 0.018 | 2.314 |
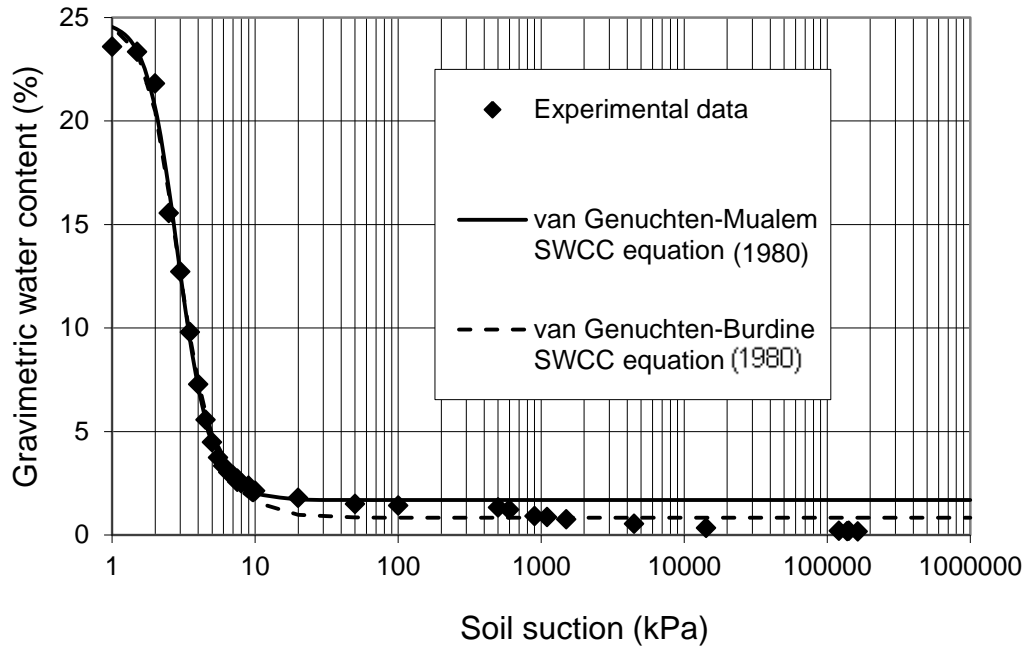
Figure 6.18 Van Genuchten-Mualem and van Genuchten-Burdine SWCC fitting curves
for Beaver Creek sand
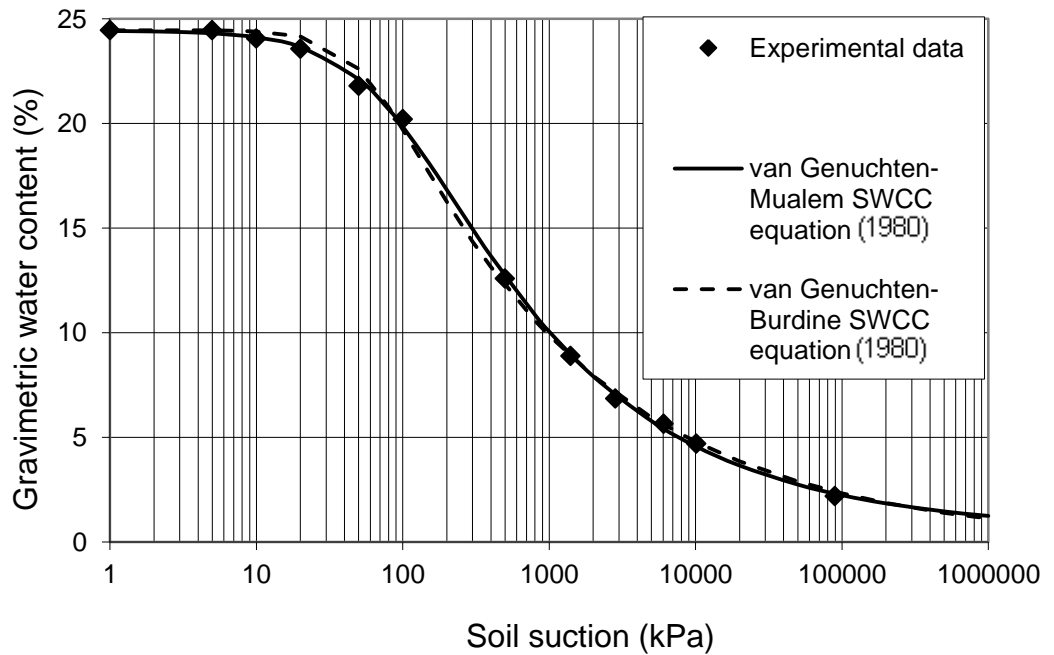


Figure 6.19 Van Genuchten-Mualem and van Genuchten-Burdine SWCC fitting curves
for Botkin silt

### 6.6.5    Determination of the Residual-State Condition Using the Proposed Method

Determination of the residual-state condition for Beaver Creek sand and Botkin silt soils, using the new method described in Chapter 3, section 3.5, is presented in this section. The results are compared with those obtained from conventionally used methods (see section 6.6.1 to 6.6.4). Figures 6.20 and 6.21 show the resulting values for the initial and final residual-state condition using the proposed method.
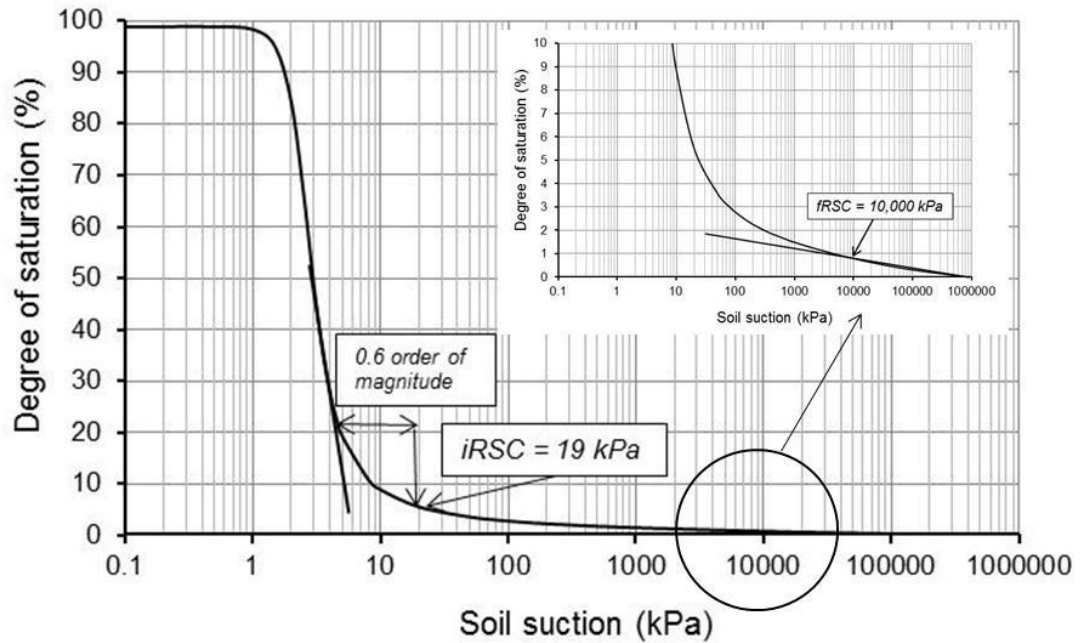


Figure 6.20 Determination of the residual-state condition using the proposed method
(Chapter 3, section 3.5) for Beaver Creek sand

### 6.6.6    Comparison of the Residual-State Condition Obtained from the Proposed Method and the Conventionally Used Methods

Table 6.4 summarizes the results of the residual-state condition for the Beaver Creek sand and Botkin silt samples using different methods. The values in bold indicate the residual-state condition derived directly using the method indicated. The volume-mass properties of the specimens were used to determine the water content in terms of gravimetric, volumetric, and degree of saturation values. The SWCCs of the soil samples (see section 6.5) were used to estimate the suction value from a given water-content value and vice versa.

228
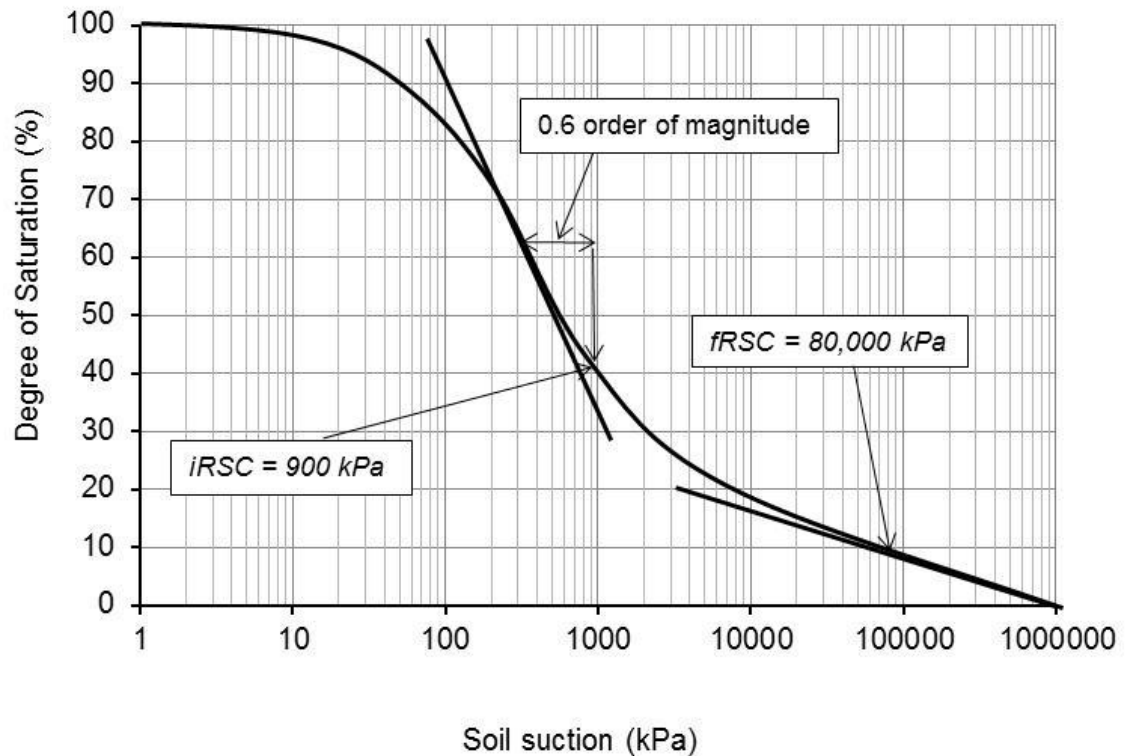
Figure 6.21 Determination of the residual-state condition using the proposed method
(Chapter 3, section 3.5) for Botkin silt

For Beaver Creek sand, using the proposed method, the initial and final suction values of the residual-state condition are 19 kPa and 10,000 kPa, respectively. The residual suction values resulting from all the conventional methods, except from the Mualem method and the Vanapalli method, are located between the initial and final values obtained by the proposed method. Based on the Mualem method the residual water content is 0. The corresponding suction value to totally dry condition is assumed to be 1,000,000 kPa. Based on the Vanapalli method the residual suction value is 5 kPa.

For Botkin Silt, using the proposed method, the initial and final suction values of the residual-state condition are 900 kPa and 80,000 kPa, respectively. The residual suction values obtained by the Vanapalli (1994) method and the van Genuchten (1980) method are located between the initial and final residual-state condition resulting from the proposed method. The suction values from the other conventionally used methods are beyond the final residual-state condition.

## 6.7 EVAPORATION TESTS SELECTED FOR THE ANALYSIS

A total of ten evaporation tests were conducted: six on Beaver Creek sand specimens and four on Botkin silt specimens (see Chapter 4, Table 4.13). The results of the tests were presented in Chapter 5. The evaporation test results were considered suitable for the analysis if all of the following conditions were met:

1- The evaporation rate becomes equal to the inflow rate at the end of the test,

2- The water-content profile at the end of the test consists of water-content values around the residual water content,

3- Evaporation occurs exclusively through the top surface of the specimen (not from the side surface of the specimen because of shrinkage), and

4- Cracks are not developed vertically or horizontally.

Table 6.4 Residual-state conditions for Beaver Creek sand and Botkin silt soils using different methods

| Soil Type | Method | | $w_r$ (%) | $\theta_r$ (%) | $S_r$(%) | $\psi_r$(kPa) |
|---|---|---|---|---|---|---|
| Beaver Creek sand | Brooks and Corey (1964) | | 1.04 | 1.63 | **4** | 1,000 |
| | Mualem (1967) | | 0 | **0** | 0 | 1,000,000 |
| | Vanapalli (1994) | | **2.00** | 3.12 | 7.68 | **5** |
| | van Genuchten (1980) | | **0.75** | 1.17 | 2.88 | **1,500** |
| | van Genuchten-Mualem (1980) | | **1.70** | 2.65 | 6.53 | 30 |
| | van Genuchten-Burdine (1980) | | **0.50** | 0.78 | 1.92 | 4,500 |
| | Proposed method | iRSC | 1.47 | 2.34 | **5.86** | **19** |
| | | fRSC | 0.21 | 0.32 | **0.79** | **10,000** |
| Botkin silt | Brooks and Corey (1964) | | 0.73 | 1.19 | **3** | 400,000 |
| | Mualem (1967) | | 0.61 | **1** | 2.52 | 500,000 |
| | Vanapalli (1994) | | **7.00** | 11.41 | 28.74 | **1,800** |
| | van Genuchten (1980) | | **8.00** | 13.04 | 32.85 | **1,500** |
| | van Genuchten-Mualem (1980) | | **0.8** | 1.30 | 3.29 | 430,000 |
| | van Genuchten-Burdine (1980) | | **0** | 0 | 0 | 1,000,000 |
| | Proposed method | iRSC | 10.00 | 16.29 | **40.88** | **900** |
| | | fRSC | 2.01 | 3.28 | **8.26** | **80,000** |

Note: Numbers in bold indicate the residual-state condition derived directly using the method indicated.

The results of five out of six evaporation tests on Beaver Creek sand (PS1, PS2, PS3, PS4, and MS1) met these conditions and were used in data analysis. The evaporation test on PS5 did not satisfy condition 2 above, as the water content remained significantly high in the soil profile (see Chapter 5, section 5.5.4.1).

The results of one of the four tests on Botkin silt (MCS2) met all the above conditions and were used in data analysis. The other three tests (PCS1, PCS2, MCS1) did not satisfy conditions 3 and/or 4. Cracks and shrinkage were the main issue with PCS1 and PCS2 evaporation tests (see Chapter 5, section 5.5.2.3), and shrinkage was the main issue with MCS1 evaporation test (see Chapter 5, section 5.5.2.4).

The main problem with development of the cracks and shrinkage during the evaporation tests is over-estimation of the evaporation rate. In addition to the cross-sectional area of the soil surface, which is used for estimation of the evaporation rate, evaporation occurs through cracks and side surface.

For the evaporation test on the MCS2 specimen, the cracking and shrinkage problems were solved by restricting the height of specimens, by consolidating the soil specimen prior to initiation of the evaporation test, and by using a triaxial test membrane around the specimen (see Chapter 5, section 5.5.2.4).

## 6.8   TEMPERATURE AND SOIL SUCTION PROFILES

The objective of conducting the steady-state evaporation processes was to determine the unsaturated coefficient of permeability function. The liquid- and vapour-phase flow equations to be used in the analysis were developed in Chapter 3, section 3.6 (Eqs. 3.4 and 3.20). Temperature and soil suction gradients are two essential terms of the developed equations and must be determined for data analysis.

In section 6.8.1, temperature profiles are discussed in general. In section 6.8.2, the results of change in evaporation rate in relation with temperature changes during the evaporation tests are discussed. An equation representing relations between the evaporation rate and soil surface temperature is then developed by analyzing the evaporation test data for MCS2, presented in Chapter 5, sections 5.5.2.4 and 5.5.3.4. In section 6.8.3, the experimental data of water content profiles are converted to the soil suction profiles using the corresponding SWCCs. Equations representing these suction

profiles are then developed. The suction gradients required for the flow equations are determined using the equations representing suction profiles.

### 6.8.1 Temperature Profiles

Temperature changes along the evaporation column at different depths were recorded in 10-minute time increments during evaporation processes. The changes in temperature with time were presented in Chapter 5, section 5.5.3. Three types of top boundary conditions were considered for the evaporation tests: i) in the first type, controlled radiation energy was emitted to the surface of the soil in order to promote the evaporation rate and to keep the temperature at a constant value along the column (PS1 and PS3); ii) in the second type, wind was created on top of the soil column to accelerate the evaporation (PS2, PS4, MS1); and iii) in the third type, there was no attempt to accelerate the evaporation rate during the test (MCS2). The evaporation tests were conducted in an environmentally controlled room. To avoid radiation from the light, all lights in the room were off during the evaporation processes, except for the controlled light which was required for the tests with the wind and radiation boundary condition type.

Figure 6.22 shows the temperature profiles at 400 min (early stages) and 7,000 min (later stages) for the evaporation process on Beaver Creek sand Specimen PS2 with no radiation. The temperature profiles for times greater than 7,000 min were constant and similar to the temperature profile at 7,000 min. A temperature gradient of about 2.5 $^{o}$C/ 145 mm is created. The temperature gradient was greater at the early stages of the test; it decreased with time, and became constant after the steady-state condition was reached. Similar results were observed in all of the evaporation processes without radiation.

Figure 6.23 shows temperature profiles at 100 min (early stage) and 2830 min (later stage) for the evaporation process on Beaver Creek sand Specimen PS3 with radiation. Small differences in temperature ($< 0.5$ $^{o}$C) with depth were observed.
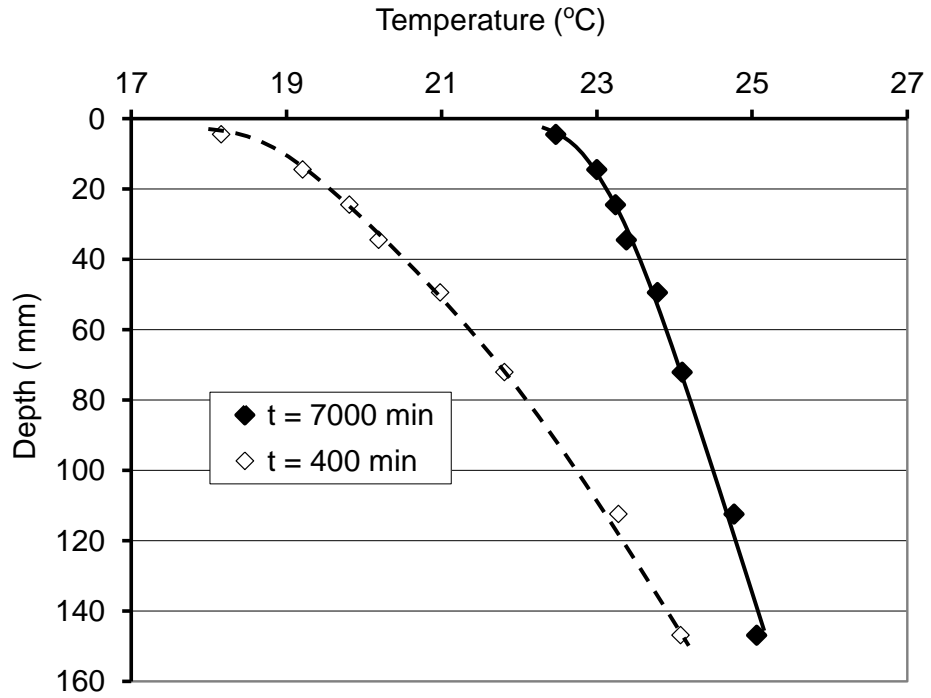
Figure 6.22 Temperature profiles at elapsed times of 400 and 7,000 minutes for "wind" treatment of Specimen PS2 (Beaver Creek sand)
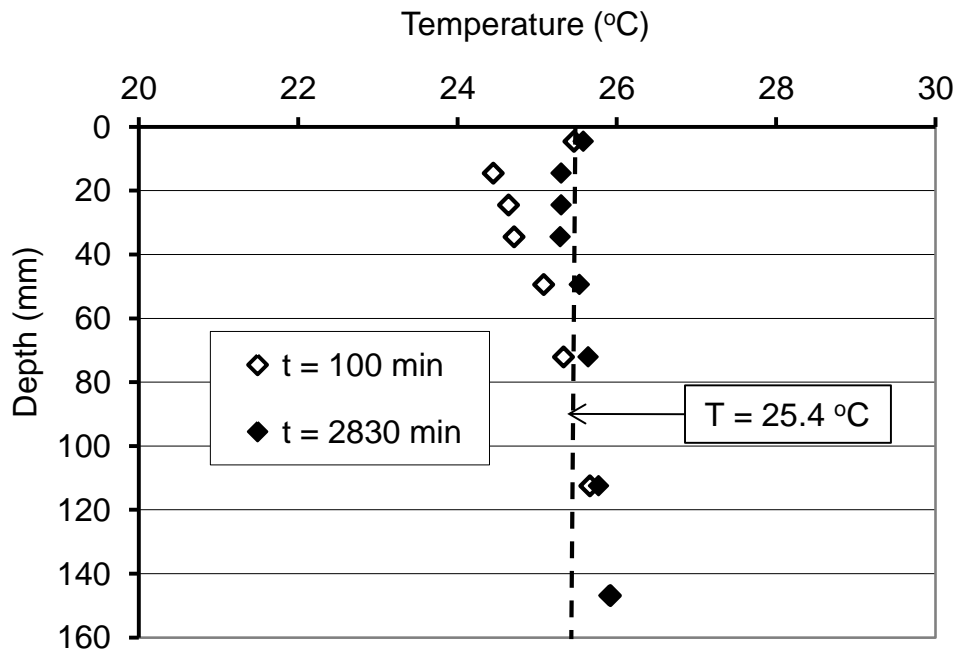


Figure 6.23 Temperature profiles at elapsed times of 100 and 2,830 minutes for "radiation and wind" treatment of the Specimen PS3 (Beaver Creek sand)

Figure 6.24 shows temperature profiles at the end of the evaporation processes for the Beaver Creek sand specimens (PS1, PS2, PS3, PS4, and MS1). The top boundary condition for the evaporation processes on Specimens PS1 and PS3 was "wind and radiation" treatment. The top boundary condition for the evaporation processes on Specimens PS2, PS4, and MS1 was "wind" treatment. The temperature gradients along the evaporation column are smaller for the tests with top boundary condition controlled by "wind and radiation." That is, the temperature was successfully controlled by the bulb and relay system used for this purpose (see Chapter 4). It should be noted that the modified evaporation column used for Specimen MS1 was shorter than the primary evaporation column.

For the evaporation test on MCS2 (Botkin silt), the temperature with time data were measured only at the surface of the specimen. Thermocouples were not inserted at the different depths, in order to prevent damage to the triaxial membrane that in turn could compromise the data analysis.

For MCS1 (Botkin silt), from the temperature changes versus time data (Chapter 5, section 5.5.3.4), it can be determined that difference in temperature along the soil column (between 5 and 50 mm distances from the surface) was about 1.2 $^{o}$C. This sample was discarded from the analysis because of the shrinkage issue.

Temperature difference along MCS2 was expected to be less than that along the MCS1 specimen, because the rate of evaporation at the end of the test was substantially larger for the latter (1.13 mm/d versus 11.49 mm/d).

## 6.8.2   Evaporation Rate and Temperature

The data for change in evaporation rate versus time were presented in Chapter 5, section 5.5.2. The change in temperature versus time at different depths of the soil column was presented in Chapter 5, section 5.5.3. A close relationship between change in evaporation rate with time and change in soil temperature with time was observed during the evaporation processes. In general, the rate of evaporation and the temperature showed an inverse relationship: an increase in evaporation rate caused a decrease in temperature, and a decrease in evaporation rate caused an increase in temperature. When the evaporation rate remained constant, so did the temperature.
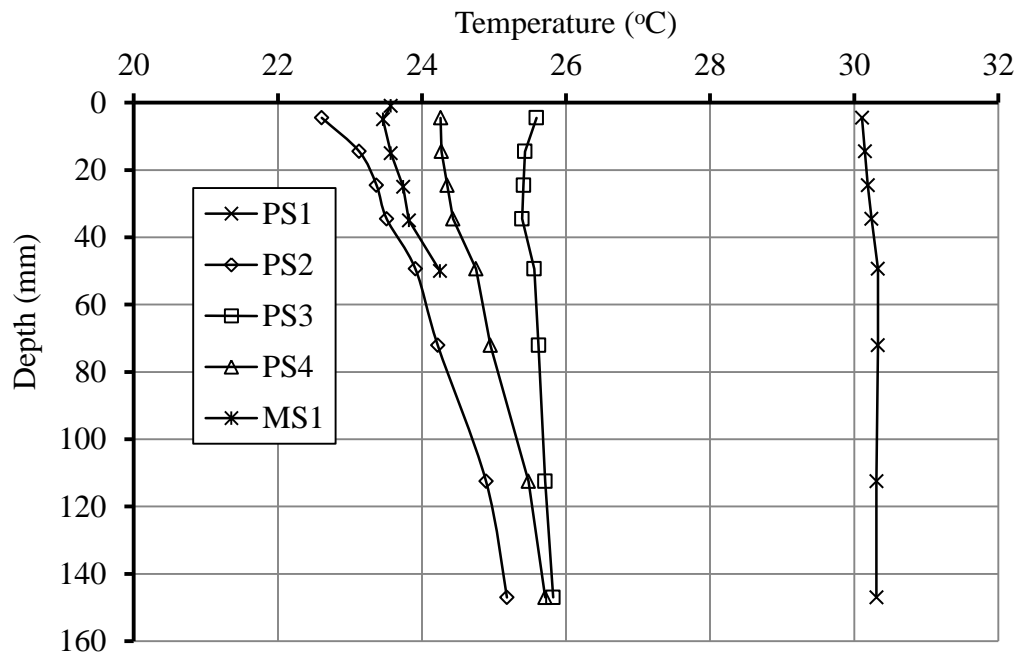
Figure 6.24 Temperature profiles at the end of the evaporation processes for Beaver
Creek sand

To explain how the change in evaporation rate caused the change in temperature, evaporation rate and temperature data for the evaporation test on Beaver Creek sand Specimen PS4, as an example, are shown on the same scale in Figure 6.25. As the cover on the evaporation column is removed, evaporation begins and increases with time. The temperature decreases at the surface of the soil due to latent heat. Heat is transferred from the depth to the surface of the soil due to temperature gradient through conduction, resulting in a decrease in temperature at lower depths of the column. After the potential evaporation (PE = 27 mm/d) for this test is reached, the evaporation rate begins to decrease; the latent heat required for evaporation decreases accordingly, resulting in the increase in temperature at the surface of the soil and at all depths of the soil column. Near the steady-state condition, both evaporation rate and temperature at different depths remained constant.

Temperature and evaporation rate versus time for Botkin silt Specimen MCS2 are shown in Figure 6.26. As with Beaver Creek sand (Specimen PS4), the rate of evaporation and the temperature show a close relationship. Temperature decreases with

increase in evaporation rate. Both the evaporation rate and the temperature remain constant for a period of time after the potential evaporation rate is reached. Then, the temperature begins to rise again when evaporation rate decreases. At a steady-state condition, both temperature and evaporation rates remain constant.

The correlation between soil surface temperature and the evaporation rate obtained from evaporation Process MCS2 for the second period of drying (from 2,800 min to 10,000 min) is shown in Figure 6.27. The relationship between the evaporation rate and soil surface temperature is linear. The linearity and accuracy of the relationship between the evaporation rate and soil surface temperature should be further assessed.

### 6.8.3 Determination of Soil Suction Profiles

Soil suction profiles were required for analyzing data obtained from the evaporation processes in order to determine the unsaturated coefficient of permeability function. The suctions at the end of the evaporation processes along the evaporation columns were determined using the water content profile and the corresponding SWCC of each specimen. To determine the suction value near the surface, a thin layer of soil was removed and its suction was measured using a WP4-T device whenever it was possible. The suction values measured using this device were used to verify the values determined through the water content profile and the SWCC.

Equation 6.1 is used to determine the fitting curve of the suction profile for each of the tests.

$$\psi(y) = a\left(1 + e^{b/y}\right) + \left(\frac{c}{y}\right)^d \qquad [6.1]$$

where

$\psi(y)$      = suction, kPa,

$y$      = distance from the surface of the soil specimen, mm, and

   $a, b, c,$ and $d$ = fitting parameters of the equation.

236
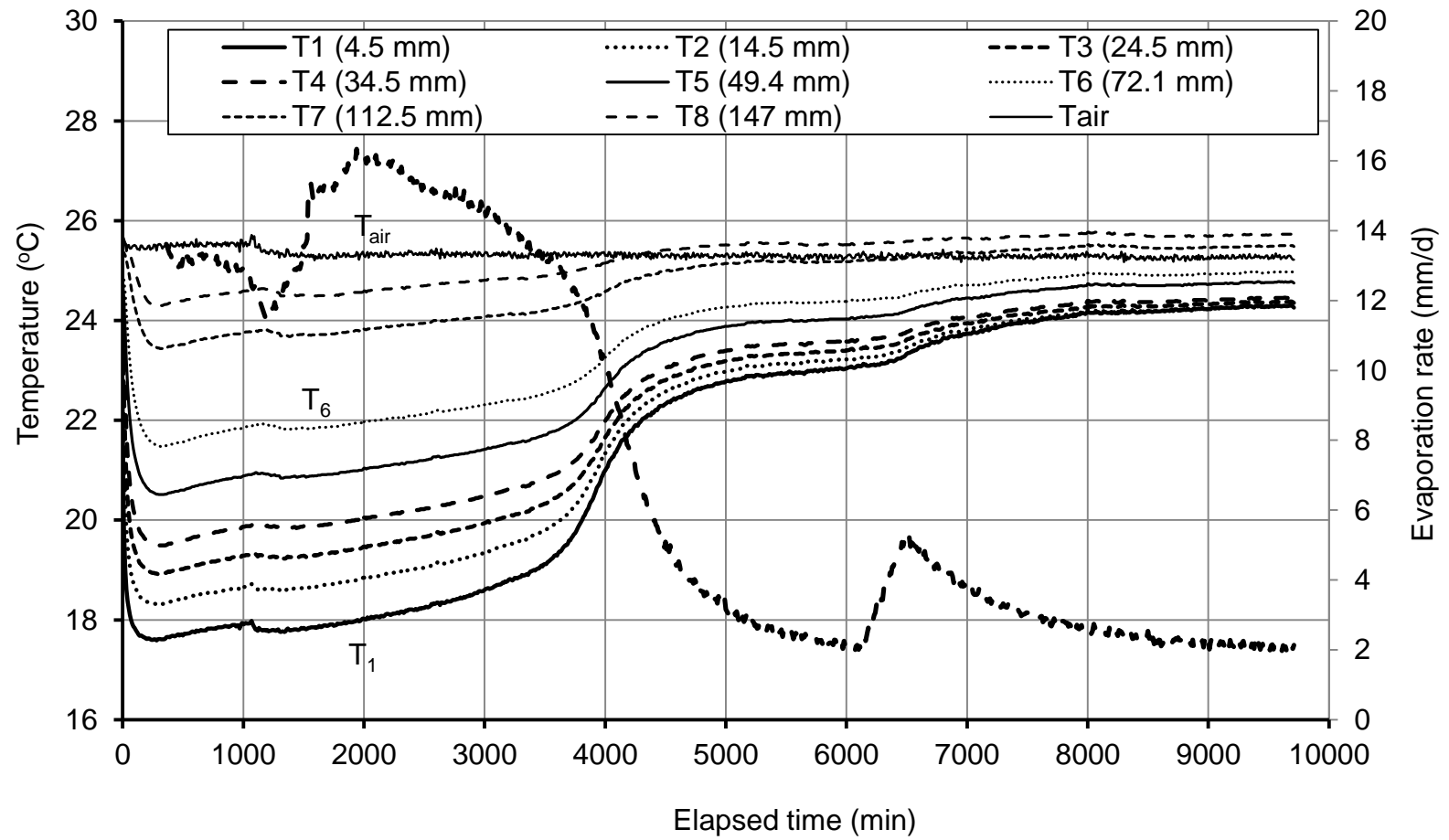
Figure 6.25 Temperature and evaporation rate versus time for Beaver Creek sand Specimen PS4
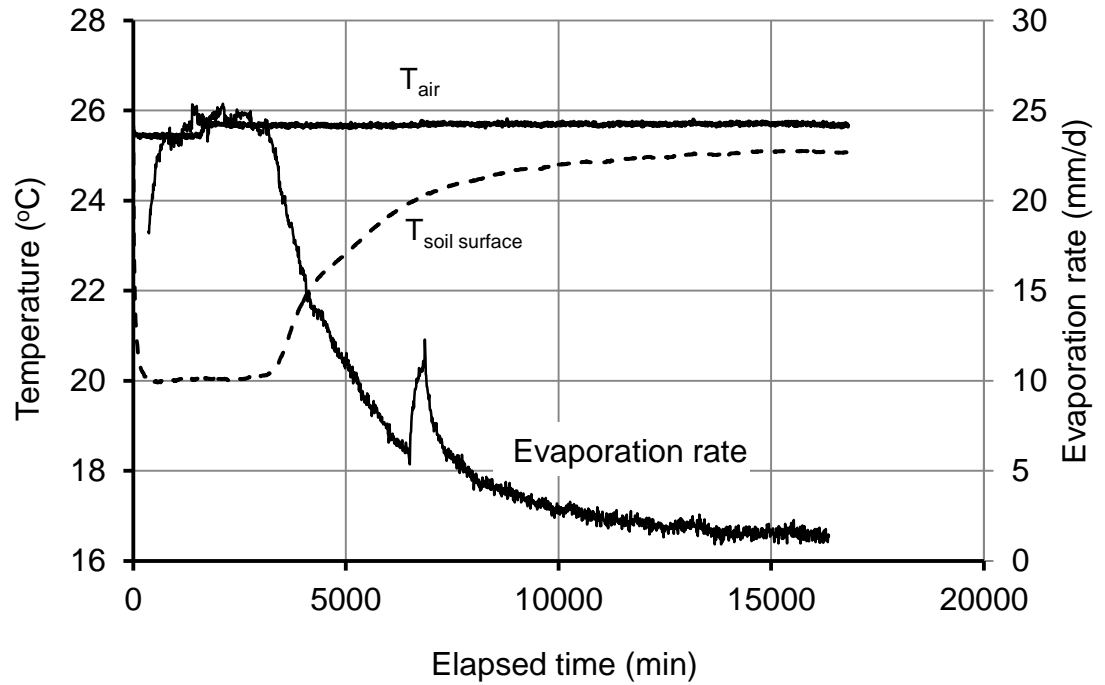
Figure 6.26 Temperature and evaporation rate versus time for Botkin silt Specimen
MCS2
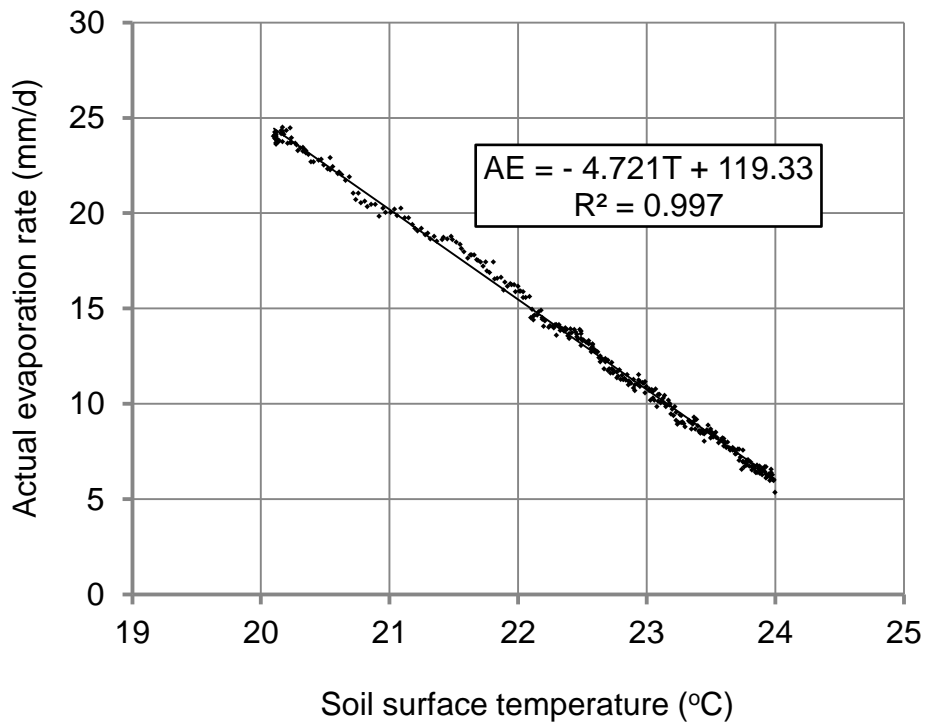


Figure 6.27 Correlation between soil surface temperature and evaporation rate for
Botkin silt Specimen MCS2

Figures 6.28 to 6.32 show experimental data and fitting curves of the soil suction profiles at the end of the evaporation tests on Beaver Creek sand Specimens PS1, PS2, PS3, PS4, and MS1. The fitting parameters are also presented in the figures. The figures show that there is generally good agreement between fitting curves and experimental data. However, discrepancies can be observed between experimental data and fitting curves for PS1 and PS2 specimens (Figures 6.28 and 6.29); they occurred mainly at depths above 20 mm for PS1 and below 25 mm for PS2. These discrepancies may cause uncertainties in determination of the coefficient of permeability in the regions where they appear. The impact of these discrepancies on determination of the unsaturated coefficient of permeability for Beaver Creek sand is discussed in section 6.10.

Figure 6.33 shows the estimated profiles for the evaporation tests on all of the Beaver Creek sand specimens.

Figure 6.34 shows experimental data and fitting curve of the soil suction profile at the end of evaporation Process MCS2. The fitting curve along with its parameters is also presented in the figure. There are discrepancies between the fitting curve and the experimental data at depths below about 55 mm.

Differentiation of Eq. 6.1 with respect to y gives Eq. 6.2. Equation 6.2 is used to compute the suction gradients required in the data analysis.

$$\frac{d\psi}{dy} = \frac{-ab}{y^2} \, e^{b/y} - \frac{dc^d}{y^{d+1}} \qquad\qquad [6.2]$$

Fitting curves for the soil suction profiles at the end of the evaporation processes for Beaver Creek sand specimens are shown in Figure 6.33. The main differences between the initial condition of MS1 and the other specimens were: i) the modified evaporation column was shorter than the primary evaporation column; therefore, the MS1 specimen was shorter than the other specimens, and ii) the boundary condition at top of the MS1 specimen was "no-radiation–no-wind" treatment. That is, the potential evaporation rate for the MS1 specimen was smaller than that for the other specimens. The smaller potential evaporation rate and the short specimen appear to cause the small suction values along the soil column.
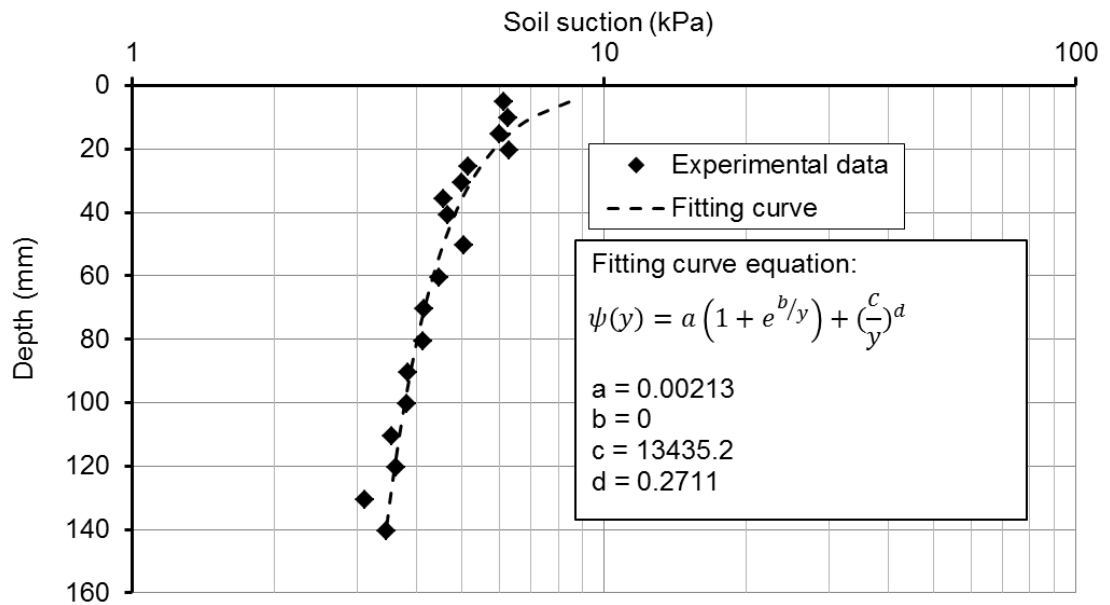
Figure 6.28 Experimental data and fitting curve for the soil suction profile at the end of evaporation Process PS1 (Beaver Creek sand)
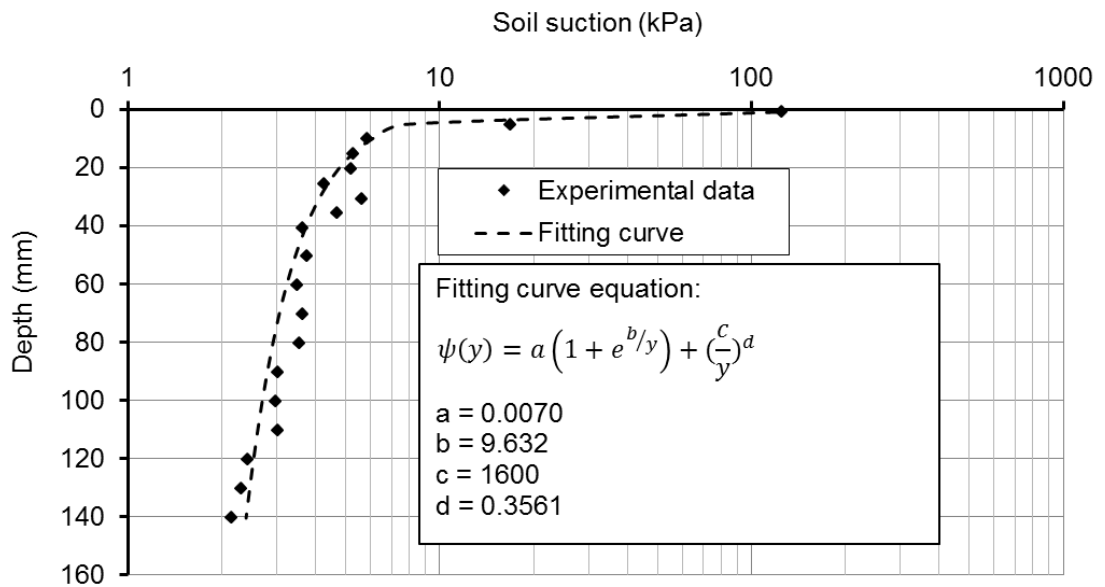


Figure 6.29 Experimental data and fitting curve for the soil suction profile at the end of evaporation Process PS2 (Beaver Creek sand)

240
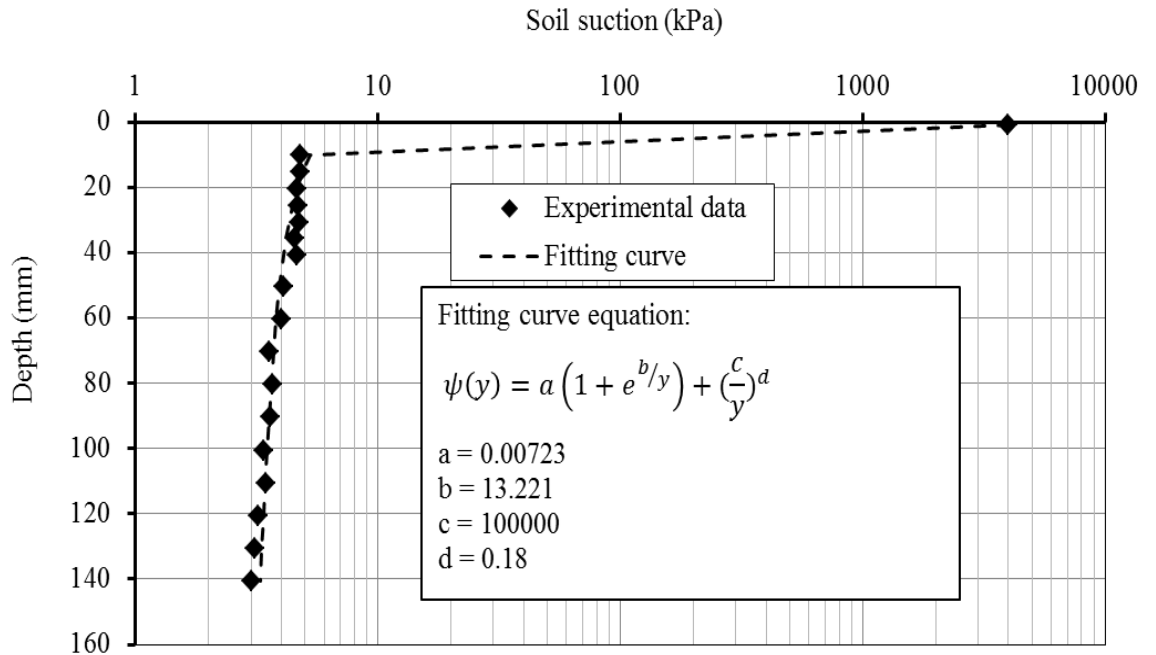
Figure 6.30 Experimental data and fitting curve for the soil suction profile at the end of evaporation Process PS3 (Beaver Creek sand)
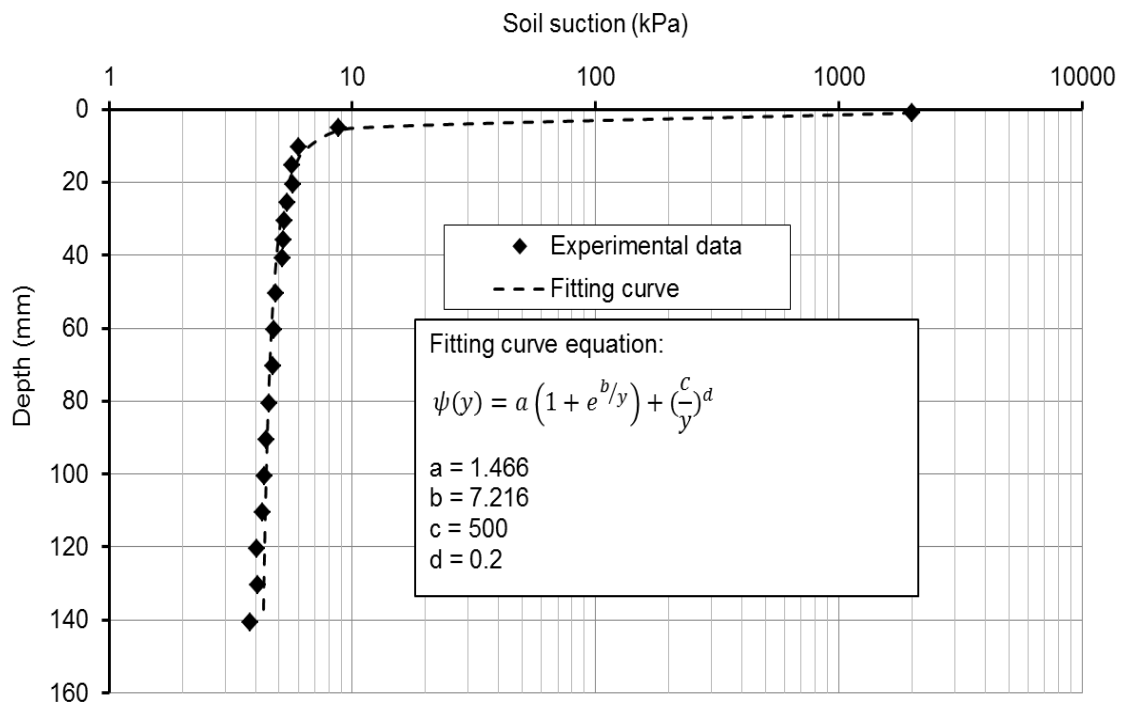


Figure 6.31 Experimental data and fitting curve for the soil suction profile at the end of evaporation Process PS4 (Beaver Creek sand)

241

Figure 6.32 Experimental data and fitting curve for the soil suction profile at the end of evaporation Process MS1 (Beaver Creek sand)



Figure 6.33 Fitting curves for the soil suction profiles at the end of the evaporation processes for Beaver Creek sand specimens
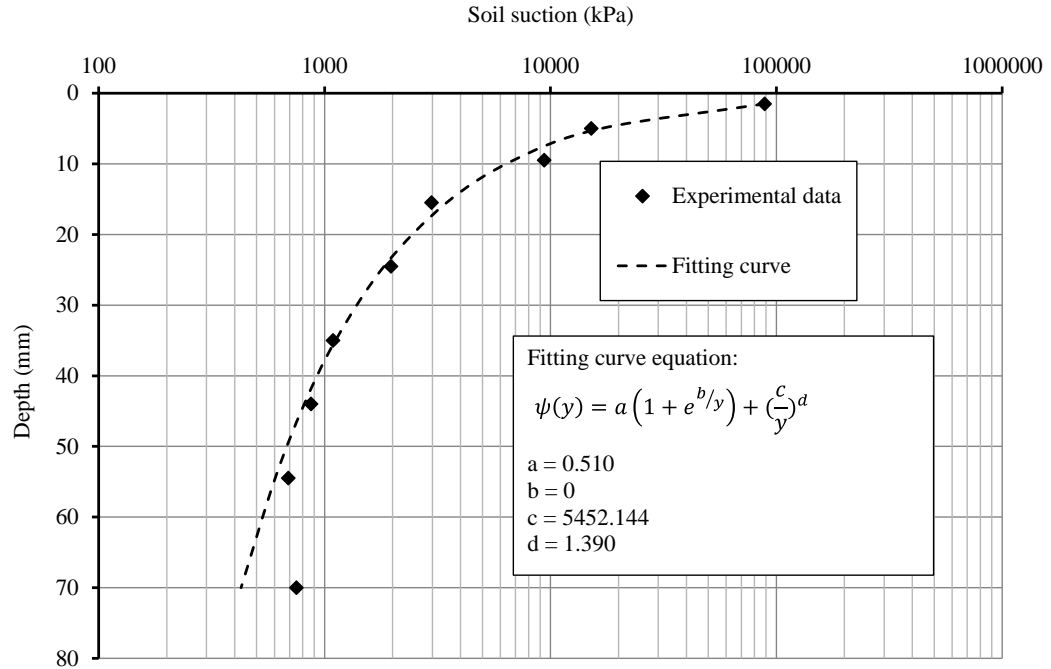
Figure 6.34 Experimental data and fitting curve for the soil suction profile at the end of evaporation Process MCS2 (Botkin silt)

Most of the changes in suction values took place within the first 20 mm of the soil surface. That is, the suction gradient was the largest within 20 mm of the soil surface. For instance, the suction value for Botkin silt varied from about 90,000 kPa at the surface to about 5 kPa at a depth of 20 mm (see Figure 6.34).

## 6.9   THE RESIDUAL-STATE CONDITION AND THE TRANSITION ZONE

The transition zone was defined as a zone on the water-content or soil-suction profile over which the mechanism of flow transfers from liquid-phase-dominated flow (lower limit) to vapour-phase-dominated flow (upper limit). Definitions of the lower and upper limits of the transition zone were described in Chapter 2, section 2.4 and Chapter 3, section 3.3.

Chapter 3, section 3.3 gave examples of soil profiles for soil-drying systems after the steady-state flow condition was reached. All the evaporation tests for this research generated type 2 profiles (Chapter 3, Figure 3.3.b). In a type 2 profile, the drying surface remains at the top of the soil column, and a transition zone develops below it. Since the evaporation surface is at the top of the soil, it is not clear whether the suction value has been reached the point below which the vapour flow becomes dominant. In this type of

profile, development of the upper part of the transition zone is considered to be incomplete.

Table 6.5 shows the lower limit of the transition zones obtained from the suction profiles presented in section 6.8. In Chapter 3, it was hypothesized that the lower and upper limits of the transition zones may be considered as the initial and final residual-state conditions. The resulting values for the lower limit of the transition zone for Specimens PS1, PS2, PS3, PS4, and MS1 (Beaver Creek sand specimens) vary between 4.3 kPa and 5 kPa (Table 6.5), which are not comparable to 19 kPa,, the estimated value for the iRSC obtained from the method proposed in Chapter 3 (see Table 6.4).

For the Botkin silt specimen MCS2, the lower limit of the transition zone is 700 kPa (Table 6.5), which is close to 900 kPa, the estimated value for the iRSC obtained from the method proposed in Chapter 3 (see Table 6.4). The upper limit of the transition zone is 90,000 kPa which is close to the estimated final residual-state condition for this soil based on the proposed method in Chapter 3 (80,000 kPa).

Table 6.5 Lower and upper limits of the transition zones for the evaporation processes

| Soil | Specimen ID | Transition zone (mm) | Lower limit (kPa) |
|---|---|---|---|
| Beaver Creek sand | PS1 | 20 – 40 | 4.5 |
| | PS2 | 1 – 20 | 4.3 |
| | PS3 | 1 – 10 | 4.3 |
| | PS4 | 1 – 20 | 5.0 |
| | MS1 | 1 – 4 | 4.3 |
| Botkin silt | MCS2 | 1 – 50 | 700 |

It is not clear from a comparison of the results presented in Tables 6.4 and 6.5 whether or not the lower and upper limits of the transition zone of the soil-suction profile indicate the initial residual-state condition (iRSC) and the final residual-state condition (fRSC).

244

## 6.10  DETERMINATION OF THE UNSATURATED COEFFICIENT OF PERMEABILITY FUNCTION USING EXPERIMENTAL DATA

The unsaturated coefficient of permeability functions for Beaver Creek sand and Botkin silt specimens, presented in this section, were determined by analysis of the experimental results obtained from the evaporation processes by means of the flow equations developed in Chapter 3.

### 6.10.1  Unsaturated Coefficient of Permeability Function for Beaver Creek Sand

Figures 6.35 to 6.39 show unsaturated coefficient of permeability functions determined by analyzing the data obtained from the evaporation processes for Specimens PS1, PS2, PS3, PS4, and MS1. It was assumed that the coefficient of permeability remains constant and equal to the saturated coefficient of permeability from near-zero suction to the air-entry value. Past air-entry value, the coefficient of permeability decreases. For the range of suction value beyond 1500 kPa, WP4-T measurements were involved in the process of determination of the coefficient of permeability.

The unsaturated coefficient of permeability data obtained from the evaporation tests on the 5 Beaver Creek sand tests are generally consistent. Inconsistencies were observed in the lower suction values, between 2 kPa to 3 kPa for the data obtained from the evaporation process PS2 (Figure 6.36). Theses inconsistencies may be attributed to the discrepancies in suction profile data for this test (see Figure 6.29).

Figure 6.40 shows experimental data from all of the 5 evaporation tests for Beaver Creek sand soils on the same scale. The initial and final residual-state conditions predicted from the proposed method (see Table 6.4) are also shown in this figure. There is a clear change in the slope of the coefficient of permeability function at suction value of about 20 kPa, which is close to the initial estimated suction value of 19 kPa. Based on the experimental data, the coefficient of permeability may be presented as a three-region function: i) near-zero to air-entry value; ii) air-entry value to the initial residual-state condition; and iii) initial to final residual-state condition.
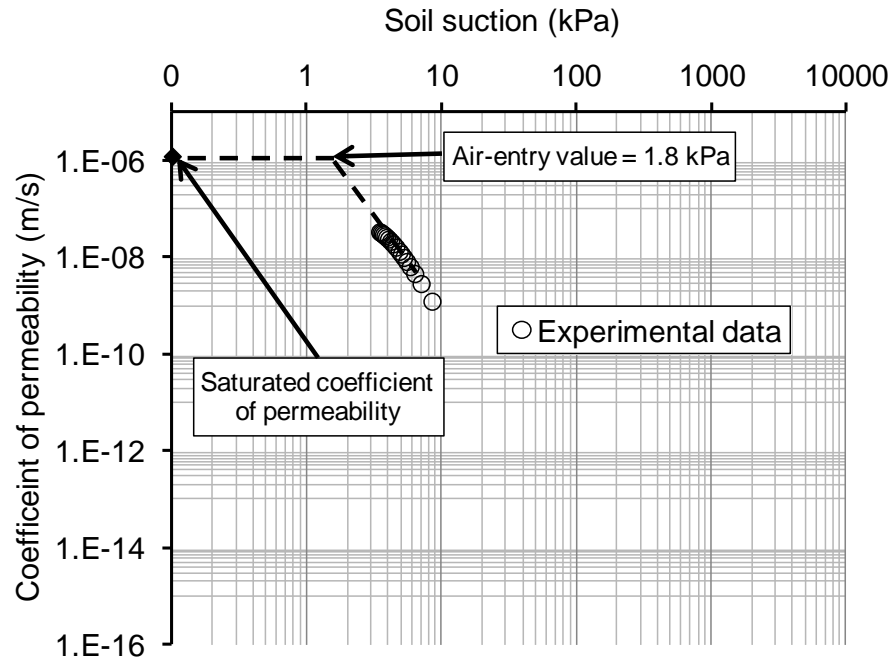
Figure 6.35 Coefficient of permeability function for Beaver Creek sand Specimen PS1
(Experimental data)
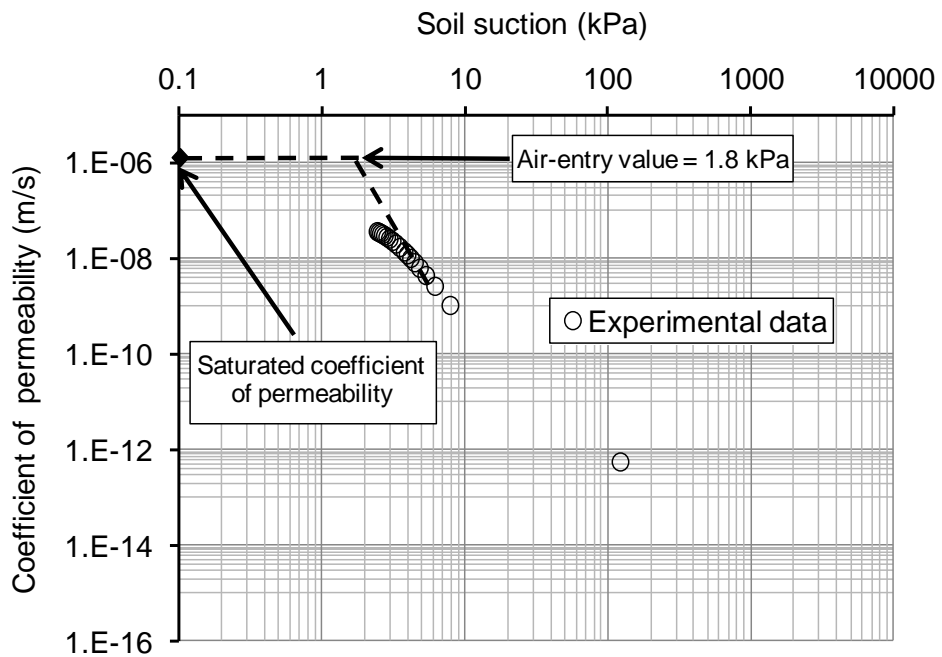


Figure 6.36 Coefficient of permeability function for Beaver Creek sand Specimen PS2
(Experimental data)
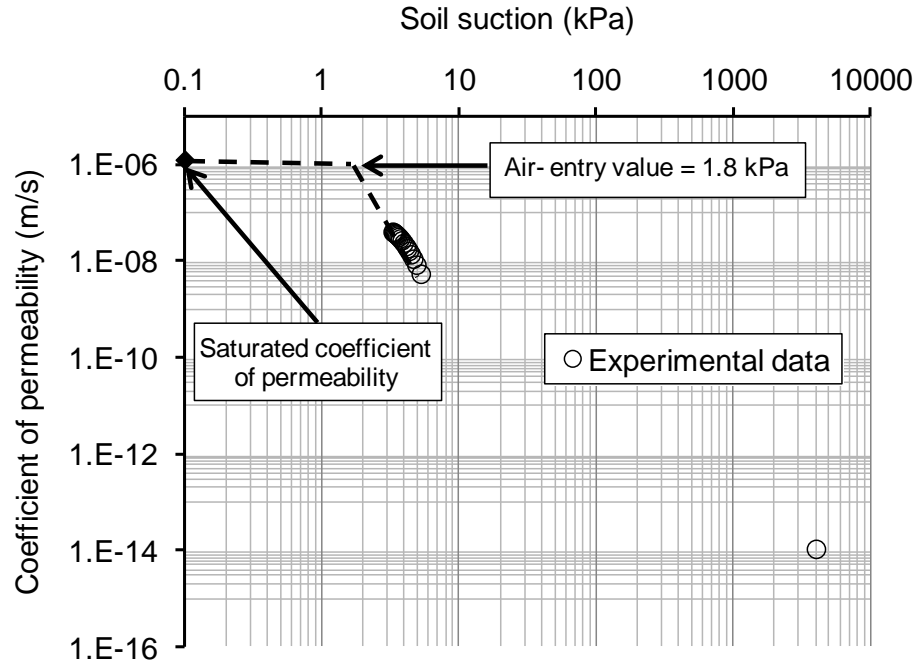
Figure 6.37 Coefficient of permeability function for Beaver Creek sand Specimen PS3 (Experimental data)
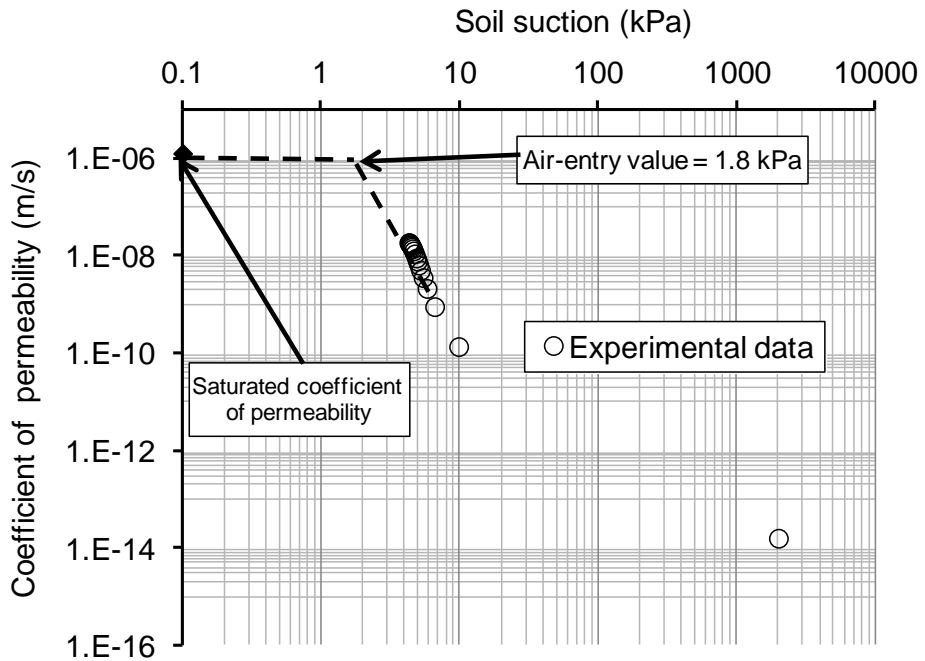


Figure 6.38 Coefficient of permeability function for Beaver Creek sand Specimen PS4 (Experimental data)
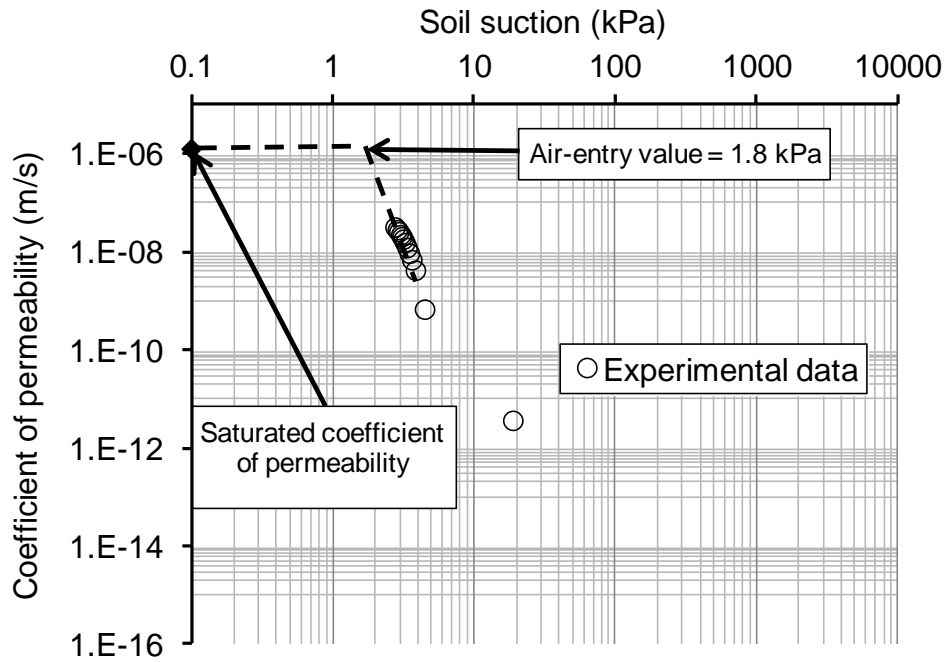
Figure 6.39 Coefficient of permeability function for Beaver Creek sand Specimen MS1
(Experimental data)
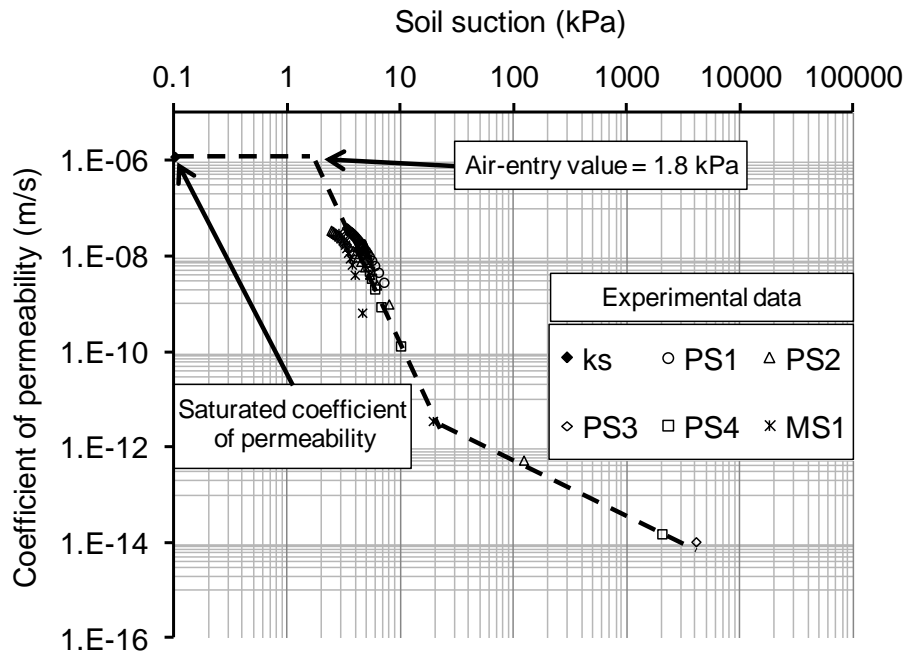


Figure 6.40 Coefficient of permeability function for Beaver Creek sand (Experimental
data)

The general form of the coefficient of permeability function for the Beaver Creek sand in Figure 6.40 is consistent with the form of the function proposed in Chapter 3, section 3.7.3 (Figure 3.12).

### 6.10.2 Unsaturated Coefficient of Permeability Function for Botkin Silt

Figure 6.41 shows experimental data for the unsaturated coefficient of permeability for Botkin silt, determined by analyzing the data obtained from the evaporation process on Specimen MCS2. The estimated initial and final residual-state conditions (iRSC and fRSC) from the proposed methods (see Table 6.4), and the experimental data for the saturated coefficient of permeability, are also shown in Figure 6.41. There is a small change in the saturated coefficient of permeability from suction values near zero to the air-entry value of 65 kPa. The change in permeability below air-entry value is mainly due to change in volume of the sample.

Past air-entry value, the soil becomes unsaturated, and a significant reduction in the coefficient of permeability with suction can be observed. Similar to the Beaver Creek sand, the general form of the coefficient of permeability function for the Botkin silt in Figure 6.41 is consistent with the form of the function proposed in Chapter 3, section 3.7.3 (Figure 3.12).

### 6.11 WATER-VAPOUR COEFFICIENT OF PERMEABILITY FUNCTION

This section presents the liquid-water and water-vapour coefficient of permeability functions ($k_l$ and $k_v$) determined for Beaver Creek sand and Botkin silt specimens. The data for the liquid-water coefficient of permeability are the same ones presented in the previous section.

Water-vapour permeability functions for Beaver Creek sand and Botkin silt soils were determined by analyzing the experimental data (Chapter 4) and using Eq. 3.19, developed in Chapter 3, section 3.6. The results of the analysis are shown in Figures 6.42 and 6.43 for Beaver Creek sand and Botkin silt soils, respectively.

For both Beaver Creek sand and Botkin silt soils, the water-vapour coefficient of permeability reaches its maximum at about $3 \times 10^{15}$ m/s at the initial residual-state condition. Figures 6.42 and 6.43 indicate that the water-vapour and liquid-water coefficients of permeability become approximately equal at the final residual-state

condition. The data analysis also shows that the total coefficient of permeability defined as $k_l + k_v$ is dominated by the liquid-water coefficient of permeability ($k_l$) from near zero to the final residual-state condition, and by the water-vapour coefficient of permeability ($k_v$) beyond the final residual-state condition.
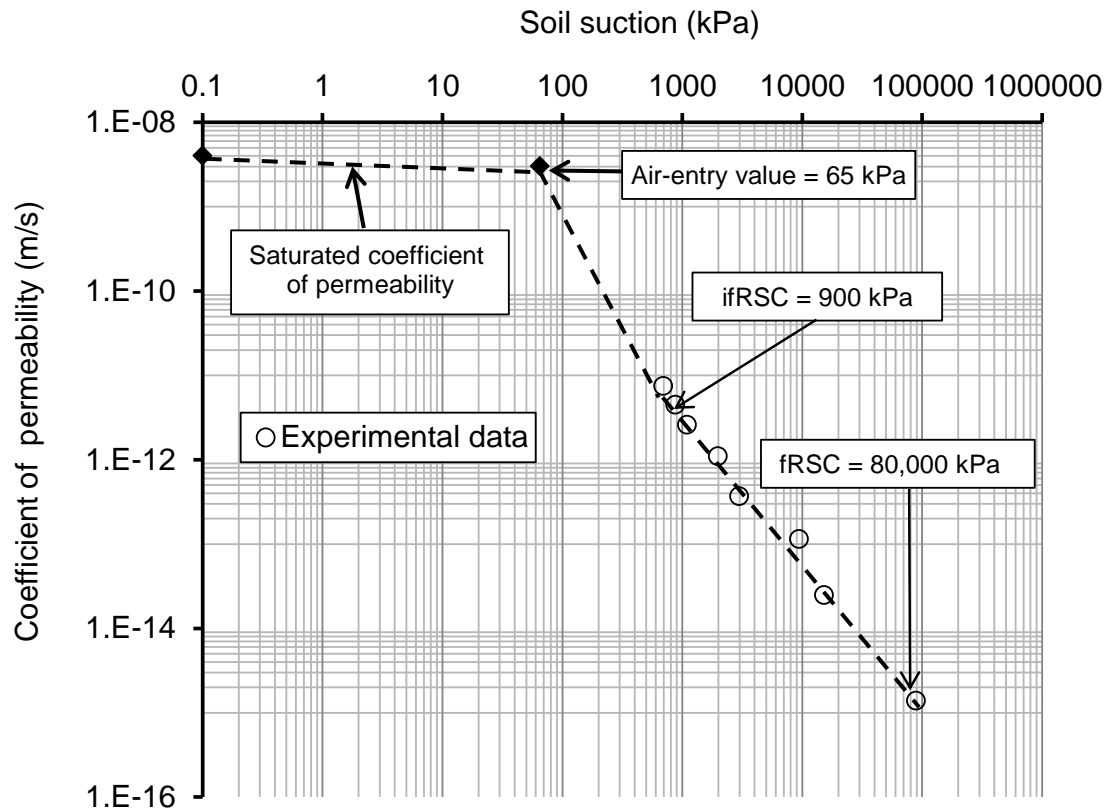


Figure 6.41 Coefficient of permeability function for Botkin silt Specimen MCS2
(Experimental data)

A physical description of the residual-state condition was given in Chapter 3, section 3.4. It was hypothesized that in a single soil pore in an unsaturated condition, the moisture flow may occur through hydraulically connected layers of water to a suction value at which the hydraulic connection is broken. The moisture flow was assumed to be dominated by the water-vapour flow mechanism after the hydraulic connection is broken. As mentioned in the previous paragraph, the experimental data show that the water-vapour coefficient of permeability becomes dominant beyond the final residual-state condition.
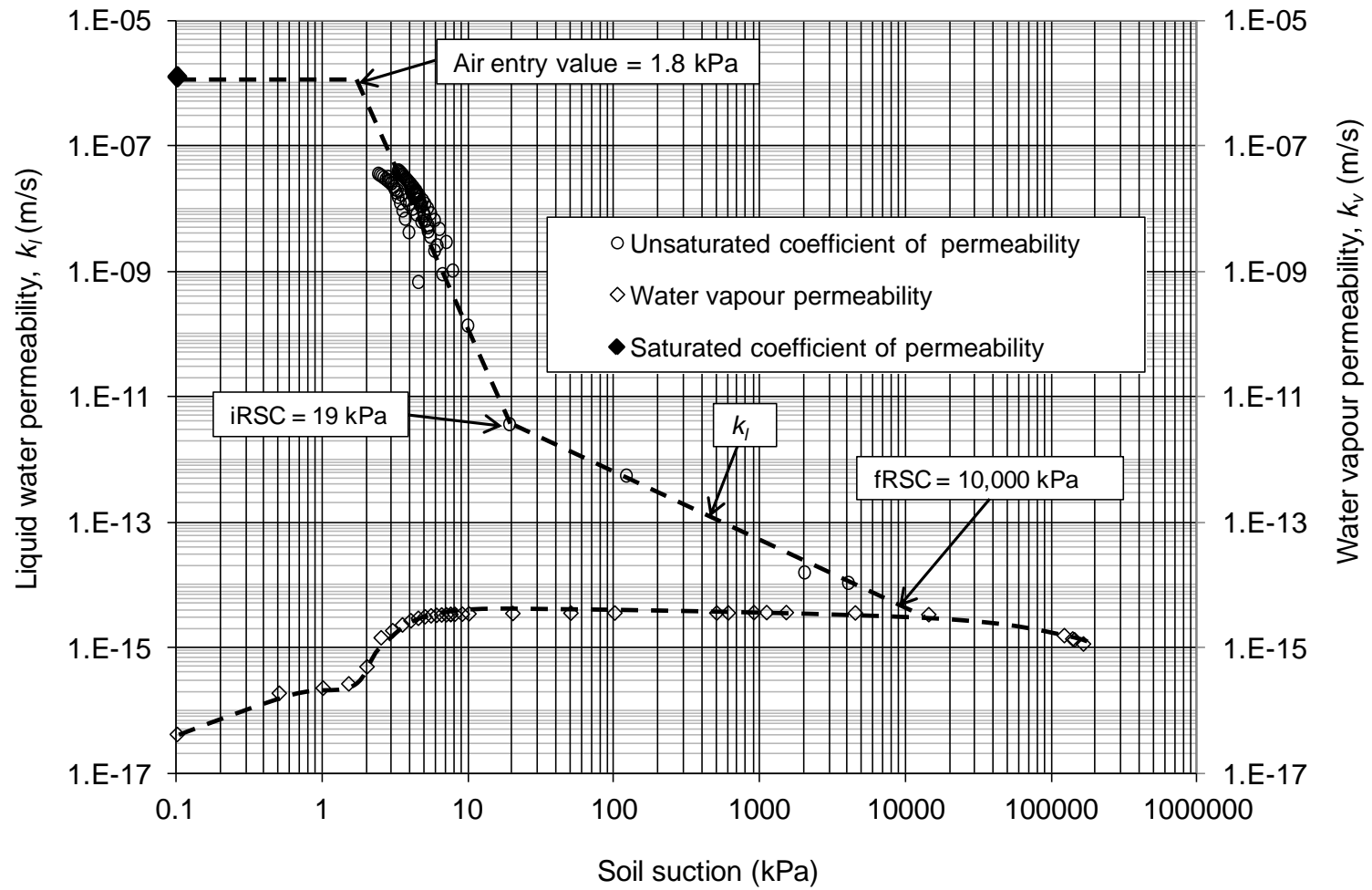
Figure 6.42 Experimental data for liquid-water permeability, and water-vapour permeability of Beaver Creek sand
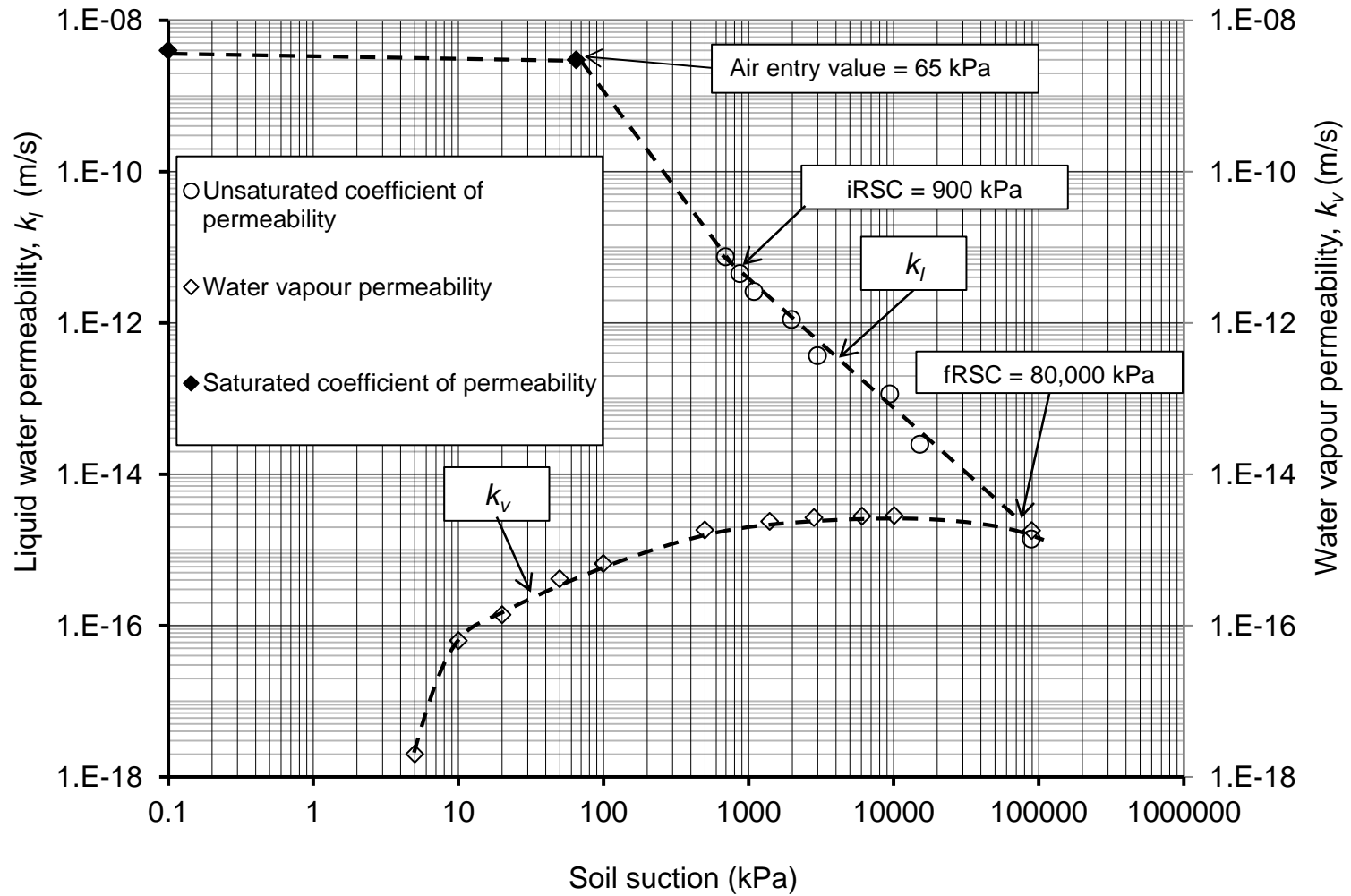
Figure 6.43 Experimental data for liquid-water permeability and water-vapour permeability of Botkin silt

## 6.12  EVALUATION OF METHODS FOR PREDICTING THE UNSATURATED COEFFICIENT OF PERMEABILITY

Methods for predicting the unsaturated coefficient of permeability were presented in the literature review chapter (i.e., Chapter 2, section 2.5). Three commonly used methods, as well as the new method proposed in Chapter 3, section 3.7.3 are used to predict the coefficient of permeability function for the soils under study. To assess the reliability of these methods, the predicted data for the Beaver Creek sand and Botkin silt soils are compared with the experimental data which were presented in sections 6.10 and 6.11.

Table 6.5 shows the methods used for prediction of the coefficient of permeability function in this section.

Table 6.6 Selected methods for predicting the unsaturated coefficient of permeability function

| Method | Reference |
|---|---|
| B-C Method | Brooks and Corey (1964) |
| Campbell Method | Campbell (1974) |
| Fredlund et al. Method | Fredlund et al. (1994) |
| Proposed Method | Chapter 3 |

### 6.12.1  Prediction of the Unsaturated Coefficient of Permeability Using the Brooks and Corey (1964) Method

The Brooks and Corey (1964) method is one of the commonly used methods for prediction of the unsaturated coefficient of permeability function. The Brooks and Corey (1964) relative permeability equation is as follows:

$$k_r = \left(\frac{\psi_b}{\psi_c}\right)^{\eta} \qquad\qquad [6.3]$$

where

$k_r$ = relative permeability, defined as the ratio of the coefficient of permeability at any soil suction value to the saturated coefficient of permeability,

$\psi_b$ = bubbling pressure (air-entry value), kPa,

$\psi_c$ = a soil-suction value greater than air-entry value, kPa,

$\eta$ = $2 + 3\lambda$, and

$\lambda$ = pore-size distribution index.

Two main parameters are required when using the Brooks and Corey (1964) predictive method: pore-size distribution index and air-entry value. These two parameters can be determined using SWCC data. The pore-size distribution index and air-entry values for Beaver Creek sand and Botkin silt soils were determined in section 6.6.1 (see Figures 6.12 and 6.13).

Figures 6.44 and 6.45 show the predicted unsaturated coefficient of permeability functions using the Brooks and Corey (1964) method for Beaver Creek sand and Botkin silt soils, respectively. Experimental data obtained from evaporation tests are also shown for comparison.

The Brooks and Corey (1964) method appears to predict the coefficient of permeability function for Beaver Creek sand for the suction range between 3 kPa and the initial residual-state condition at 5 kPa (see Figure 6.44). There are discrepancies between the experimental and predictive data for suction values beyond 5 kPa. The discrepancies become larger for suction values beyond 20 kPa.

As stated in the literature review (Chapter 2, section 2.3.1), the slow flow of liquid water at low degrees of saturation should not be included in the Brooks and Corey (1964) model. It was suggested that the analysis should be limited to residual saturation. The residual saturation and corresponding soil-suction values for Beaver Creek sand based on the Brooks and Corey (1964) method were determined to be 4% and 1,000 kPa (see Table 6.4). The discrepancies observed between the experimental and predicted data for Beaver Creek sand (Figure 6.44) suggest that application of the Brooks and Corey (1964) method must be limited to a maximum soil suction value of about 20 kPa for this soil.

The residual saturation and corresponding soil-suction values for Botkin silt  based on the Brooks and Corey (1964) method were determined to be 3% and 400,000 kPa

(see Table 6.4). The discrepancies observed between experimental and predicted data for Botkin silt (Figure 6.45) suggest that application of the Brooks and Corey (1964) method must be limited to a maximum soil-suction value of about 700 kPa for this soil.

The experimental observations in this research suggest some quantitative values beyond which the Brooks and Corey (1964) method may not predict accurate coefficient of permeability values. The initial residual-state condition (iRSC) appears to be the limit for the Brooks and Corey (1964) method.
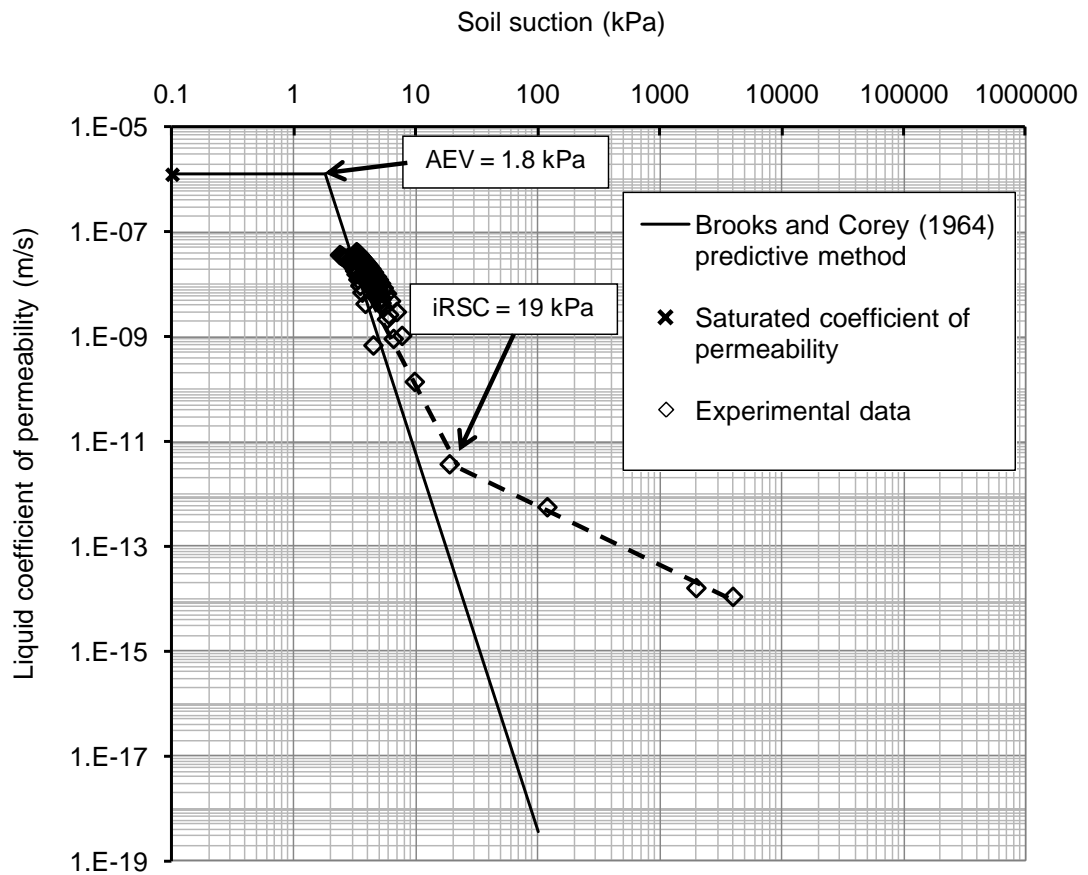
Figure 6.44 Experimental data and predicted unsaturated coefficient of permeability function using the Brooks and Corey (1964) method for Beaver Creek sand
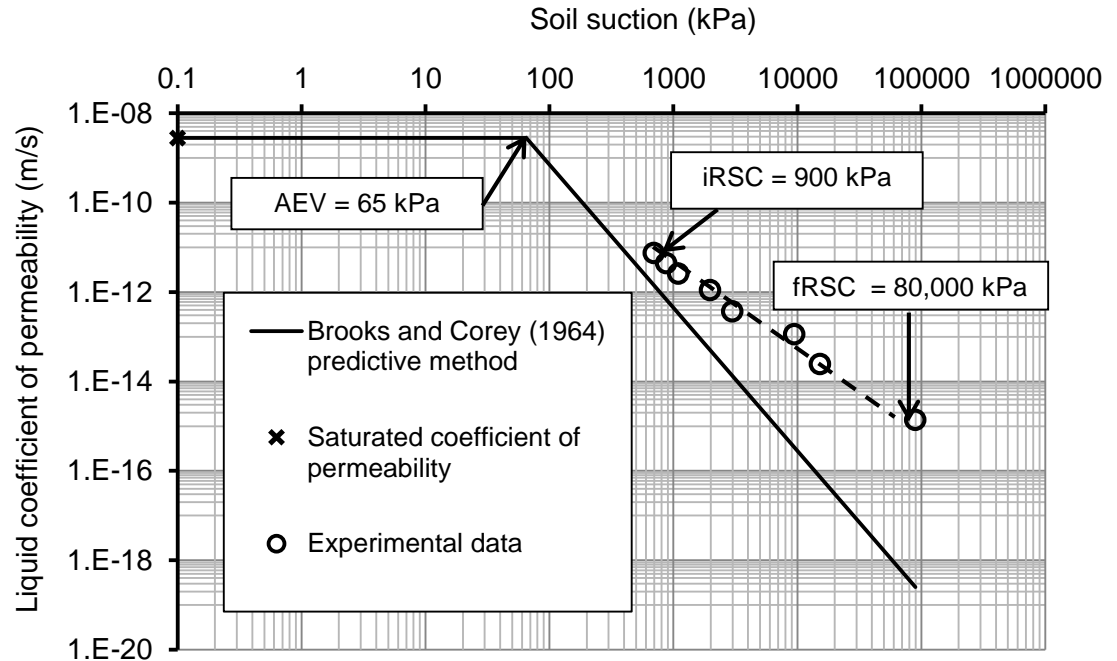
Figure 6.45 Experimental and the predicted unsaturated coefficient of permeability
function using the Brooks and Corey (1964) method for Botkin silt

### 6.12.2 Prediction of the Unsaturated Coefficient of Permeability Using the Campbell (1974) Method

The Campbell (1974) method is one of the commonly used methods for prediction of the unsaturated coefficient of permeability function. The Campbell (1974) relative permeability equation is presented as follows:

$$k_r = \left(\frac{\psi_e}{\psi}\right)^{2+2/b} \qquad\qquad [6.4]$$

where

$k_r$ = relative permeability which is defined as ratio of the coefficient of permeability at any soil-suction value to the saturated coefficient of permeability,

$\psi_e$ = air-entry value, kPa,

$\psi$ = a soil-suction value greater than air-entry value, kPa, and

$-\,b$ = slope of the soil suction versus water content plotted on a log-log scale.

256

The b values of 0.578 and 2.421 are used for Beaver Creek sand and Botkin Silt soils. Figures 6.46 and 6.47 show the predicted unsaturated coefficient of permeability using the Campbell (1974) method for Beaver Creek sand and Botkin silt soils. Experimental data obtained from evaporation tests are also shown for comparison.

The Campbell (1974) method appears to predict the coefficient of permeability function with high accuracy for Beaver Creek sand to a suction value of about 20 kPa (see Figure 6.46). However, there are discrepancies between the experimental and predictive data for suction values beyond 20 kPa. The discrepancies become larger as the suction increases. These discrepancies between the experimental and predicted data suggest that application of the Campbell (1974) method must be limited to a maximum soil-suction value.
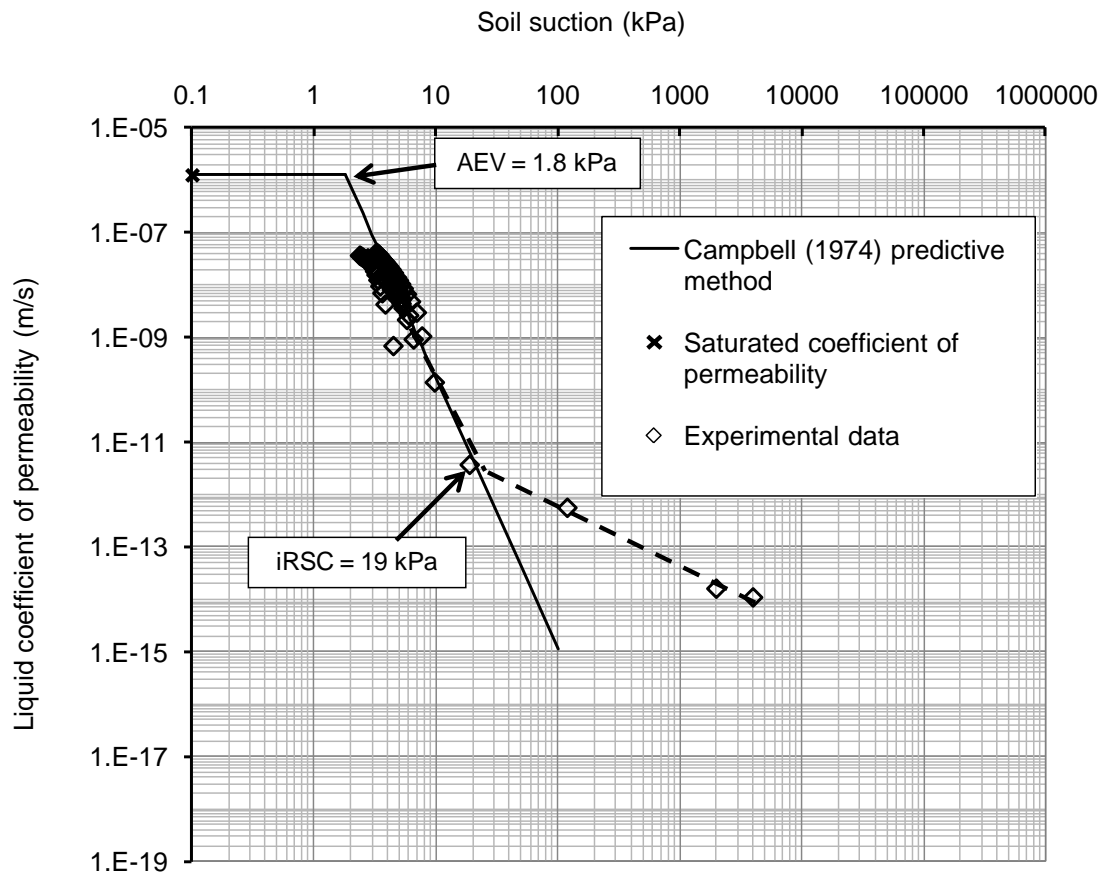


Figure 6.46 Experimental and predicted unsaturated coefficient of permeability functions using the Campbell (1974) method for Beaver Creek sand
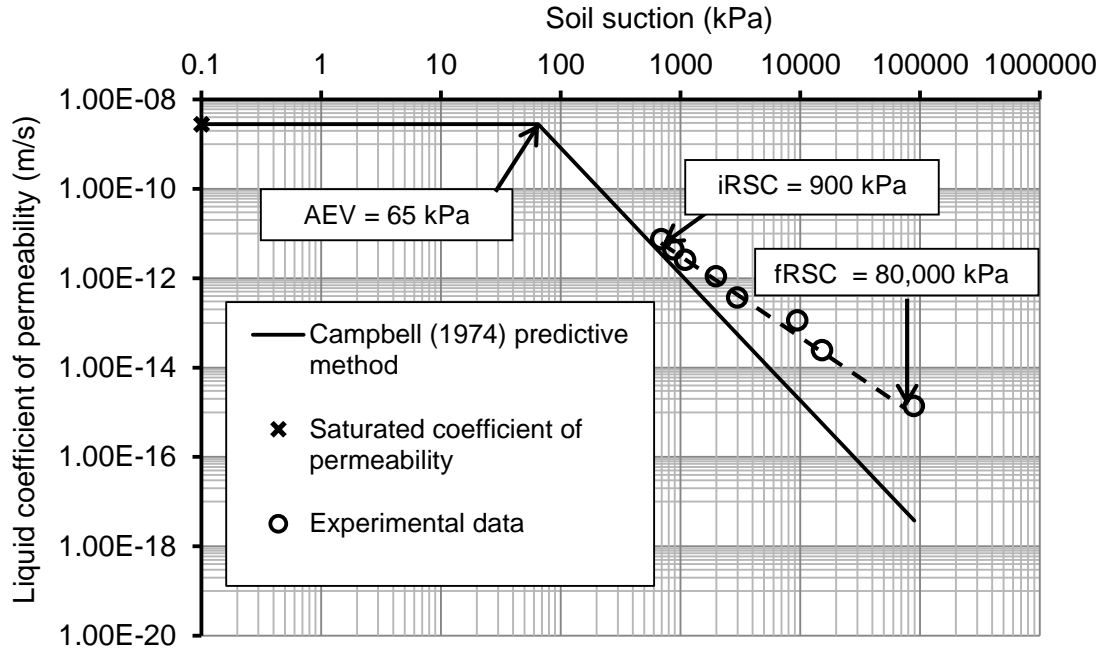
Figure 6.47 Experimental and predicted unsaturated coefficient of permeability
functions using the Campbell (1974) method for Botkin silt

Comparison of the observed and predicted unsaturated coefficient of permeability
for Botkin silt (Figure 6.47) indicates discrepancies between the experimental and
predicted data between the initial and final residual-state conditions.

As with the Brooks and Corey (1964) method, a suction value of about iRSC
appears to be the application limit for the Campbell (1964) method.

### 6.12.3 Prediction of the Unsaturated Coefficient of Permeability Function using the Fredlund et al. (1994) Method

Fredlund et al. (1994) used the Childs and Collis-George (1950) permeability equation
and the Fredlund and Xing (1994) SWCC equation to predict the permeability function
(see Chapter 2, Table 2.9). To predict the coefficient of permeability function using the
Fredlund et al. (1994) method for the Beaver Creek sand and Botkin silt, the
experimental data for the SWCC and saturated coefficient of permeability were analyzed
using Excel Spreadsheet and MathCad14.0 software.

The SWCC experimental data and the Fredlund and Xing (1994) fitting curves are
shown in Figures 6.48 and 6.49 for Beaver Creek sand and Botkin silt soils.

Figure 6.48 Soil-water characteristic curve using the Fredlund and Xing (1994) equation
for Beaver Creek sand



Figure 6.49 Soil-water characteristic curve using the Fredlund and Xing (1994) equation
for Botkin silt

The Fredlund and Xing (1994) SWCC fitting curve shows a good fit for both Beaver Creek sand and Botkin silt soils. The fitting parameters for the Fredlund and Xing (1994) SWCC equations for Beaver Creek sand and Botkin silt soils are summarized in Table 6.7.

Figures 6.50 and 6.51 show the predicted coefficient of permeability functions for the Beaver Creek sand and Botkin silt soils. The experimental data are also shown for comparison.

Table 6.7 Fitting parameters of the Fredlund and Xing (1994) SWCC equations for Beaver Creek sand and Botkin silt

| Soil ID | $a_f$ | $m_f$ | $n_f$ | $w_s$ |
|---|---|---|---|---|
| Beaver Creek sand | 2.369 | 1.208 | 5.111 | 0.2482 |
| Botkin Silt | 105.1 | 0.774 | 1.263 | 0.2446 |

Unlike the Brooks and Corey (1964) method, and the Campbell (1974) method, the Fredlund et al. (1994) method shows a change in the slope of the coefficient of permeability function beyond the initial residual-state condition (iRSC) for both Beaver Creek sand and Botkin silt soils.

### 6.12.4  Prediction of the Unsaturated Coefficient of Permeability Functions Using the Proposed Method

The experimental data for the unsaturated coefficient of permeability function which were presented in sections 6.10 and 6.11 suggest a multiple-region function for the coefficient of permeability. The two-region methods proposed by Brooks and Corey (1964) and by Campbell (1974) did not generate reliable estimations beyond the initial residual-state condition for the soils under study. The method proposed by Fredlund et al (1994) generated a nonlinear coefficient of permeability function on a log-log scale, which indicates change in slope of the function. This change in slope of the unsaturated coefficient of permeability function was also observed by Ebrahimi-Birang et al. (2004) and Poulsen et al. (2002).
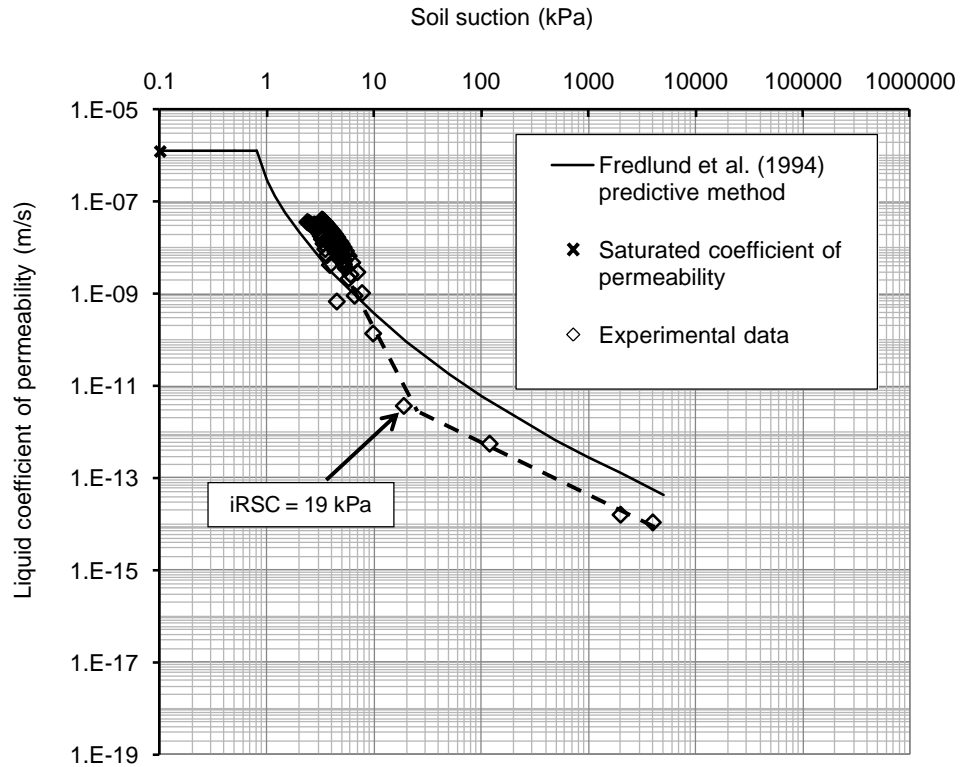
Figure 6.50 Experimental data and the predicted unsaturated coefficient of permeability functions using the Fredlund et al. (1994) method for Beaver Creek sand
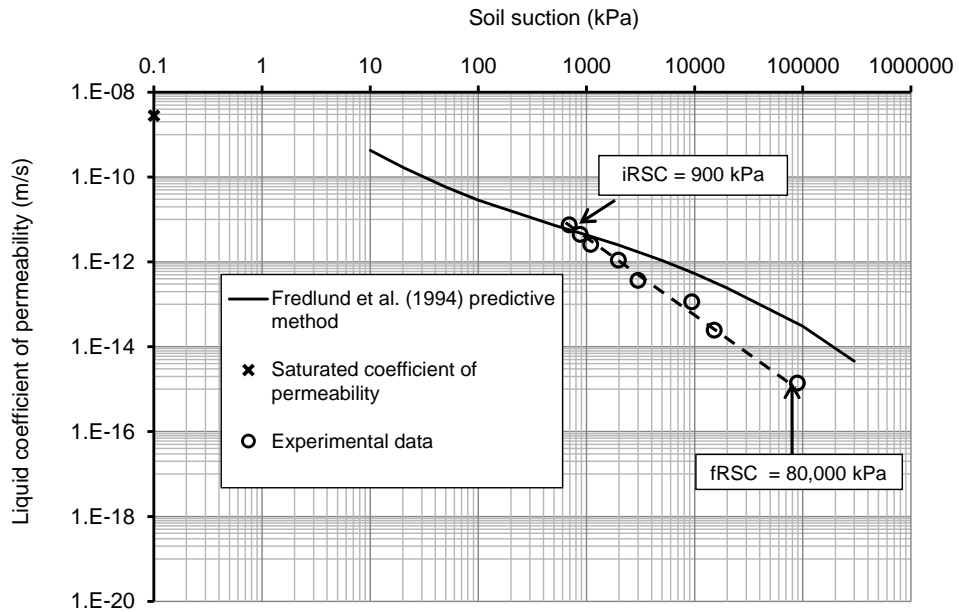


Figure 6.51 Experimental data and the predicted unsaturated coefficient of permeability functions using the Fredlund et al. (1994) method for Botkin silt

261

A four-region function for the unsaturated coefficient of permeability, proposed in Chapter 3, was used to predict the coefficient of permeability function for the Beaver Creek sand and Botkin silt soils. In the proposed method, the coefficient of permeability from saturation to air-entry value is considered as the saturated coefficient of permeability ($k = k_s$). The Campbell (1974) method is used to determine the coefficient of permeability function passed air-entry value to the initial residual state condition. The suction value at the initial residual state condition was estimated using the method described in Chapter 3, section 3.5.1. The corresponding coefficient of permeability at the initial residual state condition can then be determined using the Campbell (1974) equation (see Chapter 3, Eq. 3.25). An alternative predictive method such as Brooks and Corey (1974) or Fredlund et al. (1994) may be used to determine the coefficient of permeability function in this section.

Suction at the final residual state condition was determined using the method described in Chapter 3, section 3.5.2. The coefficient of permeability at this point was assumed to be equal to the lower limit of the liquid coefficient of permeability function, approximately $3 \times 10^{-15}$ m/s, regardless of the type of soil (see Chapter 3, section 3.7.2).

The coefficient of permeability function within the residual-state condition was drawn using Eq. 3.26 presented in Chapter 3.

The coefficient of permeability beyond the final residual state condition was assumed to follow the vapour-phase coefficient of permeability.

Figures 6.52 and 6.53 show the experimental coefficient of permeability data along with the predicted unsaturated coefficient of permeability functions using the proposed four-region method for Beaver Creek sand and Botkin silt soils. Data obtained from the Brooks and Corey (1964), Campbell (1974) and Fredlund et al. (1994) methods are also included for comparison.

The results shown in Figures 6.52 and 6.53 suggest that the proposed method in this thesis was able to predict the coefficient of permeability function within the residual-state condition for both Beaver Creek sand and Botkin silt soils more accurately than two- region predictive methods such as the Brooks and Corey (1964) method and the Campbell (1974) method.
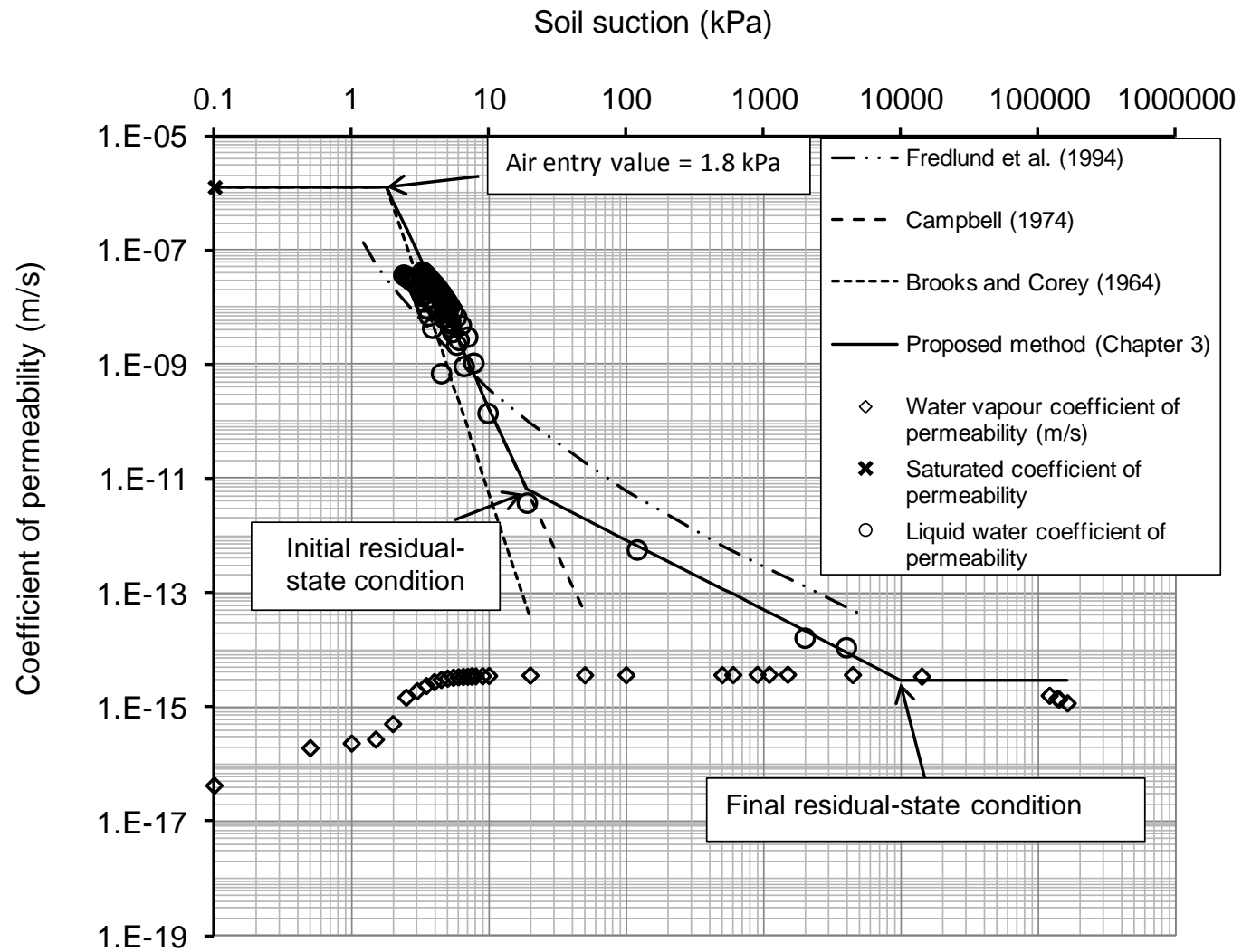
Figure 6.52 Experimental data for the unsaturated coefficient of permeability along with the predicted unsaturated coefficient of permeability functions, using the proposed method and the selected predictive methods for Beaver Creek sand
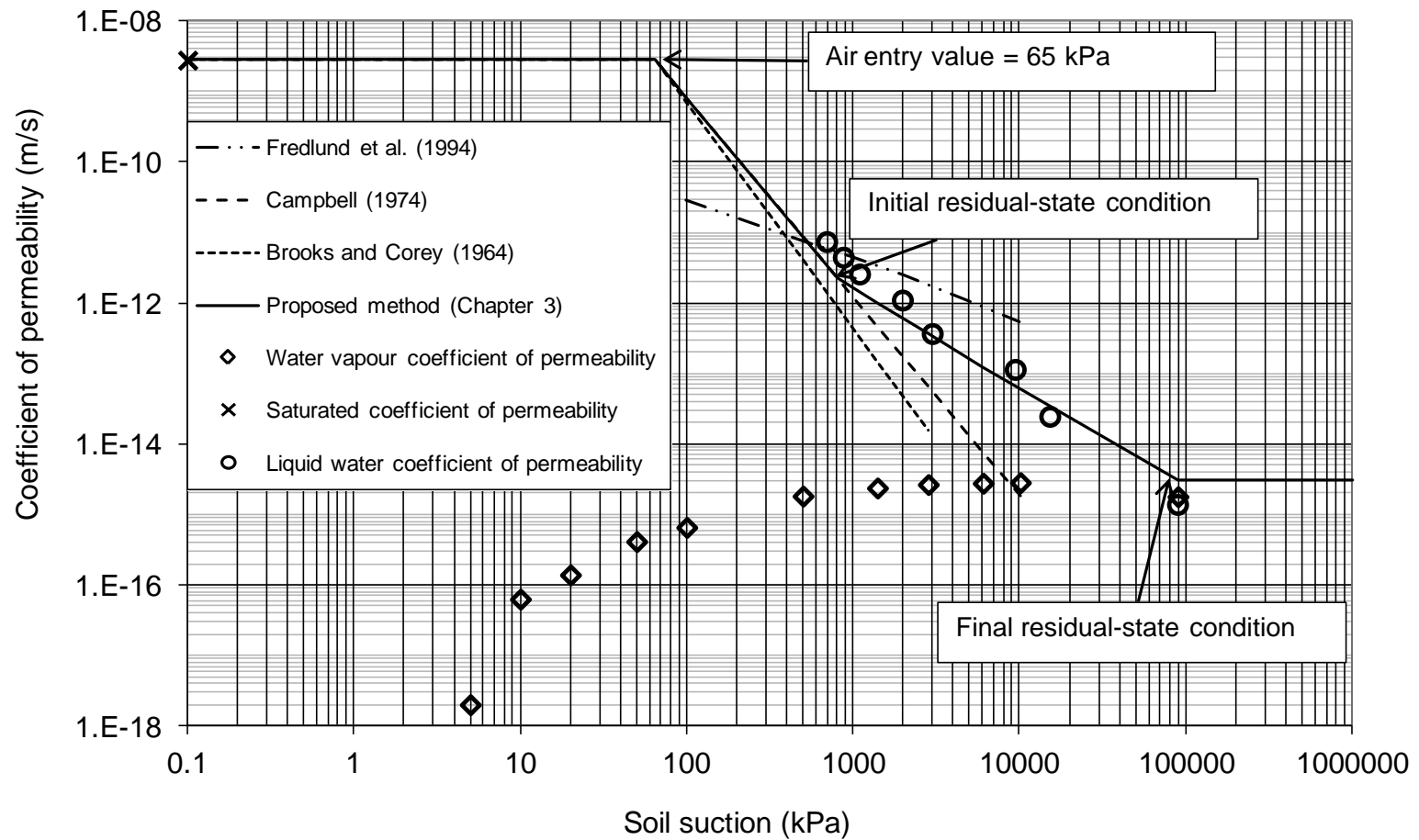
Figure 6.53 Experimental data for the unsaturated coefficient of permeability along with the predicted unsaturated coefficient of permeability functions, using the proposed method and the selected predictive methods for Botkin silt

CHAPTER 7

**SUMMARY AND CONCLUSIONS**

## 7.1    INTRODUCTION

This chapter is consists of three main sections. Section 7.2 presents a concise overview of the study objectives and the methodology used to achieve the objectives. Section 7.3 presents the conclusions reached from entire study. Section 7.4 presents some recommendations for future research.

## 7.2    BRIEF OVERVIEW OF THE RESEARCH OBJECTIVES AND METHODOLOGY

The general objective of the thesis was to study the hydraulic flow properties of sand and clayey silt soils around the residual-state condition.

The specific objectives of the thesis were as follows:

1) to review research in associated disciplines and determine an appropriate definition and description of the residual-state condition (RSC) for geotechnical engineering practice,

2) to measure the unsaturated coefficient of permeability in the moderate to low water-content ranges,

3) to evaluate relationship between the residual-state condition and the transition zone of water-content profile, and

4) to propose a methodology, or modify an existing methodology, in order to predict the unsaturated coefficient of permeability around the residual-state condition.

To meet objective 1, the topics related to the residual-state condition in associated disciplines were summarized in the literature review chapter. A definition for the

residual-state condition was proposed in Chapter 3, along with a procedure to determine the residual-sate condition using the soil-water characteristic curve (SWCC). This curve was measured for sand and clayey silt soils. The apparatuses, sample preparation, tests procedures, and results were presented in Chapters 4 and 5. Chapter 6 reports on determination of the residual-state condition for Beaver Creek sand and Botkin silt soils, by means of analysis of the SWCC results and the method proposed in Chapter 3. As a comparison, the residual-state condition was also determined by means of commonly used methods.

The chilled-mirror Water PotentiaMeter (WP4-T), a relatively new device, was used to establish the SWCC in the high-suction ranges (i.e., > 1500 kPa) for the soils under study. To assess the reliability of soil-suction results produced using the WP4-T device, the results obtained from the device were compared with the results produced by a conventionally used method in which small soil samples were placed over saturated salt solutions of known osmotic suctions. A conventional method referred to as an air-tight chamber (ATC) was introduced in Chapter 4. The WP4-T test results were compared with those obtained through ATC. The tests results were presented in Chapter 5, and were analyzed and discussed in Chapter 6.

Objective 2 was met through a series of steady-state evaporation processes, conducted in an environmentally controlled room. Details of evaporation columns, sample preparation, and steady-state evaporation process set-up were described in Chapter 4. The data obtained from the evaporation processes, presented in Chapter 5, were analyzed in Chapter 6 in order to determine the liquid-phase unsaturated coefficient of permeability function for the Beaver Creek sand and Botkin silt specimens around the residual-state condition. The data analysis was done using the liquid-water and water-vapour flux equations, developed in Chapter 3.

In analysis of the evaporation process data, the SWCC was assumed to be non-hysteretic at high-suction ranges. The hysteresis of the soil-water characteristic curve in high soil-suction ranges was investigated for two types of fine-grained soils: clay and clayey silt. The drying and wetting soil-suction values were those measured using the chilled-mirror Water PotentiaMeter (WP4-T) and the air-tight chamber (ATC) mentioned above.

Objective 3 was met through determination of the upper and lower limits of the transition zone for the soils under study. These limits were estimated by analyzing the water content and/or suction profiles at the end of the evaporation tests. The estimated values of the initial and the final residual-state conditions obtained by the method proposed in Chapter 3 were compared with the lower and upper limits of the transition zone of the water content/suction profiles for the Beaver Creek sand and Botkin silt soils.

To meet objective 4, a method was developed for the prediction of the coefficient of permeability based on the SWCC, the definition of the residual-state condition and the theory of the vapour-phase flow. The method described in Chapter 3 was used in Chapter 6 to predict the unsaturated coefficient of permeability function for the Beaver Creek sand and Botkin silt specimens. The measured SWCC and the saturated coefficient of permeability values for the sand and silt specimens were used in the prediction. The experimental coefficient of permeability functions obtained from analyzing the evaporation test data were compared with the results obtained from the proposed method, and with the results obtained from three selected conventionally used methods, described in Chapters 2 and 3.

## 7.3   CONCLUSIONS

The following conclusions have been reached:

1   The definition of the residual-state condition as a designated zone (between the initial and final residual-state conditions) on the SWCC improved the accuracy of prediction of the unsaturated coefficient of permeability function for the Beaver Creek sand and Botkin silt soils.

2   The steady-state evaporation method used in this study proved to be a relatively rapid method of measuring the unsaturated coefficient of permeability function. The function in the low water-content range was measurable by the steady-state evaporation method.

3   The main limitation of the steady-state evaporation method for the measurement of the unsaturated coefficient of permeability function was the need for enhanced control of the test environment.

4   Selection of an optimum combination of sample size, inflow rate, and outflow rate for obtaining the unsaturated coefficient of permeability function in the desired suction range was found to be essential in the steady-state evaporation process.

5   From data analysis of the SWCC and the evaporation tests results on Beaver Creek sand and Botkin silt specimens, it is not possible to withdraw a firm conclusion on whether or not the lower and upper limits of the transition zone of the water content/soil suction profile at the end of the evaporation tests (after the steady-state flow condition is reached) can represent the initial residual-state condition (iRSC) and the final residual-state condition (fRSC).

6   The predicted unsaturated coefficient of permeability function using the conventional predictive methods (Brooks and Corey, 1964; Campbell, 1974) agreed closely with the experimental data for suction values from zero to the initial-residual state condition for the Beaver Creek sand. For Botkin silt soil, the experimental data were not available between air-entry value and the initial residual-state condition.

7   The commonly used predictive methods for the unsaturated coefficient of permeability function were able to predict the coefficient of permeability from saturation to the initial residual state condition for the Beaver Creek sand and Botkin silt soils.

8   The initial residual-state condition appear to be the application limit for predicting the coefficient of permeability function using the commonly used predictive methods such as Brooks and Corey (1964) and Campbell (1974) methods.

9   The new method proposed for the prediction of the permeability function made it possible to estimate the coefficient of permeability for the higher suction range. The proposed method predicted the coefficient of permeability function within and beyond residual-state condition for both Beaver Creek sand and Botkin silt soils.

10 An unsaturated coefficient of permeability equal to $3 \times 10^{-15}$ m/s was suggested as a minimum limit value for the liquid-water coefficient of permeability based on the theory of vapour flow.

11 The liquid and vapour coefficient of permeability was determined through analysis of the results obtained from the steady-state evaporation processes for the Beaver Creek sand and Botkin silt soils. The general form of the unsaturated coefficient of permeability function was matched with the form of the conductivity function that Buckingham (1907) had proposed over a century ago.

12 Good agreement was observed between the suction values obtained from the WP4-T measurements and those determined from the theory based on relative humidity reported in the literature for saturated salt solutions.

## 7.4 RECOMMENDATIONS FOR FUTURE RESEARCH

The following are recommendations for future research:

1 Further study should be done on the hysteresis of the soils in the high suction range using the WP4-T device.

2 The behaviour of the unsaturated coefficient of permeability function was studied around and beyond the residual-state condition. Investigation should be conducted on the other behavior of the unsaturated soil such as the shear strength and the volume change behaviour around and beyond the residual-state condition.

3 Using the theory proposed in this study, a study based on the numerical model analysis should be developed for choosing the optimum potential evaporation, sample height, and inflow rate for the steady-state evaporation process.

4 The proposed predictive method in this research should be evaluated through the application of the proposed predictive method in the seepage related problems for geotechnical engineering practice.

# LIST OF REFERENCES

Agus, S.S. and Schanz, T. (2005). "Comparison of four methods for measuring total suction." Vadose Zone Journal, 4(4): 1087-1095.

Ahuja, L.R., Naney, J.W. and Williams R.D. (1985). "Estimating soil water characteristics from simpler properties or limited data." Soil Science Society of America Journal, 49: 1100-1105.

Aoda, T. (2000). "Physical definition of residual water content in usaturated soils." In Unsaturated Soils for Asia, H. Rahardjo, D.G. Toll, and E.C. Leong (Eds.), Balkema, Rotterdam.

Arya, L.M. and Dierolf, T.S. (1992). "Predicting soil moisture characteristics from particle-size distributions: an improved method to calculate pore radii from particle radii." In: Indirect Methods for Estimating the Hydraulic Properties of Unsaturated Soils, van Genuchten, M. Th., Leij, F. J., and Lund, L. J. (Eds.), Proceedings of International Workshop, Riverside, CA, 11- 13 Oct., 1989. University of California, Riverside, pp. 115-124.

Arya, L.M. and Paris, J.F. (1981). "A physicoempirical model to predict the soil moisture characteristic from particle size distribution and bulk density data". Soil Science Society of America Journal, 45: 1023-1030.

Arya, L.M., Farrell, D.A. and Blake, G.R. (1975). "A field study of water depletion patterns in presence of growing soybean roots. I. determination of hydraulic properties of the soil". Soil Science Society of American Proceedings. 39: 424-430.

ASTM D 422. (1994). "Standard test method for particle size analysis of soils." Annual Book of ASTM Standards, 4.08: 10-16.

ASTM D 4318-93. (1994). "Standard test method for liquid limit, plastic limit, and plasticity index of soils." Annual Book of ASTM Standards, 4.08: 551-561.

ASTM D 6836-02 (2003). "Test methods for determination of the soil water characteristic curve for desorption using a hanging column, pressure extractor, chilled mirror hygrometer and/or centrifuge." Annual Book of ASTM Standards, 04.08.

ASTM D 854. (1994). "Standard test methods for specific gravity of soils." Annual Book of ASTM Standards, 04.08: 80-83.

ASTM E104-85. (1996). "Standard practice for maintaining constant relative humidity by means of aqueous solutions." Annual Book of ASTM Standards.

ASTM E 104-02. (2003). "Standard practice for maintaining constant relative humidity by means of aqueous solutions." Annual Book of ASTM Standards, 11.03: 1133-1137.

Aubertin, M., Mbonimpa, B., Bussiere, B. and Chapuis, R.P. (2003). "A model to predict the water retention curve from basic geotechnical properties." Canadian Geotechnical Journal, 40: 1104-1122.

Averjanov, S.F. (1950). "About permeability of subsurface soils in case of incomplete saturation." Engineering Collect,7.

Bachmann, J., Horton, R. and van der Ploeg, R.R. (2001). "Isothermal and non-isothermal evaporation from four sandy soils of different water repellency." Soil Sci. Soc. Am. J, 65: 1599-1607.

Barbour, S.L. (1993). "Evaluation of the saturated-unsaturated groundwater conditions of a thickened tailings deposit" Canadian Geotechnical Journal, 30: 935-946.

Barbour, S.L. (1998). "Nineteenth Canadian Geotechnical Colloquium: the soil-water characteristics curve: a historical perspective." Canadian Geotechnical Journal, 35: 873-894.

Barbour, S.L. and Yanful, E.K. (1994). "A column study of static nonequilibrium fluid pressures in sand during prolonged pressure." Canadian Geotechnical Journal, 31: 299-303.

Bear, J. (1979). "Hydraulics of groundwater." Dover Publications, McGraw-Hill International Book Company, New York.

Benson, C.H. and Gribb, M.M. (1997). "Measuring unsaturated hydraulic conductivity in the laboratory and field." In: Unsaturated Soil Engineering Practice, Geotechnical Special Publication No. 68, ASCE.

Bethel, F.T. and Calhoun, J.D (1953). "Capillary desaturation in unconsolidated beads." Transactions American Institute of Mining Engineers, 198: 197-202.

Bloemen, G.W. (1980) "Calculation of hydraulic conductivities from texture and organic matter content." Zeitschrift fur Pflanzennernahrung und Bodenkunde, 143: 581-605.

271

Bouma, J. and van Lanen, J.A.J. (1987). "Transfer functions and threshold values: from soil characteristics to land qualities." Quantified Land Evaluation, Beek, K.J. (Ed.), International Institute of Aerospace Survey Earth Science ITC Publication 6: 106-110.

Brooks, R.H. and Corey, A.T. (1964). "Hydraulic properties of porous media." Hydrology paper No. 3., Colorado State University, Fort Collins, Colorado, U.S.A.

Brooks, R.H. and Corey, A.T. (1966). "Properties of porous media affecting fluid flows." Journal of the Irrigation and Drainage Divition, ASCE, 92(IR2): 61-88.

Bruch, P.G. (1993). "A laboratory study of evaporative fluxes in homogeneous and layered soils." M.Sc. Thesis, University of Saskatchewan, Saskatoon, Canada.

Brutsaert, W. (1967). "Some methods of calculating unsaturated permeability." Transactions, ASAE, 10: 400-404.

Buckingham, E. (1907). "Studies on the movements of soil moisture." United States Department of Agriculture, Bureau of Soils, Bulletin No. 38.

Burdine, N.T. (1953). "Relative permeability calculations from pore size distribution data." Transactions, American Institute of Mining and Metallurgical Engineers, 198: 71-78.

Campbell, G.S. and Shiozawa, S. (1992). "Prediction of hydraulic properties of soils using particle size distribution and bulk density data." In: Indirect Methods for Estimating the Hydraulic Properties of Unsaturated Soils, van Genuchten, M. Th., Leij, F. J., and Lund, L. J. (Eds.), Proceedings of International Workshop, Riverside, CA, 11- 13 Oct., 1989. University of California, Riverside, pp. 317-328.

Campbell, G.S. (1985). "Soil physics with basic." Elsevier Science B.V., the Netherlands.

Campbell, G.S. (1974). "A simple method for determining unsaturated conductivity from moisture retention data." Soil Science, 117: 311-314.

Campbell, G.S. and Gee, G.W. (1986). "Water potential: miscellaneous methods." Methods of Soil Analysis. Part 1. 2nd edition, A. Klute (ed.), ASA and SSSA, Madison, WI.

Campbell, G.S., Smith, D.M. and Teare, B.L. (2007)."Application of a dew point method to obtain the soil water characteristic." Proceedings of the Second International Conference on Mechanics of Unsaturated Soils, Experimental Unsaturated Soil Mechanics, Bauhaus-Universität, Weimar, Germany. March 7-9. pp.71-77.

Cardoso, R., Romero, E., Lima, A. and Ferrari, A. (2007)."A comparative study of soil suction measurement using two different high-range psychrometers." Proceedings of the Second International Conference on Mechanics of Unsaturated Soils, Experimental Unsaturated Soil Mechanics, Bauhaus-Universität, Weimar, Germany. March 7-9. pp.79-93.

Carey, S.K., Barbour, S.L. and Hendry, M.J. (2005). "Evaporation from a waste rock surface, Key Lake, Saskatchewan." Canadian Geotechnical Journal, 42: 1189-1199.

Childs, E.C., and Collis-George, N. (1950). "The permeability of porous materials." Proceedings of the Royal Society of London. Series A, Mathematical and Physical Sciences, 201(1066): 392-405.

Childs, E.C. (1969). "An introduction to the physical basis of soil water phenomena." John Wiley and Sons Ltd., pp. 493.

Choo, L.P., and Yanful, E.K. (2000). "Water flow through covers soils using modeling and experimental methods." Journal of geotechnical and geoenvironmental engineering, 126(4): 324-334.

Cosby, B.J., Hornberger, G.M., Clapp, R.B. and Ginn, T.R. (1984). "A statistical exploration of the relationship of soil and characteristics to the physical properties of soil." Water Resources Research, 20: 682-690.

Couture, F., Jomaa, W. and Puiggali, J.-R. (1996). "Relative permeability relations: a key factor for a drying model." Transport in Porous Media, 23: 303-335.

Dadgar, S. (2005). "Moisture Adsorption and Spoilage Characteristics of Pea Under Adverse Storage Conditions," M.Eng. Thesis, Department of Agricultural and Bioresource Engineering, University of Saskatchewan, Saskatoon, Canada.

Dakshanamurthy, V. and Fredlund, D.G. (1981). "A mathematical model for predicting moisture flow in an unsaturated soil under hydraulics and temperature gradients." Water Resources Research, 17: 714-722.

Dane, J.H. and Topp, G.C. (2002). "Methods of soil analysis." Part 4, Physical Methods, SSSA, Book Series 5.

Darcy. H. (1856). "Les fontaines publique de la ville de dijon." Paris: Dalmont.

Dobchuk, B.S., Barbour, S.L. and Zhou, J. (2004). "Prediction of water vapor movement through waste rock." Journal of Geotechnical and Geoenvironmental Engineering, 130(3): 293-302.

Ebrahimi-Birang, N., Fredlund, D.G. and Samarasekera, L. (2007). "Hysteresis of the soil-water characteristic curve in the high suction range " Proceedings of the 60th Canadian Geotechnical Conference, Ottawa, Oct. 21-24, pp. 1061-1068.

Ebrahimi-Birang, N., Gitirana Jr., G.F.N., Fredlund, D.G., Fredlund, M.D. and Samarasekera, L. (2004)."A lower limit for the water permeability coefficient." Proceedings of the 57th Canadian Geotechnical Conference, Quebec City, Oct. 24-27, pp.12-19

Farrel, D.A. and Larson, W.E. (1972). "Modeling the pore structure of porous media." Water Resources Research, 8(3): 699-706.

Fatt, I. and Dykstra, H. (1951). "Relative Permeability Studies." Transactions, American Institute of Mining and Metallurgical Engineers, 192: 249-255.

Fayer, M.J. and Simmons, C.S. (1995). "Modified soil water retention functions for all matric suctions." Water Resources Research, 31(5): 1233-1238.

Feasby, G., Tremblay, G. and Blanchette, M. (1991). "The mine environmental neutral drainage (MEND) program." In Proceedings of the Second International Conference on the Abatement of Acidic Drainage, Montreal, Sept. 16-18, MEND Program, CANMET, Orttawa, Ont. 1: 1-26.

Feng, M., and Fredlund, D.G. (1999). "Hysteretic influence associated with thermal conductivity sensor measurements". Proceedings of the 52nd Canadian Geotechnical Conference, Regina, Saskatchewan, October 24-27, pp. 651-657.

Fick, A. (1855). "Ueber diffusion." Ann. der Phys., (Leipzig), 94: 59-86.

Fredlund, D.G. (2000). "The 1999 R.M. Hardy Lecture: The implementation of unsaturated soil mechanics into geotechnical engineering, - R.M. Hardy Address". Canadian Geotechnical Journal, 37(5): 963-986.

Fredlund, D.G. (2006). "The 2005 Terzaghi Lecture: Unsaturated soil mechanics in engineering practice". Presented at Geo-Institute, Austin, Texas, Journal of Geotechnical and Geoenvironmental Engineering, ASCE, 132(3): 286-321.

Fredlund, D.G. and Rahardjo, H. (1993). "Soil mechanics for unsaturated soils." John Willey & Sons, New York.

Fredlund, D.G. and Morgenstern, N.R. (1977). "Stress state variables for unsaturated soils". Journal of Geotechnical Engineering Division, ASCE, 103(GT5): 447-466.

Fredlund, D.G. and Xing, A. (1994). "Equations for the soil-water characteristic curve." Canadian Geotechnical Journal, 31: 521-532.

Fredlund, D.G., Xing, A. and Huang, S. (1994). "Predicting the permeability function for unsaturated soils using the soil-water characteristic curve." Canadian Geotechnical Journal, 31: 533-546.

Fredlund, D.G., Xing, A., Fredlund, M.D. and Barbour, S.L. (1996). "The relationship of the unsaturated soil shear strength to the soil-water characteristic curve". Canadian Geotechnical Journal, 33(3): 440-448.

Fredlund, D.G. (1964). "Comparison of soil suction and one-dimensional consolidation characteristics of a highly plastic clay." M.Sc. Thesis, University of Alberta, Edmonton, Alberta, Canada.

Fredlund, M.D., Wilson, G.W. and Fredlund, D. G. (2002). "Use of grain-size distribution for the estimation of the soil-water characteristic curve". Canadian Geotechnical Journal, 39(5): 1103-1117.

Fritton, D.D., Kirkham, D. and Shaw, R.H. (1967). "Soil-water and chloride redistribution under various evaporation potentials." Soil Science Society of America Proceedings, 31: 599-603.

Fujimaki, H., and Inoue, M. (2003). "A flux-controlled steady-state evaporation method for determining unsaturated hydraulic conductivity at low matric pressure head values." Soil Science, 168(6): 385-395.

Gardner, H.R. and Hanks, R.J. (1966). "Effect of sample size and environmental conditions on evaporation of water from soil." Agricultural Research Service, U.S. Department of Agriculture, pp. 14.

Gardner, W.R. (1958). "Some steady state solutions of the unsaturated moisture flow equation with application to evaporation from a water table." Soil Science, 85: 228-232.

Gates, J.I. and Lietz, W.T. (1950). "Relative permeabilities of California cores by the capillary-pressure method." Drilling and Production Practice, American Petroleum Institute, Q: 285-298.

Gee, G.W., Campbell, M.D., Campbell, G.S. and Campbell, J.H. (1992). "Rapid measurement of low soil water potentials using a water activity meter." Soil Science Society of America Journal, 56: 1068-1070.

Gitirana Jr., G.F.N (2005). "Weather-related geo-hazard assessment model for railway embankment stability." Ph.D. Thesis, University of Saskatchewan, Saskatoon, Canada.

Gupta, S.C. and Larson, W.E. (1979). " Estimating soil water characteristic from particle size distribution, organic matter and bulk density." Water Resources Research, 15: 1633-1635.

Gvirtzman, H. and Roberts, P.V. (1991). "Pore scale spatial analysis of two immiscible fluids in porous media." Water Resources Reserch, 27(6): 1165-1176.

Gvirtzman, H., Magaritz, M., Klein, E. and Nadler, A. (1987). "A scanning electron microscopy study of water in soil." Transport in Porous Media, 2: 83-93.

Haines, W.B. (1923). "The volume change associated with variations of water content in soil." Journal of Agricultural Science, 13: 296-310.

Hanks, R.J., Gardner, H.R. and Fairbourn, M.L. (1967). "Evaporation of water from soils as influenced by drying with wind or radiation." Soil Science society of America Proceedings, 31(5): 593-598.

Haverkamp, R., Leij, F.J., Fuentes, C., Sciortino, A. and Ross, P.J. (2005). "Soil water retention: I. Introduction of a shape index." Soil Science Society of America Journal, 69: 1881-1890.

Hilf, J.W. (1956). "An investigation of pore-water pressure in compacted cohesive soils." Ph.D. Thesis, Technical Memorandum No. 654, United States Department of the Interior Bureau of Reclamation, Design, and Construction Division, Denver, Colorado, U.S.A.

Hillel, D. (1998). "Environmental soil physics." Academic Press.

Huang, S. (1994). "Evaluation and laboratory measurement of the coefficient of permeability in deformable, unsaturated soils." Ph.D. Thesis, University of Saskatchewan, Saskatoon, Canada.

Huang, S., Barbour, S.L., and Fredlund, D.G. (1998). "Development and verification of a coefficient of permeability function for a deformable unsaturated soil." Canadian Geotechnical Journal, 35: 411-425.

Irmay, S. (1954). "On the hydraulic conductivity of unsaturated soils." Transactions of American Geophysics Union, 35: 463-467.

Khalili, N. and Khabbaz, M.H. (1998). "An effective stress based approach for shear strength determination of unsaturated soils." Proceedings of the Second International Conference on Unsaturated Soils, International Academic, Beijing, pp. 84-89.

Kimball, B.A., Jackson, R.D., Reginato, R.J., Nakayama, F.S. and Idso, S.B. (1976). Comparison of field-measures and calculated soil-heat fluxes. Soil Science Society of America Proceedings, 40: 18-25.

Knight, R., Tercier, P. and Goertz, D. (1996). "A laboratory procedure for estimating irreducible water saturation from cuttings." The Log Analyst, 37(4): 18-24.

Konukcu, F., Istanbulluoglu, A. and Kocaman, I. (2004). "Determination of water content in drying soils: incorporating transition from liquid phase to vapour phase." Australian Journal of Soil Research, 42: 1-8.

Lai, S. H., Tiedje, J.M. and Erickson, A.E. 1976. In situ measurement of gas diffusion coefficient in soils, Soil Science Society of America Journal, 40: 3-6.

Laliberte, G.E., Brooks, R.H. and Corey, A.T. (1968). "Permeability calculated from desaturation data." Journal of the Irrigation and Drainage Divition, ASCE, 43(IR1): 57-71.

Leong, E.-C., Tripathy, S. and Rahardjo, H. (2003). "Total suction measurement of unsaturated soils with a device using the chilled-mirror dew-point technique." Geotechnique, 35(2): 173-182.

Luckner, L., van Genuchten, M.Th. and Nielsen, D.R. (1989). A consistent set of parametric models for the two phase flow of immiscible fluids in the subsurface. Water Resources Research, 25(10): 2187-2193.

Luckner, L., van Genuchten, M.Th. and Nielsen, D.R. (1991). "Reply to comments on the treatment of residual water content in "a consistent set of parametric models for the two phase flow of immiscible fluids in the subsurface." Water Resources Research, 27(4): 663-664.

Marshall, T J. and Gurr, C.G. (1954). "Movement of water and chloride in relatively dry soil." Soil Science, 77: 147-152.

McKee, C. and Bumb, A. (1987). "Flow-testing coal bed methane production wells in the presence of water and gas." Proceedings, 1985 SPE Formation Evaluation Paper SPE 14447, Society of Petroleum Engineers, Richardson, Texas, pp. 599–608.

Mehta, K., Shiozawa, S. and Nakano, M. (1994). "Hydraulic properties of a sandy soil at low water contents." Soil Science, 157(4): 208-214.

Marshall, C.E. (1959). "The diffusion of gas through porous media." Journal of Soil Science, 10: 79-82.

Miller, E.E and Miller R.D. (1958). "Physical theory for capillary flow phenomena." Journal of applied physics, 27(4): 324-332.

Millington, R.J. (1959). "Gas diffusion in porous media." Science, 130: 100-102.

Millington, R.J. and Quirk, J.P. (1961). "Permeability of porous solids." Trans. Faraday Soc. 57: 1200-1207.

Morrow, N.R. (1970). "Irreducible wetting-phase saturation in porous media." Chemical Engineering Science, 25: 1799-1815.

Mualem, Y. (1974). "A conceptual model of hysteresis." Water Resources Research, 10(3): 514-520.

Mualem, Y. (1976a). "Hysteretical models for prediction of the hydraulic conductivity of unsaturated porous media." Water Resources Research, 12: 1248-1254.

Mualem, Y. (1976b). "A catalogue of hydraulic properties of soils. Proj. 442. Technion, Israel Institute of Technology, Haifa.

Mualem, Y. (1976c). "A new model for predicting hydraulic conductivity of unsaturated porous media." Water Resources Research, 12(3): 513-522.

Mualem, Y. (1992). "Modeling the hydraulic conductivity of unsaturated porous media." In: van Genuchten, M.Th., Leij, F.J. and Lund, L.J. (Eds.), Indirect Methods for Estimating the Hydraulic Properties of Unsaturated Soils, Proceedings of International Workshop, Riverside, CA, 11- 13 Oct., 1989. University of California, Riverside, pp. 1-14.

Mualem, Y. and Dagan, G. (1978). "Hydraulic conductivity of soils." unified approach to the statistical models." Soil Science Society of America Journal, 42: 392-395.

Mualem, Y. (1986). "Hydraulic conductivity of unsaturated soils: Prediction and formulas." Methods of Soil Analysis, 9(1), Physical and Mineralogical Methods, Second Edition, Agronomy, Madison, Wasconsin, pp. 799-823.

Nakayama, F.S., Jackson, R.D., Kimball, B.A. and Reginato, J.G. (1973). "Diurnal soil water evaporation: Chloride movement and accumulation near the soil surface." Soil Science Society of America Proceedings, 37: 509-513.

Nielson, D.R., Kirkham, D. and Perrier, E.R. (1960). "Soil capillary conductivity: comparison of measured and calculated values." Soil Science Society of America Proceedings, 24: 157-160.

Nimmo, J.R. (1990). "Experimental testing of transient unsaturated flow theory at low water content in a centrifugal field." Water Research Research, 26(9): 1951-1960.

Nimmo J.R. (1991). "Comments on the treatment of residual water content in "a consistent set of parametric models for the two phase flow of immiscible fluids in the subsurface." Water Resources Research, 27(4): 661-662.

Nimmo, J.R., Rubin, J. and Hammermeister, D.P. (1987). "Unsaturated flow in centrifugal field: measurement of hydraulic conductivity and testing of Darcy's law." Water Resources Research, 23(1): 124-134.

Nitao, J.J. and Bear, J. (1996). "Potentials and their role in transport in porous media." Water Resources Research, 32(2): 225-250.

Oberg, A.L. and Sallfors, G. (1997). "Determination of shear strength parameters of unsaturated soils and sands based on the water retention curve." Geotechnical Testing Journal, 20(1): 40-48.

Or, D. and Tuller, M. (1999). "Liquid retention and interfacial area in variably saturated porous media: upscaling from single pore to sample scale model." Water Resources Research, 35 (12): 3591-3606.

Penman, H.L. (1940). "Gas and vapour movements in the soil. I. the diffusion of vapours through porous solids." Journal of Agricultural Science: 30: 437-462.

PDE Solutions Inc. (2003). "Flex 3.10 - Reference Manual." Antioch, CA, U.S.A.

Pham, H.Q., Fredlund, D.G. and Barbour, S.L. (2003). "A practical hysteresis model for the soil-water characteristic curve for soils with negligible volume change." Geotechnique, 53(2): 293–298.

Poulsen, T.G., Moldrup, P., Iversen, B.V. and Jacobsen O.H. (2002). "Three-region Campbell model for unsaturated hydraulic conductivity in undisturbed soils." Soil Science Society of America Journal, 66(3): 744-752.

Purcell, W.R. (1949). "Capillary pressure-their measurement using mercury and calculation of the permeability therefrom." Transactions, American Institute of Mining and Metallurgical Engineers, 186: 39-48.

Quirk, J.P. (1955). "Significance of surface areas calculated from water vapor sorption isotherms by use of the B. E. T. equation." Soil Science, 80: 423-430.

Rassam, D.W. and Cook, F. (2002). "Predicting the shear strength envelope of unsaturated soils." Geotechnical Testing Journal, 25(2): 215-220.

Rassam, D.W. and Williams, D.J. (1999). "A numerical study of steady state evaporative conditions applied to mine tailings." Canadian Geotechnical Journal, 36: 640-650.

Rawlins, S.L. and Campbell, G.S. (1986). "Water potential: thermocouple psychrometry." Methods of Soil Analysis. Part 1. 2nd edition, A. Klute (Ed.), ASA and SSSA, Madison, WI, 597-617.

Rawls, W.J. and Brakensiek, D.L. (1985). "Prediction of soil water properties for hydrologic modeling." In: Jones, E.B., Ward, T.J. (Eds.), Proceedings Symposium

Watershed Management in the Eighties, April 30-May 1, 1985, Denver, Colorado, American Society of Civil Engineers, New York, NY, pp. 293-299.

Rawls, W.J., Brakensiek, D.L. and Saxton, K.E. (1982). "Estimation of soil water properties." Transactions, ASAE, 25(5): 1316-1320.

Reinson, J.R., Fredlund, D.G. and Wilson, G.W. (2005). "Unsaturated flow in coarse porous media." Technical Note, Canadian Geotechnical Journal, 42: 252-262.

Richards, L.A. (1931). "Capillary conduction of liquids through porous medium." Journal of Physics, 1: 318-333.

Rijtema, P.E. (1965). "An analysis of actual evapotranspiration." Agricultural Research Reports, Center for Agricultural Publicationns and Documentations, Wageningen, the Netherlands.

Rose, D.A. (1963a). "Water movement in porous materials: Part 1- isothermal vapour transfer." Brit. J. Appl. Phys., 14: 256-262.

Rose, D.A. (1963b). "Water movement in porous materials: Part 2- the separation of the components of water movement." Brit. J. Appl. Phys., 14: 491-496.

Rose, D.A., Konukcu, F. and Gowing, J.W. (2005). "Effect of water table depth on evaporation and salt accumulation from saline groundwater." Australian Journal of Soil Research, 43: 565-573.

Ross, P.J., Williams, J. and Bristow, K.L. (1991). "Equations for extending water-retention curves to dryness." Soil Science Society of America Journal, 55: 923-927.

Rossi, C. and Nimmo, J.R. (1994). "Modeling of soil water retention from saturation to oven dryness." Water Resources Research, 30(3): 701-708.

Sillers, W.S., Fredlund, D.G. (2001). "Statistical assessment of soil-water characteristic curve models for geotechnical engineering". Canadian Geotechnical Journal, 38(6): 1297-1313.

Simms, P.H. and Yanful, E.K. (2004). "Estimation of the soil-water characteristic curve of a clayey till using measured pore-size distributions". ASCE Journal of Environmental Engineering, 130 (8): 847-854.

Simms, P.H. and Yanful E.K. (2002). "Predicting soil-water characteristic curves of compacted plastic soils from measured pore-size distributions. Géotechnique, 52(4): 269-278.

Sjoblom, K.J. (2000). "The mechanisms involved during the desaturation process of a porous matrix." Ph.D. Thesis, Department of Civil and Environmental Engineering, Massachusetts Institute of Technology. pp. 334.

SoilVision Systems Ltd. (2003). "SoilVision user's guide – a knowledge-based system for geotechnical engineers". Version 3.34. Saskatoon, SK, Canada.

Tami, D., Rahardjo, H., Leong, E.C. and Fredlund, D.G. (2004). "Design and laboratory verification of a physical model of sloping capillary barrier". Canadian Geotechnical Journal, 41: 814-830.

Thakur, V. K. S., Sreedeep, S., and Singh, D. N. (2006). "Laboratory investigation on extremely high suction measurements for fine-grained soils." Geotechnical and Geological Engineering, 24, 565-578.

Tietje, O. and Tapkenhinrichs, M. (1993). "Evaluation of pedo-transfer functions." Soil Science Society of America Journal, 57(4): 1088-1095.

Tuller, M., and Or, D. (2005). "Water films and scaling of soil characteristic curve at low water contents." Water Resources Research, 41, W09403, 09401-09406.

van Genuchten, M.T. (1980). "A closed-form equation for predicting the hydraulic conductivity of unsaturated soils." Soil Science Society of America Journal, 44: 892-898.

Vanapalli, S.K., Fredlund, D.G., Pufahl, D.E. and Clifton, A.W. (1996). "Model for the prediction of shear strength with respect to soil suction". Canadian Geotechnical Journal, 33(3): 379-392.

Vanapalli, S.K., Sillers, W.S. and Fredlund, M.D. (1998). "The meaning and relevance of residual state to unsaturated soils." Proceedings of the 51th Canadian Geotechnical Conference. Edmonton, Alberta, Oct. 4-7.

Vanapalli, S.K. (1994). "Simple test procedures and their interpretation in evaluating the shear strength of an unsaturated soil". Ph.D. Thesis, University of Saskatchewan, Saskatoon, Canada.

Vereecken, H., Maes, J., Feyen, J. and Darius, P. (1989). "Estimating the moisture retention characteristics from texture, bulk density, and carbon content." Soil Science, 148: 389-403.

Wheeland, K.G. and Feasby, G. (1991). "Innovative decomposition technologies via Canada's MEMD program." In Proceedings of the 12th National Conference on Hazardous Material Control/Superfund' 91. Hazardous Material Control Research Institute, pp. 23-28.

White, N.F. (1968). "The desaturation of porous materials." Ph.D. dissertation, Colorado State University, Fort Collins, U.S.A.

White, N.F., Duke, H.R., Sunada, D.K. and Corey A.T. (1970). "Physics of desaturation in porous materials." Journal of the Irrigation and Drainage Division, ASCE, 96(IR2): 165-191.

Williams, P.J. (1982). "The surface the Earth, an introduction to geotechnical science". Longman, Inc., New York.

Wilson, G.W. (1990). "Soil evaporative fluxes for geotechnical engineering problems," PhD Thesis, Department of Civil and Geological Engineering, University of Saskatchewan, Saskatoon.

Wilson, G.W., Fredlund, D.G. and Barbour, S.L. (1994). "Coupled soil-atmosphere modeling for soil evaporation." Canadian Geotechnical Journal, 31(2): 151-161.

Wilson, G.W., Fredlund, D.G. and Barbour, S.L. (1997). "The effect of soil suction on evaporative fluxes from soil surface." Canadian Geotechnical Journal, 34(4): 145-155.

Wind, G.P. (1955). "Field experiment concerning capillary rise of moisture in heavy clay soil." Netherlands Journal of Agricultural Science, 3: 60-69.

Wind, G.P. (1968). "Capillary conductivity data estimated by simple method." In: Water in the Unsaturated Zone, Proceedings of the Wageningen Symposium, P.E Rijtema and H. Wassink (Eds.), 1: 181-191, International Association of Hydrological Sciences, Gentbrugge, Belgium.

Wosten, J.H.M., Pachepsky, Ya.A. and Rawls, W.J. (2001). "Pedotransfer functions: bridging the gap between available basic soil data and missing soil hydraulic characteristics." Journal of Hydrology, 251: 123-150.

Wyllie, M.R.J and Gardner, G.H.F. (1958). "The generalized Kozeny-Carman equation 11.A novel approach to problems of fluid flow." World Oil Production, Section 146: 210-228.

Yanful, E.K., Simms, P.H. and Payant, S.C. (1999). Soil covers for controlling acid generation in mine tailings: A laboratory evaluation of the physics and geochemistry. Water, Air, and Soil Pollution, 114(3-4): 347-375.

Yanful, E.K. and Choo, L.P. (1997). "Measurement of evaporation fluxes from candidate cover soils." Canadian Geotechnical Journal, 34: 447-459.

Yuster, S.T. (1951). "Theoretical considerations of multiphase flow in idealized capillary systems." Proceedings of the 3rd World Petroleum Congress, May 28 - June 6, 1951, The Hague, the Netherlands, 2: 437-445.

Zapata, C.E., Houston, W.N., Houston, S.L. and Walsh, K.D. (2000). "Soil–water characteristic curve variability." Advances in Unsaturated Geotechnics, Geotechnical Institute Special Publication No. 99, C. D. Shackelford, S. L. Houston, and N.-Y. Chang (Eds.), ASCE, Reston, a: 84–124.

APPENDIX A


EXPERIMENTAL DATA OF THE GRAIN-SIZE ADANALYSIS FOR BEAVER
CREEK SAND, BOTKIN SILT, AND REGINA CLAY SAMPLES

Experimental Data of the Grain-Size Analysis for Beaver Greek Sand

(ASTM D 422)

Sample:          Beaver Creek Sand

Total Mass, g:   100

Test Method:     Sieve

| Sieve No | Particle Size (mm) | % Finer Than |
|----------|--------------------|--------------|
| 10       | 2.000              | 99.98        |
| 20       | 0.850              | 96.21        |
| 40       | 0.425              | 86.90        |
| 60       | 0.250              | 32.25        |
| 80       | 0.180              | 13.62        |
| 100      | 0.150              | 7.22         |
| 200      | 0.075              | 0.49         |

Experimental Data of Grain-Size Analysis for Botkin Silt Sample before and after Washing

(ASTM D 422)

Sample:        Botkin Silt

Total Mass:    49.58 g

Test Method:   Hydrometer and Sieve

| Sieve No | Particle size (mm) | Before Washing | After Washing |
|:---:|:---:|:---:|:---:|
| | | % Finer Than | % Finer Than |
| 10 | 2.000 | 100 | 100 |
| 20 | 0.850 | 99.4 | 99.3 |
| 40 | 0.425 | 97.5 | 97.4 |
| 60 | 0.250 | 81.5 | 93.6 |
| 80 | 0.180 | 75.6 | 89.3 |
| 100 | 0.150 | 74.0 | 85.1 |
| 200 | 0.075 | 62.8 | 65.4 |
| | 0.061 | 54.7 | 52.4 |
| | 0.044 | 50.2 | 45.4 |
| | 0.032 | 40.3 | 39.4 |
| | 0.021 | 34.5 | 34.0 |
| | 0.012 | 29.1 | 29.2 |
| | 0.009 | 26.9 | 27.6 |
| | 0.006 | 24.3 | 24.8 |
| | 0.003 | 20.1 | 21.9 |
| | 0.001 | 16.3 | 17.6 |

Experimental Data for Grain-Size Analysis on Regina Clay

(ASTM D 422)

Sample:            Regina Clay

Total Mass:        50 g

Test Method:       Hydrometer and Sieve

| Sieve No | Particle size (mm) | % Finer Than |
|---|---|---|
| 10 | 2.000 | 100 |
| 20 | 0.850 | 100 |
| 40 | 0.425 | 99.1 |
| 60 | 0.250 | 97.9 |
| 80 | 0.180 | 97.1 |
| 100 | 0.150 | 96.7 |
| 200 | 0.075 | 95.3 |
| | 0.071 | 95.3 |
| | 0.050 | 95.0 |
| | 0.036 | 94.7 |
| | 0.025 | 93.7 |
| | 0.016 | 91.5 |
| | 0.009 | 89.6 |
| | 0.007 | 86.4 |
| | 0.005 | 82.9 |
| | 0.002 | 73.7 |
| | 0.001 | 59.7 |

APENDIX B

EXAMPLE TEST DATA FOR CONSOLIDATION AND SATURATED
COEFFICIENT OF PERMEABILITY

Consolidation Test Data for Preparation of the Evaporation Column, CS1-2 Aug, 2009

Consolidation Pressure =12.5 kPa

| Date | Elapsed Time (min) | Deflection (mm) |
|---|---|---|
| Aug. 27, 2009 | 0 | 0 |
| Aug. 27, 2009 | 0.1 | 2.060 |
| Aug. 27, 2009 | 2 | 2.170 |
| Aug. 27, 2009 | 5 | 2.375 |
| Aug. 27, 2009 | 10 | 2.645 |
| Aug. 27, 2009 | 20 | 2.995 |
| Aug. 27, 2009 | 52 | 3.770 |
| Aug. 27, 2009 | 104 | 4.520 |
| Aug. 27, 2009 | 140 | 4.850 |
| Aug. 27, 2009 | 270 | 5.400 |
| Aug. 27, 2009 | 300 | 5.455 |
| Aug. 27, 2009 | 670 | 5.655 |
| Aug. 28, 2009 | 1446 | 5.700 |
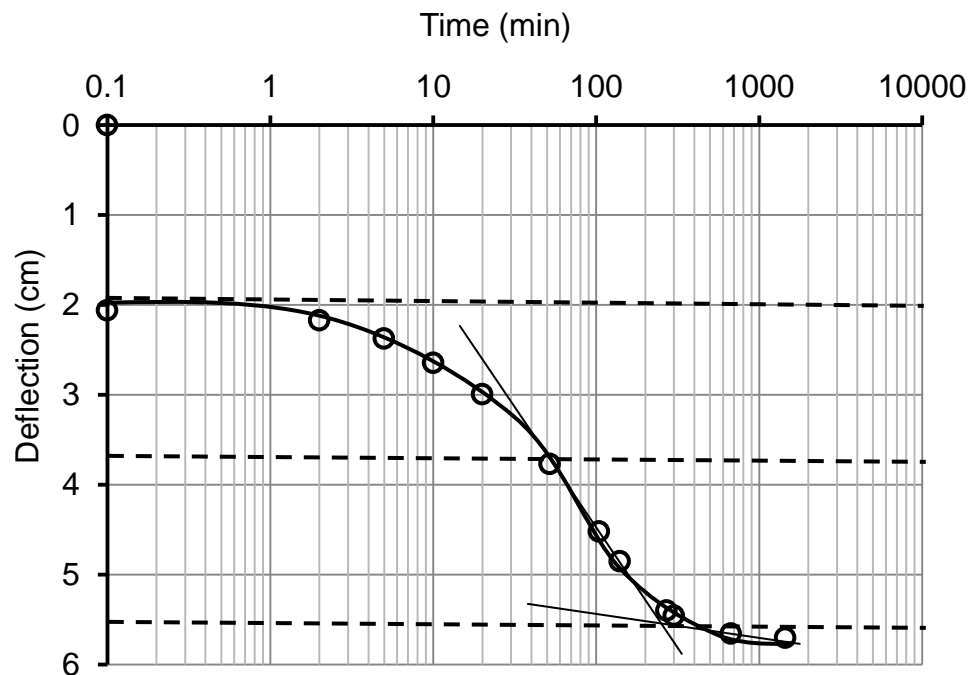
Experimental Data for the Falling Head Method of the Saturated Coefficient of Permeability Test

Saturated Coefficient of Permeability Calculations for Botkin Silt

Vertical Consolidation Pressure: 12.5 kPa

| Date | Time increment, sec | h1, cm | h2, cm | L, cm | $k_s$, m/s |
|------|---------------------|--------|--------|-------|------------|
| Aug. 28, 2009 | | | | | |
| | 225 | 33.478 | 32.878 | 4.66 | 4.01E-09 |
| | 240 | 32.878 | 31.778 | 4.66 | 7.07E-09 |
| | 3585 | 40.078 | 27.178 | 4.66 | 5.4E-09 |

Vertical Consolidation Pressure: 25 kPa

| Date | Time increment, sec | $h_1$, cm | $h_2$, cm | L, cm | $k_s$, m/s |
|------|---------------------|-----------|-----------|-------|------------|
| Aug. 30, 2009 | | | | | |
| | 900 | 32.778 | 30.528 | 4.53 | 3.83E-09 |
| | 900 | 30.528 | 28.928 | 4.53 | 2.9E-09 |
| | 900 | 28.928 | 27.678 | 4.53 | 2.38E-09 |
| | 1800 | 27.678 | 25.678 | 4.53 | 2.02E-09 |

Vertical Consolidation Pressure: 50 kPa

| Date | Time increment, sec | $h_1$, cm | $h_2$, cm | L, cm | $k_s$, m/s |
|------|---------------------|-----------|-----------|-------|------------|
| Aug. 31, 2009 | | | | | |
| | 900 | 34.078 | 31.678 | 4.41 | 3.83E-09 |
| | 900 | 31.678 | 29.928 | 4.41 | 2.98E-09 |
| | 900 | 29.928 | 28.528 | 4.41 | 2.51E-09 |
| | 3600 | 38.278 | 28.528 | 4.41 | 3.85E-09 |

Vertical Consolidation Pressure:  100 kPa

| Date | Time increment, sec | $h_1$, cm | $h_2$, cm | L, cm | $k_s$, m/s |
|------|---------------------|-----------|-----------|-------|------------|
| Sept. 1, 2009 | | | | | |
| | 420 | 29.578 | 28.778 | 4.284 | 2.99E-09 |
| | 660 | 28.778 | 28.178 | 4.284 | 1.46E-09 |
| | 720 | 28.178 | 26.678 | 4.284 | 3.48E-09 |
| | 780 | 26.678 | 25.628 | 4.284 | 2.36E-09 |

Experimental Data for the Falling Head Method of the Saturated Coefficient of
Permeability Test

Saturated Coefficient of Permeability Calculations for Beaver Creek Sand

Vertical Consolidation Pressure:  25 kPa

| Date | Time increment, sec | h1, cm | h2, cm | L, cm | $k_s$, m/s |
|------|---------------------|--------|--------|-------|------------|
| Sept. 06, 2009 | | | | | |
| | 5 | 29.674 | 19.674 | 4.75 | 4.18E-06 |
| | 8 | 19.674 | 9.674 | 4.75 | 4.51E-06 |

Vertical Consolidation Pressure:  200 kPa

| Date | Time increment, sec | h1, cm | h2, cm | L, cm | $k_s$, m/s |
|------|---------------------|--------|--------|-------|------------|
| Sept. 07, 2009 | | | | | |
| | 5 | 29.674 | 19.674 | 4.66 | 4.10E-06 |
| | 9 | 19.674 | 9.674 | 4.66 | 3.93E-06 |

APPENDIX C


DESORPTION SWCC MEASUREMENTS USING THE U OF S PRESSURE PLATE
CELL AND THE GCTS SWC 100 DEVICE

Soil: Specimen CS1-1

Mass of the Sample Holder:      81.9g

Volume of the Sample:  101.61 cm $^3$

Mass of the Sample Holder + Saturated Specimen: 287.91g

|  | Initial | Final |
|---|---|---|
| Saturated porous plate 1-bar | 139.07g | 139.10g |
| Saturated porous plate 5-bar | 141.40g | 141.39g |
| Saturated porous plate 15-bar | 140.47g | 140.46g |

| Date | Time | Mass of Tempe Cell | BFDA (g) | Mass of Tempe Cell | AFDA (g) | Suction (kPa) | Changed to | Comments |
|---|---|---|---|---|---|---|---|---|
| March 24, 2008 | 17:06 | | | 1873.49 | | 0 | | right after consolidation |
| March 25, 2008 | 14:20 | | | 1872.29 | | 0 | | saturating |
| March 30, 2008 | 14:15 | | | 1872.91 | | 0 | 1 | saturated |
| March 30, 2008 | 19:40 | | | 1872.78 | | 1 | | |
| March 31, 2008 | 11:51 | | | 1872.72 | | 1 | 5 | |
| March 30, 2008 | 21:00 | | | 1871.55 | | 5 | | |
| April 1, 2008 | 15:35 | | | 1871.45 | | 5 | 10 | |
| April 1, 2008 | 19:35 | | | 1870.33 | | 10 | | |
| April 2, 2008 | 14:55 | | | 1869.39 | | 10 | | |
| April 3, 2008 | 17:10 | | | 1869.27 | | 10 | | |
| April 4, 2008 | 13:50 | | | 1869.27 | | 10 | 20 | end of hanging column method |
| April 5, 2008 | 17:40 | | | 1867.56 | | 20 | | |

| | | | | | | |
|---|---|---|---|---|---|---|
| April 6, 2008 | 13:33 | | 1867.57 | 20 | 30 | |
| April 7, 2008 | 15:13 | | 1865.96 | 30 | | |
| April 8, 2008 | 15:20 | | 1865.82 | 30 | | |
| April 9, 2008 | 18:10 | | 1865.78 | 30 | 40 | |
| April 10, 2008 | 16:15 | | 1865.09 | 40 | 60 | |
| April 11, 2008 | 15:03 | | 1864.04 | 60 | | |
| April 12, 2008 | 16:02 | | 1863.53 | 60 | | |
| April 13, 2008 | 20:52 | | 1863.07 | 60 | | |
| April 14, 2008 | 16:10 | | 1862.87 | 60 | | |
| April 15, 2008 | 13:13 | 1862.65 | 1863.97 | 60 | | |
| April 16, 2008 | 16:32 | | 1863.25 | 70 | | little air bubble |
| April 17 2008 | 19:42 | | 1862.93 | 70 | | little air bubble |
| April 18, 2008 | 19:00 | | 1863.41 | 70 | | $M_{ring + soil}$ @ 70 kPa=278.58g, plate was changed to 5 bar |
| April 21, 2008 | 14:30 | | 1866.18 | 70 | | 5 bar, $M_{Tempe\ Cell}$ after plate was changed= 1869.39g |
| April 22, 2008 | 17:41 | | 1866.14 | 70 | | |

BFDA: Before Flushing Diffused Air,   AFDA: After Flushing Diffused Air

| Date | Time | Mass of Tempe Cell BFDA (g) | Mass of Tempe Cell AFDA (g) | Suction (kPa) | Changed to | Comments |
|---|---|---|---|---|---|---|
| April 23, 2008 | 16:30 | | 1866.05 | 70 | 90 | |
| April 24, 2008 | 15:35 | | 1865.62 | 90 | | |
| April 25, 2008 | 15:40 | | 1865.42 | 90 | | |
| April 26, 2008 | 19:28 | | 1865.42 | 90 | 100 | |
| April 28, 2008 | 20:12 | 1865.05 | 1865.30 | 100 | | |
| April 30, 2008 | 16:32 | | 1865.09 | 100 | | |
| May 01, 2008 | 17:17 | | 1865.17 | 100 | 150 | |
| May 02, 2008 | 16:05 | | 1864.90 | 150 | | 0.5 cm bubble |
| May 03, 2008 | 19:15 | 1864.66 | 1864.68 | 150 | | 0.5 cm bubble |
| May 08, 2008 | 11:08 | 1864.07 | 1864.41 | 150 | | |
| May 11, 2008 | 14:22 | 1864.07 | 1864.37 | 150 | 200 | |
| May 12, 2008 | 18:00 | 1864.28 | | 200 | | some bubbles observed |
| May 15, 2008 | 12:30 | 1863.95 | 1864.38 | 200 | 300 | |
| May 16, 2008 | 16:07 | 1864.19 | | 300 | | little bubbles |
| May 19, 2008 | 13:47 | 1863.45 | 1864.01 | 300 | 500 | |
| May 21, 2008 | 13:17 | 1863.71 | | 500 | | |
| May 26, 2008 | 20:30 | 1861.44 | 1863.49 | 500 | | |
| May 28, 2008 | 17:27 | 1862.63 | 1863.24 | | | |
| May 31, 2008 | 11:53 | 1862.06 | 1863.19 | 500 | | end of pressure Tempe Cell |

Desorption SWCC Measurements Using U of S Pressure Plate Apparatus

Soil: Specimen CS2-1

Mass of the Sample Holder: 83.04g

Volume of the Sample Holder: 101.45 cm$^3$

Mass of the Sample Holder + Saturated Specimen: 287.88 g

|  | Initial | Final |
|---|---|---|
| Saturated porous plate 1-bar | 137.28 g | 137.32 g |
| Saturated porous plate 5-bar | 135.52 g | 135.49 g |

| Date | Time | Mass of Tempe Cell | BFDA (g) | Mass of Tempe Cell | AFDA (g) | Suction (kPa) | Changed to | Comments |
|---|---|---|---|---|---|---|---|---|
| March 24, 2008 | 17:10 | | | 1888.35 | | 0 | | right after consolidation |
| March 25, 2008 | 14:20 | | | 1888.05 | | 0 | | saturating |
| March 30, 2008 | 14:15 | | | 1888.67 | | 0 | 1 | saturated |
| March 30, 2008 | 19:37 | | | 1888.46 | | 1 | | |
| March 31, 2008 | 11:50 | | | 1888.39 | | 1 | 5 | |
| March 30, 2008 | 21:00 | | | 1887.29 | | 5 | | |
| April 1, 2008 | 15:33 | | | 1887.07 | | 5 | 10 | |
| April 1, 2008 | 19:33 | | | 1885.91 | | 10 | | |
| April 2, 2008 | 14:53 | | | 1885.01 | | 10 | | |

| | | BFDA | AFDA | | | |
|---|---|---|---|---|---|---|
| April 3, 2008 | 17:07 | | 1884.83 | 10 | | |
| April 4, 2008 | 13:47 | | 1884.79 | 10 | 20 | end of hanging column method |
| April 5, 2008 | 17:37 | | 1883.02 | 20 | | |
| April 6, 2008 | 13:35 | | 1883.04 | 20 | 30 | |
| April 7, 2008 | 15:11 | | 1881.40 | 30 | | |
| April 8, 2008 | 15:17 | | 1881.23 | 30 | | |
| April 9, 2008 | 18:08 | | 1881.15 | 30 | 40 | |
| April 10, 2008 | 16:12 | | 1880.59 | 40 | 60 | |
| April 11, 2008 | 15:05 | | 1879.47 | 60 | | |
| April 12, 2008 | 16:00 | | 1878.96 | 60 | | |
| April 13, 2008 | 20:50 | | 1878.41 | 60 | | |
| April 14, 2008 | 16:12 | | 1878.22 | 60 | | |
| April 15, 2008 | 13:25 | 1877.99 | 1878.23 | 60 | 70 | |
| April 16, 2008 | 16:30 | | 1877.58 | 70 | | |
| April 17 2008 | 19:40 | | 1877.16 | 70 | | |
| April 18, 2008 | 19:27 | | 1876.84 | 70 | | |
| April 21, 2008 | 14:32 | | 1876.00 | 70 | | |
| April 22, 2008 | 17:43 | | 1875.75 | 70 | | |

BFDA: Before Flushing Diffused Air,   AFDA: After Flushing Diffused Air

| Date | Time | Weight of Tempe Cell BFDA (g) | Weight of Tempe Cell AFDA (g) | Suction (kPa) | Changed to | Comments |
|---|---|---|---|---|---|---|
| April 23, 2008 | 16:35 | | 1875.48 | 70 | | |
| April 24, 2008 | 15:10 | 1875.26 | 1878.54 | 70 | | 1 bar plate was replaced with 5 bar |
| April 24, 2008 | 15:30 | | 1877.97 | 70 | | $M_{5\text{- bar plate}}=135.52$, $M_{s\ @\ 70kPa}+M_{ring}=278.26g$ |
| April 25, 2008 | 15:36 | | 1876.77 | 70 | | |
| April 26, 2008 | 19:25 | | 1876.77 | 70 | 100 | |
| April 28, 2008 | 20:10 | | 1876.40 | 100 | | |
| April 30, 2008 | 16:30 | | 1876.26 | 100 | | |
| May 01, 2008 | 17:15 | | 1876.21 | 100 | 150 | |
| May 02, 2008 | 16:00 | | 1876.12 | 150 | | |
| May 03, 2008 | 19:15 | | 1876.04 | 150 | | |
| May 08, 2008 | 11:55 | 1875.61 | 1875.80 | 150 | | |
| May 11, 2008 | 14:30 | 1875.53 | 1875.88 | 150 | 200 | |
| May 12, 2008 | 17:58 | | 1875.86 | 200 | | |
| May 15, 2008 | 12:35 | 1875.47 | 1875.80 | 200 | 300 | |
| May 16, 2008 | 16:00 | 1875.60 | | 300 | | little bubbles |
| May 19, 2008 | 13:52 | 1874.86 | 1875.66 | 300 | 500 | |
| May 21, 2008 | 13:18 | 1875.50 | 1875.50 | 500 | | |
| May 26, 2008 | 20:35 | 1873.75 | 1875.23 | 500 | | |
| May 28, 2008 | 17:21 | 1874.53 | 1875.00 | 500 | | |
| May 31, 2008 | 11:40 | 1874.28 | 1874.95 | 500 | | end of pressure (Tempe Cell) |

May 31, 2008 @ 11:45 the specimen was removed from the Tempe Cell

$M_{s\ @\ 500kPa} + M_{ring} = 274.78g$

$M_{s\ @\ 500kPa} + M_{ring} + M_{plate} = 291.69$

$M_{s@ovendried} + M_{ring} + M_{plate} = 261.78g$

$M_{s@ovendried} + M_{ring} = 244.82g$

$M_{plate} = 16.97g$

Drying SWCC Measurements Using GCTS SWC-100 Equipment

Soil:   Specimen CS3-1

Mass of the Sample Holder:  91.50g

Volume of the Sample Holder:  100.02 cm$^3$

$M_{ring + saturated\ soil} = 268.91g$

| | | Initial | Final |
|---|---|---|---|
| Saturated porous plate 1-bar | | 179.40g | 179.26g |
| Saturated porous plate 5-bar | | 135.52g | 135.49g |

| Date | Time | Burette Reading (mm) | BFDA | Burette Reading (mm) | AFDA | Suction (kPa) | Changed to | Comments |
|---|---|---|---|---|---|---|---|---|
| March 31, 2008 | 21:20 | 91 | | 91 | | 0 | 10 | |
| April 1, 2008 | 15:52 | 123.5 | | 123.5 | | 10 | | |
| April 2, 2008 | 14:58 | 124.5 | | 124.5 | | 10 | | |
| April 3, 2008 | 17:35 | 124.5 | | 124.5 | | 10 | 20 | |
| April 4, 2008 | 13:45 | 137.5 | | 137.5 | | 20 | | |
| April 5, 2008 | 17:40 | 137.5 | | 137.5 | | 20 | 30 | |
| April 6, 2008 | 13:35 | 147.5 | | 147.5 | | 30 | | |
| April 7, 2008 | 15:15 | 147.5 | | 147.5 | | 30 | 40 | |
| April 8, 2008 | 15:22 | 152.5 | | 152.5 | | 40 | | |
| April 9, 2008 | 18;10 | 152.5 | | 152.5 | | 40 | 60 | |
| April 10, 2008 | 16:13 | 162.5 | | 162.5 | | 60 | | |
| April 11, 2008 | 15:15 | 162.5 | | 162.5 | | 60 | 80 | |

| | | | | | | |
|---|---|---|---|---|---|---|
| April 12, 2008 | 16:06 | 169.5 | 169.5 | 80 | | |
| April 13, 2008 | 20:55 | 169.5 | 169.5 | 80 | 90 | |
| April 14, 2008 | 16:14 | 172.5 | 172.5 | 90 | | |
| April 15, 2008 | 13:25 | 172.5 | 171 | 90 | 100 | |
| April 16, 2008 | | 173.5 | 173.5 | 100 | | |
| April 17, 2008 | 19:46 | 174.5 | 173.5 | 100 | | |
| April 18, 2008 | 9:40 | 173.5 | 173.5 | 100 | | Change the plate from 1 to 5-bar<br><br>5-bar saturated plate = 170.16g<br><br>$M_{s\ @\ 100kPa}+M_{ring} = 258.19g$ |
| April 18, 2008 | 19:35 | | 106.5 | 100 | | reading with 5-bar plate |
| April 21, 2008 | 15:10 | | 189 | 100 | | 5-bar plate didn't function well, so it was replaced with 15bar @ 14:45, $M_{s\ @\ 100kPa}+M_{ring} = 257.78g$ |
| April 22, 2008 | 17:48 | | 209.5 | 100 | | |
| April 23, 2008 | 16:38 | | 209.5 | 100 | 120 | |
| April 24, 2008 | 15:47 | | 210.5 | 120 | | |
| April 26, 2008 | 19:40 | | 210.5 | 120 | 150 | |

| Date | Time | Burette Reading (mm) BFDA | Burette Reading (mm) AFDA | Suction (kPa) | Changed to | Comments |
|---|---|---|---|---|---|---|
| April 28, 2008 | 20:15 | 215.5 | 213 | 150 | | |
| April 30, 2008 | 16:27 | 216.5 | 214 | 150 | | |
| May 1, 2008 | 17:25 | 215.5 | 214 | 150 | 200 | |
| May 2, 2008 | 16:00 | 220 | 218.5 | 200 | | |
| May 3, 2008 | 19:10 | 222 | 220.5 | 200 | | |
| May 8, 2008 | 12:05 | 228 | 221.5 | 200 | | |
| May 11, 2008 | 14:35 | 225 | 221.5 | 200 | 500 | |
| May 12, 2008 | 18:00 | Past 308 | 204 | 500 | 200 | the 15-bar plate was cracked $M_{15\text{-bar}}$ = 137.28 and 137.52 |
| May 15, 2008 | 12;46 | Past 308 again | | 200 | | Change the plate and start from 200kPa again |
| May 15, 2008 | 13:10 | | 199 | 500 | | Suction was set at 500kPa after installing a new 15bar plate with M = 140.71 g |
| May 15, 2008 | 14:35 | | 206 | 500 | | |
| May 16, 2008 | 16:10 | 233.5 | 231 | 500 | | |
| May 19, 2008 | 13:43 | 255 | 245.5 | 500 | | |
| May 21, 2008 | 13:20 | 253.5 | 245.5 | 500 | 1000 | |
| May 21, 2008 | 15:15 | 249.5 | | 1000 | | |
| May 22, 2008 | 10:52 | 269.5 | 256.5 (213) | 1000 | | The burrette reading was adjusted to 213 |
| May 26, 2008 | 2030 | 285 | 226.5 | 1000 | | |
| May 27, 2008 | 15:36 | 240.5 | 226.5 | 1000 | | |

| | | | | | | |
|---|---|---|---|---|---|---|
| May 28, 2008 | 17:07 | 243.5 | 226.5 | 1000 | | |
| May 29, 2008 | 10:50 | 241 | 226.5 | 1000 | 1500 | |
| May 29, 2008 | 14:44 | 240 | 228.5 | 1500 | | |
| May 29, 2008 | 17:30 | 238.5 | 228 | 1500 | | |
| May 29, 2008 | 22:20 | 244.5 | 229 | 1500 | | |
| May 30, 2008 | 9:57 | 270.5 | 228.5 | 1500 | | |
| May 30, 2008 | 22:36 | 273.5 | 229 | 1500 | | |
| May 31, 2008 | 11:10 | 275.5 | 229 | 1500 | | |

May 31, 2008 @ 11:20 AM

$M_{\text{soil @ 1500kPa}}+M_{\text{ring}} = 243.14\text{g}$

$M_{\text{soil @ 1500kPa}}+M_{\text{ring}}+M_{\text{plate}}= 349.22\text{g}$

$M_{\text{oven-dried soil}} +M_{\text{ring}}+M_{\text{plate}} = 333.38\text{g}$

$M_{\text{plate}} = 106.10\text{g}$

Desorption SWCC Measurements on Botkin Silt Using U of S Pressure Plate Apparatus

Soil: Specimen CSSlurry02

Mass of the Steel Plate:    106.32 g

Mass of the Sample Holder:    76.65 g

| Date | Time | Mass of Tempe Cell | BFDA (g) | Mass of Tempe Cell | AFDA (g) | Suction (kPa) | Changed to | Comments |
|------|------|------|------|------|------|------|------|------|
| Aug.11, 2006 | 17:06 | 1856.81 | | | | 0 | | |
| | | 1853.83 | | | | 1 | | |
| | | 1849.74 | | | | 5 | | |
| | | 1846.84 | | | | 10 | | End of hanging-column technique |
| | | 1804.23 | | | | 50 | | |
| | | 1797.72 | | | | 50 | | |
| | | 1793.05 | | | | 100 | | $M_s@100kPa + M_{ring} = 240.21$ |
| | | 1843.17 | | | | 100 | | The plate was changed |
| | | 1842.53 | | | | 100 | | |
| | | 1840.33 | | | | 200 | | |
| | | 1837.85 | | | | 300 | | |
| | | 1834.55 | | | | 420 | | |

BFDA: Before Flushing Diffused Air,   AFDA: After Flushing Diffused Air

$M_{soil\ @\ 420kPa}+M_{ring}+M_{plate}=$ 339.05g

$M_{oven\text{-}dried\ soil}+M_{ring}+M_{plate}=$ 321.40g

$M_{plate} = 107.21g$

APPENDIX D

EXAMPLE EXPERIMENTAL TEST DATA FOR EVAPORATION PROCESSES

INCLUDING RECORDED DATA FOR

MASS OF THE EVAPORATION COLUMN

TEMPERATURE

MOISTURE CONTENT AND SUCTION PROFILES

Experimental Recorded Data for the Mass of the Evaporation Column with Time
(Example Data for Evaporation Test No. MCS2, Botkin silt)

| Date | Time | Mass of the Column (g) |
|---|---|---|
| 12/04/2010 | 17:51:28 | 1510.4 |
| 12/04/2010 | 18:01:28 | 1510.46 |
| 12/04/2010 | 18:11:28 | 1504.49 |
| 12/04/2010 | 18:21:28 | 1508.74 |
| 12/04/2010 | 18:31:28 | 1510.06 |
| 12/04/2010 | 18:41:28 | 1510.56 |
| 12/04/2010 | 18:51:28 | 1510.95 |
| 12/04/2010 | 19:11:28 | 1511.41 |
| 12/04/2010 | 19:21:28 | 1511.55 |
| 12/04/2010 | 19:31:28 | 1511.66 |
| 12/04/2010 | 19:41:28 | 1511.72 |
| 12/04/2010 | 19:51:27 | 1511.7 |
| 12/04/2010 | 20:01:27 | 1511.8 |
| 12/04/2010 | 20:11:27 | 1511.73 |
| 12/04/2010 | 20:21:27 | 1511.48 |
| 12/04/2010 | 20:31:27 | 1511.52 |
| 12/04/2010 | 20:41:27 | 1511.49 |
| 12/04/2010 | 20:51:27 | 1511.52 |
| 12/04/2010 | 21:01:27 | 1511.44 |
| 12/04/2010 | 21:11:27 | 1511.39 |
| 12/04/2010 | 21:21:27 | 1511.39 |
| 12/04/2010 | 21:31:27 | 1511.23 |
| 12/04/2010 | 21:41:26 | 1511.19 |
| 12/04/2010 | 21:51:26 | 1511.12 |
| 12/04/2010 | 22:01:26 | 1511.1 |
| 12/04/2010 | 22:11:26 | 1510.92 |
| 12/04/2010 | 22:21:26 | 1510.85 |
| 12/04/2010 | 22:31:26 | 1510.76 |
| 12/04/2010 | 22:41:26 | 1510.68 |
| 12/04/2010 | 22:51:26 | 1510.6 |
| 12/04/2010 | 23:01:26 | 1510.43 |
| 12/04/2010 | 23:11:26 | 1510.41 |
| 12/04/2010 | 23:21:26 | 1510.24 |
| 12/04/2010 | 23:31:26 | 1510.17 |
| 12/04/2010 | 23:41:26 | 1510.07 |
| 12/04/2010 | 23:51:25 | 1509.86 |
| 13/04/2010 | 0:01:25 | 1509.84 |
| 13/04/2010 | 0:11:25 | 1509.67 |

| | | |
|---|---|---|
| 13/04/2010 | 0:21:25 | 1509.6 |
| 13/04/2010 | 0:31:25 | 1509.43 |
| 13/04/2010 | 0:41:25 | 1509.36 |
| 13/04/2010 | 0:51:25 | 1509.22 |
| 13/04/2010 | 1:01:25 | 1509.09 |
| 13/04/2010 | 1:11:25 | 1509 |
| 13/04/2010 | 1:21:25 | 1508.86 |
| 13/04/2010 | 1:31:25 | 1508.71 |
| 13/04/2010 | 1:41:25 | 1508.56 |
| 13/04/2010 | 1:51:24 | 1508.47 |
| 13/04/2010 | 2:01:24 | 1508.33 |
| 13/04/2010 | 2:11:24 | 1508.25 |
| 13/04/2010 | 2:21:24 | 1508.09 |
| 13/04/2010 | 2:31:24 | 1507.95 |
| 13/04/2010 | 2:41:24 | 1507.84 |
| 13/04/2010 | 2:51:24 | 1507.68 |
| 13/04/2010 | 3:01:24 | 1507.56 |
| 13/04/2010 | 3:11:24 | 1507.43 |
| 13/04/2010 | 3:21:24 | 1507.32 |
| 13/04/2010 | 3:31:24 | 1507.18 |
| 13/04/2010 | 3:41:24 | 1507.04 |
| 13/04/2010 | 3:51:24 | 1506.94 |
| 13/04/2010 | 4:01:24 | 1506.74 |
| 13/04/2010 | 4:11:23 | 1506.62 |
| 13/04/2010 | 4:21:23 | 1506.44 |
| 13/04/2010 | 4:31:23 | 1506.31 |
| 13/04/2010 | 4:41:23 | 1506.21 |
| 13/04/2010 | 4:51:23 | 1506.04 |
| 13/04/2010 | 5:01:23 | 1505.92 |
| 13/04/2010 | 5:11:23 | 1505.72 |
| 13/04/2010 | 5:21:23 | 1505.62 |
| 13/04/2010 | 5:31:23 | 1505.46 |
| 13/04/2010 | 5:41:23 | 1505.39 |
| 13/04/2010 | 6:01:23 | 1505.11 |
| 13/04/2010 | 6:11:22 | 1504.94 |
| 13/04/2010 | 6:21:22 | 1504.71 |
| 13/04/2010 | 6:31:22 | 1504.68 |
| 13/04/2010 | 6:41:22 | 1504.44 |

Experimental Recorded Data for Soil Surface and Air Temperatures with Time
(Example Data for Evaporation Test No. MCS2, Botkin silt)

| Date and Time | Elapsed Time (min) | $T_s$ ($^o$C) | $T_{air}$($^o$C) |
|---|---|---|---|
| 12/04/2010 17:50 | 0 | 25.65 | 25.51 |
| 12/04/2010 18:00 | 10 | 24.34 | 25.56 |
| 12/04/2010 18:10 | 20 | 22.91 | 25.52 |
| 12/04/2010 18:20 | 30 | 22.29 | 25.44 |
| 12/04/2010 18:30 | 40 | 21.82 | 25.46 |
| 12/04/2010 18:40 | 50 | 21.56 | 25.46 |
| 12/04/2010 18:50 | 60 | 21.33 | 25.48 |
| 12/04/2010 19:00 | 70 | 21.14 | 25.49 |
| 12/04/2010 19:10 | 80 | 20.98 | 25.46 |
| 12/04/2010 19:20 | 90 | 20.87 | 25.46 |
| 12/04/2010 19:30 | 100 | 20.77 | 25.45 |
| 12/04/2010 19:40 | 110 | 20.66 | 25.46 |
| 12/04/2010 19:50 | 120 | 20.57 | 25.41 |
| 12/04/2010 20:00 | 130 | 20.52 | 25.47 |
| 12/04/2010 20:10 | 140 | 20.47 | 25.46 |
| 12/04/2010 20:20 | 150 | 20.39 | 25.4 |
| 12/04/2010 20:30 | 160 | 20.34 | 25.47 |
| 12/04/2010 20:40 | 170 | 20.3 | 25.39 |
| 12/04/2010 20:50 | 180 | 20.29 | 25.45 |
| 12/04/2010 21:00 | 190 | 20.24 | 25.45 |
| 12/04/2010 21:10 | 200 | 20.23 | 25.42 |
| 12/04/2010 21:20 | 210 | 20.2 | 25.46 |
| 12/04/2010 21:30 | 220 | 20.19 | 25.44 |
| 12/04/2010 21:40 | 230 | 20.19 | 25.48 |
| 12/04/2010 21:50 | 240 | 20.16 | 25.44 |
| 12/04/2010 22:00 | 250 | 20.15 | 25.43 |
| 12/04/2010 22:10 | 260 | 20.12 | 25.47 |
| 12/04/2010 22:20 | 270 | 20.09 | 25.45 |
| 12/04/2010 22:30 | 280 | 20.09 | 25.44 |
| 12/04/2010 22:40 | 290 | 20.09 | 25.42 |
| 12/04/2010 22:50 | 300 | 20.09 | 25.47 |
| 12/04/2010 23:00 | 310 | 20.07 | 25.44 |
| 12/04/2010 23:10 | 320 | 20.06 | 25.42 |
| 12/04/2010 23:20 | 330 | 20.03 | 25.45 |
| 12/04/2010 23:30 | 340 | 20.03 | 25.41 |
| 12/04/2010 23:40 | 350 | 20.01 | 25.43 |
| 12/04/2010 23:50 | 360 | 20.03 | 25.45 |

| | | | |
|---|---|---|---|
| 13/04/2010 0:00 | 370 | 20.03 | 25.46 |
| 13/04/2010 0:10 | 380 | 20 | 25.42 |
| 13/04/2010 0:20 | 390 | 19.99 | 25.47 |
| 13/04/2010 0:30 | 400 | 19.99 | 25.4 |
| 13/04/2010 0:40 | 410 | 19.99 | 25.46 |
| 13/04/2010 0:50 | 420 | 19.98 | 25.45 |
| 13/04/2010 1:00 | 430 | 19.97 | 25.38 |
| 13/04/2010 1:10 | 440 | 19.97 | 25.39 |
| 13/04/2010 1:20 | 450 | 19.97 | 25.46 |
| 13/04/2010 1:30 | 460 | 19.97 | 25.41 |
| 13/04/2010 1:40 | 470 | 19.98 | 25.41 |
| 13/04/2010 1:50 | 480 | 20 | 25.46 |
| 13/04/2010 2:00 | 490 | 19.98 | 25.44 |
| 13/04/2010 2:10 | 500 | 19.97 | 25.41 |
| 13/04/2010 2:20 | 510 | 19.98 | 25.48 |
| 13/04/2010 2:30 | 520 | 19.99 | 25.43 |
| 13/04/2010 2:40 | 530 | 19.98 | 25.47 |
| 13/04/2010 2:50 | 540 | 19.99 | 25.41 |
| 13/04/2010 3:00 | 550 | 19.99 | 25.48 |
| 13/04/2010 3:10 | 560 | 19.96 | 25.4 |
| 13/04/2010 3:20 | 570 | 19.96 | 25.42 |
| 13/04/2010 3:30 | 580 | 19.97 | 25.44 |
| 13/04/2010 3:40 | 590 | 19.96 | 25.4 |
| 13/04/2010 3:50 | 600 | 19.97 | 25.47 |
| 13/04/2010 4:00 | 610 | 19.97 | 25.41 |
| 13/04/2010 4:10 | 620 | 19.99 | 25.45 |
| 13/04/2010 4:20 | 630 | 19.99 | 25.44 |
| 13/04/2010 4:30 | 640 | 19.96 | 25.38 |
| 13/04/2010 4:40 | 650 | 19.97 | 25.46 |
| 13/04/2010 4:50 | 660 | 19.99 | 25.42 |
| 13/04/2010 5:00 | 670 | 20 | 25.45 |
| 13/04/2010 5:10 | 680 | 20 | 25.46 |
| 13/04/2010 5:20 | 690 | 20 | 25.49 |
| 13/04/2010 5:30 | 700 | 20 | 25.41 |
| 13/04/2010 5:40 | 710 | 20 | 25.48 |
| 13/04/2010 5:50 | 720 | 19.99 | 25.43 |
| 13/04/2010 6:00 | 730 | 19.99 | 25.42 |
| 13/04/2010 6:10 | 740 | 20 | 25.45 |
| 13/04/2010 6:20 | 750 | 20.01 | 25.45 |
| 13/04/2010 6:30 | 760 | 19.98 | 25.41 |
| 13/04/2010 6:40 | 770 | 19.98 | 25.45 |

Experimental Moisture Content and Total Suction Data along the Soil Column after Reaching Steady State Flow Conditions (Example Data for Evaporation Test No. MCS2, Botkin silt)

| Depth (mm) | Gravimetric Water Content(%) | Suction (kPa) |
|---|---|---|
| 1.5 | 2.41 | 75980 |
| 5.0 | 4.20 | 12380 |
| 9.5 | 4.88 | 6010 |
| 15.5 | 7.00 | 4290 |
| 24.5 | 7.97 | 1860 |
| 35.0 | 9.60 | 80 |
| 44.0 | 10.30 | |
| 56.5 | 11.07 | |
| 70.0 | 10.79 | |